Characterization of a novel multiprotein complex downstream of the cytosolic nucleic acid sensors cGAS and RIG-I

Dissertation

zur Erlangung des Doktorgrades (PhD)

der Medizinischen Fakultät

der Rheinischen Friedrich-Wilhelms-Universität

Bonn

Alexander Kirchhoff

aus Melle

2021

Angefertigt mit der Genehmigung

der Medizinischen Fakultät der Universität Bonn

1. Gutachter: Prof. Dr. rer. nat. Martin Schlee

2. Gutachter: Prof. Dr. rer. nat. Matthias Geyer

Tag der Mündlichen Prüfung: 17.08.2021

Aus dem Institut für Klinische Chemie und Klinische Pharmakologie

Direktor: Prof. Dr. med. Gunther Hartmann

Table of Contents

List of abbreviations

α	Anti
°C	Degree Celsius
Δ	Deletion
∞	Infinity
λ	Wavelength
×	Times
×g	Times gravity
A	Ampere
aa	Amino acid
ADP	Adenosine diphosphate
AF	Alexa Fluor
AGS	Aicardi-Goutières syndrome
ANOVA	Analysis of variance
AP-MS	Affinity purification-mass spectrometry
APC	Antigen-presenting cell
APS	Ammonium peroxydisulfate
ARE	Adenylate-uridylate-rich element
ATP	Adenosine triphosphate
BHI	Brain-heart infusion
bp	Base pair
CARD	Caspase recruitment domain
Cas9	CRISPR associated protein 9
CCL	Cleared cellular lysate
CDN	Cyclic dinucleotide
cDNA	Complementary DNA
CRISPR	Clustered regularly interspaced short palindromic repeats
crRNA	CRISPR RNA
C_t	Cycle threshold
CTD	C-terminal domain
CTT	C-terminal tail
DMEM	Dulbecco's Modified Eagle's Medium
DNA	Deoxyribonucleic acid
dNTP	Deoxynucleoside triphosphate
ds	Double stranded
DTT	1,4-dithiothreitol
E. coli	*Escherichia coli*
e.g.	For example
EDTA	Ethylenediaminetetraacetic acid
ELISA	Enzyme-linked immunosorbent assay
ER	Endoplasmic reticulum
ERGIC	ER-Golgi intermediate compartment
et al.	And others
FCS	Fetal calf serum
Fig.	Figure
fwd	Forward

g	Gram
GFP	Green fluorescent protein
GO	Gene ontology
gRNA	Guide RNA
GST	Glutathione S-transferase
GTP	Guanosine triphosphate
h	Hour
HIV-1	Human immunodeficiency virus 1
hnRNP	Heterogeneous nuclear ribonucleoprotein
HSV-1	Herpes simplex virus-1
iBAQ	Intensity based absolute quantification
i.e.	That is
IFN	Interferon
IL	Interleukin
IP	Immunoprecipitation
ISG	IFN-stimulated gene
ISRE	IFN-stimulated response element
kb	Kilobase
kDa	Kilodalton
KD	Knockdown
KO	Knockout
LB	Lysogeny broth
LBD	Ligand-binding domain
L. monocytogenes	*Listeria monocytogenes*
LPS	Lipopolysaccharide
LRR	Leucine-rich repeat
M	Molarity
mAb	Monoclonal antibody
MAPK	Mitogen-activated protein kinase
MEF	Mouse embryonic fibroblast
min	Minute
MOI	Multiplicity of infection
mRNA	Messenger RNA
MTT	Thiazolyl blue tetrazolium bromide
NLS	Nuclear localization sequence
norm.	Normalized
nt	Nucleotide
NTD	N-terminal domain
OA	Okadaic acid
P	*P* value
PAMP	Pathogen-associated molecular pattern
PBS	Phosphate-buffered saline
PCR	Polymerase chain reaction
PFU	Plaque-forming unit
pH	Potential of hydrogen
PLA	Proximity ligation assay
PMA	Phorbol 12-myristate 13-acetate

poly(I:C)	Polyinosinic:polycytidylic acid
PRR	Pattern recognition receptor
pTBK1-Ser172	TBK1 phosphorylated at Ser172
PTM	Post-translational modification
puro	Puromycin
qPCR	Quantitative real-time PCR
RBP	RNA-binding protein
rev	Reverse
RLR	Retinoic acid inducible gene I (RIG-I)-like receptor
RNA	Ribonucleic acid
rpm	Revolutions per minute
RPMI	Roswell Park Memorial Institute
RRM	RNA recognition motif
RT	Room temperature
SAVI	STING-associated vasculopathy with onset in infancy
SD	Standard deviation
SDS	Sodium dodecyl sulfate
SEAP	Secreted alkaline phosphatase
sec	Second
SLE	Systemic lupus erythematosus
SMS	Singleton-Merten syndrome
ss	Single stranded
Tab.	Table
TLR	Toll-like receptor
TM	Transmembrane
TNF	Tumor necrosis factor
U	Unit
UTR	Untranslated region
UV	Ultraviolet
V	Volt
vs.	Versus
v/v	Volume per volume
V_HH	Single variable domain on a heavy chain (nanobody)
VSV	Vesicular stomatitis virus
w/v	Weight per volume
WT	Wildtype
YSD	Y-form short DNA

The International Union of Pure and Applied Chemistry (IUPAC) code was used for the nomenclature of incompletely specified amino acids, DNA bases, and RNA bases.

1 Introduction

The human body is permanently exposed to countless pathogens. Whether these microorganisms will cause disease is primarily determined by the integrity of the host's immune system. The immune system can be divided into two branches: innate and adaptive immune system. Mechanisms of the innate immune system act as the first line of defense and are essential to prevent, restrict, and, if possible, eliminate microbial infections within the first hours or days after infection. The adaptive immune response develops several days after the infection, as it requires the expansion and differentiation of specialized lymphocytes.

The main components of the innate immune system involve (1) mechanical, chemical, and microbial barriers of surface epithelia that prevent microbial pathogens from entering host cells; (2) cellular components, including tissue sentinel cells (e.g., macrophages, dendritic cells, or mast cells) capable of recognizing microbial pathogens that have breached natural barriers, and certain leukocyte species (e.g. monocyte-derived macrophages, neutrophils, or natural killer cells) that can enter the inflamed tissue from the blood to fight the infection; and (3) soluble effector molecules (e.g., plasma proteins of the complement system).

A theoretical framework of how the innate immune system recognizes microbial infections was first conceptualized by Charles Janeway Jr. (Janeway, 1989). Extensive research over the years solidified his theory that invariant molecular components of microbial pathogens, so-called pathogen-associated molecular patterns (PAMPs), are detected by a limited number of germline-encoded pattern recognition receptors (PRRs) (Schlee and Hartmann, 2016). A key challenge in the evolution of the innate immune system is the discrimination of self from non-self molecules. PRRs have evolved to detect highly conserved PAMPs, often essential for microbial survival. This evolutionary constraint ensures that microbes cannot mutate rapidly to escape recognition by innate immune sensors (Tan et al., 2018). Certain members of the Toll-like receptor (TLR) family can sense bacterial cell wall components (e.g., lipopolysaccharide (LPS) or peptidoglycan) that are fundamentally different from endogenous molecules and are not expressed by host cells. By contrast, viruses exploit the host cell machinery to synthesize proteins and nucleic acids for their own replication and therefore do not contain molecules that are starkly different from

the host. PRRs often recognize the core of the virus, the nucleic acid genome. Viral genomes are highly variable and consist of single stranded or double stranded DNA or RNA that can be either linear, circular, or segmented (Tan et al., 2018). Since DNA or RNA are used as the blueprint of life by all species, immune detection of foreign nucleic acids represents a fundamental biological challenge and needs to be highly specific to avoid autoimmune responses caused by recognition of endogenous molecules.

Discrimination of self from non-self in nucleic acid sensing is determined by three central ligand criteria: availability, localization, and structure (Schlee and Hartmann, 2016). Factors that contribute to the availability of nucleic acid ligands involve local concentration, thermodynamic stability, protection form degradation by nucleases, and association with shielding proteins. Virus-derived nucleic acids can also be localized in different cellular compartments (e.g., cytosol, endolysosome, extracellular space, or nucleus) and may therefore be spatially separated from certain nucleic acid sensors. Structural properties of nucleic acid ligands (e.g., length, sequence, conformation, and chemical modifications) also determine their stimulatory potential.

Nucleic acid immune sensors can be classified as (1) PRRs capable of detecting microbial infections and activating transcription factors that induce the expression of cytokines, chemokines, and antiviral effector proteins, and (2) nucleic acid receptors with direct antiviral effector functions (Schlee and Hartmann, 2016). Receptors of the second category are important to restrict microbial growth and are not involved in antiviral gene expression. The following chapters will provide a more detailed overview of the progress that has been made in the field of nucleic acid immunity, with emphasis on the principal first category nucleic acid sensors and important signaling proteins.

1.1 Innate immune sensors of pathogenic nucleic acids

The innate immune system has developed sophisticated mechanisms to sense invading microbes in different cellular compartments. Recognition of pathogenic infections by nucleic acid sensors triggers the induction of type I interferons (IFNs) and pro-inflammatory cytokines. Type I IFNs can induce the expression of a plethora of IFN-stimulated genes (ISGs), ultimately leading to the formation of an antiviral state. TLR3, TLR7, TLR8, and TLR9, the four human nucleic acid sensing TLRs, constantly monitor the endosomal lumen for pathogenic DNA or RNA (Tan et al., 2018). By contrast, cytoplasmic microbial

nucleic acids are predominantly sensed by members of the retinoic acid inducible gene I (RIG-I)-like receptor (RLR) family and the cyclic GMP-AMP (cGAMP) synthase (cGAS)-stimulator of IFN genes (STING) pathway (Ablasser and Hur, 2020).

1.1.1 Cytosolic DNA sensing by cGAS

With the exception of RNA viruses, all pathogens use DNA as their genetic material (Tan et al., 2018). Since DNA is restricted to the nucleus and mitochondria of human cells, cytosolic DNA represents an alarm signal that indicates viral or bacterial infection. cGAS is the principal type I IFN-inducing receptor of cytosolic DNA (Fig. 1.1). In addition to its well-established role in immune defense against DNA viruses, increasing evidence suggests that cGAS is also associated with autoimmune diseases and antitumor immunity, as it can be activated by both self and non-self double stranded DNA (dsDNA).

cGAS is a member of the nucleotidyl transferase (NTase) enzyme family and is composed of an unstructured, basic N-terminus and a globular C-terminal catalytic domain (Hopfner and Hornung, 2020). Crystal structures show that cGAS binds to DNA in a sequence-independent manner through interactions between positively charged residues in the catalytic domain and the negatively charged DNA sugar-phosphate backbone (Zhang et al., 2020). Interestingly, unpaired guanosines of short Y-form DNA (12 base pairs (bp) to 20 bp), as found in human immunodeficiency virus 1 (HIV-1) complementary DNA (cDNA), potently activate cGAS in a sequence- and structure-dependent manner (Herzner et al., 2015). Binding of DNA by cGAS induces a global conformational change in the catalytic domain, forming an active site that provides space for adenosine triphosphate (ATP), guanosine triphosphate (GTP), and metal ions (Hopfner and Hornung, 2020). The active site catalyzes the formation of the cyclic dinucleotide (CDN) 2'3'-cGAMP and is stabilized by the formation of a 2:2 complex of dimeric cGAS and two dsDNA molecules (Ablasser et al., 2013; Li et al., 2013; Zhang et al., 2014). 2'3'-cGAMP functions as a second messenger that binds to and activates the endoplasmic reticulum (ER)-resident adapter protein STING (Ishikawa and Barber, 2008; Jin et al., 2008; Sun et al., 2009; Zhong et al., 2008a).

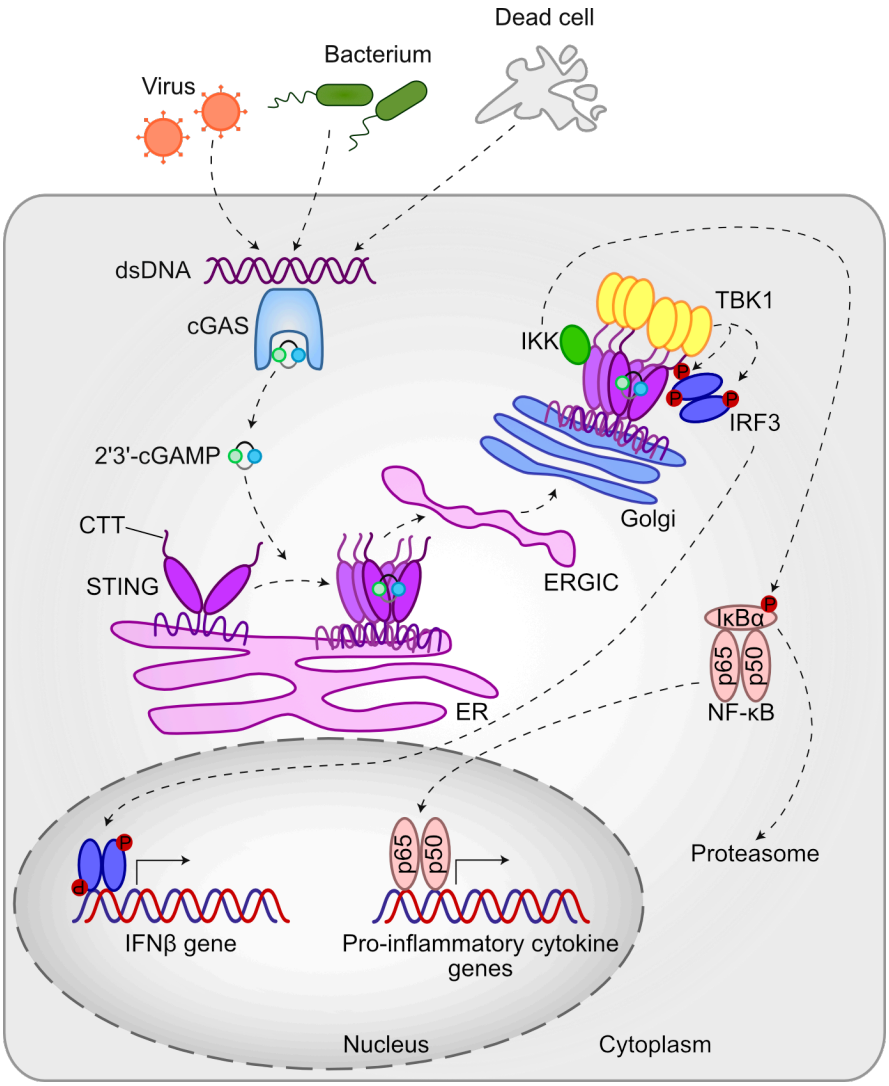

Fig. 1.1: The cGAS-STING pathway of cytosolic DNA sensing.
In the cytoplasm, dsDNA species of invading viruses, bacteria, or phagocytosed dead cells are sensed by cGAS. Upon activation, cGAS catalyzes the conversion of GTP and ATP into 2'3'-cGAMP, a second messenger that activates the ER-resident adaptor protein STING. Conformational changes in STING enable STING clustering and initiate its translocation from the ER via the ER-Golgi intermediate compartment (ERGIC) to the Golgi. Multimerized STING provides a suitable geometry for C-terminal tail (CTT)-mediated interactions with multiple TANK-binding kinase 1 (TBK1) molecules. After *trans*-autophosphorylation, TBK1 phosphorylates STING at the consensus *p*Lx*I*S motif (*p* = hydrophilic residue, *x* = any residue) at Ser366, thereby generating a docking site for IFN regulatory factor 3 (IRF3). Proximity to TBK1 triggers TBK1-dependent phosphorylation of IRF3 and, in turn, induces homodimerization and nuclear translocation of IRF3, ultimately leading to the expression of type I IFNs. The inhibitor of nuclear factor kappa-B kinase (IKK) complex mediates the phosphorylation-dependent proteasomal degradation of NF-kappa-B inhibitor alpha (IκBα), thereby releasing canonical nuclear factor kappa-light-chain-enhancer of activated B cells (NF-κB) (consisting of NF-κB subunit p65 and subunit p50) from an autoinhibited state to promote the expression of pro-inflammatory cytokines.

STING is composed of four N-terminal transmembrane (TM) domains, an internal ligand-binding domain (LBD), and a CTT, with both LBD and CTT facing the cytosol. In the resting state, STING is retained in the ER by the Ca^{2+} sensor stromal interaction molecule 1 (STIM1) and exists as a butterfly-shaped dimer with a V-shaped ligand binding pocket formed by interdomain interactions of the LBDs (Huang et al., 2012; Ouyang et al., 2012; Shang et al., 2012; Srikanth et al., 2019; Yin et al., 2012; Zhang et al., 2019). Binding of 2'3'-cGAMP to the binding pocket of STING induces a conformational change that seals the lid of the ligand binding pocket and induces a 180°-rotation of the LBD relative to the TM domain (Shang et al., 2019). These structural rearrangements generate a suitable surface for STING oligomerization and occur in concert with trafficking of the nascent STING oligomer from the ER to Golgi or post-Golgi compartment.

Oligomerized STING recruits several dimers of the serine/threonine kinase TBK1 via its CTT (Shang et al., 2019; Zhang et al., 2019; Zhao et al., 2019). This brings multiple TBK1 molecules in close proximity and promotes TBK1 activation by autophosphorylation *in trans* at Ser172, followed by TBK1-dependent phosphorylation of STING (Liu et al., 2015; Zhao et al., 2016). Current structural data suggest that each TBK1 molecule phosphorylates the adjacent, rather than the directly bound STING molecule, at multiple residues, including Ser366 in the *p*L*x*IS motif of the CTT (Liu et al., 2015; Shang et al., 2019; Zhang et al., 2019; Zhao et al., 2019). Phosphorylated *p*L*x*IS^{366} serves as a docking site for the transcription factor IRF3. The subsequent phosphorylation of IRF3 by TBK1 induces homodimerization and nuclear translocation of IRF3 (Liu et al., 2015; Shang et al., 2019; Zhao et al., 2019). STING also activates the catalytic subunits of the IKK complex, IKKα and IKKβ, which catalyze the phosphorylation of IκBα, thereby targeting IκBα to the proteasome and releasing active NF-κB. Together with other transcription factors, IRF3 and NF-κB induce the expression of type I IFNs and pro-inflammatory cytokines (e.g., interleukin (IL)-6, tumor necrosis factor (TNF), or IL-1β) (Ishikawa and Barber, 2008).

1.1.2 Cytosolic RNA sensing by RIG-I and MDA5

The presence of long double stranded RNA (dsRNA) in the cytosol is a danger signal for the innate immune system and indicates replication of RNA or DNA viruses (Schlee and Hartmann, 2016). RIG-I and melanoma differentiation associated gene 5 (MDA5; also

known as IFIH1), two ubiquitously expressed DExD/H box RNA helicases of the RLR family, are the major cytosolic sensors of viral RNA inducing a robust, TLR-independent type I IFN response via the shared adaptor protein mitochondrial antiviral signaling protein (MAVS; also known as CARDIF, IPS-1, and VISA) (Fig. 1.2) (Kang et al., 2002; Kawai et al., 2005; Meylan et al., 2005; Seth et al., 2005; Xu et al., 2005; Yoneyama et al., 2004). RIG-I and MDA5 share structural similarities and are composed of three domains: (1) the N-terminal tandem caspase recruitment domains (CARDs) mediate interactions with MAVS; (2) the intermediate RNA helicase domain binds and hydrolyzes ATP; and (3) a C-terminal domain (CTD).

While both RIG-I and MDA5 recognize dsRNA species, structural and biochemical studies have discovered different ligand preferences. RIG-I recognizes tri- or di-phosphorylated 5'-ends at short blunt dsRNA (Hornung et al., 2006; Pichlmair et al., 2006; Schlee et al., 2009). 5'-triphosphate groups are typically found in nascent RNA strands generated during viral replication. However, endogenous mRNAs also possess tri-phosphorylated 5'-ends. To prevent self-recognition by RIG-I, an additional N_1-2'O-methylation is introduced into the 5' cap of host cell mRNAs (Schuberth-Wagner et al., 2015). MDA5 preferentially binds to stem regions of long dsRNA (> 1000 bp), with RNA length and secondary structure primarily determining receptor activation (Peisley et al., 2011, 2012; Wu et al., 2013).

In uninfected cells, RIG-I is autoinhibited due to interactions between the tandem CARDs and the helicase domain. However, the flexible CTD continuously monitors the cytoplasm for pathogenic RNA. Upon recognition of 5'-tri- or di-phosphorylated dsRNA, the overall closed conformation of RIG-I is stretched, thereby exposing the tandem CARDs (Jiang et al., 2011; Kowalinski et al., 2011; Luo et al., 2011). The transition to an O-shaped, opened conformation is driven by ATP hydrolysis and additional interactions between the helicase domain and the microbial RNA. For MDA5, crystal structures imply that long dsRNA ligands are used as signaling platforms along which multiple MDA5 molecules assemble into adjacent C-shaped MDA5 subunits (Berke et al., 2012; Peisley et al., 2011; Wu et al., 2013). This cooperative arrangement might explain the observed binding specificity of MDA5 towards long dsRNA (Kato et al., 2008; Wu et al., 2013).

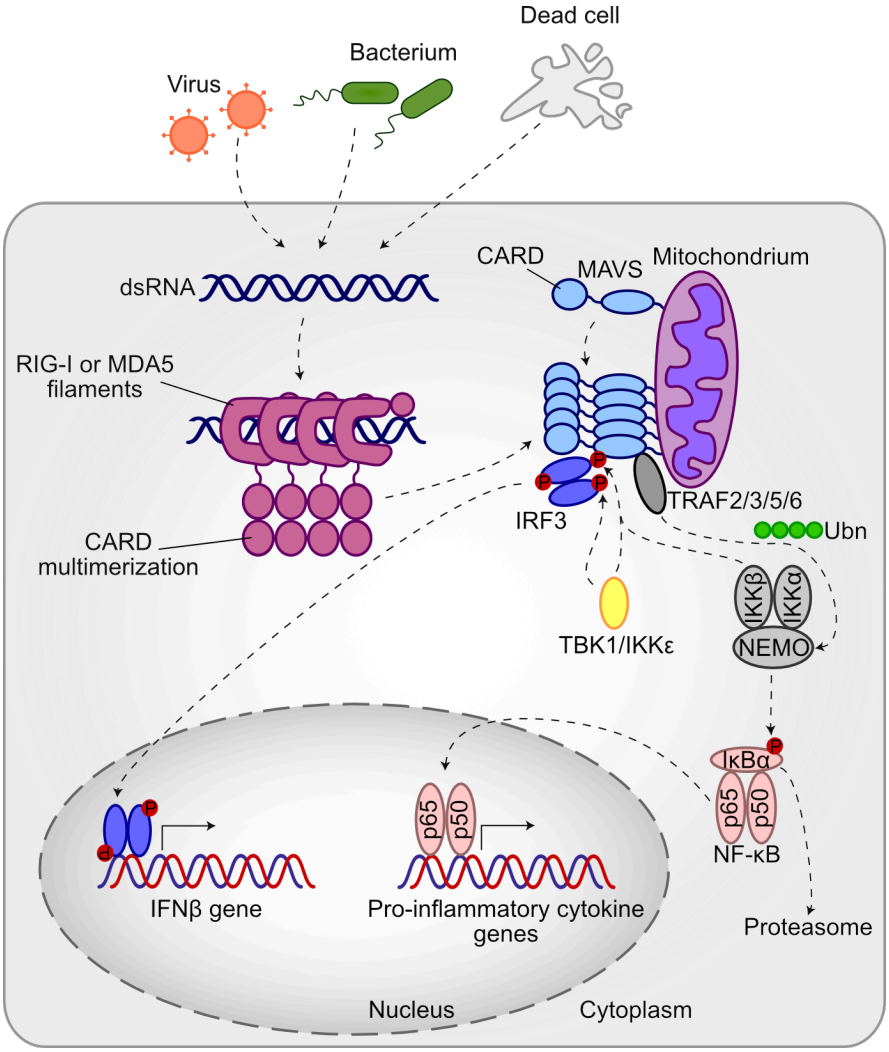

Fig. 1.2: Cytosolic sensing of RNA by RLRs.
In the cytoplasm, long dsRNA and RNA with tri-/diphosphorylated 5'-termini of viruses, bacteria, or phagocytosed dead cells are sensed by the RLR family members MDA5 and RIG-I, respectively. Upon ligand binding, the tandem CARDs of RIG-I and MDA5 are exposed and drive the formation of RIG-I tetramers or helical MDA5 filaments. Heterotypic interactions with the CARD of MAVS lead to the formation of a multimeric signaling complex at the mitochondrial membrane. TBK1, IKKε, and IKKβ phosphorylate MAVS at the consensus *p*L*x*IS motif at Ser442, thereby generating a docking site for IRF3. IRF3 is then redundantly phosphorylated by TBK1/IKKε, dimerizes, and shuttles into the nucleus to induce the expression of type I IFNs. Through a ubiquitin (Ubn)-dependent mechanism, TNF receptor-associated factor 2 (TRAF2), TRAF3, TRAF5, and TRAF6 recruit NF-kappa-B essential modulator (NEMO) to MAVS. The IKK complex mediates the phosphorylation-dependent proteasomal degradation of IκBα, thereby releasing NF-κB from an autoinhibited state. Active NF-κB induces the expression of pro-inflammatory cytokines.

Binding of RIG-I and MDA5 to their ligands is required but not fully sufficient for activation, a condition that is achieved only after oligomerization. Oligomerization critically relies on the presence of unanchored K63 polyubiquitin chains, which have high affinity for the CARDs of RIG-I and MDA5 and induce the formation of RIG-I tetramers or helical MDA5 filaments (Jiang et al., 2012; Zeng et al., 2010). The two E3 ubiquitin ligases RING finger protein leading to RIG-I activation (RIPLET) and tripartite motif-containing 25 (TRIM25) facilitate RIG-I oligomerization by catalyzing the formation of covalent K63 polyubiquitin chains in the CARDs of RIG-I (Gack et al., 2007; Oshiumi et al., 2009, 2010). Clustering of RIG-I and MDA5 enable intermolecular CARD interactions with MAVS and nucleate the multimerization of MAVS at the outer membrane of mitochondria (Wu et al., 2014; Xu et al., 2015). The self-assembly of MAVS resembles the formation of prion aggregates and coordinates the antiviral immune response (Cai et al., 2014; Hou et al., 2011).

MAVS is composed of a C-terminal TM domain, which anchors it to the outer mitochondrial membrane, and an N-terminal cytoplasm-facing CARD (Shi et al., 2015). In addition to RIG-I and MDA5, MAVS also interacts with the E3 ubiquitin ligases TRAF2, TRAF3, TRAF5, and TRAF6. These TRAFs activate NF-κB by recruiting NEMO, the regulatory subunit of the IKK complex, via a ubiquitin-dependent mechanism (Ea et al., 2006; Liu et al., 2013; Wu et al., 2006). TBK1 and IKKε, the two non-canonical IKKs, and IKKβ redundantly phosphorylate MAVS at the conserved *p*L*x*IS motif at Ser442 to generate a docking site for positively charged C-terminal amino acids of IRF3 (Fitzgerald et al., 2003; Liu et al., 2015). IRF3 is then phosphorylated by TBK1/IKKε at multiple residues, including Ser386 and Ser396, and enters the nucleus to induce the expression of type I IFNs (Liu et al., 2015; Panne et al., 2007).

1.1.3 Endosomal sensing of DNA and RNA

As most pathogens invade human cells via the endocytosis machinery, close monitoring of the endosomal compartment is crucial for the host (Tan et al., 2018). In humans, TLR3, TLR7, TLR8, and TLR9 represent the four endosomal nucleic acid sensing PRRs. In contrast to cGAS, RIG-I, and MDA5, these TLRs are mainly expressed in immune cells (except TLR3). TLR3, TLR7, TLR8, and TLR9 are structurally related and consist of three protein domains: the TM domain anchors the TLRs to the endosomal membrane; the

leucine-rich repeat (LRR)-bearing ectodomain serves as an endoluminal ligand binding site; and the cytosolic Toll IL-1 receptor (TIR) domain mediates signaling.

1.1.3.1 Activation of TLR3, TLR7, TLR8, and TLR9

TLR3 recognizes dsRNA > 35 bp through sequence-independent interactions between the N-terminal ectodomain and the RNA ribose-phosphate backbone (Alexopoulou et al., 2001; Leonard et al., 2008; Liu et al., 2008). The TLR3 ectodomain forms a horse-shoe-shaped solenoid structure and comprises 23 LRRs (Choe et al., 2005). Ligand binding is mediated by a glycan-free site in the highly glycosylated ectodomain and induces TLR3 dimerization as well as homotypic TIR domain interactions (Choe et al., 2005). In contrast to TLR7/8/9, TLR3 is primarily expressed in non-immune cells, including fibroblasts, endothelial cells, and neurons (Schlee and Hartmann, 2016).

TLR7 and TLR8 sense GU-rich single stranded RNA (ssRNA) fragments of bacterial and viral origin and can also be activated by polyU and small molecules such as the imidazoquinoline compound resiquimod (Judge et al., 2005; Jurk et al., 2002; Ostendorf et al., 2020; Tanji et al., 2015; Zhang et al., 2016b). The ectodomains of TLR7 and TLR8 are structurally related and adopt a donut-shaped fold (Zhang et al., 2016b). TLR7 is primarily expressed in plasmacytoid dendritic cells (pDCs) and B cells and forms an M-shaped dimer with two ligand binding sites upon activation. TLR8 is mainly expressed in monocytes, conventional DCs, and neutrophils and is dimeric in the resting state (Bartok and Hartmann, 2020; Zhang et al., 2016b). Ligand binding to TLR7 or TLR8 brings the cytosolic C-termini of the receptor chains in close proximity and enables oligomerization of the TIR domains (Tanji et al., 2015).

TLR9 is the sole endosomal DNA sensor and, in humans, is expressed only in B cells and pDCs (Barchet et al., 2008). The ectodomain of TLR9 has binding preferences towards unmethylated CpG motifs in single stranded DNA (ssDNA) and dsDNA sequences, which are most commonly found in bacterial and viral genomes but also occur randomly in vertebrates. Under steady state conditions, TLR9 exists as a donut-shaped monomer and dimerizes after ligand encounter (Ohto et al., 2015).

1.1.3.2 Signaling downstream of TLR3, TLR7, TLR8, and TLR9

Common to all TLRs described above is that ligand-induced conformational changes allow TIR domain-mediated recruitment of signaling proteins. While TLR7/8/9 recruit the adaptor protein myeloid differentiation primary response 88 (MyD88) to activate IRF5, IRF7, and NF-κB, TLR3 signals via the adaptor TIR-domain-containing adapter-inducing IFN-β (TRIF; also known as TICAM1) to activate IRF3 and NF-κB.

TRIF is composed of an N-terminal domain (NTD), an intermediate TIR domain, and a C-terminal receptor-interacting protein 1 (RIP-1) homotypic interaction motif (RHIM) domain. After TLR3 activation, TRIF oligomerizes at the cytosolic portion of TLR3, thereby releasing itself from an autoinhibited state (Oshiumi et al., 2003; Tatematsu et al., 2010; Yamamoto et al., 2003). Activated TRIF binds to the ubiquitin ligase TRAF3, which recruits TBK1 and IKKε to the TIR signaling complex (Häcker et al., 2006; Oganesyan et al., 2006). Similar to STING and MAVS, TRIF also contains a consensus *p*L*x*IS motif that is phosphorylated by TBK1 and required for the IRF3-dependent type I IFN response (Liu et al., 2015). Additionally, TRIF can interact with receptor-interacting serine/threonine-protein kinase 1 (RIPK1), eventually leading to the activation of NF-κB via transforming growth factor β-activated kinase 1 (TAK1) and the IKK complex (Häcker et al., 2006).

Activated TLR7/8/9 recruit MyD88 via interdomain TIR interactions (Hemmi et al., 2002; Schnare et al., 2000). In addition to the C-terminal TIR domain, MyD88 further consists of an intermediate domain and an N-terminal death domain (DD). The DD mediates MyD88 oligomerization and recruits the IL-1 receptor-associated kinase (IRAK) family members IRAK1, IRAK2, and IRAK4 (Lin et al., 2010; Motshwene et al., 2009). This large signaling complex, also known as the myddosome, provides a platform for IRAK4 *trans*-autophosphorylation and the phosphorylation-dependent activation of IRAK1/2 by IRAK4 (Li et al., 2002). In turn, IRAK1 phosphorylates IRF7, thereby inducing the expression of IFNα (Honda et al., 2005; Kawai et al., 2004; Uematsu et al., 2005). Similar to TLR3 signaling, the TLR7/9-dependent activation of NF-κB is mediated by TAK1 and the IKK complex. In addition, the TLR7/9-induced expression of type I IFNs and activation of NF-κB also requires the IKKβ-mediated phosphorylation of IRF5 at Ser462 (Lopez-Pelaez et al., 2014; Ren et al., 2014; Takaoka et al., 2005). Recently, the endolysosomal transporter solute carrier family 15 member 4 (SLC15A4) and TLR adaptor interacting with SLC15A4 (TASL)

have been described as novel components of the TLR7/8/9 signaling pathways (Heinz et al., 2020). In analogy to the well-studied adaptor proteins STING, MAVS, and TRIF, TASL also contains a functional *p*L*x*IS motif that mediates recruitment and activation of IRF5.

1.2 Type I IFN signaling

Recognition of nucleic acids by cytosolic and endosomal PRRs triggers the secretion of type I IFNs - a hallmark of antiviral defense. In humans, type I IFNs represent the largest class of IFNs and comprise IFNα, IFNβ, IFNε, IFNκ, and IFNω. They can signal in an autocrine and paracrine fashion and activate the Janus kinase (JAK)-signal transducer and activator of transcription (STAT) pathway by binding to the heterodimeric IFNα receptor (IFNAR) complex, thereby eliciting an antiviral state that is characterized by the expression and effector functions of ISGs (Schneider et al., 2014).

In the non-stimulated condition, JAK1 and tyrosine kinase 2 (TYK2), two tyrosine kinases, are pre-associated with the cytosolic chains of IFNAR2 and IFNAR1, respectively (Gauzzi et al., 1997; Kawamura et al., 1994). Binding of type I IFNs cross-links adjacent IFNAR chains and brings JAK1 and TYK2 in close proximity, which facilitates their *trans*-autophosphorylation. Upon activation, JAK1 and TYK2 phosphorylate the IFNAR complex at highly conserved tyrosine residues, which are subsequently bound by STAT1 and STAT2 (Greenlund et al., 1995; Heim et al., 1995). After phosphorylation by JAK1/TYK2, STAT1 and STAT2 dissociate from the IFNAR complex and recruit IRF9 to form a protein complex known as IFN-stimulated gene factor 3 (ISGF3) (Schindler et al., 1992). In the nucleus, ISGF3 binds to IFN-stimulated response elements (ISRE) and induces the expression of ISGs. A recent study showed that approximately 10 % of the human genes can be induced by type I IFNs (Shaw et al., 2017). Therefore, it is not surprising that ISGs have a variety of different activities, from inhibiting virus entry, intracellular trafficking, and translation to replication and assembly of viral particles. Type I IFNs can also upregulate the expression of important first category nucleic acid receptors (e.g., RIG-I, MDA5, or cGAS), thereby lowering the PRR activation threshold.

1.3 Biological and medical relevance of nucleic acid immunity

1.3.1 Microbial evasion of nucleic acid sensing

During the evolutionary arms race between host and pathogen, most successful microbes have developed strategies to evade or subvert host defense mechanisms. For example, some viruses introduce host cell-specific modifications into their RNA genome to render it invisible to the immune system. Other viruses inhibit nucleic acid sensors, adaptors, or signaling proteins. In this context, an isoform of the latency-associated nuclear antigen (LANA) of Kaposi sarcoma herpesvirus (KSHV) has been described to block the type I IFN response by interacting with cGAS (Zhang et al., 2016a). Furthermore, Dengue virus NS2B protein was reported to inhibit DNA sensing by cleaving cGAS (Aguirre et al., 2017). Although Dengue virus contains a ssRNA genome, infections can cause damage to host cell mitochondria, leading to leakage of mitochondrial DNA into the cytosol and activation of cGAS. In addition, the 3C protease of coxsackievirus B was shown to degrade TRIF and MAVS, further highlighting the central role of adaptor proteins in type I IFN expression (Mukherjee et al., 2011a). Another example is the infected cell protein 27 (ICP27) protein of Herpes simplex virus (HSV-1), which suppresses the TBK1-dependent phosphorylation of IRF3 by interfering with STING and TBK1 (Christensen et al., 2016).

1.3.2 Role of nucleic acid sensors in inflammatory and autoimmune diseases

Ongoing research investigates how dysregulation of nucleic acid immunity contributes to the development of autoimmune and inflammatory diseases. Aicardi-Goutières syndrome (AGS), a rare neurodegenerative disorder characterized by systemic inflammation and elevated type I IFN levels, can be caused by mutations in the genes encoding three prime repair exonuclease 1 (TREX1), RNase H2, SAM and HD domain containing deoxynucleoside triphosphate triphosphohydrolase 1 (SAMHD1), adenosine deaminase 1 (ADAR1), or MDA5 (Crow and Manel, 2015; Crow et al., 2006). TREX1 is a 3'-5' exonuclease that degrades cytosolic ssDNA and dsDNA species resulting from DNA damage or active retroelements (Stetson et al., 2008; Yang et al., 2007). Deficiency of TREX1 causes accumulation of cytoplasmic DNA and triggers a cGAS-STING-dependent autoimmune response. In mice, this fatal autoinflammatory phenotype can be prevented by deleting the cGAS- or STING-encoding genes (Ahn et al., 2012; Gall et al., 2012; Gao et al., 2015). Singleton-Merten syndrome (SMS) and STING-associated vasculopathy with onset in in-

fancy (SAVI) are other autoimmune diseases that can be caused by gain-of-function mutations in the RIG-I- and STING-encoding genes, respectively (Jang et al., 2015; Liu et al., 2014; Warner et al., 2017). Systemic lupus erythematosus (SLE) was the first autoinflammatory disease linked to increased type I IFN levels in the blood and is associated with dysregulated functions of TLR7, DNase I, TREX1, and MDA5 (An et al., 2017; Deane et al., 2007; Hooks et al., 1979; Namjou et al., 2011; Napirei et al., 2000; Pisitkun et al., 2006; Robinson et al., 2011).

1.3.3 Senescence and cancer

Recent findings have revealed a connection between cellular senescence, tumor immunity, and cGAS-STING signaling. Cellular senescence, primarily caused by DNA damage, is a state of permanent cell cycle arrest and represents a safety mechanism of the cell to prevent tumor development (Ablasser and Chen, 2019). DNA damage leads to the formation of cytosolic chromatin fragments and micronuclei that can activate cGAS in a cell-autonomous manner (Dou et al., 2017; Glück et al., 2017; Harding et al., 2017; Mackenzie et al., 2017). Activated cGAS, in turn, promotes senescence by inducing the secretion of inflammatory cytokines, proteases, and growth factors, a feature known as the senescence-associated secretory phenotype (SASP) (Coppé et al., 2008).

cGAS can also suppress tumor formation via a cell non-autonomous pathway. In this regard, sensing of cytosolic tumor-derived DNA of phagocytosed dying cancer cells by cGAS in antigen-presenting cells (APCs) (e.g., dendritic cells, macrophages) was shown to trigger T cell priming, expansion, and recruitment of tumor-specific T cells to the tumor microenvironment (Woo et al., 2014).

1.4 Heterogeneous nuclear ribonucleoprotein M

Prior to this thesis, Dr. A.-M. Herzner has performed a quantitative affinity purification-mass spectrometry (AP-MS) approach to identify proteins bound to G_3-YSD, a short dsDNA oligonucleotide with G_3-overhangs and potent cGAS activator (Herzner, 2013; Herzner et al., 2015). Heterogeneous nuclear ribonucleoprotein M (hnRNPM) was one of the proteins that were highly enriched after G_3-YSD precipitation. Initial experiments showed that RNA interference (RNAi) against hnRNPM inhibits the cGAS-dependent secretion of type I IFNs in THP-1 monocytes.

hnRNPM is a ubiquitously expressed multiple domain protein and consists of an N-terminal nuclear localization sequence (NLS), three RNA recognition motifs (RRMs), a glycine/methionine-rich region (GMG), and a methionine/arginine repeat motif (MR). The three hnRNPM variants (i.e., hnRNPM4, hnRNPM1/2, and hnRNPM3) are generated by alternative splicing and are shown in Fig. 1.3.

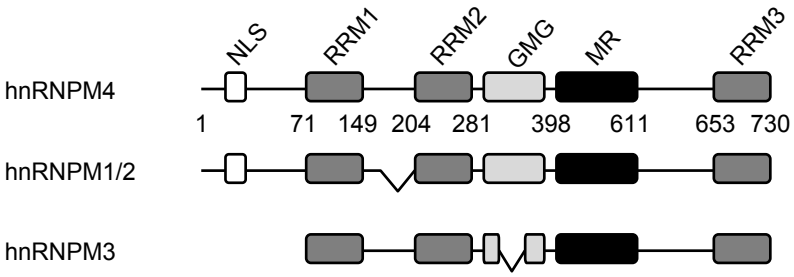

Fig. 1.3: Domain structure and isoforms of hnRNPM.
hnRNPM4, chosen as the canonical sequence of hnRNPM, comprises an NLS, three RRMs (RRM1, RRM2, RRM3), a GMG region, and an MR repeat motif. The isoforms of hnRNPM4, hnRNPM1/2 and hnRNPM3, are generated by alternative splicing.

hnRNPM preferentially binds to G/U-rich sequences in intron RNA and is primarily known for its role in pre-mRNA splicing (Datar et al., 1993; Gattoni et al., 1996; Huelga et al., 2012; Passacantilli et al., 2017). Huelga *et al.* reported that hnRNPM accumulates at distal intronic regions that are separated by > 2 kb from adjacent exon-intron junctions and resemble binding sites of TAR DNA-binding protein 43 (TDP-43) in mouse brain RNA (Polymenidou et al., 2011). hnRNPM is predominantly localized in the nucleus, where it regulates splicing together with cell division cycle 5-like (CDC5L) and pleiotropic regulator 1 (PLRG1) (Llères et al., 2010). In addition, hnRNPM was shown to interact with the splicing factors polypyrimidine tract-binding protein-associated splicing factor (PSF) and non-POU-domain-containing octamer binding protein ($p54^{nrb}$) in subpopulations of nuclear paraspeckles (Marko et al., 2010). Besides its role in splicing, increasing evidence suggests that hnRNPM is also involved in cancer biology and muscle differentiation (Chen et al., 2017; Passacantilli et al., 2017; Xu et al., 2014).

Although several groups have described hnRNPM in the context of immune responses and viral infections, it is largely unknown how hnRNPM regulates these processes. In 2012, hnRNPM has been described to inhibit the listerolysin O-induced type I IFN response in HEK293T cells and to restrict the growth of *Listeria monocytogenes* (*L. mono-*

cytogenes) in HEK293T and THP-1 cells (Luo et al., 2012). In the context of viral infections, hnRNPM was shown to block replication of Semliki Forest virus, Sindbis virus, and Chikungunya virus and to shuttle from the nucleus to the cytoplasm upon infection with these viruses (Varjak et al., 2013). Furthermore, poliovirus and coxsackievirus B3 have been described to cleave hnRNPM in a 3C protease-dependent manner and to exploit the hnRNPM degradation product for their own replication (Jagdeo et al., 2015). Recently, hnRNPM was reported to suppress the expression of a set of immune-related genes, including *IL6* and *MX1*, after infection with *Salmonella* Typhimurium in the mouse macrophage cell line RAW 264.7 (West et al., 2019). In addition, hnRNPM has been described to negatively regulate RLR-MAVS signaling by competing with RIG-I and MDA5 for binding to viral RNAs (Cao et al., 2019).

1.5 Aims of this study

The aim of this thesis was to unravel the function of hnRNPM in cGAS-STING signaling. Considering that hnRNPM is a multifunctional protein, it was intended to study the role of hnRNPM at different stages of the cGAS-STING signaling cascade, from ligand-receptor contact to kinases, RNA stability, and translation. On the one hand, global screening approaches such as mRNA expression profiling and MS-based interactome analysis were used to investigate the role of hnRNPM in innate immunity. On the other hand, biochemical and genetic techniques such as interaction assays, RNAi, CRISPR/Cas9-mediated gene knockout, and kinase assays were used to specifically elucidate the influence of hnRNPM on signaling proteins downstream of cGAS.

2 Material and Methods

2.1 Material

2.1.1 Instruments and reagents

Tab. 2.1: Instruments and equipment.

Description	Manufacturer
12-channel pipette	VWR
12-channel pipette research plus	Eppendorf AG
Agarose electrophoresis system Biometra compact M	Analytik Jena AG
ARE hot plate stirrer	VELP Scientifica
Autoclave dx-200	Systec
Autoclave vx-150	Systec
Axio Vert.A1 fluorescence microscope	Zeiss
Centrifuge 5418	Eppendorf AG
Centrifuge 5425	Eppendorf AG
Centrifuge 5430	Eppendorf AG
Centrifuge 5430 R	Eppendorf AG
Centrifuge 5810	Eppendorf AG
Centrifuge 5810 R	Eppendorf AG
Centrifuge MiniSpin	Eppendorf AG
CO_2 incubator ICO240med	Memmert
DynaMag-2	Thermo Fisher Scientific
EnVision 2104 multilabel reader	PerkinElmer
Epoch microplate spectrophotometer	BioTek
Epson perfection V370 photo	Epson
FiveEasy plus pH/mV bench meter	Mettler Toledo
Freezer (-20 °C)	Liebherr
Gel documentation system	PEQLAB
Inverted microscope Eclipse TS100	Nikon
Micro balance Cubis	Sartorius
Mini-PROTEAN tetra vertical electrophoresis cell	Bio-Rad
Mr. Frosty freezing container	Thermo Fisher Scientific
NanoDrop One	Thermo Fisher Scientific
New Brunswick Innova 42	Eppendorf AG
Odyssey Fc imaging system	LI-COR Biosciences
Orbital shaker DOS-10L	neoLab
PCR cycler XT96	VWR
Pipette controller Pipet-X	Mettler Toledo
Eppendorf research plus pipettes	Eppendorf AG
PowerPac HC high-current power supply	Bio-Rad

Tab. 2.1 (continued).

Description	Manufacturer
Precision balance MS6002TS/00	Mettler Toledo
QuantStudio 5 real-time PCR system	Thermo Fisher Scientific
Safety cabinet ScanLaf Mars	LaboGene
Single-channel pipette Pipet-Lite XLS	Mettler Toledo
Single-channel pipette Research Plus	Eppendorf AG
Sprout microcentrifuge	Biozym
TC20 automated cell counter	Bio-Rad
TE22 mighty small wet transfer tank	Hoefer Inc.
ThermoMixer C	Eppendorf AG
Tube roller	VWR
Tube rotator	VWR
Ultra-low temperature freezer MDF-C2156VANW-PE	PHCbi
Ultra-low temperature freezer MDF-DU502VH-PE VIP ECO	PHCbi
UV transilluminator UVT-22 BE-LED	Herolab
Vacuum pump 420312	ILMVAC GmbH
VialTweeter sonication device	Hielscher Ultraschalltechnik
Vortex-Genie 2	Scientific Industries
Water bath	Memmert

Tab. 2.2: Consumables.

Description	Manufacturer
Amersham Protran 0.45 µm nitrocellulose membrane	GE Healthcare
Blotting paper Whatman	GE Healthcare
Cell counting slides	Bio-Rad
Cell culture flasks (T25, T75, T175)	Sarstedt
CellCarrier-96 Ultra microplates	PerkinElmer
Centrifuge tubes (15 ml, 50 ml)	Greiner Bio-One
Corning Costar Stripette serological pipettes	Corning, Inc.
Cryogenic storage vials	Greiner Bio-One
ELISA microplate 96-well	Thermo Fisher Scientific
Kimtech precision wipes	Kimberly-Clark
LUMITRAC 96-well microplates	Greiner Bio-One
Micro reaction tubes (0.5 ml, 1.5 ml, 2.0 ml)	Sarstedt
MicroAmp optical 384-well reaction plate	Thermo Fisher Scientific
Micropipette filter tips	Aygen

Tab. 2.2 (continued).

Description	Manufacturer
Micropipette tips	Greiner Bio-One
Micropipette tips	Mettler Toledo
Microplate 96-well	Greiner Bio-One
Nitril BestGen gloves	Meditrade
Parafilm M	Brand
PCR single cap SoftStripes 0.2 ml	Biozym Scientific
Petri dish (10 cm)	Sarstedt
Reagent reservoirs	Axygen
Syringe filters (0.2 µm, 0.45 µm)	Whatman
Syringes Discardit II (10 ml, 20 ml, 50 ml)	BD Biosciences
Tissue culture test plates (96-well, 24-well, 6-well)	TPP
Tissues culture dishes (10 cm)	Sarstedt
Zymo Spin IIICG columns	Zymo Research

Tab. 2.3: Chemicals and reagents.

Description	Manufacturer
1,4-Dithiothreitol (DTT)	Carl Roth
10× DreamTaq green buffer	Thermo Fisher Scientific
10× DNase I buffer	Thermo Fisher Scientific
10× FastDigest green buffer	Thermo Fisher Scientific
10× NEBuffer 2	New England Biolabs
10× T4 DNA ligase buffer	Thermo Fisher Scientific
2-Propanol (> 99.5 % pure)	Carl Roth
2'3'-cGAMP	InvivoGen
Thiazolyl blue tetrazolium bromide (MTT)	Sigma-Aldrich
5'ppp-dsRNA	B. Putschli
5× Phusion HF buffer	Thermo Fisher Scientific
Acetic acid	Carl Roth
Adenosine-5’-triphosphate (ATP) disodium salt	Carl Roth
Agar-agar (bacteriological)	Carl Roth
Agarose UltraPure	Invitrogen
Albumin fraction V (BSA)	Carl Roth
Ammonium peroxydisulfate (APS)	Carl Roth
Ampuwa water (H_2O)	Fresenius Kabi
Bacillol AF	Hartmann
Calcium chloride ($CaCl_2$)	Carl Roth
Carbenicillin disodium salt	Carl Roth

Tab. 2.3 (continued).

Description	Manufacturer
CellMask orange plasma membrane stain	Molecular Probes
Coelenterazine native	Synchem UG & Co. KG
cOmplete Mini EDTA-free protease inhibitor	Roche
Descogen liquid	Antiseptica
Di-sodium hydrogen phosphate heptahydrate	Carl Roth
Dimethyl sulfoxide (DMSO)	Carl Roth
dNTP mix (10 mM each)	Thermo Fisher Scientific
Disodium phosphate (Na_2HPO_4)	Carl Roth
Ethanol (> 96 % denatured)	Carl Roth
Ethanol (> 99.5 % pure)	Carl Roth
Ethanol (70 % denatured)	Otto Fischar GmbH & Co. KG
Ethylenediaminetetraacetic acid (EDTA)	Carl Roth
Gelatine	Carl Roth
GeneRuler 1 kb Plus DNA ladder	Thermo Fisher Scientific
GFP-Trap magnetic agarose beads	Chromotek
Gibson assembly master mix	New England Biolabs
Glycerol (> 99.5 % pure)	Carl Roth
Glycine	Carl Roth
HEPES	Carl Roth
Hexadimethrine bromide (polybrene)	Sigma-Aldrich
Hoechst 33342	Invitrogen
Human IFN-α2a (IFNα)	Miltenyi Biotec
Human IP10 ELISA set	BD Biosciences
Hydrochloric acid (HCl)	Carl Roth
IGEPAL CA-630	Sigma-Aldrich
LB agar powder (Luria/Miller)	Carl Roth
LB medium powder (Luria/Miller)	Carl Roth
Lipofectamine 2000 transfection reagent	Thermo Fisher Scientific
Magnesium chloride hexahydrate ($MgCl_2 \cdot 6\ H_2O$)	Carl Roth
my-Budget 5× EvaGreen qPCR-Mix II	ROX
Odyssey blocking buffer	LI-COR Biosciences
Okadaic acid	Santa Cruz Biotechnology
Orange G	Carl Roth
p-Nitrophenyl phosphate disodium salt (pNPP)	Sigma-Aldrich
PageRuler plus prestained protein ladder	Thermo Fisher Scientific
Pam3CSK4	InvivoGen
Paraformaldehyde	Carl Roth
pBluescript (pDNA)	Dr. A.-M. Herzner

Tab. 2.3 (continued).

Description	Manufacturer
Phorbol 12-myristate 13-acetate (PMA)	Sigma-Aldrich
PhosSTOP phosphatase inhibitor cocktail	Roche
Pierce NeutrAvidin agarose	Thermo Fisher Scientific
Ponceau S	Carl Roth
Potassium chloride (KCl)	Carl Roth
Potassium dihydrogen phosphate (KH_2PO_4)	Carl Roth
Puromycin	InvivoGen
Random hexamer primer	IDT
RiboLock RNase inhibitor	Thermo Fisher Scientific
RLT buffer	Qiagen
RNA wash buffer	Zymo Research
RNase Zap	Thermo Fisher Scientific
Rotiphorese gel 30 (37.5:1)	Carl Roth
RW1 buffer	Qiagen
Sodium azide (NaN_3)	Carl Roth
Sodium carbonate (Na_2CO_3)	Carl Roth
Sodium chloride (NaCl)	Carl Roth
Sodium deoxycholate	Carl Roth
Sodium dodecyl sulfate (SDS)	Carl Roth
Sodium hydrogen carbonate ($NaHCO_3$)	Carl Roth
Sodium hydroxide (NaOH)	Carl Roth
Sodium orthovanadate (Na_3VO_4)	Sigma-Aldrich
Sulfuric acid (H_2SO_4)	Carl Roth
SYBR safe DNA gel stain	Thermo Fisher Scientific
TEMED	Carl Roth
TL8-506	InvivoGen
Tris	Carl Roth
Triton X-100	Carl Roth
Tween 20	Carl Roth
β-Glycerol phosphate disodium salt pentahydrate	Sigma-Aldrich

Tab. 2.4: Ready-made reaction kits.

Description	Manufacturer
Duolink in situ red kit	Sigma-Aldrich
innuPREP gel extraction kit	Analytik Jena AG
innuPREP PCRpure kit	Analytik Jena AG
NE-PER nuclear and cytoplasmic extraction kit	Thermo Fisher Scientific
Neon transfection system 10 µl kit	Invitrogen
NucleoSpin plasmid miniprep kit	Macherey-Nagel
Pierce BCA protein assay kit	Thermo Fisher Scientific
PureLink HiPure plasmid filter midiprep kit	Thermo Fisher Scientific
RevertAid first strand cDNA synthesis kit	Thermo Fisher Scientific

Tab. 2.5: Enzymes and proteins.

Description	Manufacturer
DNase I	Thermo Fisher Scientific
DreamTaq DNA polymerase	Thermo Fisher Scientific
FastDigest restriction endonucleases	Thermo Fisher Scientific
Phusion High-Fidelity DNA polymerase	Thermo Fisher Scientific
RNase A	Thermo Fisher Scientific
T4 DNA ligase	Thermo Fisher Scientific
TBK1 (active, GST-tagged, human recombinant kinase)	Sigma-Aldrich

Tab. 2.6: Cell culture media and additives.

Description	Manufacturer
DMEM	Gibco
DPBS (PBS)	Gibco
Fetal calf serum (FCS)	Gibco
Gentamicin sulfate	Sigma-Aldrich
Opti-MEM	Gibco
Penicillin-streptomycin	Gibco
Puromycin	InvivoGen
RPMI 1640	Gibco
Trypsin-EDTA (0.25 %)	Gibco

2.1.2 Buffers and solutions

Tab. 2.7: Buffers and solutions.

Description	Composition
2× HBS	280 mM NaCl, 50 mM HEPES/NaOH, 1.42 mM Na_2HPO_4, pH 7.05
Blocking buffer	5 % (w/v) BSA, 0.01 % (w/v) NaN_3 in PBS-T
Blotting buffer	192 mM glycine, 25 mM Tris, 20 % (v/v) ethanol (denatured)
Brain-heart infusion (BHI) agar	BHI medium supplemented with 15 g/l Agar-Agar
Brain-heart infusion (BHI) medium	37 g BHI powder dissolved in 1 l H_2O
ELISA assay buffer	10 % (v/v) FCS, 1× penicillin-streptomycin in PBS
ELISA coating buffer	100 mM $NaHCO_3$, 33.6 mM Na_2CO_3 in PBS, pH 9.5
FACS buffer	2 % (v/v) FCS, 2 mM EDTA in PBS, pH 7.4
Fixation buffer	4 % (w/v) paraformaldehyde in PBS, pH 6.9
Kinase assay buffer	50 mM HEPES/NaOH, 10 mM $MgCl_2$, 5 mM β-glycerol phosphate, 2 mM DTT, 0.1 mM Na_3VO_4, pH 7.5
Laemmli buffer	60 mM Tris/HCl, 10 % (v/v) glycerol, 2 % (w/v) SDS, 10 mM DTT, Orange G, pH 6.8
LB agar	40 g LB agar powder (Luria/Miller) dissolved in 1 l H_2O
LB medium	25 g LB medium powder (Luria/Miller) dissolved in 1 l H_2O
MTT substrate solution	5 mg/ml MTT in PBS
PBS	150 mM NaCl, 10 mM Na_2HPO_4, 2.5 mM KCl, 1.8 mM KH_2PO_4, pH 7.4
PBS-T	0.05 % (v/v) Tween-20 in PBS
pNPP substrate buffer	100 mM NaCl, 100 mM Tris/HCl, 5 mM $MgCl_2$, 10 mg/ml pNPP, pH 9.5
Polybrene solution	5 mg/ml polybrene in PBS
Ponceau staining solution	3 % (v/v) acetic acid, 0.1 % (w/v) Ponceau
RIPA lysis buffer	150 mM NaCl, 50 mM Tris/HCl, 1.0 % (v/v) Triton X-100, 0.5 % (w/v) sodium deoxycholate, 0.1 % (w/v) SDS, pH 8.0
SDS-PAGE running buffer	192 mM glycine, 25 mM Tris, 0.1 % (w/v) SDS
SDS-PAGE resolving gel (10 %)	375 mM Tris/HCl, 10 % (v/v) rotiphorese gel 30 (37.5:1), 0.1 % (w/v) SDS, 0.1 % (w/v) APS, 0.08 % (v/v) TEMED, pH 8.8

Tab. 2.7 (continued).

Description	Composition
SDS-PAGE stacking gel (3 %)	125 mM Tris/HCl, 3 % (v/v) rotiphorese gel 30 (37.5:1), 0.1 % (w/v) SDS, 0.1 % (w/v) APS, 0.08 % (v/v) TEMED, pH 6.8
TAE	40 mM Tris/acetic acid, 1 mM EDTA, pH 7.8
TAP lysis buffer	0.5 % (v/v) IGEPAL CA-630 in TAP wash buffer
TAP wash buffer	100 mM NaCl, 50 mM Tris/HCl, 1.5 mM $MgCl_2$, 5 % (v/v) glycerol, pH 7.5
TBS	150 mM NaCl, 10 mM Tris/HCl, pH 7.6
TBS-T	0.1 % (v/v) Tween-20 in TBS

2.1.3 Antibodies

Tab. 2.8: Primary antibodies.

Description	Origin	Clone	Supplier
α-β-actin	mouse	926-42212	LI-COR Biosciences
α-β-actin	rabbit	926-42210	LI-COR Biosciences
α-β-tubulin	rabbit	9F3	Cell Signaling Technology
α-cGAS	rabbit	D1D3G	Cell Signaling Technology
α-ELAVL1	rabbit	D9W7E	Cell Signaling Technology
α-FLAG	mouse	M2	Sigma-Aldrich
α-GFP	mouse	4B10	Cell Signaling Technology
α-hnRNPM	mouse	1D8	Santa Cruz
α-hnRNPM M1-M4	rabbit	ab177957	Abcam
α-IκBα	mouse	L35A5	Cell Signaling Technology
α-IGF2BP2	rabbit	ab124930	Abcam
α-IKKα	mouse	3G12	Cell Signaling Technology
α-IKKβ	rabbit	D30C6	Cell Signaling Technology
α-IKKε	rabbit	2690	Cell Signaling Technology
α-IRF3	rabbit	D6I4C	Cell Signaling Technology
α-Lamin A	rabbit	ab26300	Abcam
α-MAVS	rabbit	3993	Cell Signaling Technology
α-NF-κB p65	rabbit	D14E12	Cell Signaling Technology
α-Phospho-IRF3 (Ser396)	rabbit	4D4G	Cell Signaling Technology
α-Phospho-NF-κB p65 (Ser536)	rabbit	93H1	Cell Signaling Technology
α-Phospho-STAT1 (Tyr701)	rabbit	D4A7	Cell Signaling Technology
α-Phospho-STING (Ser366)	rabbit	E9A9K	Cell Signaling Technology
α-Phospho-TBK1 (Ser172)	rabbit	D52C2	Cell Signaling Technology
α-RIG-I	rabbit	D14G6	Cell Signaling Technology

Tab. 2.8 (continued).

Description	Origin	Clone	Supplier
α-SON	rabbit	HPA023535	Sigma-Aldrich
α-STING	rabbit	D2P2F	Cell Signaling Technology
α-TBK1	rabbit	D1B4	Cell Signaling Technology

Tab. 2.9: Secondary antibodies.

Description	Origin	Supplier
anti-mouse IgG IRDye 680RD	Goat	LI-COR Biosciences
anti-mouse IgG IRDye 800CW	Goat	LI-COR Biosciences
anti-rabbit IgG IRDye 680RD	Goat	LI-COR Biosciences
anti-rabbit IgG IRDye 800CW	Goat	LI-COR Biosciences
Anti-rabbit IgG, F(ab')$_2$ fragment (Alexa Fluor (AF) 488 conjugate)	Goat	Cell Signaling Technology

2.1.4 Oligonucleotides and plasmids

Tab. 2.10: YSD oligonucleotides.

Name	Sequence (5'-3')
G_3-YSD (np) fwd	GGGAAACTCCAGCAGGACCATTAGGG
G_3-YSD (np) fwd-AF647	GGGAAACTCCAGCAGGACCATTAGGG-AF647
G_3-YSD (np) fwd-biotin	GGGAAACTCCAGCAGGACCATTAGGG-biotin
G_3-YSD (np) rev	GGGTAATGGTCCTGCTGGAGTTTGGG
C_3-YSD (np) fwd-biotin	CCCAAACTCCAGCAGGACCATTACCC-biotin
C_3-YSD (np) rev	CCCTAATGGTCCTGCTGGAGTTTCCC

Tab. 2.11: qPCR primers.

Gene	Forward primer (5'-3')	Reverse primer (5'-3')
ARHGEF2	CAGGCATGACCATGTGCTATG	TTTACAGCGGTTGTGGATAGTC
CTSG	CCACCCTCAATATAATCAGCGG	GTTTCGATTCCGTCTGACTCTTC
CXCL10	GAATGCTCTTTACTTCATGGACTTC	GGTAGCCACTGAAAGAATTTGG
DDX21	CTTTGCCATCCCTTTGATTGAGA	GTAGGTGCAAGAACCAGTACC
DDX60	CCTCAGGGAGATCATCAAGG	TGGCACATCTCTTTGGAAGAA
DHX9	GGCCTCTGGCTTTTGCTACT	GGCAGTAACTCTCTCTCCTGC
DHX15	TCAAGCCAGAATGGTTGGTGA	GTTTGGCAATGATGCGGTCC
EBNA1BP2	CTCTCGGATTCGGAGTCGGA	GCCCCTCTAGCACGACATTG
EFTUD2	CAATATCATGGACACTCCAGGAC	CGGTCAATCTTGTTGATGCACA
EIF3E	ACAGTGGTTGCACAACTGAAA	CATCCCTGGTTGACTGCATTT
ELAVL1	AACTACGTGACCGCGAAGG	CGCCCAAACCGAGAGAACA

Tab. 2.11 (continued).

Gene	Forward primer (5'-3')	Reverse primer (5'-3')
GAPDH	AAGGTGAAGGTCGGAGTCAA	AATGAAGGGGTCATTGATGG
HNRNPA1	TCAGAGTCTCCTAAAGAGCCC	ACCTTGTGTGGCCTTGCAT
HNRNPAB	ACCGAGAACGGACATGAGG	GCCACCAACGAACATTTTTCC
HNRNPD	GCGTGGGTTCTGCTTTATTACC	TTGCTGATATTGTTCCTTCGACA
HNRNPH2	GGGGAAGCCTTTGTGCAGTT	CTTCAGCTCGGCTACTCTTGA
HNRNPM	GACGGAGATCAAAATGGAGG	TTCTCATTCTGAGCAGGTCG
HNRNPU	GAGCATCCTATGGTGTGTCAAA	TGACCAGCCAATACGAACTTC
HP1BP3	ATGGCGACTGATACGTCTCAA	CTTCTCACCTAACTTGTCCGC
HSV-1	TGGGACACATGCCTTCTTGG	ACCCTTAGTCAGACTCTGTTACTTACCC
IFIT1	TCCACAAGACAGAATAGCCAGAT	GCTCCAGACTATCCTTGACCTG
IFNB1	CATTACCTGAAGGCCAAGGA	CAGCATCTGCTGGTTGAAGA
IGF2BP2	AGCTAAGCGGGCATCAGTTTG	CCGCAGCGGGAAATCAATCT
ILF2	CTCAGACTCTCGTCCGAATCC	CAGAAGCAAGATAGCTGGCATC
ILF3	AGCATTCTTCCGTTTATCCAACA	GCTCGTCTATCCAGTCGGAC
INPP5D	TGGACCAGCTCATCGAGTTTT	GAGACACGACACTTTCTACTGT
LSM14A	ACCGACAGATCGTCCAATACC	GGACTGAACAATAGCTGGGTCTT
MNDA	GTTTACTCCGAATCAGGAAACCC	TAAATGGCGCTGTTGCTTTCA
MTDH	GTAAACGTGATAAGGTGCTGACT	CGGTGGTAACTGTGATGGTATTT
MYO1G	CAAACCTGACTTTGTGCTTTTGG	GGCCCTTCTCGAACCTGAG
NPM1	ACGGTCAGTTTAGGGGCTG	CTGTGGAACCTTGCTACCACC
NUP98	CGGGCTCTTTGGTTTTGGC	CAGCACCAAGAGCTGTTCCA
NUP155	TGGTTTGCTGTCCGTACCC	GATAGGAGGGAACACACCCAT
POP1	AGAGGTGTAAAGCACCACAGT	GCTGTCGTGAAGTTCCAGG
PPEF1	CAGTCCATCGAATATGCTGATGA	GGGACATCTATCGAGTCCACA
PPM1B	TCTTGCTGGCAAGCGTAATG	TTTGCCTGAGAGCTTCCACC
PPP1CA	ACTACGACCTTCTGCGACTAT	AGTTCTCGGGGTACTTGATCTT
PPP2CA	GTTCGTTACCGTGAACGCATC	TGGCGAGAGACCACCATGT
PPP2CB	GTGCAAGAGGTTCGTTGCC	TGTATCCGGTGATTTTCCACCA
PPP4C	TCACGCAGGTCTATGGCTTCT	CTGACAGGCTGAGGTAGTCAA
PRKDC	CTGTGCAACTTCACTAAGTCCA	CAATCTGAGGACGAATTGCCT
RALY	TTCAGGCAAGCAATGTAACCA	CACGGCCATACTTAGAGAAGATG
RPN1	CACCCTCAACAGTGGCAAGA	ATTTCGCTCACTCTGTCGCA
RUVBL1	TCAGGAGCTGGGTAGTAAGGT	CCCTGCGGAAGTTCTCCATC
SND1	CAGAACCGGCTTTCAGAATGT	TAGTATGTGAACCGTTCCCCT
SON	CCCTTGTGGTATCATCAGAGACA	CGATGGTACGTCTACAGGCTG
SUB1	GGTGAGACTTCGAGAGCCCT	GCGAACACTAACGTACCTCATTT

Tab. 2.11 (continued).

Gene	Forward primer (5'-3')	Reverse primer (5'-3')
SUMO2	GGAAGGAGTCAAGACTGAGAAC	GTCGTTCACAATAGGCTTTCATTAG
SUMO3	GAATGACCACATCAACCTGAAGG	GCCCGTCGAACCTGAATCT
SYNCRIP	CTGGTCTCAATAGAGGTTATGCG	TCCGGTTGGTGGTATAAAATGAC
YBX3	ACCGGCGTCCCTACAATTAC	GGTTCTCAGTTGGTGCTTCAC
ZC3HAV1	TCACGAACTCTCTGGACTGAA	ACTTTTGCATATCTCGGGCATAA
ZFR	CGGGTGTAGCCTATTCTCATCC	CAGTGGGGTAGCCTCCATAAG

Tab. 2.12: Oligonucleotides.
Oligonucleotides used for cloning of the plasmids in Tab. 2.13. The plasmids were cloned as described in chapter 2.2.1.4.1.

Name	Sequence (5'-3')	Description
5'-hnRNPM-*Xho*I	TAATCTCGAGATGGCCGCTGGCG TGGAA	Cloning of pEF-BOS-EF1α-hnRNPM-FLAG
3'-hnRNPM-*Bam*HI	TAATGGATCCGGCGTTCCGGTCG ATCCGC	Cloning of pEF-BOS-EF1α-hnRNPM-FLAG
5'-GFP-*Bam*HI	TAATGGATCCATTGAAGGAAGGA TCGTCAAGATGGTGAGCAAGGGC GAGGAG	Cloning of pEF-BOS-EF1α-hnRNPM-GFP
3'-GFP-*Not*I	TAATGCGGCCGCTTACTTGTACA GCTCGTCCATGCCG	Cloning of pEF-BOS-EF1α-hnRNPM-GFP
5'-hnRNPM1-195-*Xho*I	TAATCTCGAGATGGCCGCTGGCG TGGAAG	Cloning of a FLAG-tagged hnRNPM variant into pEF-BOS-EF1α
3'-hnRNPM-1-195-*Bam*HI	TAATGGATCCGTGGATGATCTCG TTGGGGATGTTGG	Cloning of a FLAG-tagged hnRNPM variant into pEF-BOS-EF1α
5'-hnRNPM-532-730-*Xho*I	TAATCTCGAGATGGTGCCAGCCG GAATGGG	Cloning of a FLAG-tagged hnRNPM variant into pEF-BOS-EF1α
3'-hnRNPM-196-531-*Bam*HI	TAATGGATCCGCGTTCCATAGAC AGGCCCATTCT	Cloning of a FLAG-tagged hnRNPM variant into pEF-BOS-EF1α
5'-hnRNPM-71-195-*Xho*I	TAATCTCGAGATGTACAGAGCAT TCATCACCAACATCCCTTTCG	Cloning of a FLAG-tagged hnRNPM variant into pEF-BOS-EF1α
5'-hnRNPM-*Bst*BI	TAATTTCGAAACCGCCATGGCCG CTGGCGTGGAA	Cloning of pLenti-EF1α-hnRNPM
3'-hnRNPM-*Xba*I	TAATTCTAGAGGCGTTCCGGTCG ATCCGC	Cloning of pLenti-EF1α-hnRNPM
5'-GFP-*Xba*I	TAATTCTAGAATTGAAGGAAGGA TCGTCAAGATGGTGAGC	Cloning of pLenti-EF1α-hnRNPM-GFP

Tab. 2.12 (continued).

Name	Sequence (5'-3')	Description
3'-GFP-*Nde*I	TAATCATATGTTACTTGTACAGC TCGTCCATGCCGAG	Cloning of pLenti-EF1α-hnRNPM-GFP
5'-ELAVL1-*Not*I	TAATGCGGCCGCACCGCCATGTC TAATGGTTATGAAGACCACATGG CC	Cloning of pLVX-EF1α-ELAVL1-FLAG
3'-ELAVL1-FLAG-*Mlu*I	TAATACGCGTTCAGTGGTGGTGG TGGTGGTGCTTGTCATCGTCGTC CTTGTAGTCCTTGACGATCCTTC CTTCAATTCTAGATTTGTGGGAC TTGTTGGTTTTGAAGGAA	Cloning of pLVX-EF1α-ELAVL1-FLAG
5'-ELAVL1-GFP	TTTCCTTCAAAACCAACAAGTCC CACAAATCTAGAATTGAAGGAAG GATCGTCAAGATG	Cloning of pLVX-EF1α-ELAVL1-GFP
3'-ELAVL1-GFP	GGAAAAGCGCCTCCCCTACCCGG TAGAATTCACGCGTTTACTTGTA CAGCTCGTCCATGC	Cloning of pLVX-EF1α-ELAVL1-GFP
5'-GFP-*Not*I	TAATGCGGCCGCACCGCCATGGT GAGCAAGGGCGAGGA	Cloning of pLVX-EF1α-GFP
3'-GFP-*Xba*I	TAATTCTAGATTACTTGTACAGC TCGTCCATGCCG	Cloning of pLVX-EF1α-GFP
5'-ΔRRM1-ELAVL1	GAGGAATTTCGACCCGGATCCGC GGCCGCACCGCCATGAGCTCAGA GGTGATCAAAGACG	Cloning of pLVX-EF1α-ΔRRM1-ELAVL1-FLAG
3'-ΔRRM1-ELAVL1	GTAGTCCTTGACGATCCTTCCTT CAATTCTAGATTTGTGGGACTTG TTGGTTTTG	Cloning of pLVX-EF1α-ΔRRM1-ELAVL1-FLAG
5'-ΔRRM3-ELAVL1	AGGAATTTCGACCCGGATCCGCG GCCGCACCGCCATGTCTAATGGT TATGAAGACCACAT	Cloning of pLVX-EF1α-ΔRRM3-ELAVL1-FLAG
3'-ΔRRM3-ELAVL1	GTCGTCCTTGTAGTCCTTGACGA TCCTTCCTTCAATTCTAGAGCCG GAGGAGGCGTTT	Cloning of pLVX-EF1α-ΔRRM3-ELAVL1-FLAG
5'-ELAVL1 KO guide AN	CTTCAGCCGGGAAGAAAGT	Knockout validation ELAVL1 guide AN
3'-ELAVL1 KO guide AN	TTCTGATGGAGGTTGTGGTG	Knockout validation ELAVL1 guide AN
5'-ELAVL1 KO guide AI	TGCAGTTACTAGTTTTGCCTTCA	Knockout validation ELAVL1 guide AI
3'-ELAVL1 KO guide AI	ACCCAATCAATCTGCCCAGG	Knockout validation ELAVL1 guide AI

Tab. 2.13: Plasmids.
The plasmids were cloned as described in chapter 2.2.1.4.1.

Construct	Description	Source
ELAVL1 cDNA ORF clone	Human ELAVL1 sequence	Sino Biological
pEF-BOS-EF1α-1-195-hnRNPM-FLAG	Expression vector encoding a human hnRNPM variant with C-terminal FLAG tag	This thesis
pEF-BOS-EF1α-1-531-hnRNPM-FLAG	Expression vector encoding a human hnRNPM variant with C-terminal FLAG tag	This thesis
pEF-BOS-EF1α-194-730-hnRNPM-FLAG	Expression vector encoding a human hnRNPM variant with C-terminal FLAG tag	This thesis
pEF-BOS-EF1α-532-730-hnRNPM-FLAG	Expression vector encoding a human hnRNPM variant with C-terminal FLAG tag	This thesis
pEF-BOS-EF1α-69-730-hnRNPM-FLAG	Expression vector encoding a human hnRNPM variant with C-terminal FLAG tag	This thesis
pEF-BOS-EF1α-hnRNPM-FLAG	Expression vector encoding human hnRNPM with C-terminal FLAG tag	This thesis
pEF-BOS-EF1α-hnRNPM-GFP	Expression vector encoding human hnRNPM with C-terminal GFP tag	This thesis
pLenti-EF1α-GFP	Lentiviral expression vector encoding GFP	Julia Wegner
pLenti-EF1α-hnRNPM	Lentiviral expression vector encoding human hnRNPM	Dr. A.-M. Herzner
pLenti-EF1α-hnRNPM-FLAG	Lentiviral expression vector encoding human hnRNPM with C-terminal FLAG tag	This thesis
pLenti-EF1α-hnRNPM-GFP	Lentiviral expression vector encoding human hnRNPM with C-terminal GFP tag	This thesis
pLVX-EF1α-ΔRRM1-ELAVL1-FLAG	Lentiviral expression vector encoding human ΔRRM1-ELAVL1 with C-terminal FLAG tag	This thesis
pLVX-EF1α-ΔRRM3-ELAVL1-FLAG	Lentiviral expression vector encoding human ΔRRM3-ELAVL1 with C-terminal FLAG tag	This thesis

Tab. 2.13 (continued).

Construct	Description	Source
pLVX-EF1α-ELAVL1-FLAG	Lentiviral expression vector encoding human ELAVL1 with C-terminal FLAG tag	This thesis
pLVX-EF1α-ELAVL1-GFP	Lentiviral expression vector encoding human ELAVL1 with C-terminal GFP tag	This thesis
pLVX-EF1α-GFP	Lentiviral expression vector encoding GFP	This thesis
pMD2.G	Lentiviral packaging plasmid encoding VSV-G	Addgene
pMDL.G	Third generation lentiviral packaging plasmid encoding Gag and Pol	Addgene
pRSV-Rev	Third generation lentiviral packaging plasmid encoding Rev	Addgene
psPAX2	Second generation lentiviral packaging plasmid	Addgene

Tab. 2.14: Oligonucleotides for cloning of shRNA expression vectors.
Oligonucleotides used for cloning of the shRNA-encoding pLKO.1 vectors in Tab. 2.15. The plasmids were cloned as described in chapter 2.2.1.4.2.

Name	Forward sequence (5'-3')	Reverse sequence (5'-3')
shARHGEF2.1	CCGGCCCAACCTGCAATGTGACTATC TCGAGATAGTCACATTGCAGGTTGGG TTTTTG	AATTCAAAAACCCAACCTGCAATGTG ACTATCTCGAGATAGTCACATTGCAG GTTGGG
shARHGEF2.2	CCGGGCGGCGAATTAAGATGGAGTTC TCGAGAACTCCATCTTAATTCGCCGC TTTTTG	AATTCAAAAAGCGGCGAATTAAGATG GAGTTCTCGAGAACTCCATCTTAATT CGCCGC
shCTSG.1	CCGGTCCTGGTGCGAGAAGACTTTGC TCGAGCAAAGTCTTCTCGCACCAGGA TTTTTG	AATTCAAAAATCCTGGTGCGAGAAGA CTTTGCTCGAGCAAAGTCTTCTCGCA CCAGGA
shCTSG.2	CCGGCGGCATCGTCTCCTATGGAAAC TCGAGTTTCCATAGGAGACGATGCCG TTTTTG	AATTCAAAAACGGCATCGTCTCCTAT GGAAACTCGAGTTTCCATAGGAGACG ATGCCG
shDDX21.1	CCGGCCCATATCTGAAGAAACTATTC TCGAGAATAGTTTCTTCAGATATGGG TTTTTG	AATTCAAAAACCCATATCTGAAGAAA CTATTCTCGAGAATAGTTTCTTCAGA TATGGG
shDDX21.2	CCGGCCTGAGGTTGATTTGGTTATAC TCGAGTATAACCAAATCAACCTCAGG TTTTTG	AATTCAAAAACCTGAGGTTGATTTGG TTATACTCGAGTATAACCAAATCAAC CTCAGG

Tab. 2.14 (continued).

Name	Forward sequence (5'-3')	Reverse sequence (5'-3')
shDHX9.1	CCGGACGACAATGGAAGCGGATATAC TCGAGTATATCCGCTTCCATTGTCGT TTTTTG	AATTCAAAAAACGACAATGGAAGCGG ATATACTCGAGTATATCCGCTTCCAT TGTCGT
shDHX9.2	CCGGGAAGGATTACTACTCAAGAAAC TCGAGTTTCTTGAGTAGTAATCCTTC TTTTTG	AATTCAAAAAGAAGGATTACTACTCA AGAAACTCGAGTTTCTTGAGTAGTAA TCCTTC
shDHX15.1	CCGGTTGGTGACAGCTATTAGTAAAC TCGAGTTTACTAATAGCTGTCACCAA TTTTTG	AATTCAAAAATTGGTGACAGCTATTA GTAAACTCGAGTTTACTAATAGCTGT CACCAA
shDHX15.2	CCGGGTGGAGTACATGCGATCATTAC TCGAGTAATGATCGCATGTACTCCAC TTTTTG	AATTCAAAAAGTGGAGTACATGCGAT CATTACTCGAGTAATGATCGCATGTA CTCCAC
shEBNA1BP2.1	CCGGGCCCATATGATGAATGCTATTC TCGAGAATAGCATTCATCATATGGGC TTTTTG	AATTCAAAAAGCCCATATGATGAATG CTATTCTCGAGAATAGCATTCATCAT ATGGGC
shEBNA1BP2.2	CCGGCTGGCAAGAAAGGGTCAAATAC TCGAGTATTTGACCCTTTCTTGCCAG TTTTTG	AATTCAAAAACTGGCAAGAAAGGGTC AAATACTCGAGTATTTGACCCTTTCT TGCCAG
shEFTUD2.1	CCGGGCTTTGCTGAAACGCCTAATAC TCGAGTATTAGGCGTTTCAGCAAAGC TTTTTG	AATTCAAAAAGCTTTGCTGAAACGCC TAATACTCGAGTATTAGGCGTTTCAG CAAAGC
shEFTUD2.2	CCGGCCCATTATTAAGCCAGTGAAAC TCGAGTTTCACTGGCTTAATAATGGG TTTTTG	AATTCAAAAACCCATTATTAAGCCAG TGAAACTCGAGTTTCACTGGCTTAAT AATGGG
shEIF3E.1	CCGGGCCACAATATCTTAATGCAATC TCGAGATTGCATTAAGATATTGTGGC TTTTTG	AATTCAAAAAGCCACAATATCTTAAT GCAATCTCGAGATTGCATTAAGATAT TGTGGC
shEIF3E.2	CCGGGATACCAACATGGTAGACTTTC TCGAGAAAGTCTACCATGTTGGTATC TTTTTG	AATTCAAAAAGATACCAACATGGTAG ACTTTCTCGAGAAAGTCTACCATGTT GGTATC
shELAVL1.1	CCGGCGAGCTCAGAGGTGATCAAAGC TCGAGCTTTGATCACCTCTGAGCTCG TTTTTG	AATTCAAAAACGAGCTCAGAGGTGAT CAAAGCTCGAGCTTTGATCACCTCTG AGCTCG
shELAVL1.2	CCGGTACCAGTTTCAATGGTCATAAC TCGAGTTATGACCATTGAAACTGGTA TTTTTG	AATTCAAAAATACCAGTTTCAATGGT CATAACTCGAGTTATGACCATTGAAA CTGGTA
shhnRNPA1.1	CCGGAGATATTTGTTGGTGGCATTAC TCGAGTAATGCCACCAACAAATATCT TTTTTG	AATTCAAAAAAGATATTTGTTGGTGG CATTACTCGAGTAATGCCACCAACAA ATATCT
shhnRNPA1.2	CCGGCAACAATCAGTCTTCAAATTTC TCGAGAAATTTGAAGACTGATTGTTG TTTTTG	AATTCAAAAACAACAATCAGTCTTCA AATTTCTCGAGAAATTTGAAGACTGA TTGTTG
shhnRNPAB.1	CCGGTGAGGCCATTGAATTGCCAATC TCGAGATTGGCAATTCAATGGCCTCA TTTTTG	AATTCAAAAATGAGGCCATTGAATTG CCAATCTCGAGATTGGCAATTCAATG GCCTCA
shhnRNPAB.2	CCGGTGAATTGCCAATGGATCCAAAC TCGAGTTTGGATCCATTGGCAATTCA TTTTTG	AATTCAAAAATGAATTGCCAATGGAT CCAAACTCGAGTTTGGATCCATTGGC AATTCA

Tab. 2.14 (continued).

Name	Forward sequence (5'-3')	Reverse sequence (5'-3')
shhnRNPD.1	CCGGTCGAAGGAACAATATCAGCAAC TCGAGTTGCTGATATTGTTCCTTCGA TTTTTG	AATTCAAAAATCGAAGGAACAATATC AGCAACTCGAGTTGCTGATATTGTTC CTTCGA
shhnRNPD.2	CCGGAGAGTGGTTATGGGAAGGTATC TCGAGATACCTTCCCATAACCACTCT TTTTTG	AATTCAAAAAAGAGTGGTTATGGGAA GGTATCTCGAGATACCTTCCCATAAC CACTCT
shhnRNPH2.1	CCGGGCCTTAAAGAAACACAAGGAAC TCGAGTTCCTTGTGTTTCTTTAAGGC TTTTTG	AATTCAAAAAGCCTTAAAGAAACACA AGGAACTCGAGTTCCTTGTGTTTCTT TAAGGC
shhnRNPH2.2	CCGGCCATGAGAGTACATATTGAAAC TCGAGTTTCAATATGTACTCTCATGG TTTTTG	AATTCAAAAACCATGAGAGTACATAT TGAAACTCGAGTTTCAATATGTACTC TCATGG
shhnRNPM.1	CCGGAGAGCCTTCATTACAAACATAC TCGAGTATGTTTGTAATGAAGGCTCT TTTTTG	AATTCAAAAAAGAGCCTTCATTACAA ACATACTCGAGTATGTTTGTAATGAA GGCTCT
shhnRNPM.2	CCGGACAAGCATAGTCTGAGCGGAAC TCGAGTTCCGCTCAGACTATGCTTGT TTTTTG	AATTCAAAAAACAAGCATAGTCTGAG CGGAACTCGAGTTCCGCTCAGACTAT GCTTGT
shhnRNPU.1	CCGGGCAACTGTGAGACTGAAGATTC TCGAGAATCTTCAGTCTCACAGTTGC TTTTTG	AATTCAAAAAGCAACTGTGAGACTGA AGATTCTCGAGAATCTTCAGTCTCAC AGTTGC
shhnRNPU.2	CCGGAGATCATGGCCGTGGATATTTC TCGAGAAATATCCACGGCCATGATCT TTTTTG	AATTCAAAAAAGATCATGGCCGTGGA TATTTCTCGAGAAATATCCACGGCCA TGATCT
shHP1BP3.1	CCGGCAATCTTAACTGAGGCCATTAC TCGAGTAATGGCCTCAGTTAAGATTG TTTTTG	AATTCAAAAACAATCTTAACTGAGGC CATTACTCGAGTAATGGCCTCAGTTA AGATTG
shHP1BP3.2	CCGGGGAGTCATCAAACAGGTTAAAC TCGAGTTTAACCTGTTTGATGACTCC TTTTTG	AATTCAAAAAGGAGTCATCAAACAGG TTAAACTCGAGTTTAACCTGTTTGAT GACTCC
shIGF2BP2.1	CCGGAGTGAAGCTGGAAGCGCATATC TCGAGATATGCGCTTCCAGCTTCACT TTTTTG	AATTCAAAAAAGTGAAGCTGGAAGCG CATATCTCGAGATATGCGCTTCCAGC TTCACT
shIGF2BP2.2	CCGGTTCCCGCATCATCACTCTTATC TCGAGATAAGAGTGATGATGCGGGAA TTTTTG	AATTCAAAAATTCCCGCATCATCACT CTTATCTCGAGATAAGAGTGATGATG CGGGAA
shILF2.1	CCGGTCGACAGGTGGGATCCTATAAC TCGAGTTATAGGATCCCACCTGTCGA TTTTTG	AATTCAAAAATCGACAGGTGGGATCC TATAACTCGAGTTATAGGATCCCACC TGTCGA
shILF2.2	CCGGCCAACGAAACTGGCTTTGAAAC TCGAGTTTCAAAGCCAGTTTCGTTGG TTTTTG	AATTCAAAAACCAACGAAACTGGCTT TGAAACTCGAGTTTCAAAGCCAGTTT CGTTGG
shILF3.1	CCGGCCAGAGGACGACAGTAAAGAAC TCGAGTTCTTTACTGTCGTCCTCTGG TTTTTG	AATTCAAAAACCAGAGGACGACAGTA AAGAACTCGAGTTCTTTACTGTCGTC CTCTGG
shILF3.2	CCGGCCTTCCAAGATGCCCAAGAAAC TCGAGTTTCTTGGGCATCTTGGAAGG TTTTTG	AATTCAAAAACCTTCCAAGATGCCCA AGAAACTCGAGTTTCTTGGGCATCTT GGAAGG

Tab. 2.14 (continued).

Name	Forward sequence (5'-3')	Reverse sequence (5'-3')
shLSM14A.1	CCGGGCCGATGAAGAAGATCCACTTC TCGAGAAGTGGATCTTCTTCATCGGC TTTTTG	AATTCAAAAAGCCGATGAAGAAGATC CACTTCTCGAGAAGTGGATCTTCTTC ATCGGC
shLSM14A.2	CCGGCTTGCCAAAGTTCGATCCTTTC TCGAGAAAGGATCGAACTTTGGCAAG TTTTTG	AATTCAAAAACTTGCCAAAGTTCGAT CCTTTCTCGAGAAAGGATCGAACTTT GGCAAG
shMNDA.1	CCGGCAATGGTGTATGGGTTGTTTAC TCGAGTAAACAACCCATACACCATTG TTTTTG	AATTCAAAAACAATGGTGTATGGGTT GTTTACTCGAGTAAACAACCCATACA CCATTG
shMNDA.2	CCGGTCCCAAGATCAGTCAACTTTAC TCGAGTAAAGTTGACTGATCTTGGGA TTTTTG	AATTCAAAAATCCCAAGATCAGTCAA CTTTACTCGAGTAAAGTTGACTGATC TTGGGA
shMTDH.1	CCGGCGTGATAAGGTGCTGACTGATC TCGAGATCAGTCAGCACCTTATCACG TTTTTG	AATTCAAAAACGTGATAAGGTGCTGA CTGATCTCGAGATCAGTCAGCACCTT ATCACG
shMTDH.2	CCGGCCAATACTACAAGAGACAGATC TCGAGATCTGTCTCTTGTAGTATTGG TTTTTG	AATTCAAAAACCAATACTACAAGAGA CAGATCTCGAGATCTGTCTCTTGTAG TATTGG
shMYO1G.1	CCGGACCATCACTGACCGAATCTTCC TCGAGGAAGATTCGGTCAGTGATGGT TTTTTG	AATTCAAAAAACCATCACTGACCGAA TCTTCCTCGAGGAAGATTCGGTCAGT GATGGT
shMYO1G.2	CCGGTGTCCTCTGCCACTGACAATCC TCGAGGATTGTCAGTGGCAGAGGACA TTTTTG	AATTCAAAAATGTCCTCTGCCACTGA CAATCCTCGAGGATTGTCAGTGGCAG AGGACA
shNPM1.1	CCGGCCTAGTTCTGTAGAAGACATTC TCGAGAATGTCTTCTACAGAACTAGG TTTTTG	AATTCAAAAACCTAGTTCTGTAGAAG ACATTCTCGAGAATGTCTTCTACAGA ACTAGG
shNPM1.2	CCGGGTTCAGGGCCAGTGCATATTAC TCGAGTAATATGCACTGGCCCTGAAC TTTTTG	AATTCAAAAAGTTCAGGGCCAGTGCA TATTACTCGAGTAATATGCACTGGCC CTGAAC
shNUP98.1	CCGGGCACCAGTGTATTACTGCTATC TCGAGATAGCAGTAATACACTGGTGC TTTTTG	AATTCAAAAAGCACCAGTGTATTACT GCTATCTCGAGATAGCAGTAATACAC TGGTGC
shNUP98.2	CCGGTCCTACTGGGACTACTATTAAC TCGAGTTAATAGTAGTCCCAGTAGGA TTTTTG	AATTCAAAAATCCTACTGGGACTACT ATTAACTCGAGTTAATAGTAGTCCCA GTAGGA
shNUP155.1	CCGGCATGCAGGTGTTAGGTTATATC TCGAGATATAACCTAACACCTGCATG TTTTTG	AATTCAAAAACATGCAGGTGTTAGGT TATATCTCGAGATATAACCTAACACC TGCATG
shNUP155.2	CCGGGGATTTACTCTGGCGGTATTAC TCGAGTAATACCGCCAGAGTAAATCC TTTTTG	AATTCAAAAAGGATTTACTCTGGCGG TATTACTCGAGTAATACCGCCAGAGT AAATCC
shPOP1.1	CCGGGCTTACGAAGAACCTTCTGTAC TCGAGTACAGAAGGTTCTTCGTAAGC TTTTTG	AATTCAAAAAGCTTACGAAGAACCTT CTGTACTCGAGTACAGAAGGTTCTTC GTAAGC
shPOP1.2	CCGGCTCCAACCACAGGCATTATAAC TCGAGTTATAATGCCTGTGGTTGGAG TTTTTG	AATTCAAAAACTCCAACCACAGGCAT TATAACTCGAGTTATAATGCCTGTGG TTGGAG

Tab. 2.14 (continued).

Name	Forward sequence (5'-3')	Reverse sequence (5'-3')
shPPM1B.1	CCGGGACTGAATCCACATAGAGAAAC TCGAGTTTCTCTATGTGGATTCAGTC TTTTTG	AATTCAAAAAGACTGAATCCACATAG AGAAACTCGAGTTTCTCTATGTGGAT TCAGTC
shPPM1B.2	CCGGGCTGGGAATGGTTTACGTTATC TCGAGATAACGTAAACCATTCCCAGC TTTTTG	AATTCAAAAAGCTGGGAATGGTTTAC GTTATCTCGAGATAACGTAAACCATT CCCAGC
shPP1.1	CCGGTGAGTGCAAGAGACGCTACAAC TCGAGTTGTAGCGTCTCTTGCACTCA TTTTTG	AATTCAAAAATGAGTGCAAGAGACGC TACAACTCGAGTTGTAGCGTCTCTTG CACTCA
shPP1.2	CCGGACTACGACCTTCTGCGACTATC TCGAGATAGTCGCAGAAGGTCGTAGT TTTTTG	AATTCAAAAAACTACGACCTTCTGCG ACTATCTCGAGATAGTCGCAGAAGGT CGTAGT
shPP2A.1	CCGGGCTAGTGATGGAGGGATATAAC TCGAGTTATATCCCTCCATCACTAGC TTTTTG	AATTCAAAAAGCTAGTGATGGAGGGA TATAACTCGAGTTATATCCCTCCATC ACTAGC
shPP2A.2	CCGGTGGAACTTGACGATACTCTAAC TCGAGTTAGAGTATCGTCAAGTTCCA TTTTTG	AATTCAAAAATGGAACTTGACGATAC TCTAACTCGAGTTAGAGTATCGTCAA GTTCCA
shPP2B.1	CCGGTAGACACACTGGATCATATAAC TCGAGTTATATGATCCAGTGTGTCTA TTTTTG	AATTCAAAAATAGACACACTGGATCA TATAACTCGAGTTATATGATCCAGTG TGTCTA
shPP2B.2	CCGGAGCCGACAAATTACCCAAGTAC TCGAGTACTTGGGTAATTTGTCGGCT TTTTTG	AATTCAAAAAAGCCGACAAATTACCC AAGTACTCGAGTACTTGGGTAATTTG TCGGCT
shPP4.1	CCGGGCAGGTCTATGGCTTCTACGAC TCGAGTCGTAGAAGCCATAGACCTGC TTTTTG	AATTCAAAAAGCAGGTCTATGGCTTC TACGACTCGAGTCGTAGAAGCCATAG ACCTGC
shPP4.2	CCGGGGACGAGCATCTCCAGAAAGAC TCGAGTCTTTCTGGAGATGCTCGTCC TTTTTG	AATTCAAAAAGGACGAGCATCTCCAG AAAGACTCGAGTCTTTCTGGAGATGC TCGTCC
shPP7.1	CCGGGGATTATGTGGACTCGATAGAC TCGAGTCTATCGAGTCCACATAATCC TTTTTG	AATTCAAAAAGGATTATGTGGACTCG ATAGACTCGAGTCTATCGAGTCCACA TAATCC
shPP7.2	CCGGGATTATGTGGACTCGATAGATC TCGAGATCTATCGAGTCCACATAATC TTTTTG	AATTCAAAAAGATTATGTGGACTCGA TAGATCTCGAGATCTATCGAGTCCAC ATAATC
shPRKDC.1	CCGGCCGGTAAAGATCCTAATTCTAC TCGAGTAGAATTAGGATCTTTACCGG TTTTTG	AATTCAAAAACCGGTAAAGATCCTAA TTCTACTCGAGTAGAATTAGGATCTT TACCGG
shPRKDC.2	CCGGCCTGAAGTCTTTACAACATATC TCGAGATATGTTGTAAAGACTTCAGG TTTTTG	AATTCAAAAACCTGAAGTCTTTACAA CATATCTCGAGATATGTTGTAAAGAC TTCAGG
shRALY.1	CCGGCAGGACACAGACGCGGATGATC TCGAGATCATCCGCGTCTGTGTCCTG TTTTTG	AATTCAAAAACAGGACACAGACGCGG ATGATCTCGAGATCATCCGCGTCTGT GTCCTG
shRALY.2	CCGGCAACACAGCTCTGGTGAAGAAC TCGAGTTCTTCACCAGAGCTGTGTTG TTTTTG	AATTCAAAAACAACACAGCTCTGGTG AAGAACTCGAGTTCTTCACCAGAGCT GTGTTG

Tab. 2.14 (continued).

Name	Forward sequence (5'-3')	Reverse sequence (5'-3')
shRPN1.1	CCGGGCCTTTCTCACGCTATGATTAC TCGAGTAATCATAGCGTGAGAAAGGC TTTTTG	AATTCAAAAAGCCTTTCTCACGCTAT GATTACTCGAGTAATCATAGCGTGAG AAAGGC
shRPN1.2	CCGGGTGAAGCTTGCCTCTCGAAATC TCGAGATTTCGAGAGGCAAGCTTCAC TTTTTG	AATTCAAAAAGTGAAGCTTGCCTCTC GAAATCTCGAGATTTCGAGAGGCAAG CTTCAC
shRUVBL1.1	CCGGGCCACAGAATTCGACCTTGAAC TCGAGTTCAAGGTCGAATTCTGTGGC TTTTTG	AATTCAAAAAGCCACAGAATTCGACC TTGAACTCGAGTTCAAGGTCGAATTC TGTGGC
shRUVBL1.2	CCGGGTGGCGTCATAGTAGAATTAAC TCGAGTTAATTCTACTATGACGCCAC TTTTTG	AATTCAAAAAGTGGCGTCATAGTAGA ATTAACTCGAGTTAATTCTACTATGA CGCCAC
shSHIP1.1	CCGGGCTCATTAAGTCACAGAAATTC TCGAGAATTTCTGTGACTTAATGAGC TTTTTG	AATTCAAAAAGCTCATTAAGTCACAG AAATTCTCGAGAATTTCTGTGACTTA ATGAGC
shSHIP1.2	CCGGGCAGAAGGTCTTCCTACACTTC TCGAGAAGTGTAGGAAGACCTTCTGC TTTTTG	AATTCAAAAAGCAGAAGGTCTTCCTA CACTTCTCGAGAAGTGTAGGAAGACC TTCTGC
shSND1.1	CCGGTCTCGTCTCAAACTCTATTTGC TCGAGCAAATAGAGTTTGAGACGAGA TTTTTG	AATTCAAAAATCTCGTCTCAAACTCT ATTTGCTCGAGCAAATAGAGTTTGAG ACGAGA
shSND1.2	CCGGGCTGATGATGCAGACGAATTTC TCGAGAAATTCGTCTGCATCATCAGC TTTTTG	AATTCAAAAAGCTGATGATGCAGACG AATTTCTCGAGAAATTCGTCTGCATC ATCAGC
shSON.1	CCGGAGATACAGAACTACGATATAAC TCGAGTTATATCGTAGTTCTGTATCT TTTTTG	AATTCAAAAAAGATACAGAACTACGA TATAACTCGAGTTATATCGTAGTTCT GTATCT
shSON.2	CCGGACACCATGGAGACCCATATATC TCGAGATATATGGGTCTCCATGGTGT TTTTTG	AATTCAAAAAACACCATGGAGACCCA TATATCTCGAGATATATGGGTCTCCA TGGTGT
shSUB1.1	CCGGGAACAGATTTCTGACATTGATC TCGAGATCAATGTCAGAAATCTGTTC TTTTTG	AATTCAAAAAGAACAGATTTCTGACA TTGATCTCGAGATCAATGTCAGAAAT CTGTTC
shSUB1.2	CCGGAGCCAGCTGAAGGAACAGATTC TCGAGAATCTGTTCCTTCAGCTGGCT TTTTTG	AATTCAAAAAAGCCAGCTGAAGGAAC AGATTCTCGAGAATCTGTTCCTTCAG CTGGCT
shSUMO2.1	CCGGTACACCACTTAGTAAACTAATC TCGAGATTAGTTTACTAAGTGGTGTA TTTTTG	AATTCAAAAATACACCACTTAGTAAA CTAATCTCGAGATTAGTTTACTAAGT GGTGTA
shSUMO2.2	CCGGACAATTGATGTGTTCCAACAGC TCGAGCTGTTGGAACACATCAATTGT TTTTTG	AATTCAAAAAACAATTGATGTGTTCC AACAGCTCGAGCTGTTGGAACACATC AATTGT
shSUMO3.1	CCGGCGAGGACACCATCGACGTGTTC TCGAGAACACGTCGATGGTGTCCTCG TTTTTG	AATTCAAAAACGAGGACACCATCGAC GTGTTCTCGAGAACACGTCGATGGTG TCCTCG
shSUMO3.2	CCGGGAATGACCACATCAACCTGAAC TCGAGTTCAGGTTGATGTGGTCATTC TTTTTG	AATTCAAAAAGAATGACCACATCAAC CTGAACTCGAGTTCAGGTTGATGTGG TCATTC

Tab. 2.14 (continued).

Name	Forward sequence (5'-3')	Reverse sequence (5'-3')
shSYNCRIP.1	CCGGTATATGGGATCTTCGTCTAATC TCGAGATTAGACGAAGATCCCATATA TTTTTG	AATTCAAAAATATATGGGATCTTCGT CTAATCTCGAGATTAGACGAAGATCC CATATA
shSYNCRIP.2	CCGGGCAAAGTAACAGAGGGTCTTAC TCGAGTAAGACCCTCTGTTACTTTGC TTTTTG	AATTCAAAAAGCAAAGTAACAGAGGG TCTTACTCGAGTAAGACCCTCTGTTA CTTTGC
shYBX3.1	CCGGCGGTTCATCGAAATCCAACTTC TCGAGAAGTTGGATTTCGATGAACCG TTTTTG	AATTCAAAAACGGTTCATCGAAATCC AACTTCTCGAGAAGTTGGATTTCGAT GAACCG
shYBX3.2	CCGGCAGAAATGGATATGGATTTATC TCGAGATAAATCCATATCCATTTCTG TTTTTG	AATTCAAAAACAGAAATGGATATGGA TTTATCTCGAGATAAATCCATATCCA TTTCTG
shZC3HAV1.1	CCGGGCTCCTTCTTCACATCGTAGAC TCGAGTCTACGATGTGAAGAAGGAGC TTTTTG	AATTCAAAAAGCTCCTTCTTCACATC GTAGACTCGAGTCTACGATGTGAAGA AGGAGC
shZC3HAV1.2	CCGGACGAACTCTCTGGACTGAACAC TCGAGTGTTCAGTCCAGAGAGTTCGT TTTTTG	AATTCAAAAAACGAACTCTCTGGACT GAACACTCGAGTGTTCAGTCCAGAGA GTTCGT
shZFR.1	CCGGGCCTAGTATTCGAGCAAGAAAC TCGAGTTTCTTGCTCGAATACTAGGC TTTTTG	AATTCAAAAAGCCTAGTATTCGAGCA AGAAACTCGAGTTTCTTGCTCGAATA CTAGGC
shZFR.2	CCGGCCCTGAGAAGTATGACATAAAC TCGAGTTTATGTCATACTTCTCAGGG TTTTTG	AATTCAAAAACCCTGAGAAGTATGAC ATAAACTCGAGTTTATGTCATACTTC TCAGGG

Tab. 2.15: pLKO.1 shRNA expression vectors.
The plasmids were cloned as described in chapter 2.2.1.4.2.

Construct	Source
pLKO.1 shC001	Sigma-Aldrich
pLKO.1 shC002	Sigma-Aldrich
pLKO.1 shARHGEF2.1	This thesis
pLKO.1 shARHGEF2.2	This thesis
pLKO.1 shCTSG.1	This thesis
pLKO.1 shCTSG.2	This thesis
pLKO.1 shDDX21.1	This thesis
pLKO.1 shDDX21.2	This thesis
pLKO.1 shDHX9.1	This thesis
pLKO.1 shDHX9.2	This thesis
pLKO.1 shDHX15.1	This thesis
pLKO.1 shDHX15.2	This thesis
pLKO.1 shEBNA1BP2.1	This thesis
pLKO.1 shEBNA1BP2.2	This thesis

Tab. 2.15 (continued).

Construct	Source
pLKO.1 shEFTUD2.1	This thesis
pLKO.1 shEFTUD2.2	This thesis
pLKO.1 shEIF3E.1	This thesis
pLKO.1 shEIF3E.2	This thesis
pLKO.1 shELAVL1.1	This thesis
pLKO.1 shELAVL1.2	This thesis
pLKO.1 shhnRNPA1.1	This thesis
pLKO.1 shhnRNPA1.2	This thesis
pLKO.1 shhnRNPAB.1	This thesis
pLKO.1 shhnRNPAB.2	This thesis
pLKO.1 shhnRNPD.1	This thesis
pLKO.1 shhnRNPD.2	This thesis
pLKO.1 shhnRNPH2.1	This thesis
pLKO.1 shhnRNPH2.2	This thesis
pLKO.1 shhnRNPM.1	Dr. A.-M. Herzner
pLKO.1 shhnRNPM.2	Dr. A.-M. Herzner
pLKO.1 shhnRNPU.1	This thesis
pLKO.1 shhnRNPU.2	This thesis
pLKO.1 shHP1BP3.1	This thesis
pLKO.1 shHP1BP3.2	This thesis
pLKO.1 shIGF2BP2.1	This thesis
pLKO.1 shIGF2BP2.2	This thesis
pLKO.1 shILF2.1	This thesis
pLKO.1 shILF2.2	This thesis
pLKO.1 shILF3.1	This thesis
pLKO.1 shILF3.2	This thesis
pLKO.1 shLSM14A.1	This thesis
pLKO.1 shLSM14A.2	This thesis
pLKO.1 shMNDA.1	This thesis
pLKO.1 shMNDA.2	This thesis
pLKO.1 shMTDH.1	This thesis
pLKO.1 shMTDH.2	This thesis
pLKO.1 shMYO1G.1	This thesis
pLKO.1 shMYO1G.2	This thesis
pLKO.1 shNPM1.1	This thesis
pLKO.1 shNPM1.2	This thesis
pLKO.1 shNUP98.1	This thesis

Tab. 2.15 (continued).

Construct	Source
pLKO.1 shNUP98.2	This thesis
pLKO.1 shNUP155.1	This thesis
pLKO.1 shNUP155.2	This thesis
pLKO.1 shPOP1.1	This thesis
pLKO.1 shPOP1.2	This thesis
pLKO.1 shPPM1B.1	This thesis
pLKO.1 shPPM1B.2	This thesis
pLKO.1 shPP1.1	This thesis
pLKO.1 shPP1.2	This thesis
pLKO.1 shPP2A.1	This thesis
pLKO.1 shPP2A.2	This thesis
pLKO.1 shPP2B.1	This thesis
pLKO.1 shPP2B.2	This thesis
pLKO.1 shPP4.1	This thesis
pLKO.1 shPP4.2	This thesis
pLKO.1 shPP7.1	This thesis
pLKO.1 shPP7.2	This thesis
pLKO.1 shPRKDC.1	This thesis
pLKO.1 shPRKDC.2	This thesis
pLKO.1 shRALY.1	This thesis
pLKO.1 shRALY.2	This thesis
pLKO.1 shRPN1.1	This thesis
pLKO.1 shRPN1.2	This thesis
pLKO.1 shRUVBL1.1	This thesis
pLKO.1 shRUVBL1.2	This thesis
pLKO.1 shSHIP1.1	This thesis
pLKO.1 shSHIP1.2	This thesis
pLKO.1 shSND1.1	This thesis
pLKO.1 shSND1.2	This thesis
pLKO.1 shSON.1	This thesis
pLKO.1 shSON.2	This thesis
pLKO.1 shSUB1.1	This thesis
pLKO.1 shSUB1.2	This thesis
pLKO.1 shSUMO2.1	This thesis
pLKO.1 shSUMO2.2	This thesis
pLKO.1 shSUMO3.1	This thesis
pLKO.1 shSUMO3.2	This thesis

Tab. 2.15 (continued).

Construct	Source
pLKO.1 shSYNCRIP.1	This thesis
pLKO.1 shSYNCRIP.2	This thesis
pLKO.1 shYBX3.1	This thesis
pLKO.1 shYBX3.2	This thesis
pLKO.1 shZC3HAV1.1	This thesis
pLKO.1 shZC3HAV1.2	This thesis
pLKO.1 shZFR.1	This thesis
pLKO.1 shZFR.2	This thesis

2.1.5 Bacterial strains and cell lines

Tab. 2.16: Bacterial strains.

Name	Genotype	Source
Stbl3 chemo-competent *E. coli*	F– *mcr*B *mrr hsd*S20 (rB–, mB–) *rec*A13 *sup*E44 *ara*-14 *gal*K2 *lac*Y1 *pro*A2 *rps*L20 (StrR) *xyl*-5 λ– *leu mtl*-1	Invitrogen

Tab. 2.17: Human cell lines.

Name	Description	Source
HEK293FT	Human embryonic kidney cell line	Invitrogen
HeLa	Human cervix carcinoma-derived epithelial cell line	Dr. Martin Schlee
THP-1 dual	THP-1-derived cells stably expressing constructs that encode a Gaussia luciferase gene driven by an ISG54 minimal promoter with five ISREs and a secreted embryonic alkaline phosphatase (SEAP) reporter gene under the control of an IFNβ minimal promoter with five NF-κB response elements and three c-Rel binding sites	InvivoGen
THP-1 dual KO-cGAS	cGAS-deficient THP-1 dual cells	InvivoGen
THP-1 dual KO-IFNAR2	IFNAR2-deficient THP-1 dual cells	InvivoGen

2.1.6 Pathogens

Tab. 2.18: Pathogens.

Name	Source
HSV-1 (strain F)	Dr. Maria Hønholt Christensen
L. monocytogenes (wildtype strain EGD)	Dr. Martin Schlee

2.1.7 Software

Tab. 2.19: Software.

Description	Application	Developer
Affinity Designer (version 1.9.1)	Graphic editing	Serif Europe
ApE (version 2.0.49)	DNA sequence analysis	Wayne Davis
Fiji (version 2.0.0-rc-69/1.52p)	Processing of microscopy images	NIH
ImageStudio Lite (version 5.2.5)	Immunoblot analysis	LI-COR Biosciences
Mendeley Desktop (version 1.19.8)	Bibliography	Elsevier
Microsoft Office 2016 (version 16.16.22)	Text editing and calculation	Microsoft
Prism (version 7.0e)	Graphic editing and statistical analysis	GraphPad
RStudio (version 1.4.1106)	Graphic editing	PBC

2.2 Methods

2.2.1 Molecular biology methods

2.2.1.1 Annealing of DNA oligonucleotides

For annealing of two complementary single-stranded DNA sequences, the oligonucleotides were mixed in equal ratios in 1× NEBuffer 2 and incubated in a thermocycler at 95 °C for 5 min. To allow hybridization of the oligonucleotides, the temperature was decreased by 1 °C/min to 8 °C.

2.2.1.2 Polymerase chain reaction

Polymerase chain reaction (PCR) was used to amplify DNA fragments for cloning purposes and to screen for bacterial colonies harboring the desired genetic construct. To amplify insert DNA for cloning, 0.4 U Phusion High-Fidelity DNA polymerase, 1× Phusion HF buffer, 0.2 µM of each primer, 200 µM dNTPs, and 50 ng template DNA (plasmid DNA or cDNA) were mixed in a total volume of 25 µl. To screen bacterial colonies containing

the desired plasmid, 0.5 U DreamTaq DNA polymerase, 1× DreamTaq green buffer, 0.08 µM of each primer, and 80 µM dNTPs were mixed in a total volume of 25 µl and inoculated with one bacterial colony. The cycler conditions for Phusion and DreamTaq PCR are summarized in Tab. 2.20 and Tab. 2.21, respectively. After an initial denaturation step (step 1), an amplification cycle (step 2.1 to 2.3) that included denaturation, primer annealing, and elongation was repeated 30× to 35×, followed by a final elongation step (step 5). Annealing temperatures were chosen according to the melting temperatures (T_m) of the primers.

Tab. 2.20: Phusion PCR program.

Step	Specification	Temperature /°C	Time	Number of cycles
1	Initial denaturation	98	30 sec	1
2.1	Denaturation	98	30 sec	30 - 35
2.2	Annealing	55 - 62	30 sec	30 - 35
2.3	Elongation	72	30 sec/kb	30 - 35
4	Final elongation	72	5 min	1
5	End of reaction	8	∞	1

Tab. 2.21: DreamTaq PCR program.

Step	Specification	Temperature /°C	Time	Number of cycles
1	Initial denaturation	95	2 min	1
2.1	Denaturation	95	30 sec	30 - 35
2.2	Annealing	T_m - 5	30 sec	30 - 35
2.3	Elongation	72	30 sec/kb	30 - 35
4	Final elongation	72	5 min	1
5	End of reaction	8	∞	1

2.2.1.3 Agarose gel electrophoresis

PCR products and endonuclease-treated vectors were routinely separated by size on 1 % (w/v) TAE-buffered agarose gels containing 5 µl SYBR safe DNA gel stain. Smaller DNA fragments (< 500 bp) were resolved on 1.5 % (w/v) agarose gels. After electrophoresis at 110 V for 30 min, the DNA fragments were visualized on an LED blue light transilluminator. If the DNA fragments were used for further experiments, the desired target bands were excised and isolated by gel extraction using the innuPREP gel extraction kit according to the manufacturer's instructions.

2.2.1.4 Cloning

2.2.1.4.1 Standard cloning protocol

Preparation of recipient vectors:

To generate complementary single-stranded DNA overhangs for ligation of two DNA fragments, the recipient plasmid was digested with specific restriction endonucleases. Unless indicated otherwise, 1 µg plasmid DNA was mixed with 1 µl of each restriction enzyme and digested in 1× FastDigest green buffer in a total volume of 20 µl at 37 °C for 1 h. The digested vector was separated by agarose gel electrophoresis and isolated from the gel under blue light using a scalpel. The innuPREP gel extraction kit was used to isolate the DNA from the gel according to the manufacturer's instructions.

Preparation of insert DNA:

Phusion PCR was used to generate insert DNA with restriction sites compatible with those of the recipient plasmid. After PCR, the amplification product was separated by agarose gel electrophoresis and purified from the gel using the innuPREP gel extraction kit according to the manufacturer's instructions. Following, the purified insert DNA was digested at 37 °C for 1 h with 1 µl of each restriction endonuclease that were used for the digestion of the recipient vector. Afterwards, the digested PCR product was purified using the innuPREP PCRpure kit according to the manufacturer's instructions.

Ligation of DNA fragments:

After treating vector and insert DNA with the respective restriction endonucleases, 1 µl recipient plasmid, 10 µl insert DNA, 1 µl T4 DNA ligase (5 U/µl), 2 µl 10× T4 DNA ligase buffer, and 6 µl H_2O were mixed and incubated at room temperature (RT) for 1 h.

Gibson assembly:

Gibson assembly was used as an alternative way to ligate insert DNA and recipient vector in an isothermal, exonuclease-based reaction. Routinely, 0.5 µl digested vector, 2.5 µl insert DNA, and 3 µl 2× Gibson assembly master mix were mixed and incubated at 50 °C for 1 h.

Transformation of chemically competent *Escherichia coli* (*E. coli*):
Chemically competent *E. coli* Stbl3 were incubated with 2 µl ligation product or 2 µl Gibson assembly mix on ice for 20 min. After heat shock at 42 °C for 30 sec, the cells were incubated on ice for 3 min. For recovery, the bacteria were resuspended in 1 ml LB medium and incubated in a ThermoMixer at 800 rpm at 37 °C for 60 min. Following, the cells were centrifuged at 10,000 ×g for 1 min, resuspended in 100 µl LB medium, and plated on 50 µg/ml carbenicillin-containing LB plates for incubation at 37 °C overnight.

2.2.1.4.2 Specific cloning protocols

For cloning of shRNA-expressing plasmids, the pLKO.1 shC001 recipient vector was digested with *Age*I and *Eco*RI and purified by agarose gel electrophoresis as described above. To generate the insert DNA, 1 µl sense oligonucleotide (100 µM), 1 µl antisense oligonucleotide (100 µM) (both listed in Tab. 2.14), 5 µl 10× NEBuffer 2, and 43 µl H_2O were mixed and annealed as described above. Following, 2 µl annealed oligonucleotide mix were ligated with 0.5 µl *Age*I/*Eco*RI-digested pLKO.1 shC001 and transformed into *E. coli* Stbl3 as described above. After transformation, the plasmid DNA was isolated from bacterial colonies and sequenced at Microsynth Seqlab (Göttingen).

2.2.1.5 Isolation of plasmid DNA

LB medium supplemented with 50 µg/ml carbenicillin was inoculated with single colonies from bacterial plates and grown at 37 °C overnight. The plasmid DNA was isolated from 2 ml or 50 ml bacterial suspension cultures using the NucleoSpin plasmid miniprep kit or the PureLink HiPure plasmid midiprep kit according to the manufacturer's instructions. Plasmid DNA concentrations were determined using a NanoDrop One UV-Vis spectrophotometer. The plasmids were sequenced at Microsynth Seqlab.

2.2.1.6 Isolation of RNA

To isolate cellular RNA, 0.1 × 10^6 to 1.0 × 10^6 cells (THP-1 dual, HeLa) were harvested and resuspended in 350 µl RLT buffer. 350 µl 70 % (v/v) ethanol were added and the samples were mixed by pipetting. Following, the solutions were loaded onto Zymo Spin IIICG columns and centrifuged at 10,000 ×g for 1 min. After discarding the flow through, the columns were washed with 350 µl RW1 buffer and centrifuged again at 10,000 ×g for

1 min. The columns were washed a second time with 350 µl RNA wash buffer and centrifuged at 10,000 ×g for 1 min. Subsequently, the empty columns were centrifuged at 10,000 ×g for 2 min and the RNA was eluted in 30 µl RNase-free H_2O. RNA concentrations were determined using a NanoDrop One UV-Vis spectrophotometer.

2.2.1.7 DNase I treatment of RNA preparations

If required, contaminating genomic DNA was removed from RNA preparations by DNase I digest. 10 µl RNA preparation, 10 µl H_2O, 2 µl 10× DNase I buffer, and 1 µl DNase I (1 U/µl) were mixed and incubated at 37 °C for 30 min. Following, 1 µl EDTA (50 mM) was added and the reaction was stopped by incubating the samples at 70 °C for 10 min.

2.2.1.8 cDNA synthesis

Routinely, 100 ng to 500 ng RNA were used to synthesize cDNA by random hexamer-primed reverse transcription using the RevertAid first strand cDNA synthesis kit according to the manufacturer's instructions. Per reaction, 5.75 µl RNA preparation, 2 µl 5× reaction buffer, 1 µl dNTPs (10 mM each), 0.5 µl random hexamer primer (IDT) (100 µM), 0.5 µl RevertAid reverse transcriptase (200 U/µl), and 0.25 µl RiboLock RNase inhibitor (40 U/µl) were mixed and the cDNA was synthesized by incubating the samples at 25 °C for 10 min, 42 °C for 60 min, and 85 °C for 5 min. The reaction product was diluted 1:4 with H_2O.

2.2.1.9 Quantitative real-time PCR

mRNA was reverse transcribed into cDNA as described above (see chapter 2.2.1.8). The target-specific cDNA levels were determined by SYBR green-based quantitative real-time PCR (qPCR). qPCR primers were preferentially designed on exon-exon junctions and are listed in Tab. 2.11. Per reaction, 1 µl diluted cDNA solution was mixed with 6.4 µl H_2O, 0.6 µl primer solution (0.15 µM forward and reverse primer), and 2 µl my-Budget 5× EvaGreen qPCR-Mix II and pipetted into a 384-well qPCR plate. After sealing the plate with optically clear foil, the qPCR was performed on a QuantStudio 5 real-time PCR system using the cycler parameters shown in Tab. 2.22.

Tab. 2.22: Cycler parameters for qPCR.

Step	Specification	Temperature /°C	Time	Number of cycles
1	Initial denaturation	95	15 min	1
2.1	Denaturation	95	15 sec	40
2.2	Annealing	60	20 sec	40
2.3	Elongation	72	20 sec	40
4	Final elongation	54	30 sec	1
5	End of reaction	8	∞	1

The target cDNA levels were normalized to the cDNA levels of *GAPDH*, which was used as an endogenous housekeeping gene. The relative ratio R was calculated using the target- and *GAPDH*-specific cycle threshold (C_t) values according to equation (1):

$$R = \frac{2^{C_t(\mathrm{GAPDH})}}{2^{C_t(\mathrm{target})}} . \quad (1)$$

2.2.2 Cell biology methods

2.2.2.1 Cultivation of human cell lines

Human cell lines were cultivated at 37 °C in a humidified atmosphere with 5 % (v/v) CO_2 and passaged under laminar flow in a biological safety cabinet. Suspension cells (THP-1 dual) were cultured in RPMI 1640 supplemented with 10 % (v/v) FCS and 1× penicillin-streptomycin. Adherent cells (HEK293FT, HeLa) were cultured in DMEM supplemented with 10 % (v/v) FCS and 1× penicillin-streptomycin. Complete RPMI 1640 and DMEM will be referred to hereafter as solely RPMI and DMEM, respectively.

2.2.2.2 Harvesting and counting of cells

All human cell lines were harvested by centrifugation at 500 ×g for 5 min. To enzymatically release adherent cells from the plate, HEK293FT and HeLa were washed with PBS and treated with trypsin-EDTA at 37 °C for 5 min. The dissociated cell suspensions were diluted 1:10 with DMEM. To determine cell concentration and viability, the cells were counted by trypan blue exclusion using a TC20 automated cell counter.

2.2.2.3 Freezing and thawing of cells

Routinely, 0.1 × 10^7 to 1 × 10^7 human cells were harvested, resuspended in 1 ml cold freezing medium (10 % (v/v) DMSO in FCS), and slowly frozen to -80 °C in Mr. Frosty freezing containers. For long-term storage, the frozen cells were transferred to -150 °C freezers. To thaw frozen cells, the cryogenic vials were incubated in a water bath at 37 °C, washed with 10 ml RPMI/DMEM, resuspended in fresh medium, and cultured as described above.

2.2.2.4 Production of lentiviral particles

$CaPO_4$ transfection of HEK293FT cells:

HEK293FT cells were used as packaging cells for the production of lentiviral particles. One day before the transfection, 4 × 10^5 HEK293FT cells were seeded in 6-well plates. On the next day, the plasmids were delivered into the cells by $CaPO_4$ transfection. Depending on the lentiviral transfer vector, different packaging and envelope plasmids were used. For the vectors pLenti and pLVX, 10 µl $CaCl_2$ solution (2.5 M) were mixed with 1.6 µg lentiviral transfer vector, 0.4 µg pRSV-rev, 1.1 µg pMDL.G, and 0.6 µg pMD2.G and adjusted to 100 µl with H_2O. For the vector pLKO.1, 10 µl $CaCl_2$ solution (2.5 M) were mixed with 1 µg lentiviral transfer vector, 0.75 µg psPAX2, and 0.25 µg pMD2.G and adjusted to 100 µl with H_2O. After preparing the aforementioned solutions, 100 µl 2× HBS buffer were added, the reagents were mixed by pipetting, incubated at RT for 5 min, and then the transfection mix was added dropwise to the cells. All of the following steps were performed under biosafety level 2 (BSL-2) conditions. 6 h after transfection, the medium was replaced with 4 ml DMEM and the cells were incubated for 72 h to allow production of lentiviral particles. The lentivirus-containing cell culture supernatants were harvested and passed through 0.45 µm filters to remove debris and remaining HEK293FT cells.

Lentiviral transduction of THP-1 dual cells and HeLa cells:

Routinely, 5 × 10^5 THP-1 dual cells were infected with 3 ml virus solution spiked with 5 µg/ml polybrene by spinning in a centrifuge at 600 ×g at 32 °C for 1 h. For the infection of HeLa cells, 1 × 10^5 cells were seeded in 6-well plates one day before the infection. On the next day, the medium was replaced and the cells were infected with 3 ml virus solution supplemented with 5 µg/ml polybrene. For both cell lines, the infection was stopped after

24 h by replacing the virus-containing medium with fresh medium. Following, the cells were cultured for 24 h to allow expression of the antibiotic resistance gene or transgenic GFP fusion proteins. If a puromycin-resistance gene was introduced by the lentiviral construct, the cells were selected for 72 h in puromycin-containing medium (THP-1: 2 µg/ml puromycin; HeLa: 1 µg/ml puromycin). Cells expressing hnRNPM-GFP, ELAVL1-GFP, or GFP fusion proteins were sorted by fluorescence activated cell sorting (FACS) at the Flow Cytometry Core Facility (FCCF) at the University Hospital Bonn.

2.2.2.5 CRISPR/Cas9-mediated knockout cell line generation

The Alt-R CRISPR/Cas9 system (IDT) was used to generate knockout (KO) cell lines. gRNAs targeting the human *ELAVL1* gene were designed using the Alt-R HDR design tool (IDT) and listed in Tab. 2.23. To form the crRNA:tracrRNA hybrid, 0.5 µl crRNA (IDT) and 0.5 µl tracrRNA (IDT) (200 µM each) were mixed with 1.28 µl IDTE buffer (IDT) and incubated at 95 °C for 5 min. The mixture was cooled down to RT on the bench top to allow RNA hybridization. Following, 0.75 µl recombinant Cas9 enzyme (IDT) was diluted with 0.5 µl resuspension buffer R from the Neon transfection system 10 µl kit. To form the RNP complex, 1.25 µl diluted Cas9 and 1.25 µl crRNA:tracrRNA duplex were mixed and incubated at RT for 20 min. During the incubation time, 1.25×10^6 THP-1 dual cells were harvested, washed with PBS, and resuspended in 22.5 µl resuspension buffer R. 2 µl crRNA:tracrRNA:Cas9 RNP complex, 4 µl electroporation enhancer (10.8 µM) (IDT), and 18 µl cell suspension were mixed and then 10 µl of the mixture were transferred to a Neon electroporation system using a 10 µl Neon tip. The electroporation was performed at 1600 V with 3 pulses and 10 ms pulse width. Single cells were cloned by limiting dilution and expanded to verify *ELAVL1* deletion by immunoblotting and/or Sanger sequencing.

Tab. 2.23: CRISPR/Cas9 gRNAs specific for the human *ELAVL1* gene.

gRNA	Sequence (5'-3')
Hs.Cas9.ELAVL1.1.AN (gRNA AN)	GGGTTTATGACCATTGAAAC
Hs.Cas9.ELAVL1.1.AI (gRNA AI)	CTTCACCAATGCTGCTGAAC

2.2.2.6 Lipofection and stimulation of cells

For stimulation experiments, cells were treated with agonists for cGAS (0.1 µg/ml pDNA, 0.5 µg/ml G_3-YSD), RIG-I (0.1 µg/ml 5'ppp-dsRNA), STING (10 µg/ml 2'3'-cGAMP), TLR8 (1.0 µg/ml TL8-506), TLR1/TLR2 (0.5 µg/ml Pam3CSK4), IFNAR (1000 U/ml or 5000 U/ml IFNα), or left non-stimulated (Opti-MEM) G_3-YSD was prepared by annealing the single-stranded DNA oligonucleotides G_3-YSD (np) fwd and G_3-YSD (np) rev (listed in Tab. 2.10) as described above. Unless indicated otherwise, the cells were seeded in 150 µl medium (THP-1 dual: 6 × 10^4 cells/well, HeLa: 2 × 10^4 cells/well) as duplicates in 96-well plates. cGAS and RIG-I agonists were transfected using Lipofectamine 2000 reagent. Per 96-well, 0.5 µl Lipofectamine 2000 (1 µg/µl) was mixed with 24.5 µl Opti-MEM and, in a second tube, 20 ng pDNA, 100 ng G_3-YSD, or 20 ng 5'ppp-dsRNA were diluted in a total volume of 25 µl Opti-MEM. Both solutions were mixed, incubated at RT for 5 min, and then added to the cells. To stimulate TLR8, TLR1/TLR2, STING, or IFNAR, the respective stimuli were diluted in 50 µl Opti-MEM and directly added to the cells (96-well format). After incubation for 6 h to 20 h, the cell culture supernatants were harvested and used for downstream assays. If the stimulated cells and not the cell culture supernatants were used for downstream assays, the experiments were performed in 24-well plates (e.g., immunoblotting, isolation of RNA) or 6-well plates (e.g., nuclear/cytoplasmic extraction). Based on the surface area of the well, the experimental parameters used for the 96-well format were adjusted by multiplying by the factors 6.1 (24-well) or 31 (6-well).

2.2.2.7 Quantification of ISRE and NF-κB reporter activities in THP-1 dual cells

THP-1 dual cells express ISRE and NF-κB reporter constructs. To determine ISRE reporter activity, which was used as a surrogate parameter for type I interferon production, 30 µl cell culture supernatant were mixed with 30 µl coelenteracine solution (diluted to 1 µg/ml in H_2O) and then the Gaussia luciferase activity was analyzed using an EnVision 2104 Multilabel Reader Device (PerkinElmer). To determine NF-κB reporter activity, 40 µl cell culture supernatant were mixed with pNPP substrate buffer, incubated for 30 min to 60 min, and then the absorbance was measured at λ = 405 nm using an Epoch microplate reader.

2.2.2.8 Infection of THP-1 dual cells with HSV-1 and *L. monocytogenes*

3×10^5 THP-1 dual cells were seeded in 300 µl RPMI and infected with HSV-1 (strain F, kindly provided by Dr. Maria Hønholt Christensen) at the indicated multiplicity of infection (MOI) for 24 h. Following, ISRE reporter activation was determined as described above and the cellular RNA was isolated to analyze HSV-1 RNA copy numbers by qPCR.
L. monocytogenes (wildtype strain EGD) was cultivated in BHI medium until log phase was reached and then stored at -80 °C. 3×10^5 THP-1 dual cells were washed with PBS, seeded in 300 µl RPMI devoid of antibiotics, and infected with *L. monocytogenes* at MOI 1 at 37 °C for 2 h. After washing with antibiotics-free RPMI, the cells were cultured in RPMI containing 50 µg/ml gentamicin for 24 h and then ISRE reporter activity was determined.

2.2.2.9 Treatment of THP-1 dual cells with okadaic acid

Wildtype and ELAVL1-deficient THP-1 dual cells were seeded in 96-well plates (see chapter 2.2.2.6) and pre-incubated with DMSO (control) or different concentrations of okadaic acid (OA) for 6 h. Following, the cells were kept in DMSO- or OA-containing medium and lipofected with 0.1 µg/ml 5'ppp-dsRNA, 0.5 µg/ml G_3-YSD, or left non-stimulated. 16 h after stimulation, ISRE reporter activation was analyzed by measuring the secreted Gaussia luciferase activity.

2.2.2.10 3'-mRNA sequencing analysis

THP-1 dual wildtype and THP-1 dual *ELAVL1*$^{-/-}$ cells (AN #39) were stimulated with 0.1 µg/ml 5'ppp-dsRNA, 0.5 µg/ml G_3-YSD, 1000 U/ml IFNα, or left non-stimulated. After 6 h, the cells were harvested and the total cellular RNA was extracted as described above. The RNA sequencing libraries were generated at the Next Generation Sequencing Core Facility at the University Hospital Bonn using the QuantSeq 3' mRNA-Seq Library Prep kit FWD (Lexogen). The samples were sequenced on a HiSeq1500 device (Illumina). Data analysis was kindly performed by Thais Schlee-Guimaraes. Briefly, the reads were aligned to the human reference genome (Ensembl genome version 96) using STAR aligner, quantified with HTSeq, and differential expression analysis was performed using DESeq2 (Anders et al., 2015; Dobin et al., 2013; Love et al., 2014).

2.2.2.11 MTT assay

MTT assay was used to determine the metabolic activity of cells, a surrogate parameter for viability. Metabolically active cells are capable of reducing the yellow tetrazole substrate compound MTT to purple formazan crystals, whose formation can be quantified colorimetrically. Routinely, MTT assay was performed after stimulation of THP-1 dual cells (96-well format) (see chapter 2.2.2.6). After isolating the cell culture supernatants, the volume of each well was adjusted to 80 µl with RPMI. Following, 20 µl MTT substrate solution were added and the cells were incubated at 37 °C for 1 h. The reaction was stopped by adding 100 µl 10 % (v/v) SDS solution. After dissolution of the crystals, the absorbance was measured at λ = 595 nm using an Epoch microplate reader.

2.2.2.12 Confocal immunofluorescence microscopy

Confocal immunofluorescence microscopy was used to analyze the subcellular localization of hnRNPM, cGAS, and TBK1 phosphorylated at Ser172 (pTBK1-Ser172). 6×10^5 THP-1 dual cells were seeded in 150 µl RPMI in CellCarrier-96 Ultra imaging microplates and treated overnight with 100 ng/ml PMA to induce differentiation into a macrophage-like state. On the next morning, the PMA-containing medium was removed by two washes with 150 µl warm PBS and replaced with 150 µl warm RPMI. G_3-YSD-AF647 was prepared by annealing the single-stranded DNA oligonucleotides G_3-YSD (np) fwd-AF647 and G_3-YSD (np) rev as described above (listed in Tab. 2.10). Following, the cells were stimulated with 0.5 µg/ml G_3-YSD-AF647 or left non-stimulated (see chapter 2.2.2.6). After 4 h, the cells were washed thrice with 150 µl warm PBS (5 min each wash) and fixed with 50 µl fixation buffer at RT for 10 min. Following, the fixation solution was removed and the cells were permeabilized with 50 µl 0.3 % (v/v) Triton X-100-PBS at RT for 10 min. After washing twice with 150 µl warm PBS (5 min each wash), 50 µl 3 % (w/v) BSA-PBS were added and the samples were incubated at RT for 1 h to block non-specific antibody binding. The primary antibodies were diluted in 1 % (w/v) BSA-PBS (α-hnRNPM M1-M4 (1:500, rabbit mAb); α-pTBK1-Ser172 (1:100, rabbit mAb); α-cGAS (1:50, rabbit mAb)) and added to the samples on ice for 2 h. Afterwards, the specimens were washed thrice with 150 µl warm PBS (5 min each wash) and incubated with rabbit-specific AF488-conjugated secondary antibody (1 µg/ml in 1 % (w/v) BSA-PBS) on ice for 1 h. After three

washes with 150 µl PBS (5 min each wash), the samples were incubated with 0.5 µg/ml CellMask orange at RT for 5 min. Subsequently, the samples were washed thrice with 150 µl PBS (5 min each wash) and the nuclei were counterstained with 5 µg/ml Hoechst 33342-PBS for 10 min. After three final washes with PBS (5 min each wash), the samples were imaged on a Leica SP8 confocal microscope (HC PL APO CS2 63×/12.0 water immersion objective) in line sequential scan mode as z stacks with zoom factor 4 and line average 4 at the Microscopy Core Facility at the University Hospital Bonn. Fiji was used for image processing.

2.2.2.13 Proximity ligation assay

The Duolink in situ red kit rabbit/mouse was used according to the manufacturer's instructions to analyze protein:protein interactions *in cellulo* by proximity ligation assay (PLA). Per 96-well, 6 × 10^5 THP-1 dual cells stably expressing hnRNPM-GFP, ELAVL1-GFP, or GFP were seeded in 150 µl RPMI in CellCarrier-96 Ultra imaging microplates and differentiated overnight with 100 ng/ml PMA. On the next morning, the cells were stimulated with 0.5 µg/ml G_3-YSD-AF647 or left non-stimulated (see chapter 2.2.2.12). After 4 h, the cells were washed thrice with 150 µl warm PBS (5 min each wash) and fixed with 50 µl fixation buffer at RT for 10 min. Following, the cells were permeabilized with 50 µl 0.3 % (v/v) Triton X-100-PBS at RT for 10 min, washed twice with 150 µl warm PBS (5 min each wash), and blocked with 40 µl Duolink blocking solution at 37 °C for 60 min. The blocking solution was removed and the samples were incubated with the primary antibodies (α-pTBK1-Ser172 (1:100, rabbit mAb), α-GFP (1:200, mouse mAb), α-ELAVL1 (1:100, rabbit mAb)) diluted in Duolink antibody diluent on ice for 2 h (combinations: α-pTBK1-Ser172 or α-ELAVL1 + α-GFP; α-pTBK1-Ser172 or α-ELAVL1; α-GFP; no primary antibody). Following, the specimens were washed four times with 150 µl warm Duolink wash buffer A (5 min each wash) and incubated with 40 µl Duolink PLA probes solution at 37 °C for 1 h. After three washes with 150 µl warm Duolink wash buffer A (5 min each wash), 40 µl Duolink ligase solution were added and the samples were incubated at 37 °C for 30 min. The samples were washed thrice with 150 µl warm Duolink wash buffer A (5 min each wash) and incubated with Duolink polymerase solution at 37 °C for 100 min. After three washes with 150 µl warm Duolink wash buffer B (10 min each wash), the samples

were incubated with 5 µg/ml Hoechst 33342-PBS for 10 min, washed thrice with PBS (5 min each wash), and imaged on a Leica SP8 confocal microscope (HC PL APO CS2 63×/12.0 water immersion objective) in line sequential scan mode as z stacks (0.5 µm z step size) with zoom factor 4 and line average 4. Fiji was used to quantify the PLA signals. For this, the PLA channel of individual cells was duplicated and a threshold was applied (Default: 6 to 255 or 10 to 255) to the duplicated images. All particles above the threshold with a size of 5 to ∞ pixel units or 10 to ∞ pixel units were counted. Threshold and particle size were adjusted only between independent experiments. The total number of detected PLA signals per cell was defined as the PLA score, providing a proportional measure to the degree of target protein:protein interactions.

2.2.3 Biochemical methods

2.2.3.1 Preparation of cleared cellular lysates

Cleared cellular lysates (CCLs) were prepared to analyze protein expression and protein phosphorylation by immunoblotting. Routinely, 3.6×10^5 THP-1 dual cells were harvested, washed with ice-cold PBS, resuspended in 25 µl RIPA lysis buffer supplemented with protease and phosphatase inhibitor cocktails, and then incubated on ice for 20 min, with vortexing the tube every 5 min at highest speed. After centrifugation of the crude lysates at 20,000 ×g at 4 °C for 20 min, the supernatants (i.e., CCLs) were isolated, mixed with equal volumes of 2× Laemmli buffer, and incubated at 95 °C for 5 min.

2.2.3.2 Quantification of protein concentrations

Bicinchoninic acid assay (BCA) was used to determine the protein concentration in CCLs. Routinely, 2.5 µl CCL were mixed with 197.5 µl BCA reagent, incubated at 37 °C for 25 min, and then the absorbance was measured at λ = 562 nm using an Epoch microplate reader. A blank-corrected standard curve was plotted to determine the protein concentration.

2.2.3.3 SDS polyacrylamide gel electrophoresis

To separate proteins by size under denaturing conditions, discontinuous SDS polyacrylamide gel electrophoresis (SDS-PAGE) was performed in a vertical Mini-Protean tetra cell system (Bio-Rad). Routinely, the protein samples were concentrated in 3 % (v/v)

SDS-PAGE stacking gels and separated by size in 10 % (v/v) SDS-PAGE resolving gels. To efficiently separate high and low molecular weight proteins, 8 % (v/v) or 12 % (v/v) resolving gels were used. Electrophoresis was performed in SDS-PAGE running buffer at 110 V until the desired separation was achieved. PageRuler plus prestained protein ladder was loaded onto the gel as a size standard.

2.2.3.4 Immunoblotting

After electrophoresis, the size-separated proteins were transferred from the resolving polyacrylamide gels to nitrocellulose membranes. Sponges, Whatman papers, 0.45 µm nitrocellulose membrane, and the polyacrylamide gel were soaked in transfer buffer, assembled, and placed onto the holder cassette of a TE22 mighty small wet transfer tank system according to the manufacturer's instructions. The proteins were transferred at 450 mA for 90 min and the success of the transfer was determined by Ponceau S staining. The membranes were destained using TBS-T and blocked for 1 h with 5 % (w/v) BSA-PBS-T. Primary antibodies (listed in Tab. 2.8) were diluted to working concentrations with Odyssey blocking buffer and incubated with the membranes at 4 °C overnight. On the next day, the membranes were washed three times with TBS-T (10 min each wash) and incubated with the target-specific secondary antibody (listed in Tab. 2.9) (diluted 1:12,500 in TBS) at RT for 2 h. After three additional washes with TBS-T (10 min each wash), the membranes were rinsed twice with TBS and the protein signals were detected using an Odyssey Fc near-infrared imaging instrument. The Image Studio Lite software was used to quantify signal intensities. If multiple targets were analyzed, the CCLs were subdivided, loaded onto multiple SDS-PAGE gels, and the resulting membranes were probed sequentially with different primary antibodies.

2.2.3.5 Immunoprecipitation

Immunoprecipitation (IP) was performed to analyze protein interactions. Prior to IP, THP-1 dual cells were lentivirally transduced to stably express hnRNPM-GFP, ELAVL1-GFP, or GFP and sorted at the FCCF to isolate populations with comparable GFP expression. For each IP, 1.5×10^7 cells were harvested, resuspended in 15 ml RPMI medium, and seeded in 10-cm cell culture plates. The cells were stimulated with 0.1 µg/ml pDNA using a total amount of 64 µl Lipofectamine 2000 reagent. 3 h after stimulation, the cells were har-

vested, washed with 10 ml PBS, and lysed in 700 µl ice-cold TAP lysis buffer supplemented with protease and phosphatase inhibitor on ice for 20 min, with vortexing the tube every 5 min at highest speed. Using a short sonication burst (15 sec, amplitude 90 %, cycle 1, VialTweeter Sonication Device), the nuclei were mechanically disrupted and then the crude lysates were centrifuged at 20,000 ×g at 4 °C for 30 min. Following, the supernatants were collected and the protein concentrations were determined by BCA. Per IP, 700 µg to 800 µg total protein were used and 5 % of the CCLs were analyzed as input controls. For each IP, 12.5 µl equilibrated GFP-Trap magnetic agarose beads (agarose beads coupled to anti-GFP nanobodies/V_HH) were incubated with the CCLs on a rotating wheel at 4 °C overnight. On the next morning, the beads were washed three times with 700 µl TAP wash buffer and, if indicated, the samples were additionally incubated with 300 µl TAP wash buffer supplemented with 100 µg/ml RNase A and protease/phosphatase inhibitor cocktail on a rotating wheel at 4 °C for 90 min. Afterwards, the beads were washed with TAP lysis buffer (three times, 700 µl) and TAP wash buffer (three times, 700 µl). Bound proteins were eluted by incubating the beads with 30 µl 2× Laemmli buffer at 95 °C for 10 min. Eluates and input controls were analyzed by immunoblotting.

2.2.3.6 Streptavidin pull-down

Streptavidin pull-down was used to analyze interactions between hnRNPM variants and biotinylated G_3-YSD or C_3-YSD. 2.5 × 10^6 HEK293FT cells were seeded in 10-cm plates and cultured overnight. pEF-BOS plasmids encoding FLAG-tagged hnRNPM variants were delivered into the cells by $CaPO_4$ transfection. 10 µg pEF-BOS plasmid were diluted in a total volume of 450 µl H_2O and mixed with 50 µl $CaCl_2$ solution (2.5 M). Following, 500 µl 2× HBS buffer were added, the solutions were mixed by pipetting, incubated for 5 min at RT, and then added dropwise to the cells. After incubation for 6 h, the medium was replaced with fresh DMEM and the cells were incubated for 72 h. Following, the cells were harvested, washed twice with ice-cold PBS, and lysed in 500 µl TAP lysis buffer supplemented with protease and phosphatase inhibitor on ice for 20 min. After centrifugation of the crude lysates at 20,000 ×g at 4 °C for 20 min, the CCLs were isolated. The biotinylated G_3-YSD and C_3-YSD oligonucleotides were prepared by annealing G_3-YSD (np) fwd-biotin and G_3-YSD (np) rev or C_3-YSD (np) fwd-biotin and C_3-YSD (np) rev (listed in Tab. 2.10). For each pull-down, 225 µl CCL were incubated with 20 µg annealed

G_3-YSD-biotin or C_3-YSD-biotin on ice for 30 min. Following, 30 µl NeutrAvidin agarose beads were equilibrated by three washes with 500 µl TAP wash buffer (30 sec, 6000 rpm, 4 °C) and incubated with the CCL-DNA mix on a rotating wheel at 4 °C overnight. Afterwards, the beads were washed three times with 500 µl TAP lysis buffer, resuspended in 40 µl 1× Laemmli buffer, and incubated at 95 °C for 5 min to elute bound proteins. Eluates and input controls were analyzed by immunoblotting.

2.2.3.7 Affinity purification-mass spectrometric analysis

In this thesis, two different AP-MS analyses were performed. In the initial analysis, the hnRNPM interactome was mapped in non-stimulated and cGAS-activated THP-1 dual cells. Here, 5 × 10^7 THP-1 dual cells expressing hnRNPM-GFP or GFP (biological quadruplicates) were lipofected with 0.5 µg/ml G_3-YSD or left non-stimulated (similar as described in chapter 2.2.3.5). After 3 h, the cells were harvested, washed with ice-cold PBS, and lysed in 2 ml TAP lysis buffer supplemented with protease and phosphatase inhibitor cocktail on ice for 20 min. For each replicate, 3.0 mg total protein were mixed with 25 µl equilibrated GFP-Trap magnetic agarose beads and incubated on a rotating wheel at 4 °C for 2 h. Afterwards, the beads were washed three times with 700 µl TAP lysis buffer, three times with 700 µl TAP wash buffer, and then the dried beads were stored at -80 °C.

In the second AP-MS analysis, the interactomes of hnRNPM and ELAVL1 were determined in the non-stimulated condition. Here, 5 × 10^7 THP-1 dual cells expressing hnRNPM-GFP, ELAVL1-GFP, or GFP (biological quadruplicates) were lysed in 2 ml TAP lysis buffer supplemented with protease and phosphatase inhibitor cocktail on ice for 20 min. Different from the AP-MS analysis described above, in this experiment, 1.5 mg total protein were used for each IP and the GFP fusion proteins were immunoprecipitated on a rotating wheel at 4 °C overnight.

In both experiments, bound proteins were identified by AP-MS in the laboratory of Prof. Andreas Pichlmair at TU Munich (Germany). The processing steps after IP and data analysis were kindly performed by Christian Urban and Dr. Antonio Piras. Briefly, co-immunoprecipitated proteins were denatured, reduced, alkylated, and digested with LysC and trypsin. After peptide purification on StageTips, the samples were loaded on a reverse-phase analytical column and separated with an EASY-nLC 1200 system (Thermo Fisher Scientific). The eluting peptides were directly analyzed on a Q-Exactive HF mass spec-

trometer (Thermo Fisher Scientific). MaxQuant (version 1.6.17.0) was used to process RAW files and output data were analyzed with Perseus (version 1.6.14.0) (Tyanova et al., 2016), R (version 4.0.2) and RStudio (version 1.3.1073). Intensity based absolute quantification (iBAQ) values, a measure of protein abundance, of each protein group were normalized using an experiment-specific normalization factor and differential enrichment of the protein groups was statistically analyzed by two-sided Welch's t-tests, with protein groups removed from the analysis if not detected in at least three replicates.

2.2.3.8 *In vitro* TBK1 kinase assay

To analyze TBK1 kinase activity *in vitro*, 7.5 × 10^6 THP-1 dual cells stably expressing hnRNPM-GFP or GFP were stimulated with 0.1 µg/ml pDNA for 3 h or left non-stimulated and lysed as described above (see chapter 2.2.3.5). Per IP, 700 µg to 800 µg total protein were incubated with 12.5 µl equilibrated GFP-Trap magnetic agarose beads on a rotating wheel at 4 °C overnight. Following, the beads were washed with TAP lysis buffer (three times, 700 µl) and TAP wash buffer (three times, 700 µl). The washed beads were incubated with 1 ng recombinant, catalytically active TBK1-GST in 25 µl kinase assay buffer supplemented with 20 µM unlabeled ATP at 30 °C for 30 min. The reaction was stopped by adding 5 µl 5× Laemmli buffer and incubating the samples at 95 °C for 10 min. After magnetic separation, the eluates were analyzed by immunoblotting.

2.2.3.9 Extraction of cytoplasmic and nuclear protein fractions

Cytoplasmic and nuclear protein fractions were prepared to determine the subcellular localization of proteins. Routinely, 1.86 × 10^6 THP-1 dual cells were seeded in 4.65 ml RPMI and stimulated with 0.5 µg/ml G_3-YSD, 0.1 µg/ml 5'ppp-dsRNA, 1000 U/ml IFNα, or left non-stimulated (see chapter 2.2.2.6). After 1 h to 4 h, the cells were harvested, washed with 5 ml PBS, and then the cytoplasmic and nuclear fractions were isolated using the NE-PER nuclear and cytoplasmic extraction kit according to the manufacturer's instructions. For each extraction 70 µl CERI buffer, 3.85 µl CERII buffer, and 35 µl NER buffer were used. The protein concentrations in the isolated fractions were determined by BCA and equal protein amounts (5 µg to 10 µg) were analyzed by immunoblotting.

2.2.3.10 Enzyme-linked immunosorbent assay

The secretion of interferon-gamma induced protein 10 kD (IP10) (also known as C-X-C motif chemokine ligand 10 (CXCL10)) to the cell culture supernatant was measured by enzyme-linked immunosorbent assay (ELISA) according to the manufacturer's instructions, using half the originally recommended amounts of each reagent. ELISA plates were coated by adding IP10-specific capture antibody diluted in ELISA coating buffer at 4 °C overnight. On the next morning, the plates were washed with ELISA wash buffer (three times, 150 µl) and incubated with 100 µl ELISA assay buffer at RT for 1 h to block non-specific binding. After three washes with 150 µl ELISA wash buffer, the cell culture supernatants were diluted in ELISA assay buffer and added to the plates at RT for 2 h. Following, the plates were washed with ELISA wash buffer (five times, 150 µl) and incubated with the biotinylated, cytokine-specific detection antibody and streptavidin-HRP, both diluted in 50 µl ELISA assay buffer, at RT for 1 h. After seven washing steps with 150 µl ELISA wash buffer, 50 µl TMB substrate reagent (BD BioSciences) were added to each well and the plates were incubated in the dark. The enzymatic reaction was stopped by adding 50 µl 1 M H_2SO_4 and the absorbance was measured at λ = 450 nm and λ = 570 nm using an Epoch microplate reader. Background-corrected absorbances at λ = 450 nm and an IP10 standard curve were used to calculate the cytokine concentrations.

2.2.4 Statistics

Statistical significance was determined with GraphPad Prism 7 using one-way ANOVA with Dunnett's or Tukey's multiple comparisons test or two-way ANOVA with Dunnett's, Tukey's, or Sidak's multiple comparisons test and a confidence interval of 95 %. Significances are indicated as follows: * (P < 0.05), ** (P < 0.01), *** (P < 0.001), **** ($P \leq 0.0001$), ns: not significant.

3 Results

Nucleic acid sensing by receptors of the innate immune system is essential for the host to fight viral infections. cGAS is the principal type I IFN-inducing sensor of pathogen-derived cytosolic dsDNA. Prior to this thesis, Dr. A.-M. Herzner has performed a quantitative AP-MS analysis to identify novel cofactors of the cGAS-STING signaling axis and novel immune sensors of exogenous DNA (Herzner, 2013). One of the proteins that selectively co-precipitated with G_3-YSD, a short dsDNA with G-overhangs and potent cGAS agonist, was hnRNPM. First RNAi experiments indicated that hnRNPM positively regulates the cGAS-dependent production of type I IFNs, but the underlying mechanism remained elusive. The aim of this study was to elucidate the molecular function of hnRNPM in cGAS-STING signaling.

3.1 hnRNPM promotes the RIG-I- and cGAS-dependent type I IFN response

3.1.1 The N-terminus of hnRNPM contains the core G_3-YSD-binding domain

To identify the protein domain that mediates binding to G_3-YSD, C-terminally FLAG-tagged hnRNPM deletion mutants were transiently expressed in HEK293FT cells for 72 h. The CCLs were incubated with biotinylated G_3-YSD or C_3-YSD and affinity-purified with biotin-specific NeutrAvidin beads at 4 °C overnight. Differential co-precipitation of the hnRNPM fusion proteins with G_3-YSD/C_3-YSD was analyzed by immunoblotting (Fig. 3.1). As expected, full-length hnRNPM (amino acids (aa) 1-730) selectively co-precipitated with G_3-YSD. However, low signal intensities were also detectable after pull-down of C_3-YSD. Expression of an hnRNPM variant lacking C-terminal amino acids (aa 1-531) did not affect the interaction with the G_3-YSD. Consistently, the C-terminal 198 amino acids of hnRNPM (aa 532-730) did not co-precipitate with G_3-YSD, suggesting that RRM3 of hnRNPM is not involved in binding of G_3-YSD. Deletions in the N-terminal portion of hnRNPM (aa69-730 and aa194-730) abrogated binding to G_3-YSD, whereas selective co-precipitation with G_3-YSD was observed for an N-terminal hnRNPM fusion protein (aa 1-195). Although these results do not prove whether binding of hnRNPM to G_3-YSD promotes cGAS activation *in cellulo*, these experiments demonstrate that the N-terminus of hnRNPM mediates direct or indirect interactions with G_3-YSD *in vitro*.

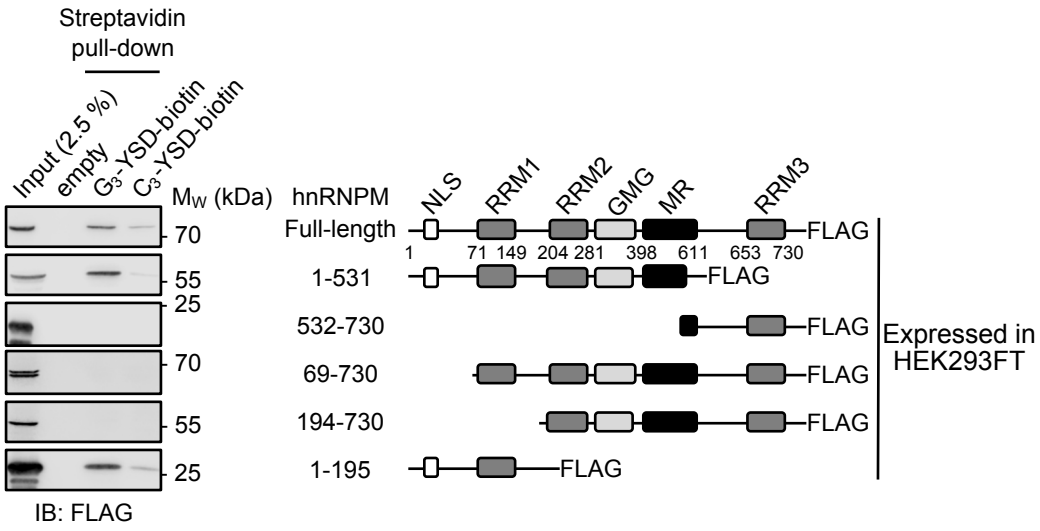

Fig. 3.1: The N-terminus of hnRNPM mediates interactions with G_3-YSD.
The indicated FLAG-tagged hnRNPM fusion proteins were transiently expressed in HEK293FT cells. 72 h after transfection, CCLs were generated and incubated with NeutrAvidin beads and biotinylated G_3-YSD (G_3-YSD-biotin) or biotinylated C_3-YSD (C_3-YSD-biotin) at 4 °C overnight. Bound proteins were eluted and analyzed by immunoblotting with a FLAG-specific antibody. 2.5 % of the CCLs were used as input controls.

3.1.2 hnRNPM is a positive regulator of cGAS and RIG-I signaling and functions downstream of cGAS, STING, and RIG-I

Considering the *in vitro* interaction with G_3-YSD, it was hypothesized that hnRNPM functions as a direct sensor of exogenous DNA. To further investigate the role of hnRNPM in nucleic acid immunity, CRISPR/Cas9 was used to target the *HNRNPM* gene in THP-1 dual cells. THP-1 dual cells are derived from the human monocyte cell line THP-1 and express ISRE and NF-κB reporter constructs (for details see chapter 2.1.5). However, several attempts to delete the *HNRNPM* gene failed, suggesting that hnRNPM is required for cell survival. For subsequent experiments, control short hairpin RNAs (shRNAs) (i.e., shC001, shC002) and shRNAs specific for the mRNA of *HNRNPM* (i.e., shhnRNPM.1, shhnRNPM.2) were constitutively expressed in THP-1 dual cells. For simplicity, knockdown (KD) of *HNRNPM* mRNA expression will henceforth be referred to as hnRNPM KD. qPCR analysis showed that the expression of hnRNPM-specific shRNAs reduces the mRNA levels of *HNRNPM* by approximately 60 % compared to control cells (THP-1 dual, THP-1 dual shC001) (Fig. 3.2A), without impairing cellular viability (Fig. 3.2B).

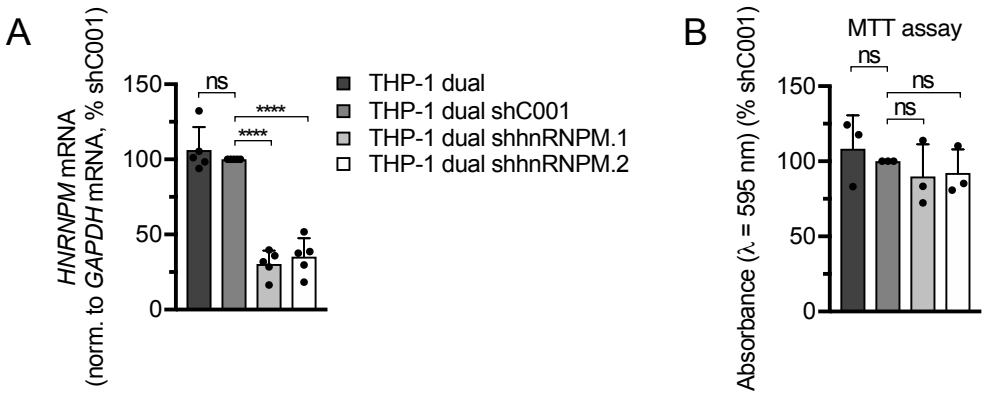

Fig. 3.2: THP-1 dual hnRNPM KD cells are viable.
(**A**) Control cells (THP-1 dual, THP-1 dual shC001) and cells expressing hnRNPM-specific shRNAs (THP-1 dual shhnRNPM.1, THP-1 dual shhnRNPM.2) were analyzed by qPCR to determine the relative hnRNPM KD efficiency. *HNRNPM* mRNA expression was normalized to *GAPDH* mRNA (n = 5, mean + SD, one-way ANOVA, Tukey's multiple comparisons test). (**B**) The viability of the cell lines depicted in (A) was determined by MTT assay (n = 3, mean + SD, one-way ANOVA, Tukey's multiple comparisons test). Significances are indicated as follows: * (P < 0.05), ** (P < 0.01), *** (P < 0.001), **** ($P \leq 0.0001$), ns: not significant.

To analyze the function of hnRNPM in nucleic acid immunity, THP-1 dual hnRNPM KD cells were stimulated with ligands activating RIG-I (0.1 µg/ml 5'ppp-dsRNA), cGAS (0.1 µg/ml pDNA, 0.5 µg/ml G_3-YSD), STING (10 µg/ml 2'3'-cGAMP), TLR8 (1.0 µg/ml TL8-506), TLR1/TLR2 (0.5 µg/ml Pam3CSK4), or IFNAR (1000 U/ml IFNα). ISRE and NF-κB reporter activities were used as surrogate parameters for type I IFN production and pro-inflammatory gene expression, respectively. Of note, KD of hnRNPM robustly inhibited the RIG-I-, cGAS-, or STING-induced ISRE reporter activity relative to the controls (THP-1 dual, THP-1 dual shC001) (Fig. 3.3A). The inhibition of the ISRE reporter correlated with the expression of hnRNPM, indicating an hnRNPM-specific effect (Fig. 3.2A). By contrast, ISRE reporter activation induced by TLR8 or IFNAR was largely unchanged between THP-1 dual hnRNPM KD cells and the controls (Fig. 3.3A-3.3B). Unexpectedly, not only signaling downstream of cGAS (pDNA, G_3-YSD) but also downstream of RIG-I (5'ppp-dsRNA) was attenuated in THP-1 dual hnRNPM KD cells, arguing against the theory that hnRNPM constitutes a novel sensor of exogenous DNA. This reasoning is further supported by the observation that KD of hnRNPM also impaired the production of type I IFNs after direct stimulation of STING (Fig. 3.3A).

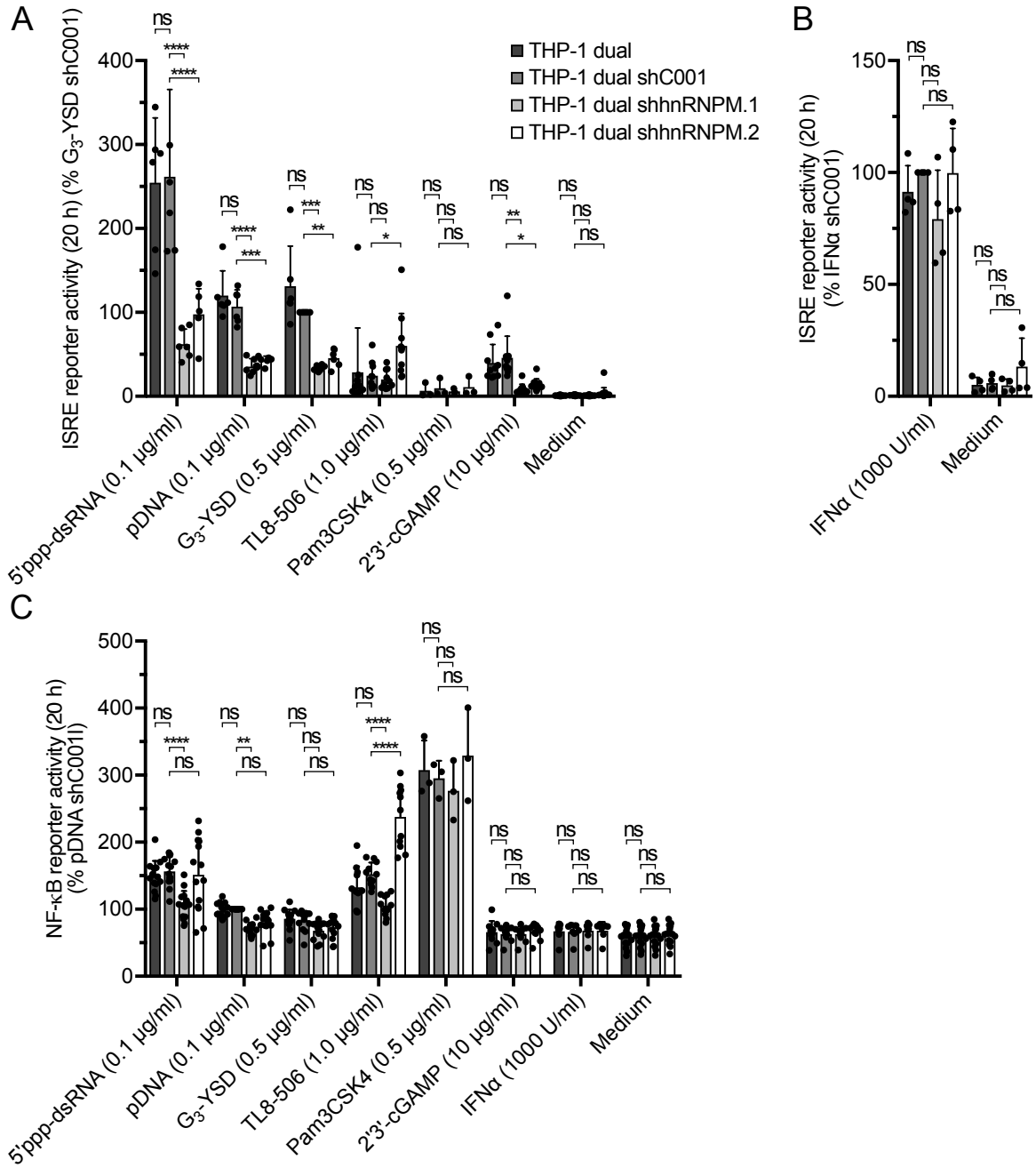

Fig. 3.3: hnRNPM positively regulates the RIG-I-, cGAS-, and STING-dependent induction of type I IFNs.

(**A**-**B**) Control cells (THP-1 dual, THP-1 dual shC001) and cells expressing hnRNPM-specific shRNAs (THP-1 dual shhnRNPM.1, THP-1 dual shhnRNPM.2) were stimulated with ligands activating RIG-I (5'ppp-dsRNA), cGAS (pDNA, G_3-YSD), TLR8 (TL8-506), TLR1/TLR2 (Pam3CSK4), STING (2'3'-cGAMP), IFNAR (IFNα), or left non-stimulated (Medium). 20 h after stimulation, ISRE reporter activation was determined (n ≥ 3, mean + SD, two-way ANOVA, Dunnett's (A) or Tukey's multiple comparisons test (B)). (**C**) The cell lines depicted in (A) were stimulated with the indicated ligands. After 20 h, NF-κB reporter activation was determined (n ≥ 3, mean + SD, two-way ANOVA, Dunnett's multiple comparisons test). Significances are indicated as follows: * (P < 0.05), ** (P < 0.01), *** (P < 0.001), **** (P ≤ 0.0001), ns: not significant.

For NF-κB, only Pam3CSK4 induced a potent reporter activation, which was unchanged between control and THP-1 dual hnRNPM KD cells (Fig. 3.3C). All other stimuli tested either induced very low or no detectable NF-κB reporter activities. Stimulation of RIG-I or TLR8 induced inconsistent NF-κB reporter activities in both THP-1 dual hnRNPM KD cell lines, indicating a non-specific response. In the following chapters, it will be analyzed whether hnRNPM promotes the cGAS- and RIG-I-dependent type I IFN production at (1) the translational level, (2) the transcriptional level, or (3) by controlling the activation of relevant signaling proteins.

3.1.3 KD of hnRNPM reduces *IFNB1* mRNA levels after cGAS activation

G_3-YSD induces a cGAS-dependent type I IFN response (Herzner et al., 2015).

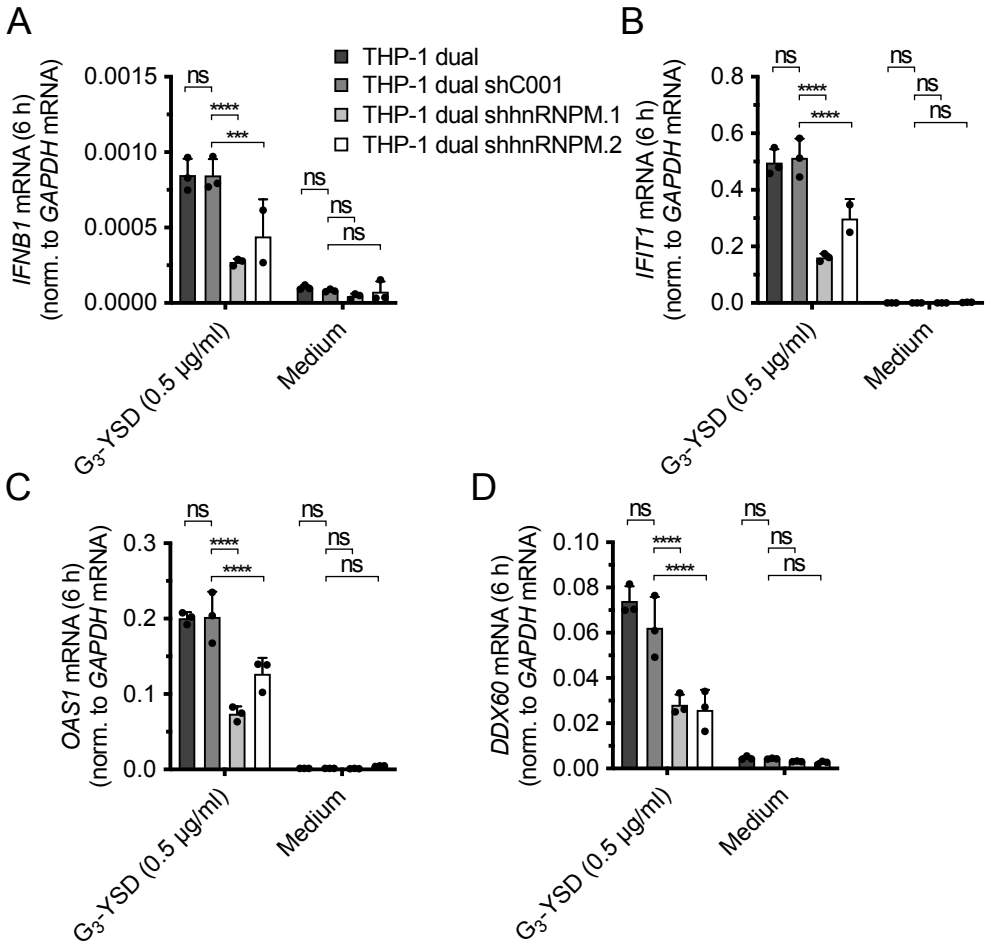

Fig. 3.4: hnRNPM promotes the cGAS-dependent expression of *IFNB1* mRNA.
(legend continued on next page)

Fig. 3.4 (continued).
(**A**-**D**) Control cells (THP-1 dual, THP-1 dual shC001) and cells expressing hnRNPM-specific shRNAs (THP-1 dual shhnRNPM.1, THP-1 dual shhnRNPM.2) were stimulated with 0.5 µg/ml G_3-YSD for 6 h or left non-stimulated (Medium). Following, the mRNA levels of *IFNB1*, *IFIT1*, *OAS1*, and *DDX60* were determined by qPCR and normalized to *GAPDH* mRNA (n ≥ 2, mean + SD, two-way ANOVA, Dunnett's multiple comparisons test). Significances are indicated as follows: * (P < 0.05), ** (P < 0.01), *** (P < 0.001), **** (P ≤ 0.0001), ns: not significant.

As shown by qPCR analysis, KD of hnRNPM in THP-1 dual cells reduced the cGAS-dependent mRNA expression of *IFNB1*, *IFIT1*, *OAS1*, and *DDX60*, suggesting that hnRNPM is not involved in the translation of *IFNB1* mRNA (Fig. 3.4). The expression of these transcripts correlated with the expression of hnRNPM (Fig. 3.2A), indicating an hnRNPM-dependent effect.

3.1.4 hnRNPM promotes the phosphorylation of IRF3 and TBK1

To further analyze how hnRNPM regulates the production of type I IFNs, phosphorylation of TBK1 and IRF3 was analyzed by immunoblotting 3 h after activation of cGAS or RIG-I. Intriguingly, KD of hnRNPM substantially decreased the levels of IRF3 phosphorylated at Ser396 (pIRF3-Ser396) after stimulation of cGAS or RIG-I, without lowering total IRF3 expression (Fig. 3.5A). Of note, THP-1 dual hnRNPM KD cells also exhibited diminished levels of TBK1 phosphorylated at Ser172 (pTBK1-Ser172) after cGAS activation (Fig. 3.5A). By contrast, stimulation of RIG-I only induced low levels of pTBK1-Ser172, which were unchanged between control and THP-1 dual hnRNPM KD cells.
To evaluate whether the observed phenotype is specific for IRF3 and TBK1 or whether other immune-related phosphorylation events are also diminished in THP-1 dual hnRNPM KD cells, phosphorylation of STAT1 was analyzed 30 min and 60 min after stimulation with 1000 U/ml IFNα. Compared to wildtype and shC001-expressing THP-1 dual cells, KD of hnRNPM did not affect the IFNα-induced phosphorylation of STAT1 at Tyr701 (pSTAT1-Tyr701), demonstrating that hnRNPM has a specific effect upstream of TBK1 phosphorylation and that the JAK-STAT signaling pathway is intact (Fig. 3.5B). In summary, these results suggest that hnRNPM amplifies the cGAS- and RIG-I-mediated type I IFN induction in a non-redundant manner by controlling the phosphorylation of IRF3 and/or TBK1 through a yet unknown mechanism.

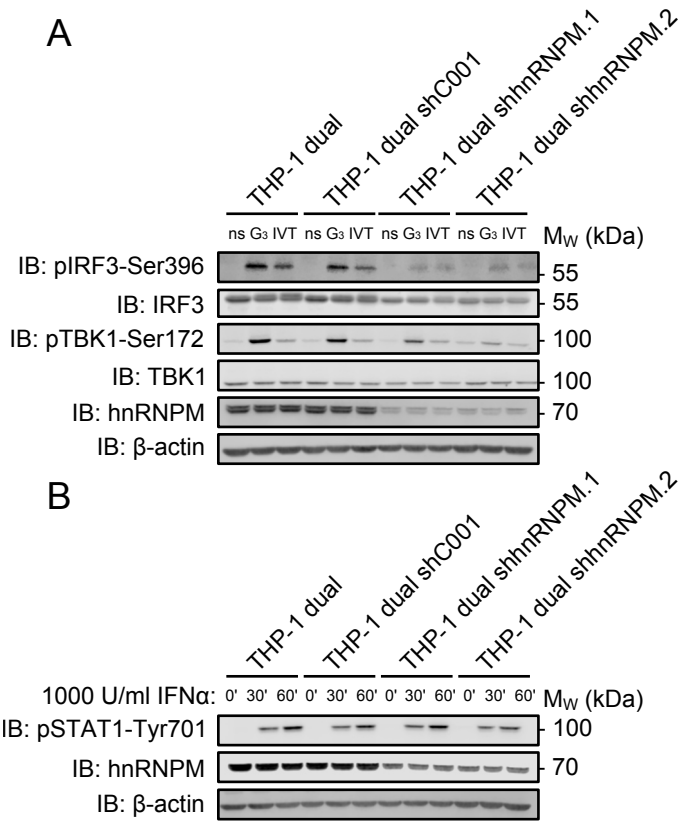

Fig. 3.5: hnRNPM promotes the cGAS- and RIG-I-dependent phosphorylation of IRF3 and the cGAS-dependent phosphorylation of TBK1.
(**A**) Control cells (THP-1 dual, THP-1 dual shC001) and cells expressing hnRNPM-specific shRNAs (THP-1 dual shhnRNPM.1, THP-1 dual shhnRNPM.2) were stimulated with 0.5 µg/ml G_3-YSD (G_3), 0.1 µg/ml 5'ppp-dsRNA (IVT), or left non-stimulated (ns). After 3 h, CCLs were generated and analyzed by immunoblotting with the indicated antibodies. One representative experiment of two independent experiments is shown. (**B**) The cell lines depicted in (A) were stimulated with 1000 U/ml IFNα for 30 min (30'), 60 min (60'), or left non-stimulated (0'). Afterwards, CCLs were generated and analyzed by immunoblotting with the indicated antibodies. One representative experiment of two independent experiments is shown.

3.1.5 hnRNPM positively regulates the RIG-I-induced secretion of IP10 in HeLa cells

In principle, any cell is susceptible to viral infections, thus antiviral defense mechanisms are not a privilege of immune cells. To test the type I IFN-inducing capacities of hnRNPM in non-immune cells, KD of hnRNPM was performed in HeLa cells. Notably, HeLa hnRNPM KD cells secreted lower amounts of IP10, a surrogate parameter for type I IFNs, after stimulation of RIG-I with 5'ppp-dsRNA (Fig. 3.6B). Similar to THP-1 dual cells, the expression of shhnRNPM.1 resulted in a stronger KD of hnRNPM as compared to

shhnRNPM.2 (Fig. 3.6A). The RIG-I-induced secretion of IP10 correlated with the hnRNPM KD efficiency, indicating that hnRNPM is a specific modulator of the type I IFN response in HeLa cells. In contrast to 5'ppp-dsRNA, no IP10 was secreted after lipofection of pDNA or G_3-YSD, suggesting that HeLa cells do not contain a functional cGAS-STING signaling axis. Collectively, these results indicate that the type I IFN-inducing function of hnRNPM is not restricted to myeloid cells but is also present in certain somatic cell lines.

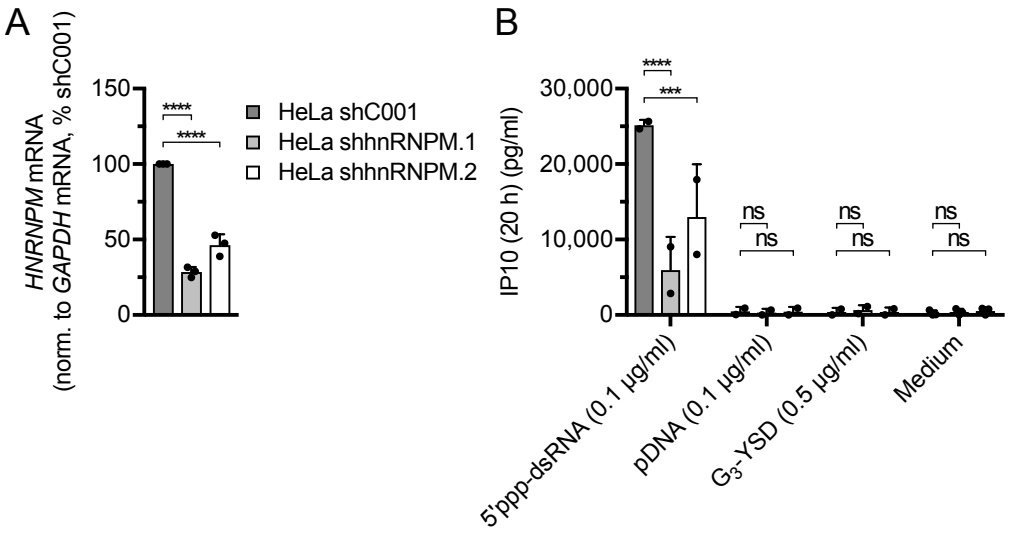

Fig. 3.6: hnRNPM promotes the RIG-I-induced secretion of IP10 in HeLa cells.
(**A**) HeLa cells were lentivirally transduced to stably express shC001 or shRNAs directed against hnRNPM (shhnRNPM.1, shhnRNPM.2). The mRNA expression of *HNRNPM* was determined by qPCR and normalized to *GAPDH* mRNA (n = 3, mean + SD, one-way ANOVA, Dunnett's multiple comparisons test). (**B**) The cell lines depicted in (A) were stimulated with ligands activating RIG-I (5'ppp-dsRNA), cGAS (pDNA, G_3-YSD), or left non-stimulated (Medium). After 20 h, the secretion of IP10 was analyzed by ELISA (n = 2, mean + SD, two-way ANOVA, Dunnett's multiple comparisons test). Significances are indicated as follows: * ($P < 0.05$), ** ($P < 0.01$), *** ($P < 0.001$), **** ($P \leq 0.0001$), ns: not significant.

3.1.6 hnRNPM mediates type I IFN production in response to HSV-1 and *L. monocytogenes* infections and prevents replication of HSV-1

To examine whether hnRNPM controls the induction of type I IFNs after infection with relevant pathogens, THP-1 dual hnRNPM KD cells were infected with HSV-1 (strain F; MOI 5) and live *L. monocytogenes* (strain EGD; MOI 1). HSV-1, a DNA virus, can be sensed by the cGAS-STING pathway (Sun et al., 2013). *L. monocytogenes* is an intracellular gram-positive bacterium capable of infecting a broad range of cell types and known to cause listeriosis (Barbuddhe and Chakraborty, 2009). In macrophages, *L. monocyto-*

genes ruptures the phagosomal membrane with its hemolysin listerolysin O to escape into the cytoplasm, its preferred replication niche. In human myeloid cells, the *L. monocytogenes*-induced production of type I IFNs is primarily dependent on cGAS, STING, and gamma-interferon-inducible protein 16 (IFI16) (Hansen et al., 2014). For both HSV-1 and *Listeria* infection, ISRE reporter activation was hnRNPM-dependent in THP-1 dual cells (Fig. 3.7A and Fig. 3.7B). Similar to previous experiments, the degree of ISRE reporter inhibition correlated with the expression of hnRNPM (Fig. 3.2A), suggesting that hnRNPM is a specific modulator of the innate immune response against HSV-1 and *Listeria*.

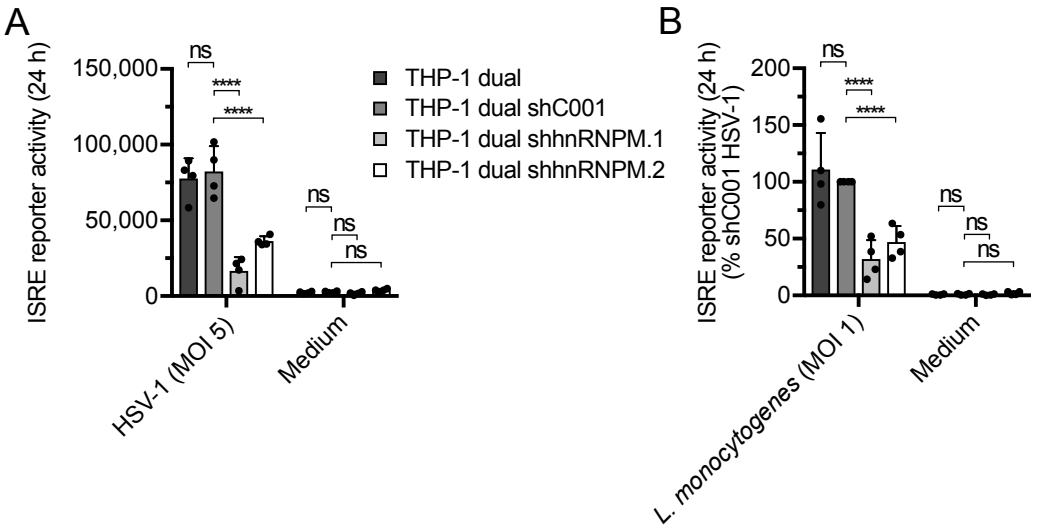

Fig. 3.7: hnRNPM promotes the production of type I IFNs induced by infections with HSV-1 and *L. monocytogenes*.
(**A**) Control cells (THP-1 dual, THP-1 dual shC001) and cells expressing hnRNPM-specific shRNAs (THP-1 dual shhnRNPM.1, THP-1 dual shhnRNPM.2) were infected with HSV-1 (strain F; MOI 5) or left non-stimulated (Medium). 24 h after infection, ISRE reporter activation was analyzed (n = 4, mean + SD, two-way ANOVA, Dunnett's multiple comparisons test). (**B**) The cell lines depicted in (A) were infected with *L. monocytogenes* (strain EGD; MOI 1) or left non-stimulated (Medium). 24 h after infection, ISRE reporter activation was analyzed (n = 4, mean + SD, two-way ANOVA, Dunnett's multiple comparisons test). Significances are indicated as follows: * ($P < 0.05$), ** ($P < 0.01$), *** ($P < 0.001$), **** ($P \leq 0.0001$), ns: not significant.

Type I IFNs can signal via the JAK-STAT pathway in an autocrine and paracrine fashion, eventually leading to the formation of an antimicrobial state. Because hnRNPM positively regulates the HSV-1-induced production of type I IFNs in THP-1 dual cells, replication of HSV-1 was examined by qPCR (Fig. 3.8). Of note, the RNA levels of HSV-1 at MOI 0.1 (Fig. 3.8A) and MOI 0.01 (Fig. 3.8B) were significantly increased in hnRNPM-depleted

cells 24 h after infection, indicating that hnRNPM restricts HSV-1 replication. By contrast, HSV-1 infection did not alter the *HNRNPM* mRNA expression (Fig. 3.8). Collectively, the results of this chapter suggest that hnRNPM is a positive regulator of the innate immune response against HSV-1 and *Listeria* and that hnRNPM is capable of blocking HSV-1 propagation.

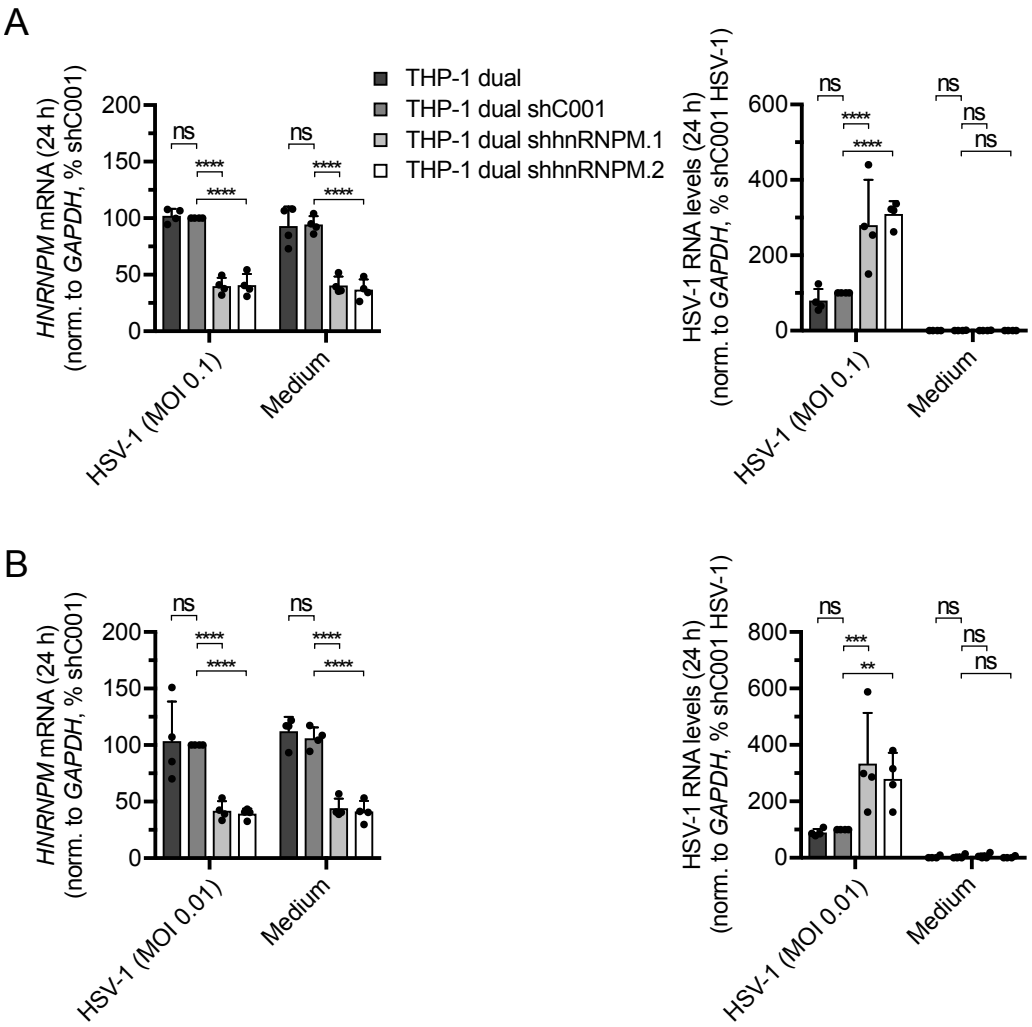

Fig. 3.8: hnRNPM is an antiviral restriction factor for HSV-1.
(**A**-**B**) Control cells (THP-1 dual, THP-1 dual shC001) and cells expressing hnRNPM-specific shRNAs (THP-1 dual shhnRNPM.1, THP-1 dual shhnRNPM.2) were infected with HSV-1 (strain F; MOI 0.1), HSV-1 (strain F; MOI 0.01), or left non-stimulated (Medium). After 24 h, HSV-1-specific transcript levels and *HNRNPM* mRNA expression were determined by qPCR and normalized to *GAPDH* mRNA (n = 4, mean + SD, two-way ANOVA, Dunnett's multiple comparisons test). Significances are indicated as follows: * ($P < 0.05$), ** ($P < 0.01$), *** ($P < 0.001$), **** ($P \leq 0.0001$), ns: not significant.

3.1.7 hnRNPM is a predominantly nuclear protein

Previously, RNAi against hnRNPM was shown to enhance the replication of Semliki Forest virus, Sindbis virus, and Chikungunya virus (Varjak et al., 2013). In addition, these viruses have been described to induce translocation of hnRNPM from the nucleus to the cytoplasm (Varjak et al., 2013). Although the results of this thesis indicate that hnRNPM is an important factor of the cGAS- and RIG-I-dependent type I IFN response, it remained elusive how hnRNPM, a nuclear protein, influences these signaling cascades. It was hypothesized that hnRNPM translocates from the nucleus to the cytosol after activation of cGAS or RIG-I to amplify the production of type I IFNs. Therefore, the distribution of endogenous hnRNPM was analyzed in nuclear and cytoplasmic extracts of THP-1 dual cells stimulated with 0.5 µg/ml G_3-YSD or 0.1 µg/ml 5'ppp-dsRNA. The localization of β-tubulin (cytoplasmic marker) and lamin A (nuclear marker) was analyzed to determine the separation efficiency. hnRNPM was predominantly detected in the nuclear fraction of THP-1 dual cells, with weaker signals also present in the cytoplasmic extracts (Fig. 3.9). Stimulation of cGAS (Fig. 3.9A) or RIG-I (Fig. 3.9B) induced no evident nucleocytoplasmic shuttling of hnRNPM.

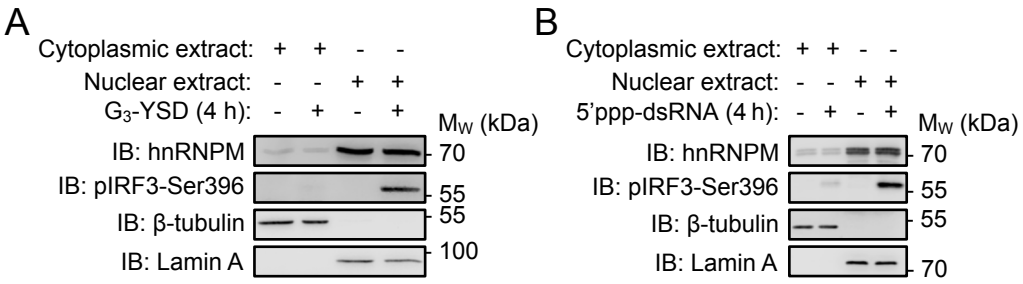

Fig. 3.9: hnRNPM is predominantly localized in the nucleus.
(**A**-**B**) THP-1 dual cells were stimulated with 0.5 µg/ml G_3-YSD, 0.1 µg/ml 5'ppp-dsRNA, or left non-stimulated. After 4 h, cytoplasmic and nuclear extracts were prepared and equal protein levels of each fraction were analyzed by immunoblotting with the indicated antibodies. One representative experiment of two independent experiments is shown.

To further evaluate the subcellular localization of hnRNPM, confocal immunofluorescence microscopy was performed. In order to facilitate sample preparation and imaging, THP-1 dual cells were treated with 100 ng/ml PMA overnight to induce maturation into an adherent, macrophage-like state. After differentiation, the cells were stimulated with AF647-labelled G_3-YSD for 4 h. Consistent with previous experiments, hnRNPM was

mostly enriched in the nuclear compartment, but weak signals were also detectable in the cytoplasm (Fig. 3.10A). No significant nucleocytoplasmic shuttling and no punctate forms of hnRNPM colocalizing with G_3-YSD were observed after cGAS activation. As a control, colocalization of cGAS and G_3-YSD was examined (Fig. 3.10B). In contrast to hnRNPM, endogenous cGAS formed distinct cytoplasmic puncta that colocalized with G_3-YSD, indicating cGAS activation (Du and Chen, 2018).

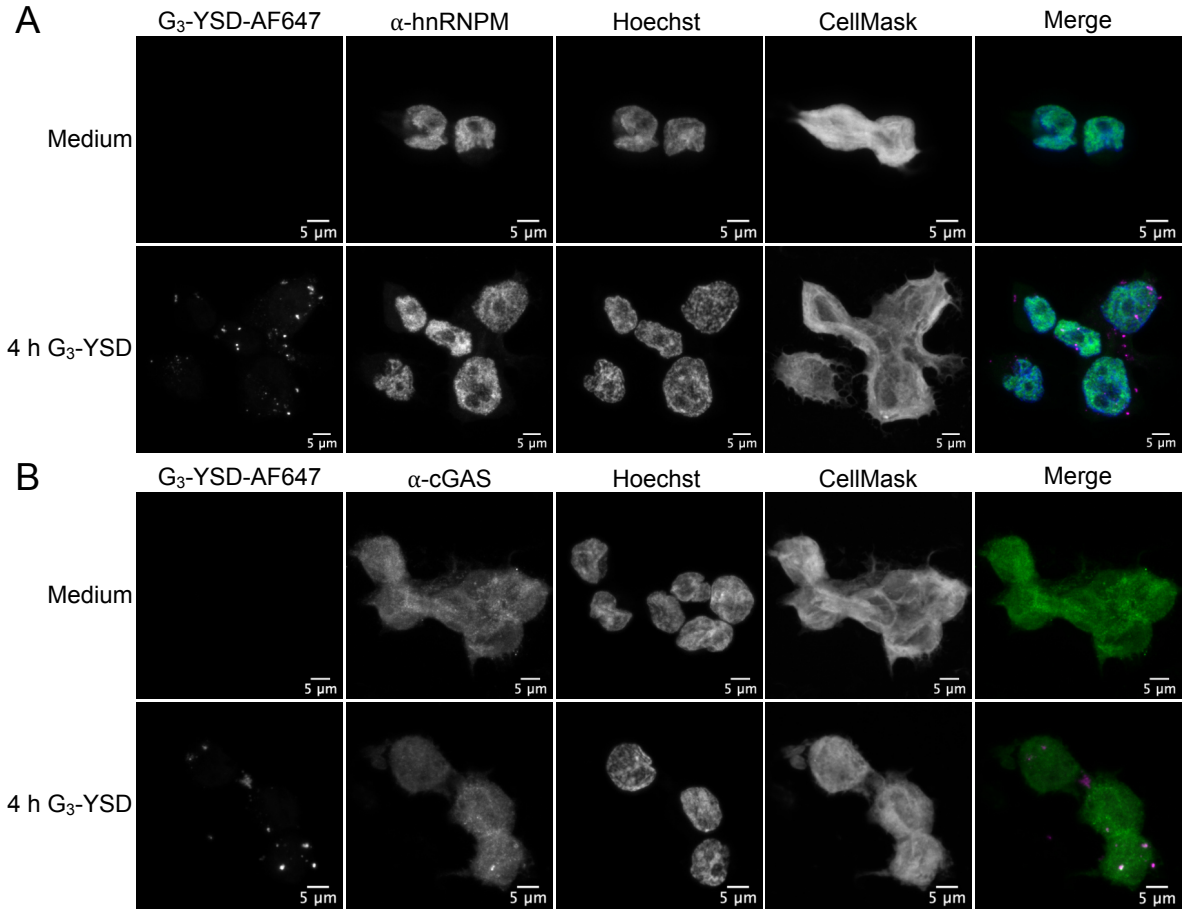

Fig. 3.10: hnRNPM is a predominantly nuclear protein.
(**A-B**) THP-1 dual cells were treated with 100 ng/ml PMA overnight. After differentiation, the cells were lipofected with 0.5 µg/ml AF647-labelled G_3-YSD or left non-stimulated (Medium). 4 h after stimulation, the cells were fixed, permeabilized, blocked, and incubated with an hnRNPM-specific antibody (A) or a cGAS-specific antibody (B) for 2 h. Following, the cells were incubated with an AF488-conjugated secondary antibody for 1 h. Nuclei and plasma membrane were counterstained with Hoechst 33342 and CellMask Orange, respectively. Z stack images were recorded in line sequential scan mode on a confocal microscope and are shown as maximum intensity projections (magenta: G_3-YSD, green: hnRNPM or cGAS, blue: Hoechst 33342). In (A), one representative experiment of two independent experiments is shown. In (B), one representative experiment is shown.

Collectively, these results suggest that hnRNPM is not actively recruited to the cytoplasm after activation of cGAS or RIG-I. Although hnRNPM exhibits distinct G_3-YSD-binding preferences *in vitro*, the *in cellulo* results presented so far imply that hnRNPM functions downstream of RIG-I, cGAS, and STING and does not meet the requirements of a novel first category nucleic acid receptor.

3.1.8 hnRNPM does not regulate the expression of the main PRRs, adaptor proteins, kinases, and transcription factors of the cGAS and RIG-I signaling pathways

Considering that hnRNPM is an RNA-binding protein involved in various cellular processes, it was hypothesized that hnRNPM indirectly regulates cGAS and RIG-I signaling by modulating the expression of active antiviral signaling proteins. Therefore, the protein levels of several components of the cytosolic nucleic acid sensing machinery in THP-1 dual hnRNPM KD cells were analyzed by immunoblotting (Fig. 3.11A).

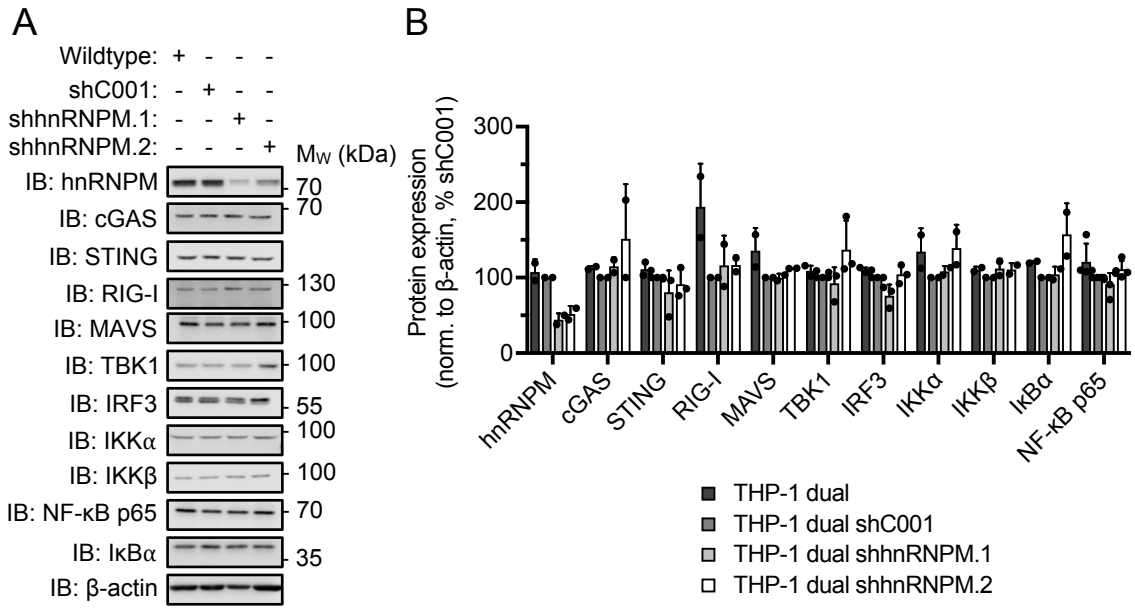

Fig. 3.11: KD of hnRNPM does not alter the protein levels of prominent components of the cGAS and RIG-I signaling pathways.
(**A**) CCLs of control cells (THP-1 dual wildtype, THP-1 dual shC001) and cells expressing hnRNPM-specific shRNAs (THP-1 dual shhnRNPM.1, THP-1 dual shhnRNPM.2) were analyzed by immunoblotting with the indicated antibodies. One representative experiment of two independent experiments is shown. (**B**) The protein intensities detected in (A) were quantified and normalized to β-actin (n = 2, mean + SD).

Quantification of the detected signal intensities revealed that KD of hnRNPM does not reduce the expression of cGAS, RIG-I, adaptor proteins (i.e., STING, MAVS), kinases (i.e., TBK1, IKKα, IKKβ), and transcription factors (i.e., IRF3, NF-κB p65) at the protein level (Fig. 3.11B). Because only a small fraction of signaling proteins was tested, it cannot be excluded that hnRNPM regulates the expression or splicing of other proteins involved in cGAS and RIG-I signaling. Profiling of the global mRNA landscape showed that the expression of genes associated with cGAS and RIG-I signaling is not downregulated in THP-1 dual hnRNPM KD cells (data not shown). However, since the KD efficiency of hnRNPM was relatively low, the results of this analysis were not included in this thesis.

3.2 Mass spectrometric identification of hnRNPM interaction partners

3.2.1 Mapping the interactome of hnRNPM by MS

Many proteins are part of protein complexes and rely on direct protein:protein interactions to fulfill their functions (Hein et al., 2015). Considering that hnRNPM has no enzymatic activity, it was hypothesized that hnRNPM promotes the production of type I IFNs by interacting with proteins involved in cGAS and RIG-I signaling. To identify novel hnRNPM interactors with functional relevance for cGAS and RIG-I signaling, a combined AP-MS/RNAi screening approach was performed. The first step of this workflow was the infection of THP-1 dual cells with lentiviral constructs encoding for C-terminally GFP-tagged hnRNPM or GFP (biological control). GFP-positive cells were sorted by FACS to isolate populations with comparable GFP expression levels. Following, the fusion proteins were immunoprecipitated from lysates of resting or cGAS-activated cells (0.5 µg/ml G_3-YSD for 3 h) using GFP-Trap magnetic agarose beads. After extensive washing, bound proteins were identified by MS (collaboration with Prof. Andreas Pichlmair (TU Munich, Germany); sample processing after IP and MS data analysis were performed by Dr. Antonio Piras and Christian Urban).

Immunoblot analysis confirmed that hnRNPM-GFP (above 100 kDa) and GFP (below 35 kDa) were expressed and that constitutive expression of these fusion proteins did not alter the cGAS- or RIG-I-induced phosphorylation of TBK1 and IRF3 (Fig. 3.12A). Although the cell lines were sorted by FACS, hnRNPM-GFP was significantly less expressed than GFP. Nonetheless, the fusion proteins could be efficiently immunoprecipitated, with degradation products detectable for hnRNPM-GFP below the 100 kDa marker

(Fig. 3.12B). By contrast, β-actin did not co-immunoprecipitate with hnRNPM-GFP or GFP, indicating high specificity of the GFP-Trap magnetic agarose beads towards the GFP tag (Fig. 3.12B). Lipofection of G_3-YSD induced a robust pTBK1-Ser172 signature, indicating cGAS activation (Fig. 3.12B).

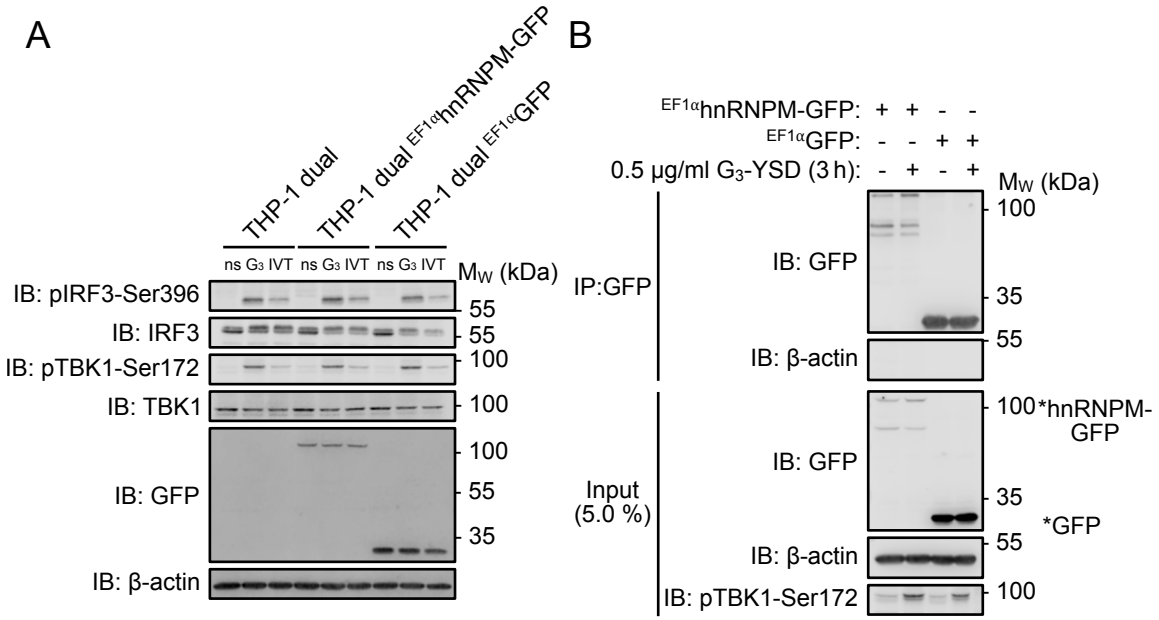

Fig. 3.12: IP of hnRNPM.
(**A**) THP-1 dual wildtype cells and THP-1 dual cells stably expressing hnRNPM-GFP or GFP (EF1α promoter) were stimulated with 0.5 µg/ml G_3-YSD (G_3), 0.1 µg/ml 5'ppp-dsRNA (IVT), or left non-stimulated (ns). After 3 h, CCLs were generated and analyzed by immunoblotting with the indicated antibodies. One representative experiment is shown. (**B**) THP-1 dual cells stably expressing hnRNPM-GFP or GFP (EF1α promoter) were stimulated for 3 h with 0.5 µg/ml G_3-YSD or left non-stimulated. After 3 h, the GFP fusion proteins were immunoprecipitated at 4 °C for 2 h and bound proteins were detected by immunoblotting with the indicated antibodies. 5.0 % of the CCLs were used as input controls. One representative experiment of two independent experiments is shown.

The hnRNPM interactomes in the non-stimulated state (Fig. 3.13A) and after cGAS activation (Fig. 3.13B) are visualized as volcano plots (for the full data sets see the reference in chapter 9.1 of the appendix). Because different MS analyses were performed and due to the shear mass of detected signals, it should be noted that not all identified proteins could be depicted in Fig. 3.13.

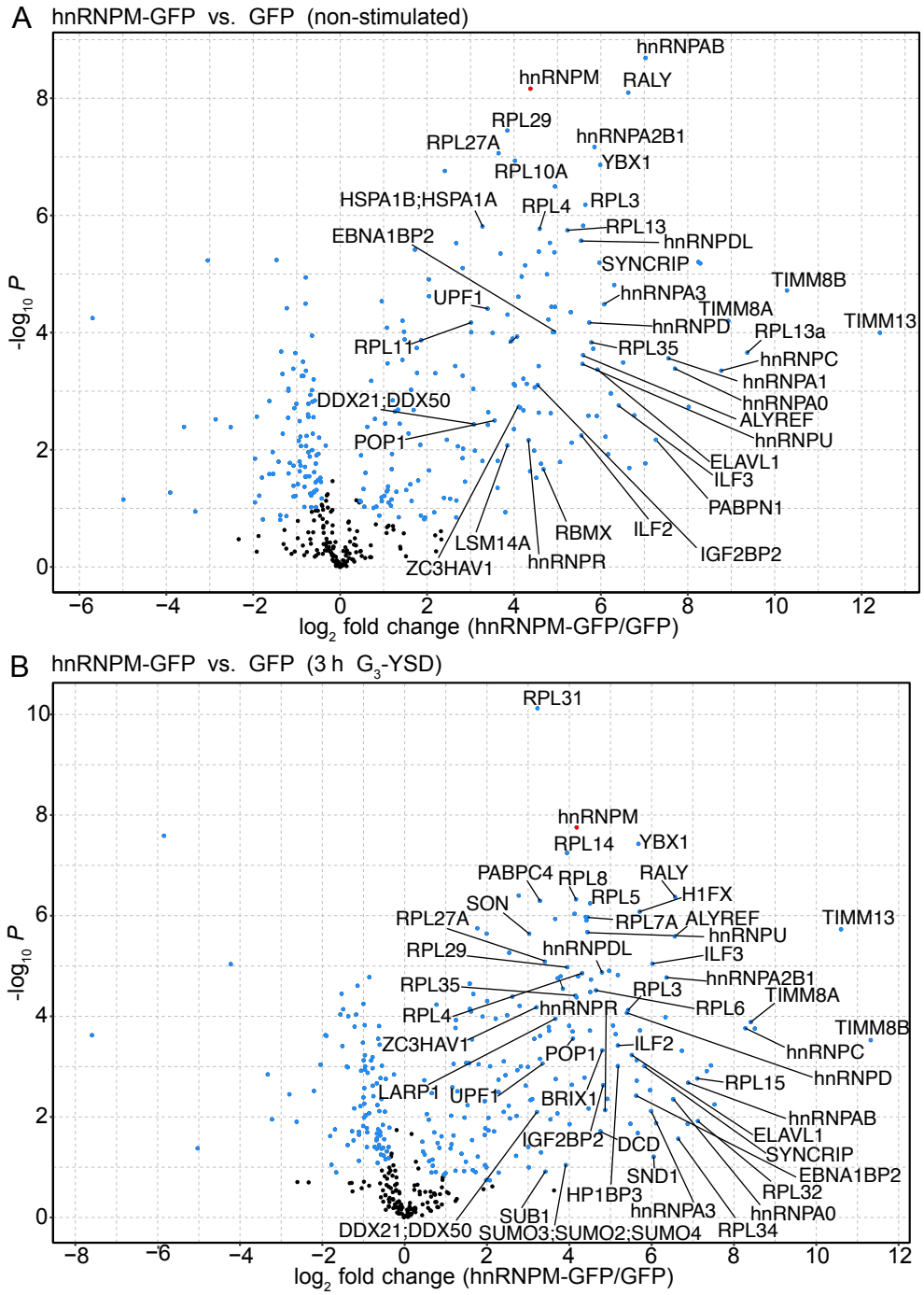

Fig. 3.13: Interactome of hnRNPM in the resting state and after cGAS activation. (**A**-**B**) THP-1 dual cells stably expressing hnRNPM-GFP or GFP were stimulated with 0.5 µg/ml G_3-YSD or left non-stimulated. After 3 h, CCLs were generated and the GFP fusion proteins were immunoprecipitated at 4 °C for 2 h. Bound proteins were identified by MS. Welch's t-test was used to determine the statistical significance. The $\log_2$ fold change of hnRNPM-GFP vs. GFP is plotted against the statistical significance ($-\log_{10} P$). hnRNPM is highlighted in red. Some of the significantly enriched proteins (blue) are highlighted with name tags. Proteins that are not significantly enriched are shown as black data points (MS analysis was performed by Dr. Antonio Piras and Christian Urban).

Several proteins specifically co-immunoprecipitated with hnRNPM, including members of the hnRNP family, RNA-binding proteins (e.g., RNA-binding protein raly (RALY), insulin-like growth factor 2 mRNA-binding protein 2 (IGF2BP2), probable rRNA-processing protein EBP2 (EBNA1BP2)), ribosomal proteins (RPL, RPS), and components of the spliceosome. Interestingly, some hnRNPM interactors have already been described in the context of nucleic acid immunity (i.e., DNA-dependent protein kinase catalytic subunit (PRKDC; also known as DNA-PKcs), ELAV-like protein 1 (ELAVL1), protein LSM14 homolog A (LSM14A), ATP-dependent RNA helicase A (DHX9), pre-mRNA-splicing factor ATP-dependent RNA helicase DHX15 (DHX15), and zinc finger CCCH-type antiviral protein 1 (ZC3HAV1)) (Burleigh et al., 2020; Ferguson et al., 2012; Hayakawa et al., 2011; Herdy et al., 2015; Kim et al., 2010; Liu et al., 2016; Pattabhi et al., 2019; Sueyoshi et al., 2018; Zhang et al., 2011). Some hnRNPM interactors were primarily enriched in the non-stimulated condition (i.e., LSM14A), while other proteins were only detected after cGAS activation (i.e., activated RNA polymerase II transcriptional coactivator p15 (SUB1), monocarboxylate transporter 10 (SLC16A10), and dermcidin (DCD)), indicating that some interactions of hnRNPM are dynamically regulated.

3.2.2 RNAi confirms ELAVL1 and SON as modulators of cGAS and RIG-I signaling

To identify novel proteins that regulate the cGAS- and RIG-I-dependent type I IFN response in a manner similar to hnRNPM, 39 different candidate hnRNPM interactors were targeted by RNAi.

The target gene KD was evaluated by qPCR. Except for *HNRNPU* and *LSM14A*, the KD of the respective target gene was confirmed in two independent shRNA-expressing cell lines (Fig. 3.14). After KD validation, the THP-1 dual KD cell lines were stimulated with cGAS or RIG-I agonists and then the ISRE reporter activation was analyzed (Fig. 3.15). For simplicity, ISRE reporter activities were normalized to the signals measured in shC001-expressing cells treated with the same stimuli (Fig. 3.15). In the non-stimulated condition, no ISRE reporter activation was detected (data not shown). As expected, the cGAS- or RIG-I-mediated type I IFN response was not consistently downregulated in most THP-1 dual KD cell lines (36/39). This included nuclear pore complex protein 155 (NUP155) and NUP98, different hnRNPs, and unexpectedly, also reported modulators of

the type I IFN response (i.e., PRKDC and ZC3HAV1). For cathepsin G (CTSG), DHX9, DHX15, hnRNPAB, and dolichyl-diphosphooligosaccharide-protein glycosyltransferase subunit 1 (RPN1), cGAS and RIG-I signaling was inhibited in one KD cell line. However, since this inhibitory effect could not be observed in the second target-specific THP-1 dual KD cell line, this phenotype was considered non-specific. Similarly, ISRE reporter activation was not attenuated in hnRNPU KD or LSM14A KD THP-1 dual cells.

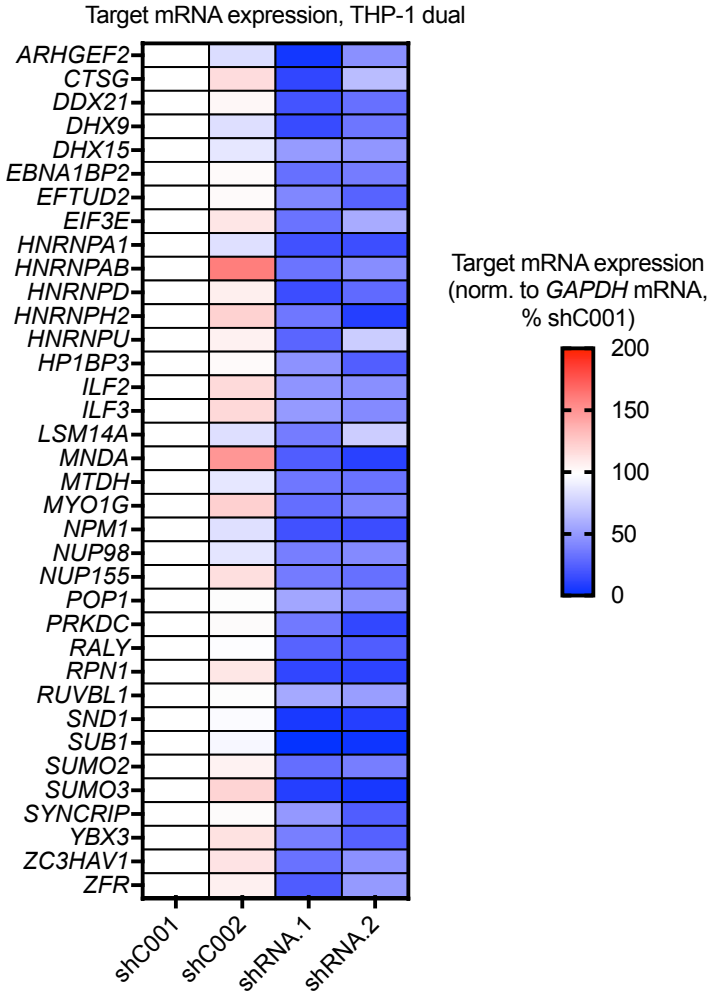

Fig. 3.14: KD validation of hnRNPM candidate interactors.
Control cells (THP-1 dual shC001, THP-1 dual shC002) and cells expressing target-specific shRNAs were analyzed by qPCR to determine the relative target gene KD efficiencies. The target mRNA expression (row labels indicate target genes) was normalized to *GAPDH* mRNA and correlated with the normalized target mRNA expression in THP-1 dual shC001 cells (n ≥ 2, mean).

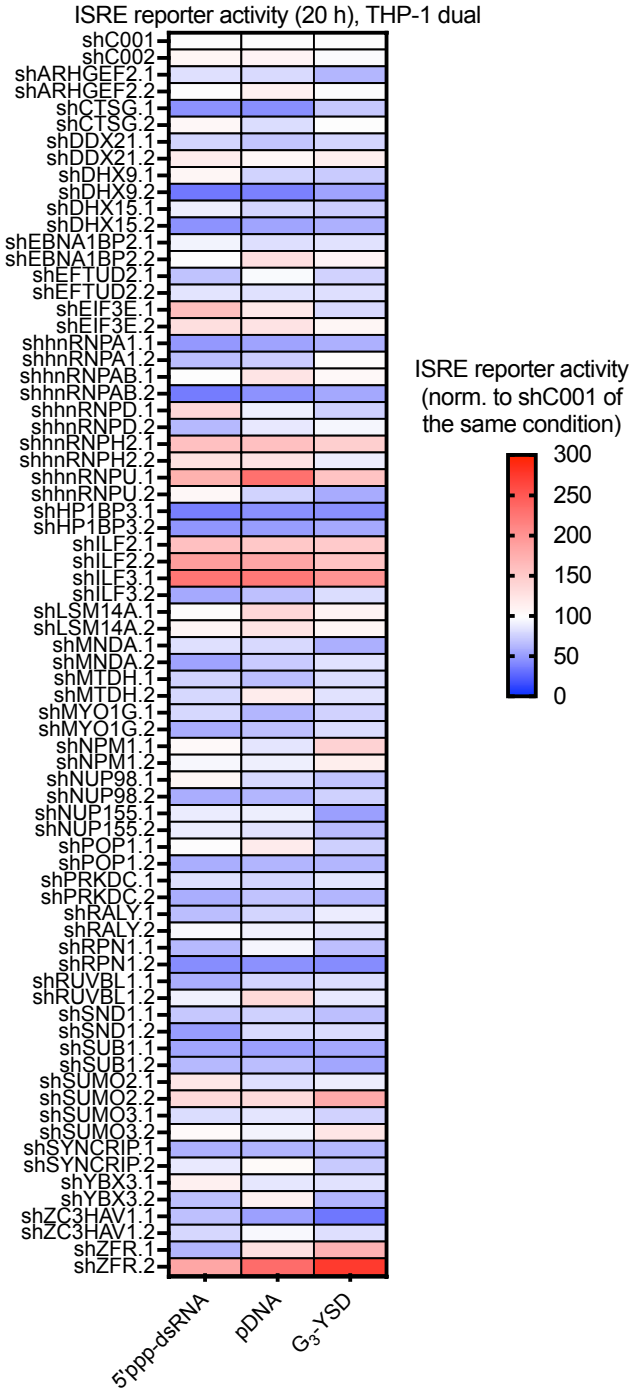

Fig. 3.15: ISRE reporter analysis after KD of different hnRNPM candidate interactors.

Control cells (THP-1 dual shC001, THP-1 dual shC002) and cells expressing target-specific shRNAs (row labels indicate control and target-specific shRNAs) were stimulated with ligands activating RIG-I (0.1 µg/ml 5'ppp-dsRNA), cGAS (0.1 µg/ml pDNA, 0.5 µg/ml G_3-YSD), or left non-stimulated. After 20 h, ISRE reporter activation was analyzed. For simplicity, the stimulation-specific ISRE reporter activation was normalized to the respective signal measured in shC001-expressing cells. No ISRE reporter activation was detected in the non-stimulated condition (data not shown) (n ≥ 2, mean).

Of note, KD of protein SON (SON), ELAVL1, and IGF2BP2 substantially reduced the secretion of type I IFNs in response to cytosolic 5'ppp-dsRNA or pDNA (Fig. 3.16A-3.16B, Fig. 3.17A-3.17B, Fig. 3.18A-3.18B). SON and IGF2BP2 have not yet been described in the context of innate antiviral immunity. For ELAVL1, two different groups have already reported a link to type I IFN production. In 2015, Herdy *et al.* have proposed that ELAVL1 stabilizes *IFNB1* mRNA, while Sueyoshi *et al.* have postulated that ELAVL1 stabilizes the mRNA of *PLK2* (encodes for serine/threonine-protein kinase PLK2 (PLK2)), a gene associated with the nuclear transport of IRF3 (Herdy et al., 2015; Sueyoshi et al., 2018).

To further investigate how SON, ELAVL1, and IGF2BP2 promote the expression of type I IFNs in THP-1 dual cells, the phosphorylation of TBK1 and IRF3 was analyzed by immunoblotting. Intriguingly, depletion of SON and ELAVL1 markedly impaired both the cGAS- and RIG-I-mediated phosphorylation of IRF3 at Ser396 (Fig. 3.16C, Fig. 3.17C). Moreover, the phosphorylation of TBK1 at Ser172 was inhibited in SON and ELAVL1 KD THP-1 dual cells after cGAS activation (Fig. 3.16C, Fig. 3.17C). The phosphorylation of IRF3 and TBK1 correlated with the KD efficiency of SON and ELAVL1, indicating specific pathway inhibition. Consistent with previous observations, RIG-I signaling only induced low levels of pTBK1-Ser172, which were unaltered in SON and ELAVL1 KD cells. Due to the low antibody specificity, KD of SON could not be detected at the protein level. In contrast to SON and ELAVL1, KD of IGF2BP2 did not affect the phosphorylation of IRF3 and TBK1 after cytosolic DNA or RNA challenge, indicating that IGF2BP2 might be involved in the transcriptional or translational regulation of the type I IFN response (Fig. 3.18C). In summary, a combined AP-MS/RNAi screening approach identified SON, ELAVL1, and IGF2BP2 as novel candidate hnRNPM interactors that are required for the type I IFN induction by cGAS and RIG-I in THP-1 dual monocytes.

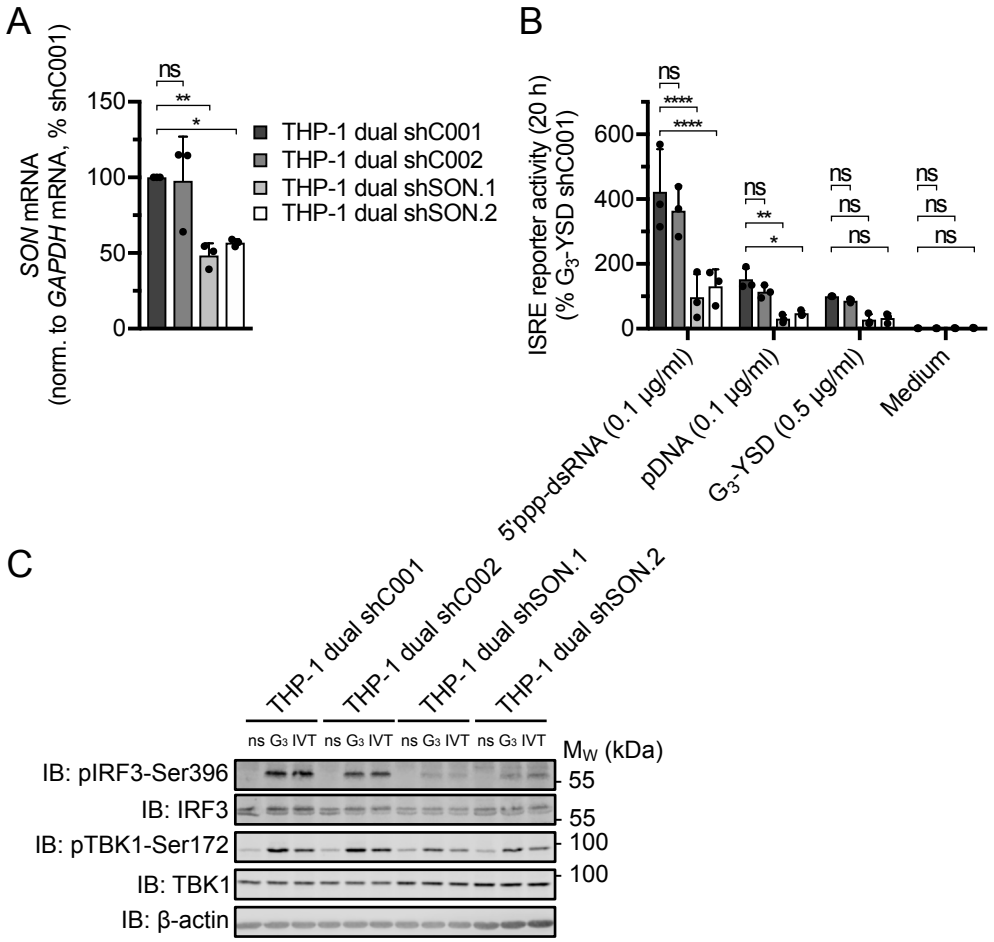

Fig. 3.16: SON promotes cGAS and RIG-I signaling.
(**A**) Control cells (THP-1 dual shC001, THP-1 dual shC002) and cells expressing SON-specific shRNAs (THP-1 dual shSON.1, THP-1 dual shSON.2) were analyzed by qPCR to determine the relative SON KD efficiency. *SON* mRNA expression was normalized to *GAPDH* mRNA (n = 3, mean + SD, one-way ANOVA, Dunnett's multiple comparisons test). (**B**) The cell lines depicted in (A) were stimulated with ligands activating RIG-I (5'ppp-dsRNA), cGAS (pDNA, G_3-YSD), or left non-stimulated (Medium). 20 h after stimulation, cell culture supernatants were harvested and ISRE reporter activation was analyzed (n = 3, mean + SD, two-way ANOVA, Dunnett's multiple comparisons test). (**C**) The cell lines depicted in (A) were stimulated with 0.5 µg/ml G_3-YSD (G_3), 0.1 µg/ml 5'ppp-dsRNA (IVT), or left non-stimulated (ns). After 3 h, CCLs were generated and analyzed by immunoblotting with the indicated antibodies. One representative experiment of two independent experiments is shown. Significances are indicated as follows: * ($P < 0.05$), ** ($P < 0.01$), *** ($P < 0.001$), **** ($P \leq 0.0001$), ns: not significant.

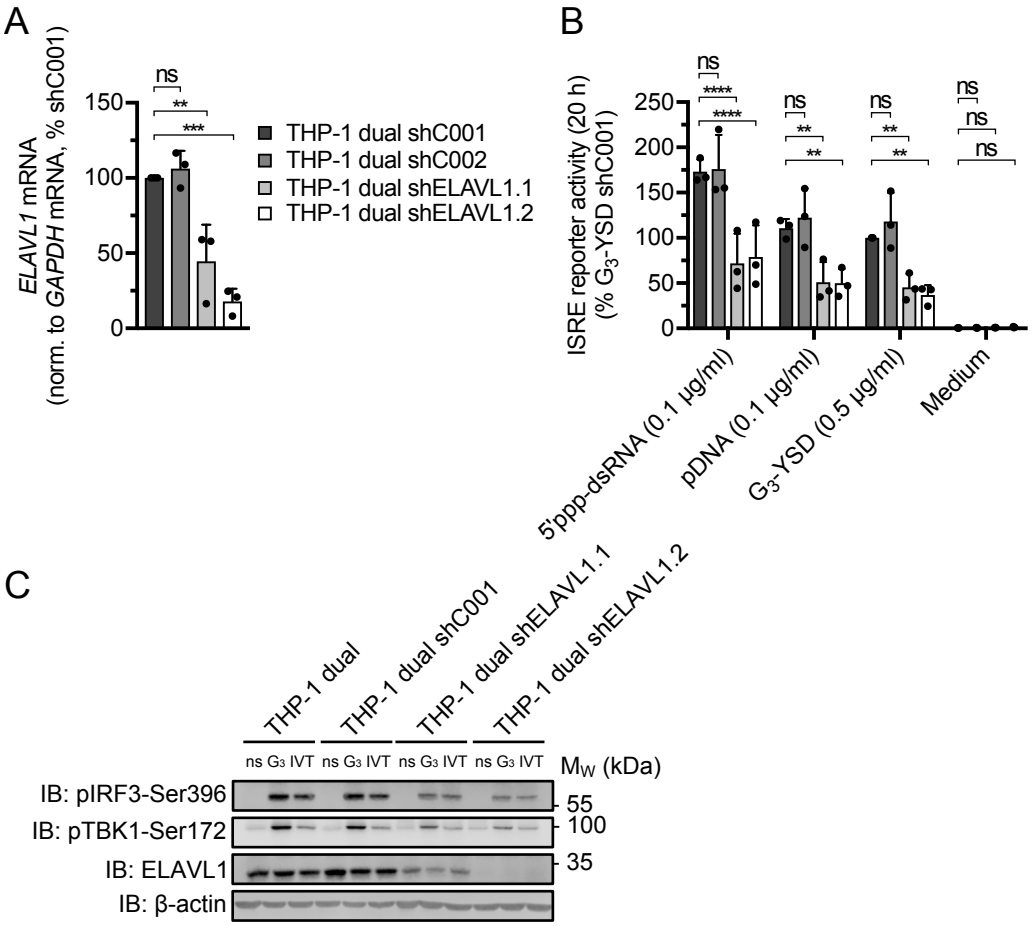

Fig. 3.17: ELAVL1 promotes cGAS and RIG-I signaling.
(**A**) Control cells (THP-1 dual shC001, THP-1 dual shC002) and cells expressing ELAVL1-specific shRNAs (THP-1 dual shELAVL1.1, THP-1 dual shELAVL1.2) were analyzed by qPCR to determine the relative ELAVL1 KD efficiency. *ELAVL1* mRNA expression was normalized to *GAPDH* mRNA (n = 3, mean + SD, one-way ANOVA, Dunnett's multiple comparisons test). (**B**) The cell lines depicted in (A) were stimulated with ligands activating RIG-I (5'ppp-dsRNA), cGAS (pDNA, G_3-YSD), or left non-stimulated (Medium). 20 h after stimulation, cell culture supernatants were harvested and ISRE reporter activation was analyzed (n = 3, mean + SD, two-way ANOVA, Dunnett's multiple comparisons test). (**C**) The indicated cell lines were stimulated with 0.5 µg/ml G_3-YSD (G_3), 0.1 µg/ml 5'ppp-dsRNA (IVT), or left non-stimulated (ns). After 3 h, CCLs were generated and analyzed by immunoblotting with the indicated antibodies. One representative experiment of two independent experiments is shown. Significances are indicated as follows: * ($P < 0.05$), ** ($P < 0.01$), *** ($P < 0.001$), **** ($P \leq 0.0001$), ns: not significant.

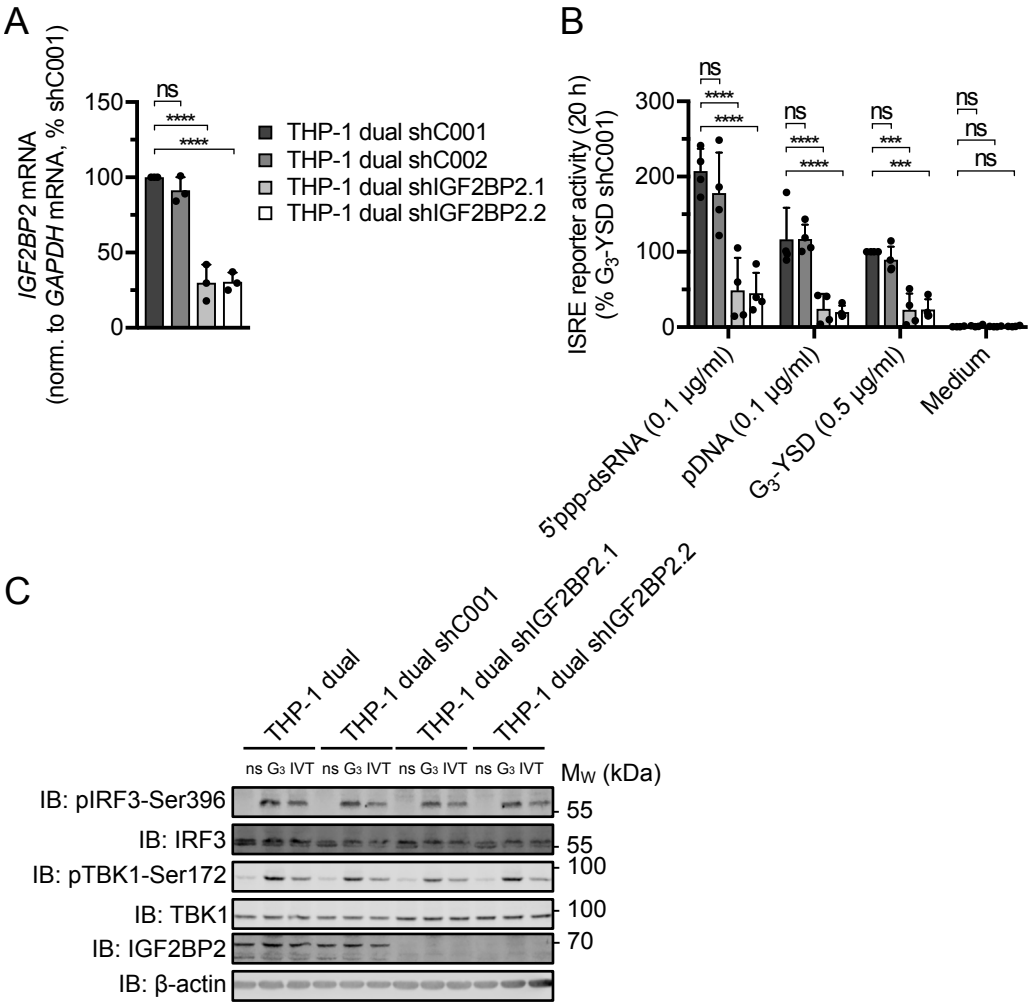

Fig. 3.18: IGF2BP2 promotes the cGAS- and RIG-I-dependent production of type I IFNs but is not involved in the phosphorylation of TBK1 and IRF3.
(**A**) Control cells (THP-1 dual shC001, THP-1 dual shC002) and cells expressing IGF2BP2-specific shRNAs (THP-1 dual shIGF2BP2.1, THP-1 dual shIGF2BP2.2) were analyzed by qPCR to determine the relative IGF2BP2 KD efficiency. *IGF2BP2* mRNA expression was normalized to *GAPDH* mRNA (n = 3, mean + SD, one-way ANOVA, Dunnett's multiple comparisons test). (**B**) The cell lines depicted in (A) were stimulated with ligands activating RIG-I (5'ppp-dsRNA), cGAS (pDNA, G_3-YSD), or left non-stimulated (Medium). 20 h after stimulation, cell culture supernatants were harvested and ISRE reporter activation was analyzed (n = 4, mean + SD, two-way ANOVA, Dunnett's multiple comparisons test). (**C**) The indicated cell lines were stimulated with 0.5 µg/ml G_3-YSD (G_3), 0.1 µg/ml 5'ppp-dsRNA (IVT), or left non-stimulated (ns). After 3 h, CCLs were generated and analyzed by immunoblotting with the indicated antibodies. One representative experiment of two independent experiments is shown. Significances are indicated as follows: * ($P < 0.05$), ** ($P < 0.01$), *** ($P < 0.001$), **** ($P \leq 0.0001$), ns: not significant.

3.2.3 SON and ELAVL1 co-immunoprecipitate with hnRNPM

To evaluate the interactions of hnRNPM with SON and ELAVL1, co-immunoprecipitations (co-IPs) were performed. Similar to the interactome analysis, hnRNPM-GFP and GFP were immunoprecipitated from lysates of resting and cGAS-activated THP-1 dual cells (Fig. 3.19A). Because hnRNPM is an RNA-binding protein, the IPs were also treated with RNase A to analyze whether the interactions occur in an RNA-dependent or -independent manner. It should be noted that IPs and immunofluorescence experiments were usually performed in cGAS-activated cells because DNA stimuli (i.e., pDNA, G_3-YSD) are more readily available in larger quantities compared to the RIG-I ligand 5'ppp-dsRNA. Since hnRNPM regulates cGAS and RIG-I signaling to similar extents, this was used as an experimental simplification.

In line with the interactome analysis, SON and IGF2BP2 selectively co-immunoprecipitated with hnRNPM (Fig. 3.19A). SON interacted with hnRNPM in an RNA-independent manner and irrespective of cGAS activation, while interactions with IGF2BP2 were sensitive to RNase A treatment (Fig. 3.19A). By contrast, no significant signals were detectable after IP of hnRNPM-GFP/GFP with an antibody recognizing endogenous ELAVL1 (data not shown), presumably due to the low sensitivity of the ELAVL1-specific antibody. To overcome this technical problem, ELAVL1-GFP was stably expressed in THP-1 dual cells and then co-immunoprecipitation of endogenous hnRNPM with ELAVL1-GFP/GFP was analyzed (Fig. 3.19B). Endogenous hnRNPM selectively co-immunoprecipitated with ELAVL1 in a stimulation-independent manner. It should be noted that ELAVL1-GFP was not easily detectable in CCLs using a GFP-specific antibody. However, bands at the expected size below the 70 kDa marker were detected after IP of ELAVL1-GFP, indicating that ELAVL1-GFP is indeed expressed. These observations further suggest that the epitope recognized by the GFP-specific antibody is masked by the ELAVL1 portion of the fusion protein. In summary, these data confirm the interactome analysis of hnRNPM and suggest that hnRNPM, ELAVL1, and SON form a multiprotein complex *in vitro*.

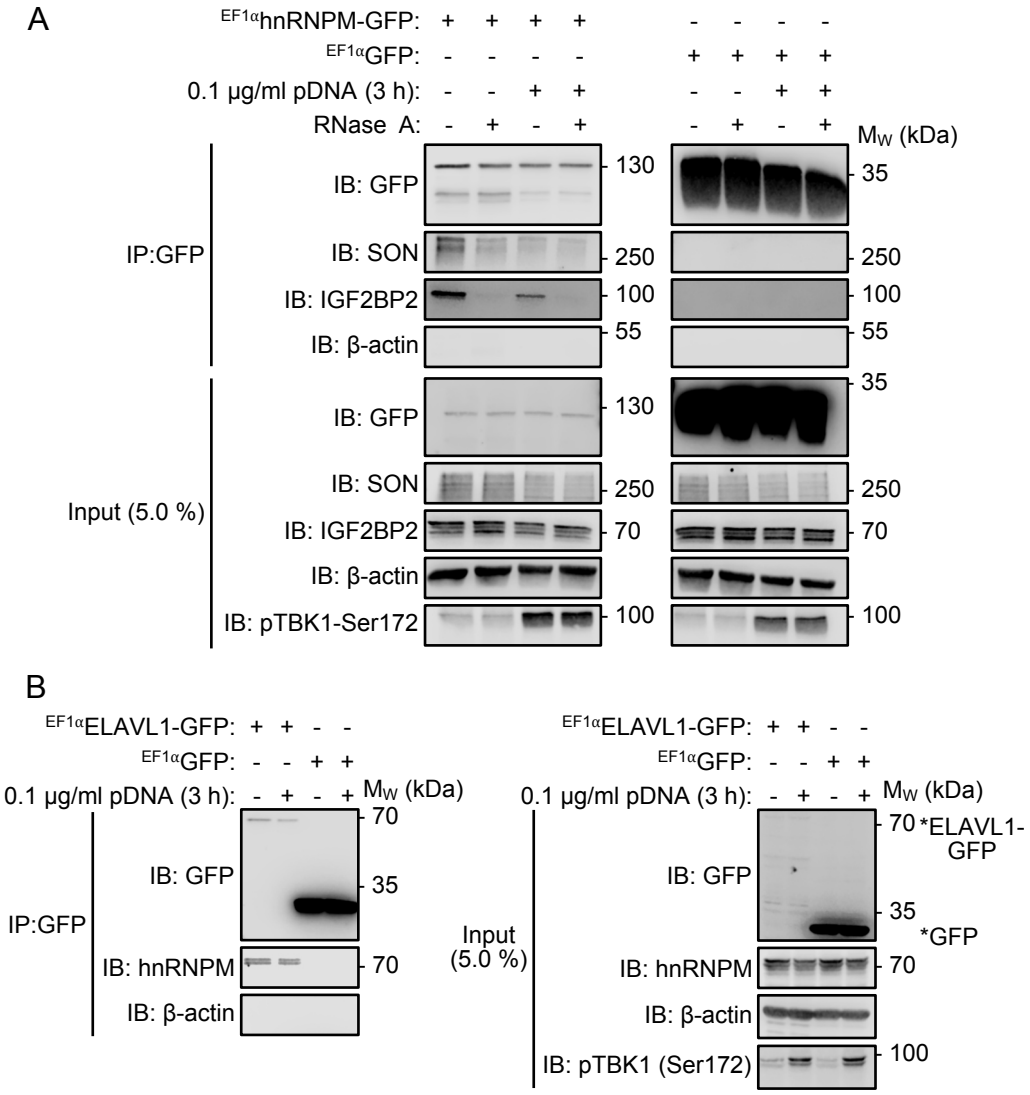

Fig. 3.19: SON co-immunoprecipitates with hnRNPM and hnRNPM co-immunoprecipitates with ELAVL1.

(**A**) THP-1 dual cells stably expressing hnRNPM-GFP or GFP were stimulated with 0.1 µg/ml pDNA or left non-stimulated. After 3 h, CCLs were generated and the GFP fusion proteins were immunoprecipitated at 4 °C overnight. If indicated, the beads were additionally treated with RNase A at 4 °C for 1.5 h. Bound proteins were eluted and analyzed by immunoblotting with the indicated antibodies. 5.0 % of the CCLs were used as input controls. One representative experiment of two independent experiments is shown. (**B**) The experiment depicted in (A) was performed with ELAVL1-GFP- or GFP-expressing THP-1 dual cells without RNase A treatment after IP. One representative experiment of two independent experiments is shown.

3.3 ELAVL1 is a positive regulator of the innate antiviral immune response

3.3.1 ELAVL1 promotes the cGAS- and RIG-I-dependent production of type I IFNs and activation of NF-κB

To provide further genetic evidence for the involvement of ELAVL1 in cGAS and RIG-I signaling, two CRISPR/Cas9 gRNAs were designed to delete the *ELAVL1* gene in THP-1 dual cells. ELAVL1 deficiency was validated by immunoblotting and/or Sanger sequencing. For three clones (gRNA AN: clone #39, clone #44; gRNA AI: clone #7), ELAVL1 protein expression was undetectable in several independent experiments (Fig. 3.20A). Sanger sequencing of the *ELAVL1* gene locus revealed that clone AN #39 contains a homozygous T insertion in the coding sequence at base position 499 of 978, inducing a frameshift in the coding sequence and a premature stop codon after 4 amino acids (data not shown). For the clones AN #44 and AI #7, the exact genomic DNA sequences could not be resolved due to sequence overlap. Notably, all ELAVL1-deficient THP-1 dual clones (ELAVL1 KO) displayed an approximate 6-fold to 8-fold inhibition of the ISRE reporter after stimulation of cGAS or RIG-I, whereas the IFNAR-induced ISRE reporter activity was ELAVL1-independent (Fig. 3.20B-3.20C).

To further verify that the inhibition of the cGAS and RIG-I signaling pathways was specifically caused by ELAVL1 deficiency and not by non-specific cleavage of Cas9, ELAVL1-FLAG was stably expressed in THP-1 dual *ELAVL1*$^{-/-}$ (AN #39) cells. Of note, in contrast to GFP overexpression, ELAVL1-FLAG expression rescued the cGAS-, STING-, and RIG-I-dependent ISRE reporter activation in ELAVL1-deficient THP-1 dual cells, indicating that ELAVL1 is a specific modulator downstream of these PRRs (Fig. 3.21A-3.21B). By contrast, the IFNα-induced ISRE reporter activity was independent of ELAVL1, suggesting that the IFNAR signaling pathway is intact (Fig. 3.21C). The TL8-506- or Pam3CSK4-triggered ISRE reporter activation was close to the detection limit in all tested cell lines (Fig. 3.21A). However, Pam3CSK4 induced a robust, ELAVL1-independent NF-κB response (Fig. 3.21D). In contrast to TLR1/TLR2, NF-κB reporter activation induced by cGAS or RIG-I was suppressed in ELAVL1-deficient THP-1 dual cells and rescued by overexpression of ELAVL1-FLAG (Fig. 3.21D). Stimulation with 2'3'-cGAMP or IFNα did not trigger a detectable NF-κB response, whereas TLR8 stimulation activated the NF-κB reporter only in wildtype cells but not in cells with *ELAVL1*$^{-/-}$ genetic background

(Fig. 3.21D). However, this effect could not be rescued by overexpression of ELAVL1-FLAG, indicating that the observed phenotype is caused by a clonal abnormality. Collectively, these results provide genetic evidence that ELAVL1, similar to its interactor hnRNPM, is a specific positive regulator of both cGAS and RIG-I signaling.

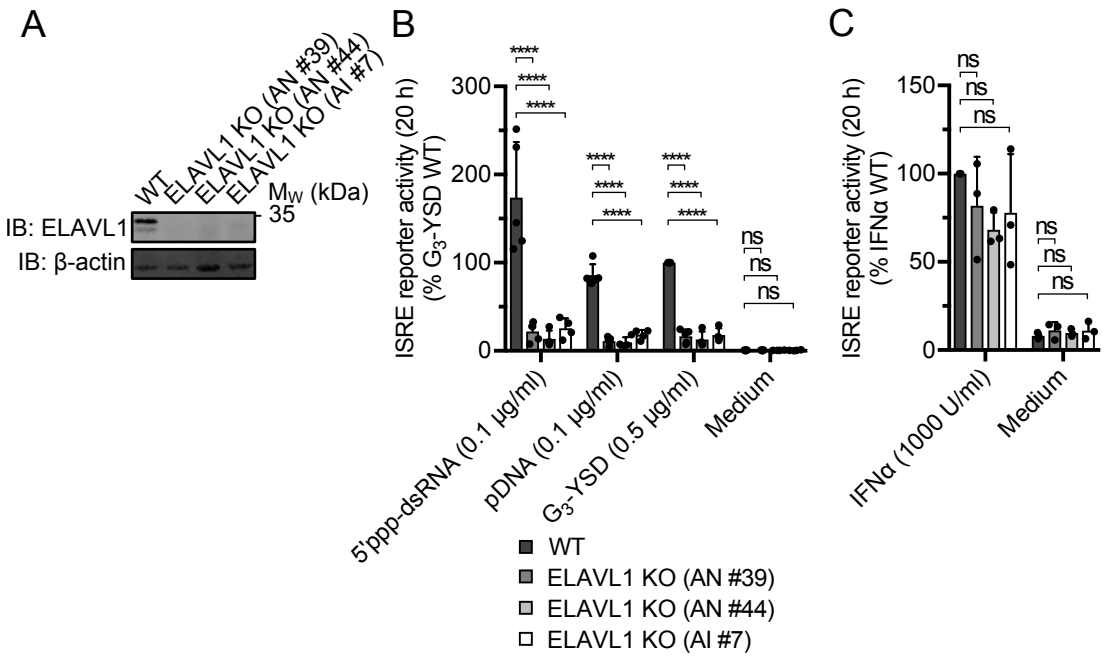

Fig. 3.20: ELAVL1 promotes the type I IFN production induced by cGAS and RIG-I. (**A**) Immunoblot analysis of THP-1 dual wildtype (WT) cells and ELAVL1-deficient THP-1 dual cells (ELAVL1 KO) (generated by CRISPR/Cas9 using gRNA AN or gRNA AI). One representative experiment of three independent experiments is shown. (**B**) The cell lines depicted in (A) were stimulated with ligands activating RIG-I (5'ppp-dsRNA), cGAS (pDNA, G_3-YSD), or left non-stimulated (Medium). After 20 h, ISRE reporter activation was analyzed (n ≥ 3, mean + SD, two-way ANOVA, Dunnett's multiple comparisons test). (**C**) The cell lines depicted in (A) were stimulated with 1000 U/ml IFNα or left non-stimulated (Medium). After 20 h, ISRE reporter activity was analyzed (n ≥ 3, mean + SD, two-way ANOVA, Dunnett's multiple comparisons test). Significances are indicated as follows: * (P < 0.05), ** (P < 0.01), *** (P < 0.001), **** (P ≤ 0.0001), ns: not significant.

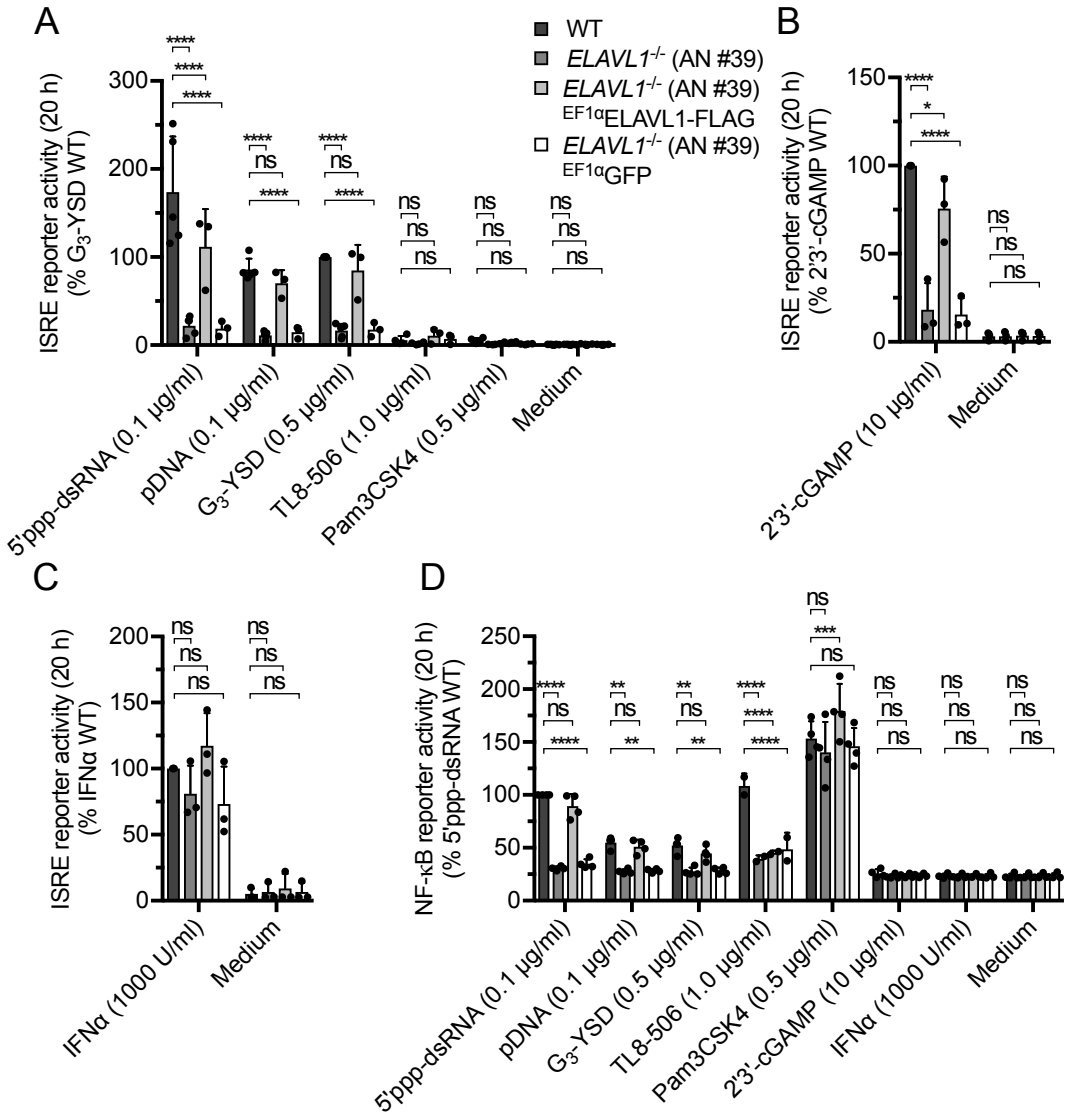

Fig. 3.21: ELAVL1 is a specific positive regulator of the cGAS- and RIG-I-dependent production of type I IFNs and activation of NF-κB.
(**A**) THP-1 dual cells (WT), THP-1 dual *ELAVL1*$^{-/-}$ (AN #39) cells, and THP-1 dual *ELAVL1*$^{-/-}$ (AN #39) cells expressing ELAVL1-FLAG or GFP (EF1α promoter) were stimulated with ligands activating RIG-I (5'ppp-dsRNA), cGAS (pDNA, G_3-YSD), TLR8 (TL8-506), TLR1/TLR2 (Pam3CSK4), or left non-stimulated (Medium). After 20 h, ISRE reporter activation was analyzed (n ≥ 3, mean + SD, two-way ANOVA, Dunnett's multiple comparisons test). (**B**) The cell lines depicted in (A) were stimulated with 10 µg/ml 2'3'-cGAMP or left non-stimulated. After 20 h, ISRE reporter activation was analyzed (n = 3, mean + SD, two-way ANOVA, Dunnett's multiple comparisons test). (**C**) The cell lines depicted in (A) were stimulated with 1000 U/ml IFNα or left non-stimulated. After 20 h, ISRE reporter activation was analyzed (n = 3, mean + SD, two-way ANOVA, Dunnett's multiple comparisons test). (**D**) The cell lines depicted in (A) were stimulated with the indicated ligands. After 20 h, NF-κB reporter activation was analyzed (n ≥ 2, mean + SD, two-way ANOVA, Dunnett's multiple comparisons test). Significances are indicated as follows: * (P < 0.05), ** (P < 0.01), *** (P < 0.001), **** (P ≤ 0.0001), ns: not significant.

Because ELAVL1 has been described to regulate mRNA stability, it was evaluated whether reduced viability of ELAVL1-deficient THP-1 dual cells leads to inhibition of cGAS and RIG-I signaling (Mukherjee et al., 2011b). MTT assay showed that the metabolic activity is unchanged between wildtype and ELAVL1-deficient THP-1 dual cells under steady state conditions and after challenge with TL8-506, Pam3CSK4, 2'3'-cGAMP, or IFNα (Fig. 3.22). By contrast, reconstitution of THP-1 dual *ELAVL1*$^{-/-}$ cells with ELAVL1-FLAG decreased the metabolic activity after activation of cGAS or RIG-I compared to ELAVL1-deficient cells.

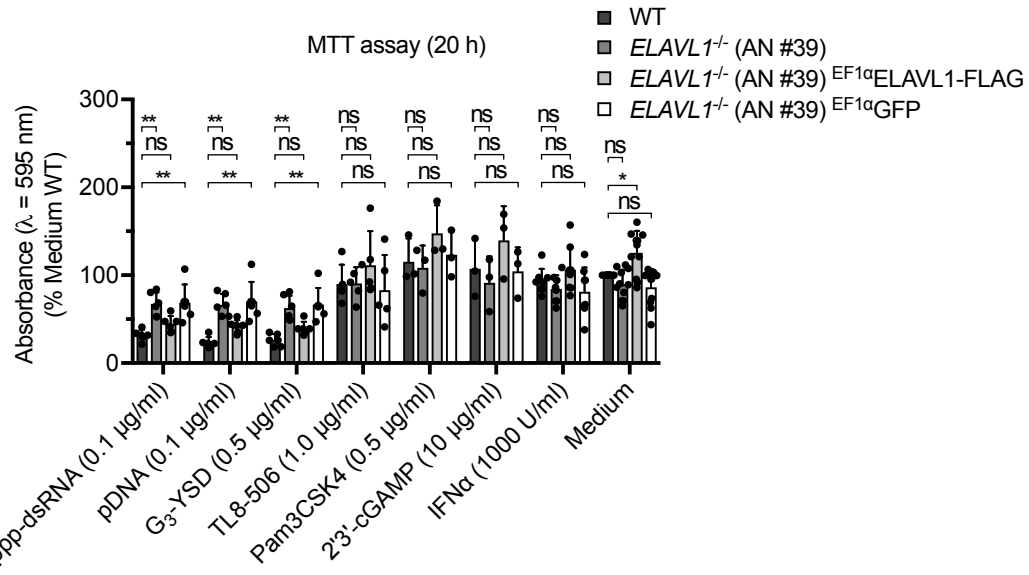

Fig. 3.22: ELAVL1-deficient THP-1 dual cells are viable.
THP-1 dual cells (WT), THP-1 dual *ELAVL1*$^{-/-}$ (AN #39) cells, and THP-1 dual *ELAVL1*$^{-/-}$ (AN #39) cells expressing ELAVL1-FLAG or GFP (EF1α promoter) were stimulated with ligands activating RIG-I (5'ppp-dsRNA), cGAS (pDNA, G_3-YSD), TLR8 (TL8-506), STING (2'3'-cGAMP), TLR1/TLR2 (Pam3CSK4), or left non-stimulated (Medium). After 20 h, cellular viability was determined by MTT assay (n ≥ 3, mean + SD, two-way ANOVA, Dunnett's multiple comparisons test). Significances are indicated as follows: * (P < 0.05), ** (P < 0.01), *** (P < 0.001), **** (P ≤ 0.0001), ns: not significant.

ELAVL1 consists of 326 amino acids and comprises three RRMs (Fig. 3.23A). To test whether these domains are required for type I IFN induction, FLAG-tagged ELAVL1 fusion proteins lacking RRM1 (ΔRRM1, deletion of amino acids 1-98) or RRM3 (ΔRRM3, deletion of amino acids 244-326) were stably expressed in ELAVL1-deficient THP-1 dual cells (Fig. 3.23B). Interestingly, overexpression of ΔRRM1-ELAVL1-FLAG or ΔRRM3-ELAVL1-FLAG in THP-1 dual *ELAVL1*$^{-/-}$ cells did not rescue the cGAS- and RIG-I-dependent ISRE reporter activation, indicating that the RRMs of ELAVL1 are required for

type I IFN induction (Fig. 3.23C). Altogether, the data of this chapter suggest that ELAVL1 promotes the expression of type I IFNs downstream of RIG-I, cGAS, and STNG. The results further indicate that the cGAS- and RIG-I-dependent production of type I IFNs and activation of NF-κB are interconnected via ELAVL1, whereas the TLR1/TLR2-mediated NF-κB response is ELAVL1-independent.

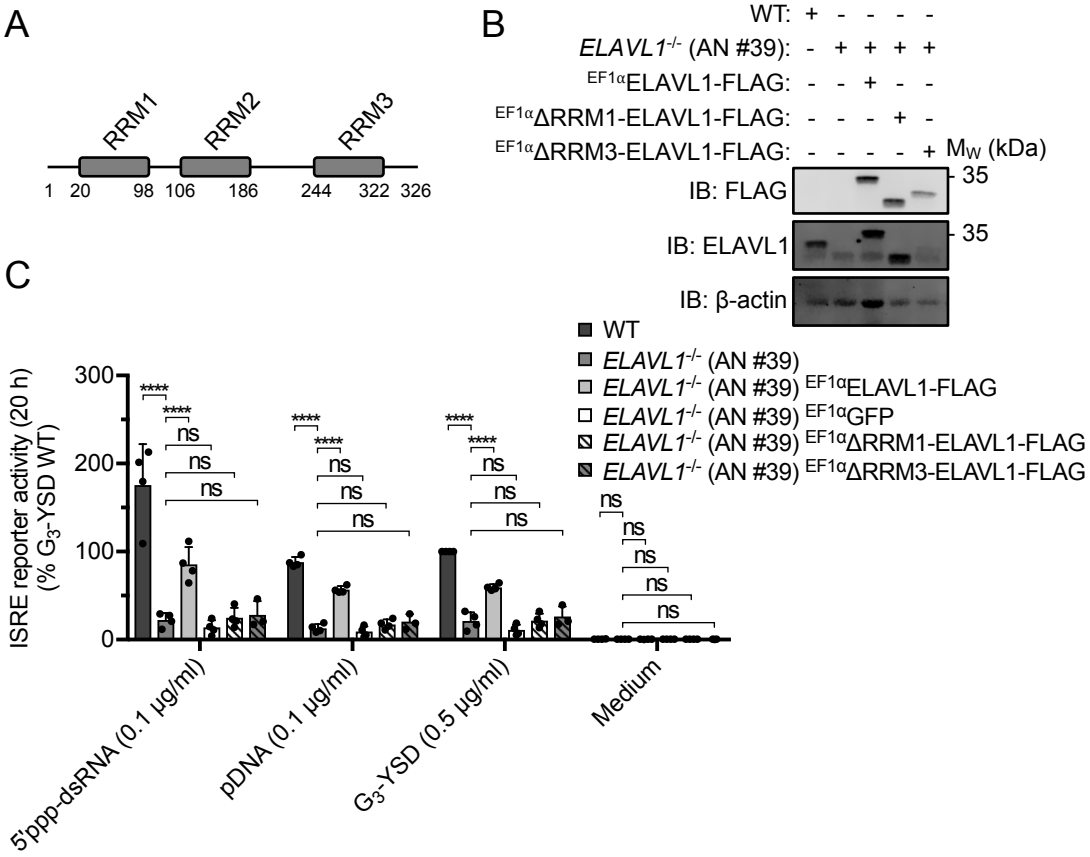

Fig. 3.23: RRM1 and RRM3 of ELAVL1 are required for the cGAS- and RIG-I-dependent induction of type I IFNs.
(**A**) Domain structure of human ELAVL1. (**B**) CCLs of THP-1 dual cells (WT), THP-1 dual *ELAVL1*$^{-/-}$ (AN #39) cells, and THP-1 dual *ELAVL1*$^{-/-}$ (AN #39) cells expressing FLAG-tagged full-length ELAVL1, ΔRRM1-ELAVL1, or ΔRRM3-ELAVL1 (EF1α promoter) were analyzed by immunoblotting with the indicated antibodies. One representative experiment is shown. (**C**) The cell lines depicted in (B) were stimulated with the indicated ligands. After 20 h, ISRE reporter activation was analyzed (n ≥ 3, mean + SD, two-way ANOVA, Dunnett's multiple comparisons test). Significances are indicated as follows: * (P < 0.05), ** (P < 0.01), *** (P < 0.001), **** (P ≤ 0.0001), ns: not significant.

3.3.2 Knockout of *ELAVL1* reduces *IFNB1* mRNA levels after cGAS or RIG-I activation

In the previous chapter, ELAVL1 was shown to promote the expression of type I IFNs downstream of cGAS-STING and RIG-I. It was hypothesized that ELAVL1-deficient THP-1 dual monocytes also fail to mount an antiviral gene expression program at the transcriptional stage. Therefore, ELAVL1-deficient THP-1 dual cells were stimulated with 5'ppp-dsRNA, G_3-YSD, or IFNα and then mRNA induction of *IFNB1*, *CXCL10*, and *IFIT1* was analyzed by qPCR (Fig. 3.24).

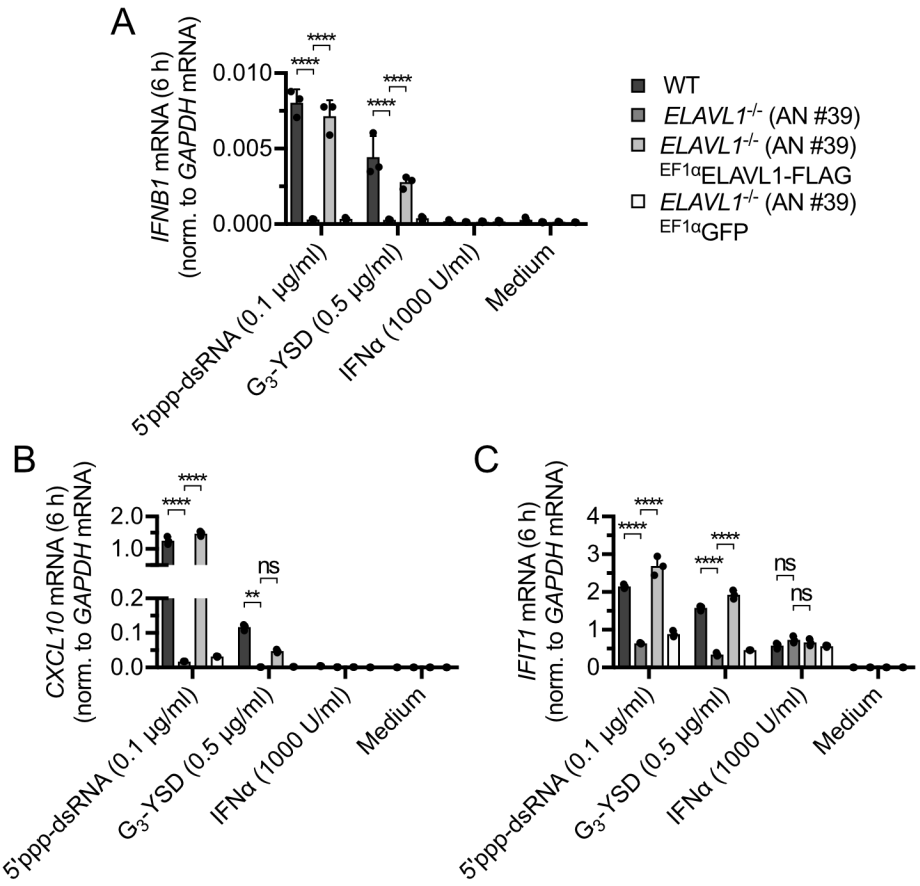

Fig. 3.24: ELAVL1 promotes the cGAS- and RIG-I-mediated mRNA induction of *IFNB1*, *CXCL10,* and *IFIT1*.
(**A**-**C**) THP-1 dual cells (WT), THP-1 dual *ELAVL1*$^{-/-}$ (AN #39) cells, and THP-1 dual *ELAVL1*$^{-/-}$ (AN #39) cells expressing ELAVL1-FLAG or GFP (EF1α promoter) were stimulated with 0.1 µg/ml 5'ppp-dsRNA, 0.5 µg/ml G_3-YSD, 1000 U/ml IFNα, or left non-stimulated (Medium). After 6 h, mRNA expression of *IFNB1*, *CXCL10*, and *IFIT1* was determined by qPCR and normalized to *GAPDH* mRNA (n = 3, mean + SD, two-way ANOVA, Dunnett's multiple comparisons test). Significances are indicated as follows: * $P < 0.05$), ** ($P < 0.01$), *** ($P < 0.001$), **** ($P \leq 0.0001$), ns: not significant.

Intriguingly, KO of ELAVL1 abrogated the cGAS- and RIG-I-dependent mRNA expression of *IFNB1* (Fig. 3.24A) and *CXCL10* (Fig. 3.24B). Reconstitution of THP-1 dual *ELAVL1*$^{-/-}$ cells with ELAVL1-FLAG reestablished the expression of these transcripts. It should be noted that the G_3-YSD-induced mRNA expression of *CXCL10* was visibly but insignificantly upregulated in ELAVL1-FLAG-expressing THP-1 dual *ELAVL1*$^{-/-}$ cells. In contrast to *IFNB1* and *CXCL10*, *IFIT1* mRNA levels were markedly, but not completely, downregulated in ELAVL1-deficient THP-1 dual cells after stimulation with cytosolic DNA or RNA. These data indicate that stabilization of certain mRNA species by ELAVL1 may contribute to its type I IFN-inducing capacities, as previously described for *IFNB1* mRNA (Herdy et al., 2015). The IFNα-induced mRNA expression of *IFIT1* was independent of ELAVL1, further demonstrating that the IFNAR signaling pathway is intact in ELAVL1-deficient THP-1 dual monocytes (Fig. 3.24C).

3.3.3 ELAVL1 controls the phosphorylation of TBK1 and IRF3

It was previously shown that KD of hnRNPM and ELAVL1 inhibits the phosphorylation of TBK1 and IRF3 induced by cGAS and/or RIG-I. Therefore, the phosphorylation of IRF3, TBK1, and STING was also analyzed in ELAVL1-deficient THP-1 dual cells (Fig. 3.25). Immunoblot analysis showed that endogenous ELAVL1 is not present in THP-1 dual cells with *ELAVL1*$^{-/-}$ genetic background and that ELAVL1-FLAG is expressed at levels similar to endogenous ELAVL1 (Fig. 3.25B). Of note, the phosphorylation of TBK1 at Ser172 and IRF3 at Ser396 was severely diminished in ELAVL1-deficient THP-1 dual cells after stimulation of cGAS or RIG-I and rescued by overexpression of ELAVL1-FLAG (Fig. 3.25C, Fig. 3.25E). Similarly, the cGAS-induced phosphorylation of STING at Ser366 (pSTING-Ser366) was ELAVL1-dependent (Fig. 3.25D). Interestingly, the TLR1/TLR2-triggered phosphorylation of TBK1 at Ser172 was independent of ELAVL1 (Fig. 3.26A-3.26B). These data are in line with the observation that ELAVL1 is not required for the TLR1/TLR2-mediated NF-κB response. In summary, these data show that ELAVL1 promotes cGAS and RIG-I signaling in a non-redundant manner by promoting the phosphorylation of essential signaling components like TBK1, IRF3, and, in the case of cGAS activation, STING. Furthermore, these data demonstrate that ELAVL1 promotes the phosphorylation of TBK1 in a PRR-dependent manner, suggesting that ELAVL1 may be capable of discriminating distinct TBK1 populations.

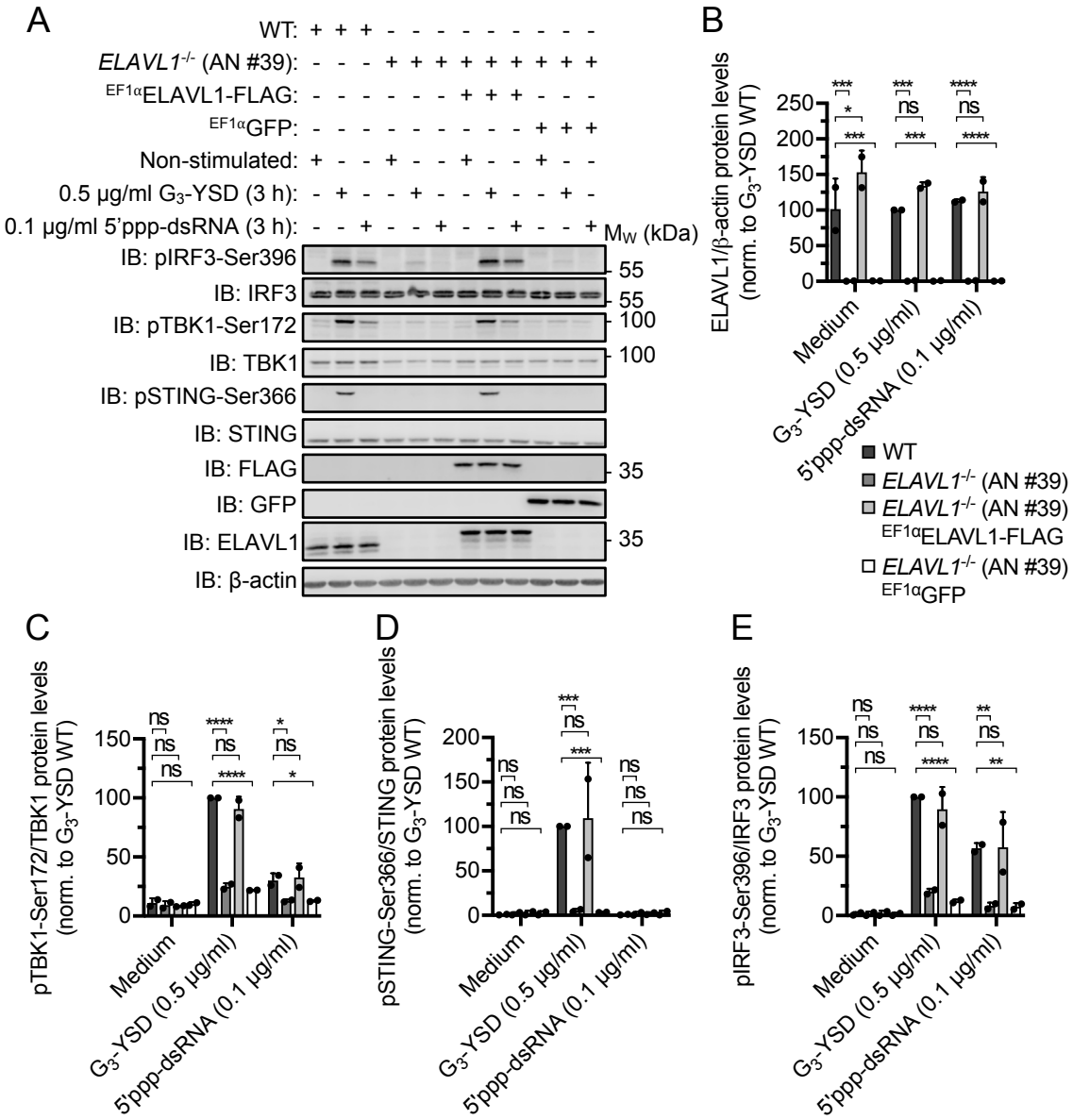

Fig. 3.25: ELAVL1 controls the phosphorylation of TBK1 and IRF3 induced by cGAS or RIG-I.

(**A**) THP-1 dual cells (WT), THP-1 dual *ELAVL1*$^{-/-}$ (AN #39) cells, and THP-1 dual *ELAVL1*$^{-/-}$ (AN #39) cells expressing ELAVL1-FLAG or GFP (EF1α promoter) were stimulated with 0.5 µg/ml G_3-YSD, 0.1 µg/ml 5'ppp-dsRNA, or left non-stimulated (Medium). After 3 h, CCLs were generated and analyzed by immunoblotting with the indicated antibodies. One representative experiment of two independent experiments is shown. (**B**) ELAVL1 signals detected in (A) were quantified and normalized to β-actin. (**C**) pTBK1-Ser172 signals detected in (A) were quantified and normalized to total TBK1. (**D**) pSTING-Ser366 signals detected in (A) were quantified and normalized to total STING. (**E**) pIRF3-Ser396 signals detected in (A) were quantified and normalized to total IRF3. (B-E) n = 2, mean + SD, two-way ANOVA, Dunnett's multiple comparisons test. Significances are indicated as follows: * ($P < 0.05$), ** ($P < 0.01$), *** ($P < 0.001$), **** ($P \leq 0.0001$), ns: not significant.

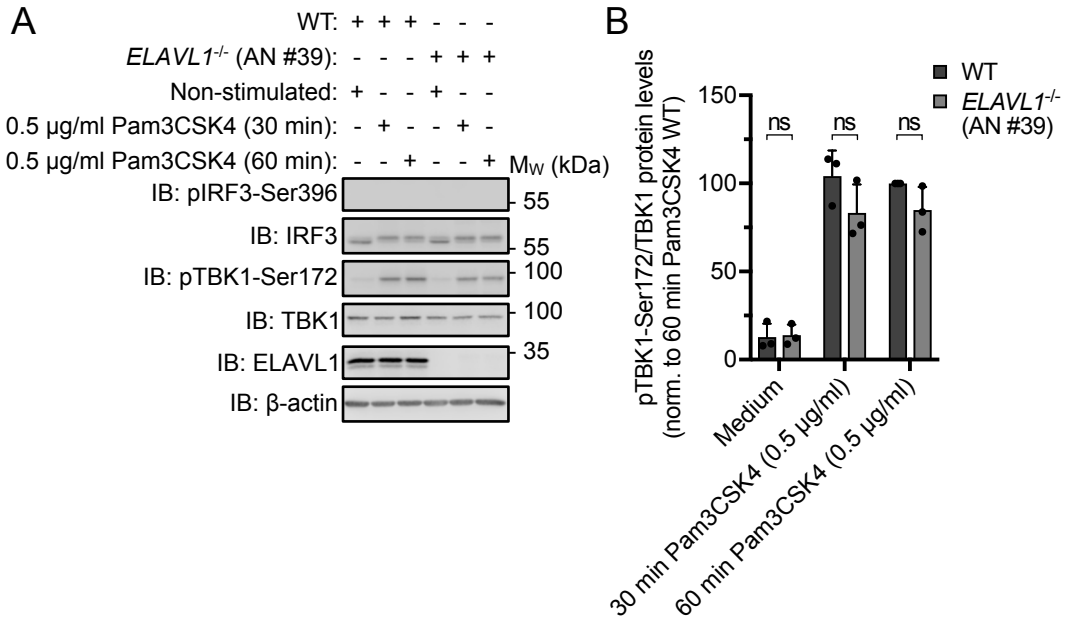

Fig. 3.26: TBK1 phosphorylation induced by TLR1/TLR2 is independent of ELAVL1. (**A**) THP-1 dual cells (WT) and THP-1 dual *ELAVL1*$^{-/-}$ (AN #39) cells were stimulated with 0.5 µg/ml Pam3CSK4 for 30 min, 60 min, or left non-stimulated (Medium). Following, CCLs were generated and analyzed by immunoblotting with the indicated antibodies. One representative experiment of three independent experiments is shown. (**B**) pTBK1-Ser172 signals detected in (A) were quantified and normalized to total TBK1 (n = 3, mean + SD, two-way ANOVA, Sidak's multiple comparisons test. Significances are indicated as follows: * ($P < 0.05$), ** ($P < 0.01$), *** ($P < 0.001$), **** ($P \leq 0.0001$), ns: not significant.

For the cGAS-STING signaling pathway, current data imply that 2'3'-cGAMP induces the formation of STING oligomers. STING clustering generates a surface geometry for the recruitment of TBK1 and phosphorylation of STING by TBK1, which licenses IRF3 for phosphorylation by TBK1. Consequently, TBK1 functions downstream of STING clustering and TBK1 *trans*-autophosphorylation precedes STING and IRF3 phosphorylation. The data of this thesis indicate that ELAVL1 and hnRNPM function upstream of TBK1 and regulate a signaling event shared by both cGAS and RIG-I.

3.3.4 ELAVL1 promotes signaling downstream of cGAS and RIG-I

Previously, ELAVL1 was shown to promote the cGAS- and RIG-I-dependent phosphorylation of TBK1 and IRF3. However, qPCR analysis showed that ELAVL1 may also stabilize *IFNB1* and *CXCL10* mRNAs. To elucidate how ELAVL1 primarily promotes cGAS and RIG-I signaling in THP-1 dual cells, ELAVL1-specific shRNAs were expressed in THP-1 dual *IFNAR2*$^{-/-}$ cells. It was hypothesized that stabilization of *IFNB1* mRNA by ELAVL1

may indirectly increase the sensitivity of the cytosolic nucleic acid sensing machinery, because the expression of RIG-I and cGAS can be upregulated by type I IFNs in a positive feedback loop. In THP-1 dual *IFNAR2*$^{-/-}$ cells, this effect should not be present. Therefore, inhibition of the cGAS- and RIG-I-mediated type I IFN response in THP-1 dual *IFNAR2*$^{-/-}$ ELAVL1 KD cells should indicate that ELAVL1 predominantly augments signal transduction.

THP-1 dual cells with *IFNAR2*$^{-/-}$ genetic background did not activate the ISRE reporter after stimulation with IFNα, indicating disruption of the JAK-STAT signaling pathway (Fig. 3.27). Of note, the ISRE reporter activation induced by cGAS or RIG-I was still markedly diminished in THP-1 dual *IFNAR2*$^{-/-}$ ELAVL1 KD cells (Fig. 3.27).

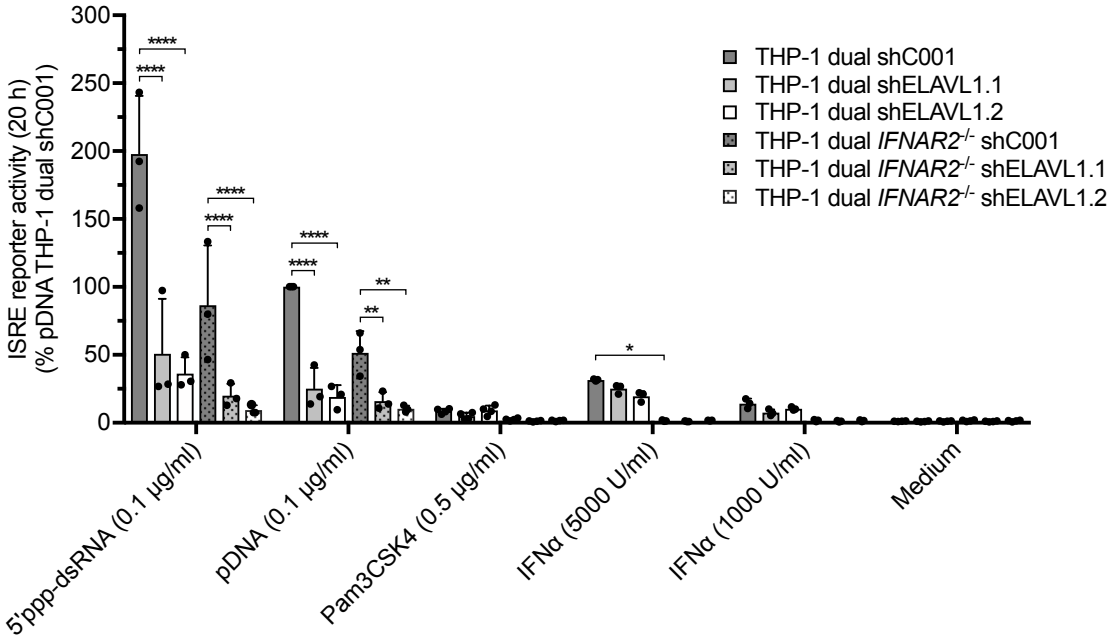

Fig. 3.27: ELAVL1 primarily promotes the cGAS- and RIG-I-dependent induction of type I IFNs by regulating signal transduction.

THP-1 dual cells and THP-1 dual *IFNAR2*$^{-/-}$ cells were infected with lentiviral particles encoding for control shRNA (shC001) or ELAVL1-specific shRNAs (shELAVL1.1, shELAVL1.2) and stimulated with ligands activating RIG-I (5'ppp-dsRNA), cGAS (pDNA), TLR1/TLR2 (Pam3CSK4), IFNAR (IFNα), or left non-stimulated (Medium). After 20 h, ISRE reporter activation was analyzed (n ≥ 3, mean + SD, two-way ANOVA, Tukey's multiple comparisons test). Significances are indicated as follows: * (P < 0.05), ** (P < 0.01), *** (P < 0.001), **** (P ≤ 0.0001), ns: not significant.

3.3.5 3'-mRNA sequencing analysis of ELAVL1-deficient THP-1 cells

Previously, ELAVL1 was shown to promote the cGAS- and RIG-I-mediated type I IFN induction by regulating signal transduction. To evaluate whether ELAVL1 also controls the mRNA expression of proteins associated with cGAS and RIG-I signaling, a global 3'-mRNA sequencing approach was performed. Wildtype and ELAVL1-deficient THP-1 dual cells were stimulated with 0.1 µg/ml 5'ppp-dsRNA, 0.5 µg/ml G_3-YSD, 1000 U/ml IFNα, or left non-stimulated. After 6 h, the cellular RNA was extracted and sequencing libraries were prepared at the Next Generation Sequencing (NGS) Core Facility at the University Hospital Bonn using the QuantSeq 3' mRNA-Seq Library Prep kit FWD (Lexogen). The samples were sequenced on an Illumina HiSeq 1500 device. Data analysis in R was kindly performed by Thais Schlee-Guimaraes. Briefly, the reads were aligned to the human reference genome (Ensembl genome version 96) using STAR (Dobin et al., 2013). The aligned sequencing reads were counted with HTSeq (Dobin et al., 2013) and the DESeq2 package was used for differential gene expression analysis (Love et al., 2014). Genes with an adjusted $P < 0.05$ and a $\log_2$ fold change of > 1.5 or < -1.5 were considered significantly regulated genes. Volcano plots were used to visualize the significantly regulated genes and show the $\log_2$ fold change of THP-1 dual *ELAVL1*$^{-/-}$ (AN #39) vs. THP-1 dual wildtype cells ($\log_2$ fold change) against the statistical significance ($-\log_{10}$ adjusted *P*) (Fig. 3.28-3.31). In addition, a Gene Ontology (GO) analysis of the differentially expressed genes (up- and downregulated) was performed to comprehensively analyze which cellular signaling pathways and processes are ELAVL1-dependent (Fig. 3.28-3.31). It should be noted that only *CXCL10*, *DDX58*, *CGAS*, *IFI16*, *IFI44L*, *IFIH1*, *IFIT1*, *IFIT2*, *IFIT3*, *IFITM3*, *IFNB1*, *ISG15*, *MX1*, *MX2*, *OASL*, *OAS1*, *OAS2*, *OAS3*, *PMAIP1*, and *RSAD2* were highlighted in Fig. 3.28-3.31 (for the full data sets see the references in chapter 9.2 of the appendix). If one of these genes is not depicted in any of the figures, it was not significantly regulated.

Under steady state conditions, 118 genes were identified with a $\log_2$ fold change of > 1.5 and 221 genes with a $\log_2$ fold change of < -1.5 (adjusted $P < 0.05$) in ELAVL1-deficient THP-1 dual cells (Fig. 3.28). The ten pathways that were most significantly regulated (up- or downregulated) by KO of ELAVL1 included processes such as 'regulated exocytosis', 'response to zinc ion', or immune-related processes. For the category 'immune response', altered mRNA levels were detected for *CTSG*, *SERPINB10*, *EGR1*, *MT2A*, *CHI3L1*,

IL1RN, *FCER1G*, *DEFB1*, *CTSB*, *S100A8*, *S100A9*, *ASS1*, *PTAFR*, and *NPC2*. The mRNA expression of the cGAS-, STING-, RIG-I-, MAVS-, TBK1-, IKK-, IRF3-, and IRF7-encoding genes was not affected by ELAVL1 deficiency. Curiously, *PLK2* mRNA expression, a gene described to be stabilized by ELAVL1 and associated with the nuclear translocation of IRF3 (Sueyoshi et al., 2018), was not downregulated in ELAVL1-deficient THP-1 dual cells.

For stimulation of IFNAR, 167 genes were identified with a $\log_2$ fold change of > 1.5 and 251 genes with a $\log_2$ fold change of < -1.5 (adjusted $P < 0.05$) in ELAVL1-deficient THP-1 dual cells relative to wildtype cells (Fig. 3.29). The mRNA expression of common ISGs such as *IFI16*, *IFIH1*, *IFIT1*, *IFIT2*, *IFIT3*, *IFITM3*, *ISG15*, *MX1*, *MX2*, *OASL*, *OAS1*, *OAS2*, and *OAS3* was not downregulated in ELAVL1-deficient THP-1 dual cells, indicating that the JAK-STAT signaling pathway is intact. For the IFNα condition, the GO analysis largely resembled the situation in the non-stimulated state and significantly regulated genes were associated with 'secretion by cells', 'response to stress', 'response to zinc ion', 'cytokine production', or 'response to other organism'. The category 'cytokine production' included the genes *CHI3L1*, *FCER1G*, *AGT*, *S100A8*, and *PTAFR*, while *CTSG*, *PRTN3*, *EGR1*, *MT2A*, *FCER1G*, *DEFB1*, *S100A8*, *IFI44L*, *ASS1*, *PTAFR*, *PLAC8*, and *NPC2* belonged to the category 'response to other organism'. Neither of these categories contained essential components of the cGAS-STING, RIG-I-MAVS, or JAK-STAT signaling cascades. For stimulation of RIG-I, 207 genes were identified with a $\log_2$ fold change of > 1.5 and 584 genes with a $\log_2$ fold change of < -1.5 (adjusted $P < 0.05$) in ELAVL1-deficient THP-1 dual cells (Fig. 3.30), whereas stimulation of cGAS with 0.5 µg/ml G_3-YSD induced a significant upregulation of 186 genes and a downregulation of 557 genes (Fig. 3.31). In both conditions, *IFNB1*, *CXCL10*, and also relevant ISGs (i.e., *IFI44L*, *IFI16*, *DDX58*, *IFIH1*, *IFIT1*, and *OASL*) were significantly downregulated in ELAVL1-deficient THP-1 dual cells. GO analysis showed that particularly immune-related processes such as 'defense response to virus' are downmodulated in THP-1 dual ELAVL1 KO cells after activation of cGAS or RIG-I.

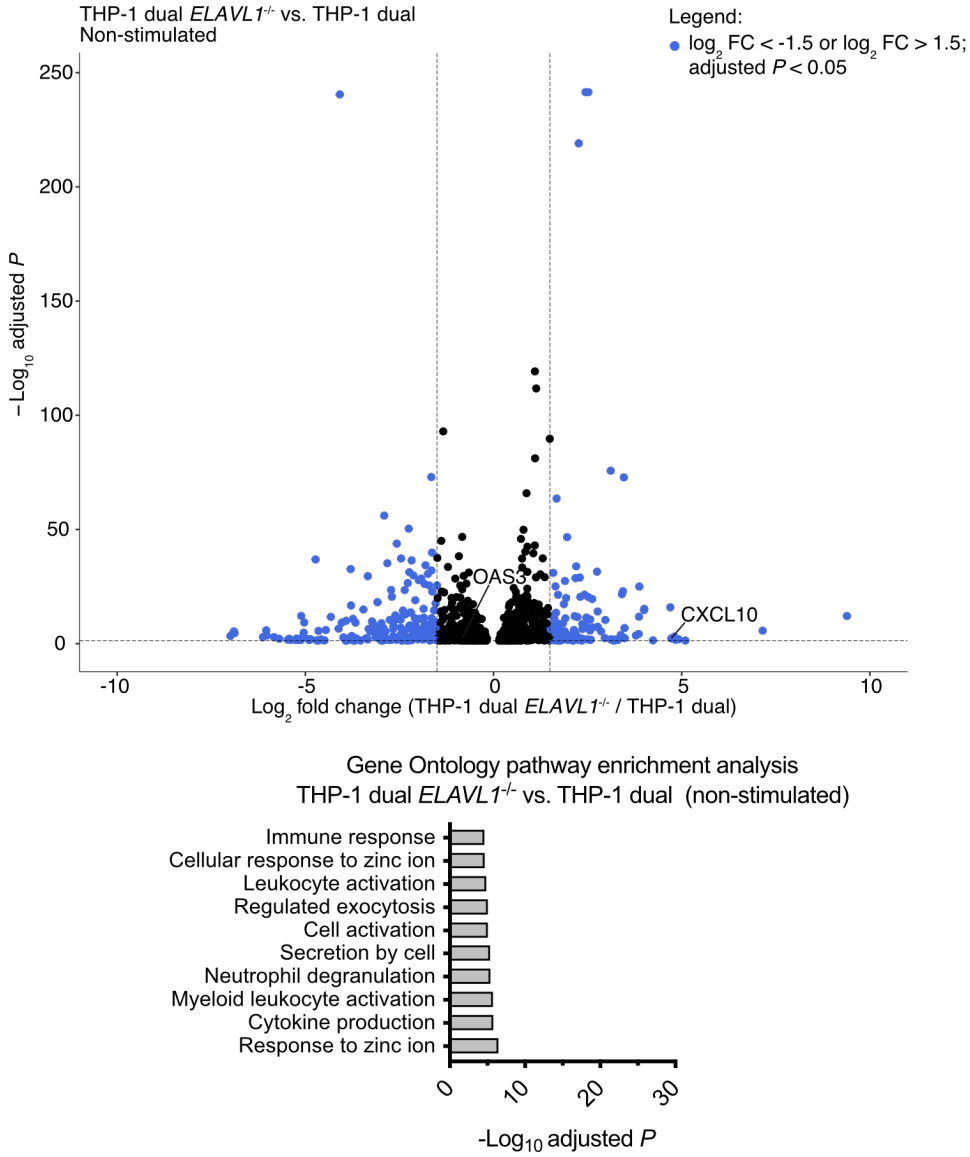

Fig. 3.28: mRNA expression profiling of THP-1 dual *ELAVL1*$^{-/-}$ cells in the non-stimulated condition.

Non-stimulated THP-1 dual *ELAVL1*$^{-/-}$ (AN #39) cells and THP-1 dual wildtype cells (biological triplicates) were harvested and used for total cellular RNA extraction. After library preparation, the samples were sequenced on an Illumina HiSeq 1500 device at the NGS core facility (University Hospital Bonn). The reads were aligned to the human reference genome (Ensembl genome version 96) using STAR, quantified with HTSeq, and differential gene expression analysis was performed using DESeq2. Data analysis in R was kindly performed by Thais Schlee-Guimaraes. The Volcano plot displays the $\log_2$ fold change (FC) of THP-1 dual *ELAVL1*$^{-/-}$ (AN #39) cells vs. THP-1 dual wildtype cells against the statistical significance ($-\log_{10}$ adjusted *P*). Each dot represents one gene. Genes with an adjusted $P < 0.05$ and a $\log_2$ fold change of > 1.5 or < -1.5 were considered significantly regulated genes (blue). The ten most significantly enriched pathways (up- and downregulated) are visualized as bar graphs.

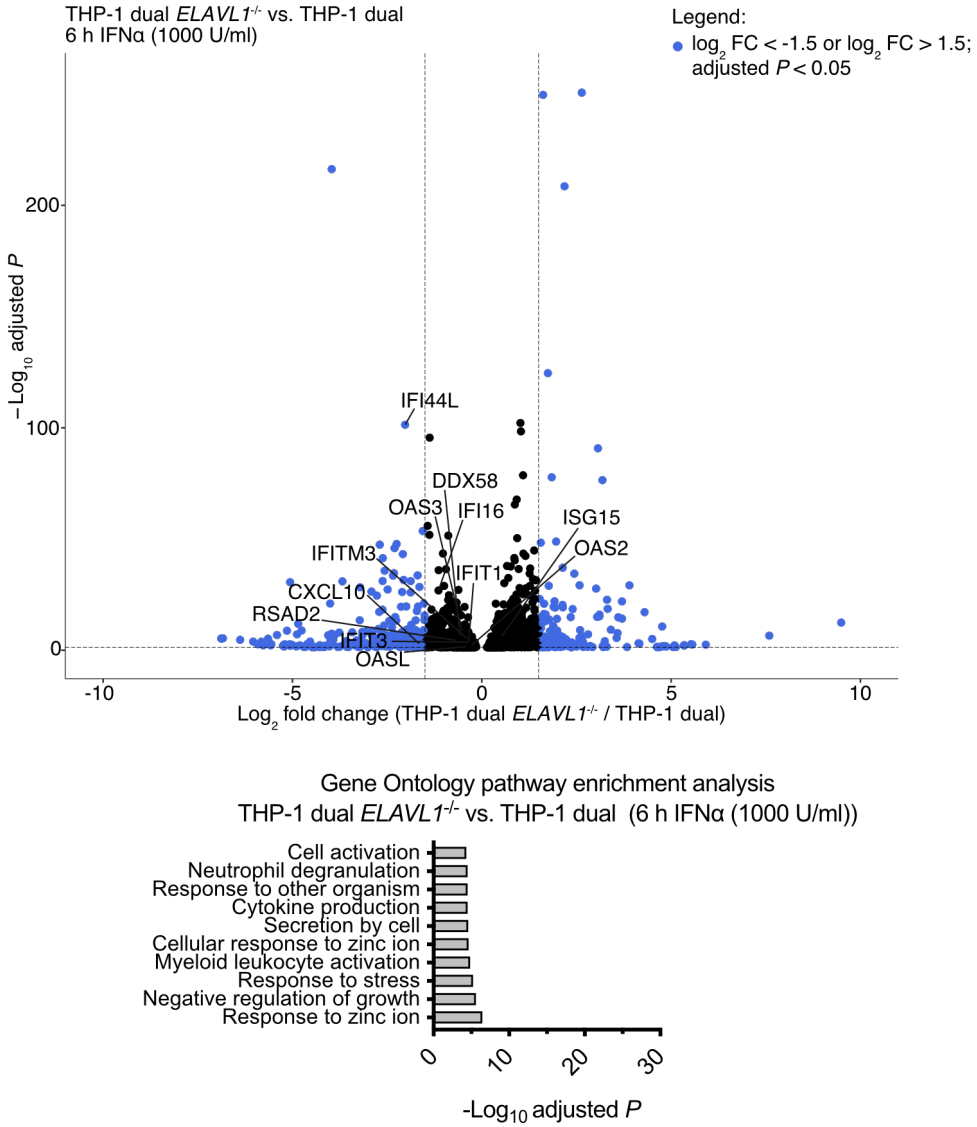

Fig. 3.29: mRNA expression profiling of THP-1 dual *ELAVL1*$^{-/-}$ cells after stimulation of IFNAR.

THP-1 dual *ELAVL1*$^{-/-}$ (AN #39) cells and THP-1 dual wildtype cells were stimulated with 1000 U/ml IFNα (biological triplicates). 6 h after stimulation, the total cellular RNA was isolated. After library preparation, the samples were sequenced on an Illumina HiSeq 1500 device at the NGS core facility (University Hospital Bonn). The reads were aligned to the human reference genome (Ensembl genome version 96) using STAR, quantified with HTSeq, and differential gene expression analysis was performed using DESeq2. Data analysis in R was kindly performed by Thais Schlee-Guimaraes. The Volcano plot displays the $\log_2$ fold change (FC) of THP-1 dual *ELAVL1*$^{-/-}$ (AN #39) cells vs. THP-1 dual wildtype cells against the statistical significance ($-\log_{10}$ adjusted *P*). Each dot represents one gene. Genes with an adjusted $P < 0.05$ and a $\log_2$ fold change of > 1.5 or < -1.5 were considered significantly regulated genes (blue). The ten most significantly enriched pathways (up- and downregulated) are visualized as bar graphs.

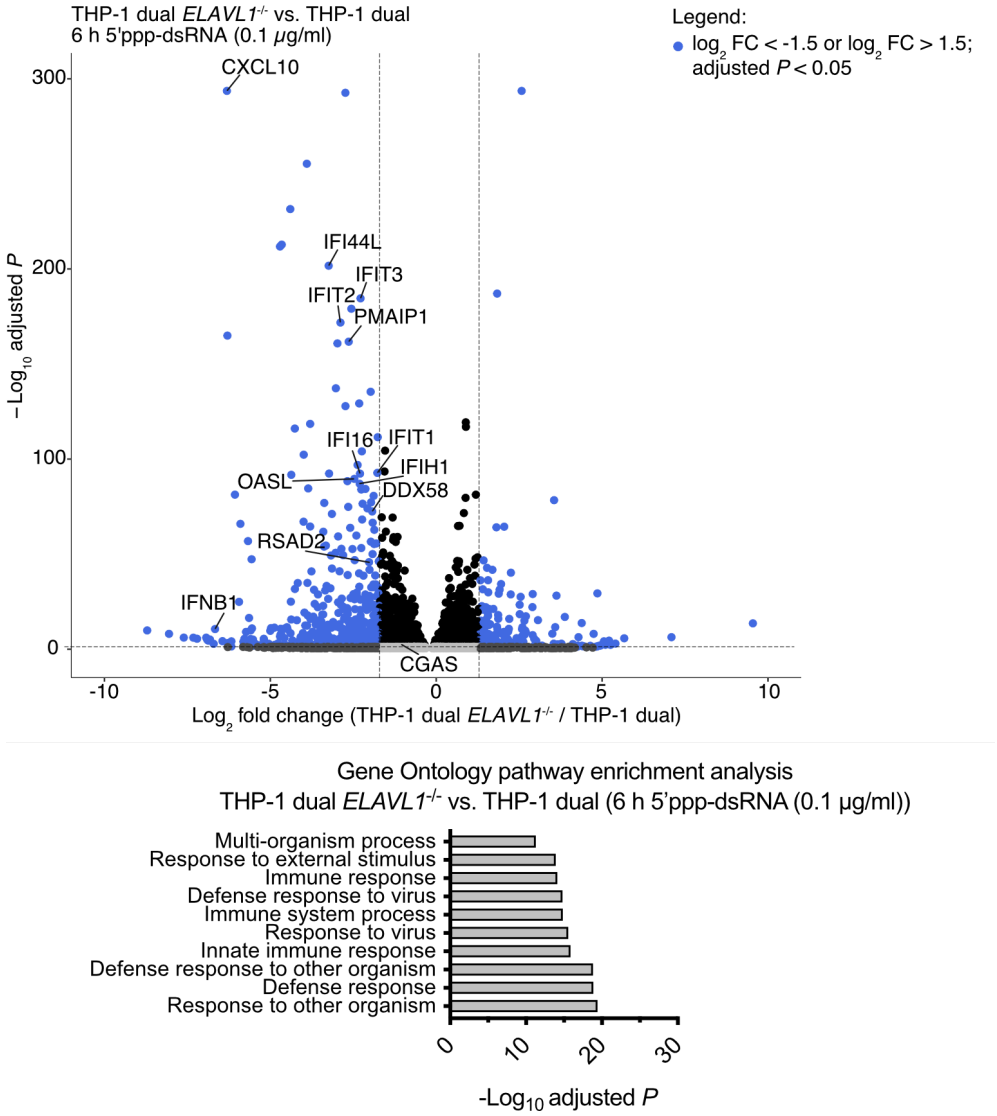

Fig. 3.30: mRNA expression profiling of THP-1 dual *ELAVL1*$^{-/-}$ cells after stimulation of RIG-I.

THP-1 dual *ELAVL1*$^{-/-}$ (AN #39) cells and THP-1 dual wildtype cells were lipofected with 0.1 µg/ml 5'ppp-dsRNA (biological triplicates). 6 h after stimulation, the total cellular RNA was isolated. After library preparation, the samples were sequenced on an Illumina HiSeq 1500 device at the NGS core facility (University Hospital Bonn). The reads were aligned to the human reference genome (Ensembl genome version 96) using STAR, quantified with HTSeq, and differential gene expression analysis was performed using DESeq2. Data analysis in R was kindly performed by Thais Schlee-Guimaraes. The Volcano plot displays the $\log_2$ fold change (FC) of THP-1 dual *ELAVL1*$^{-/-}$ (AN #39) cells vs. THP-1 dual wildtype cells against the statistical significance ($-\log_{10}$ adjusted *P*). Each dot represents one gene. Genes with an adjusted $P < 0.05$ and a $\log_2$ fold change of > 1.5 or < -1.5 were considered significantly regulated genes (blue). The ten most significantly enriched pathways (up- and downregulated) are visualized as bar graphs.

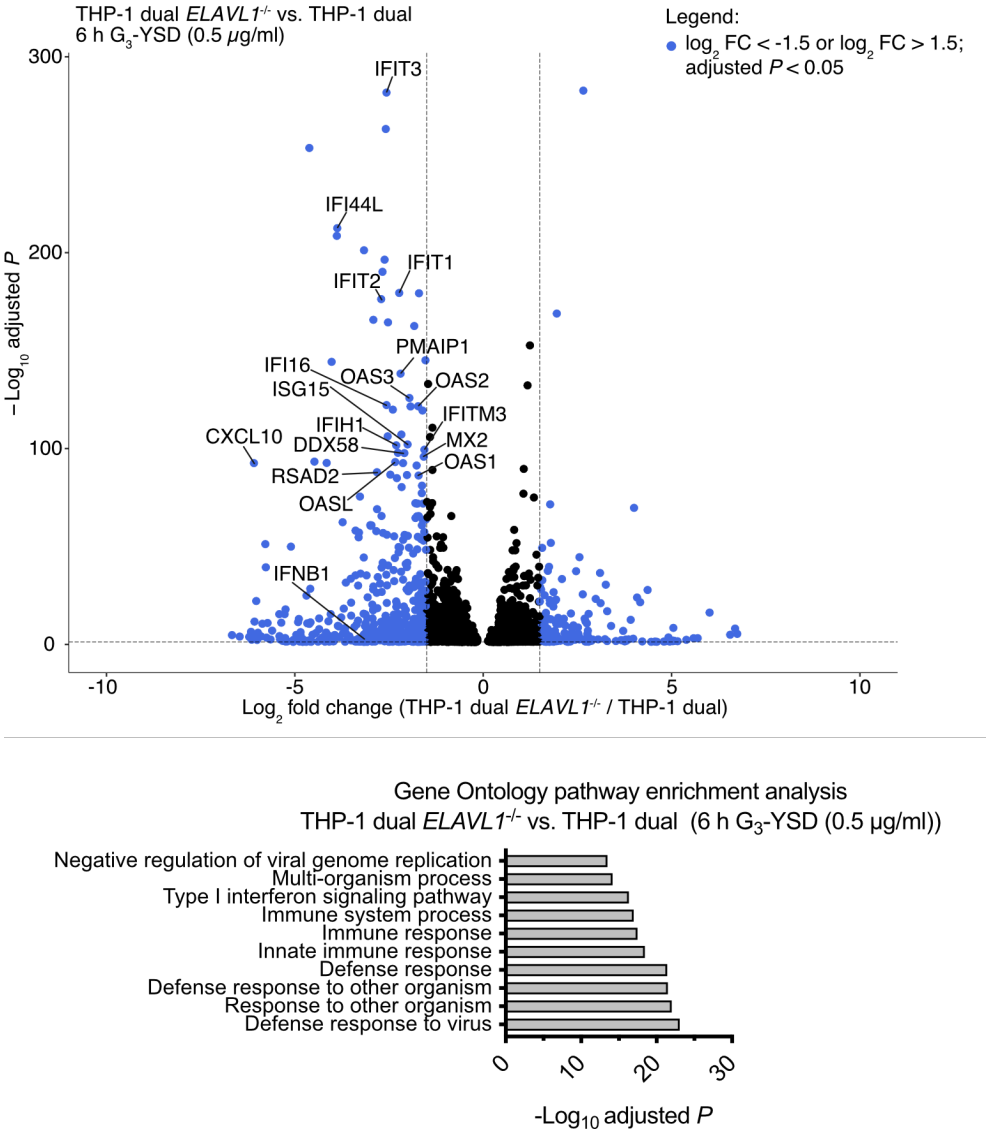

Fig. 3.31: mRNA expression profiling of THP-1 dual *ELAVL1*$^{-/-}$ cells after stimulation of cGAS.

THP-1 dual *ELAVL1*$^{-/-}$ (AN #39) cells and THP-1 dual wildtype cells were lipofected with 0.5 µg/ml G_3-YSD (biological triplicates). 6 h after stimulation, the total cellular RNA was isolated. After library preparation, the samples were sequenced on an Illumina HiSeq 1500 device at the NGS core facility (University Hospital Bonn). The reads were aligned to the human reference genome (Ensembl genome version 96) using STAR, quantified with HTSeq, and differential gene expression analysis was performed using DESeq2. Data analysis in R was kindly performed by Thais Schlee-Guimaraes. The Volcano plot displays the $\log_2$ fold change (FC) of THP-1 dual *ELAVL1*$^{-/-}$ (AN #39) cells vs. THP-1 dual wildtype cells against the statistical significance ($-\log_{10}$ adjusted *P*). Each dot represents one gene. Genes with an adjusted $P < 0.05$ and a $\log_2$ fold change of > 1.5 or < -1.5 were considered significantly regulated genes (blue). The ten most significantly enriched pathways (up- and downregulated) are visualized as bar graphs.

In the G_3-YSD condition, the category 'defense response to virus' involved *OAS3*, *OASL*, *IFIH1*, *HERC5*, *CXCL10*, *PMAIP1*, *MX2*, *OAS2*, *IFI16*, *IFI44L*, *IFIT1*, *IFIT2*, *IFIT3*, *ISG15*, *DDX58*, *RSAD2*, *IFITM3*, and *OAS1*. Similarly, *OASL*, *IFIH1*, *HERC5*, *CXCL10*, *ISG20*, *PMAIP1*, *IFNL1*, *IFI16*, *IFI44L*, *IFIT1*, *IFIT2*, *IFIT3*, and *DDX58* were assigned to this category in the 5'ppp-dsRNA condition. Collectively, the results of the global mRNA expression analysis largely exclude the possibility that ELAVL1 controls the expression of genes downstream of or at the level of ligand recognition by cGAS or RIG-I.

3.3.6 Interactome analysis of hnRNPM and ELAVL1

Because hnRNPM and ELAVL1 promote the cGAS- and RIG-I-dependent type I IFN production, it was hypothesized that both proteins have overlapping interactomes. Therefore, binding partners of hnRNPM and ELAVL1 were mapped by AP-MS (collaboration with the laboratory of Prof. Andreas Pichlmair (TU Munich, Germany)). After generating CCLs of non-stimulated THP-1 dual cells stably expressing hnRNPM-GFP, ELAVL1-GFP, or GFP, the fusion proteins were immunoprecipitated at 4 °C overnight and bound proteins were identified by MS. Fig. 3.32 compares the interactomes of ELAVL1 (log_2 fold change (ELAVL1-GFP/GFP)) and hnRNPM (log_2 fold change (hnRNPM-GFP/GFP)) and shows that both baits share many common interactors (for the full data set see the reference in chapter 9.3 of the appendix). Especially RNA-binding proteins, components of the spliceosome, and ribosomal proteins were detected in both interactomes (not highlighted). In general, ELAVL1 interacted with fewer proteins than hnRNPM and common protein interactors were more enriched after IP of hnRNPM as compared to ELAVL1 (Fig. 3.32, Fig. 3.33F). While strong interactions were detected between ELAVL1 and hnRNPM (Fig. 3.33A-3.33B), interactions with SON were restricted to hnRNPM (Fig. 3.33C), indicating that hnRNPM may form distinct protein complexes that could independently regulate the type I IFN response. Among the proteins that were previously associated with the expression of type I IFNs, DDX3X and DHX9 were the only common binding partners of ELAVL1 and hnRNPM (Fig. 3.32, Fig. 3.33E). However, this thesis has demonstrated that DHX9 is not required for cGAS and RIG-I signaling in THP-1 dual cells.

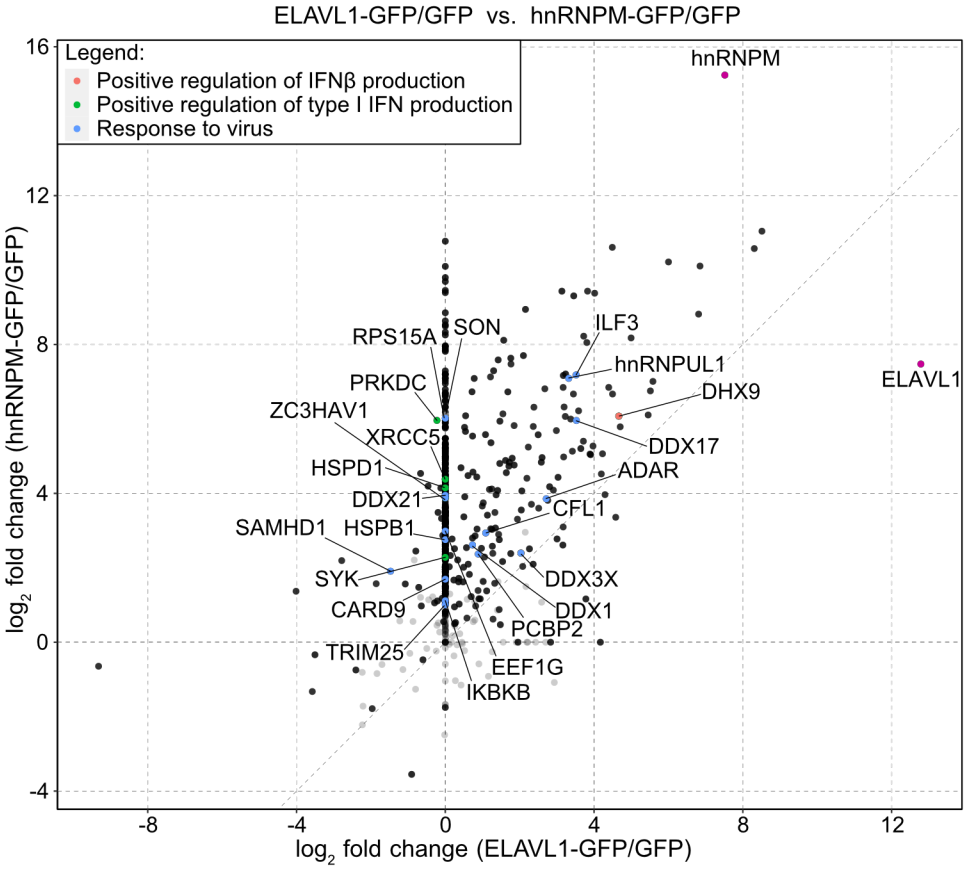

Fig. 3.32: Interactome analysis of hnRNPM and ELAVL1 under steady state conditions.
GFP fusion proteins were immunoprecipitated at 4 °C overnight from CCLs of non-stimulated THP-1 dual cells stably expressing hnRNPM-GFP, ELAVL1-GFP, or GFP. Bound proteins were identified by MS. Welch's t-test was used to determine the statistical significance. The double scatter plot shows the correlation between the $\log_2$ fold change of ELAVL1-GFP vs. GFP and the $\log_2$ fold change of hnRNPM-GFP vs. GFP of the significantly enriched proteins ($P < 0.05$) (black or colored data points). hnRNPM and ELAVL1 are highlighted in magenta. Proteins that are enriched in different pathways/processes (i.e., 'positive regulation of IFNβ production', 'positive regulation of type I IFN production', 'response to virus') are labeled with name tags and highlighted in different colors (MS analysis was done by Dr. Antonio Piras and Christian Urban).

Pathway enrichment analysis revealed that ADAR, hnRNPUL1, DDX17, and ILF3 are additional common interactors of hnRNPM and ELAVL1 that belong to the category 'response to virus' (Fig. 3.32). Different from the previous hnRNPM interactome analysis (IP at 4 °C for 2 h), the current analysis (IP at 4 °C overnight) identified IKBKB (also known as IKKβ) as a putative hnRNPM interactor (Fig. 3.33D), indicating that IP at 4 °C overnight may have enhanced the detection of weak interactions. In contrast to hnRNPM, no inter-

actions were detected between ELAVL1 and IKKβ. Collectively, these results demonstrate that hnRNPM and ELAVL1 have overlapping interactomes. Some of the common binding partners represent promising candidates for further investigation (i.e., DDX3X). IKKβ represents a particularly interesting candidate because it is structurally and functionally related to TBK1 and has been shown to phosphorylate MAVS at the consensus *p*L*x*IS motif at Ser442 (Liu et al., 2015). Although the interactions between hnRNPM and IKKβ were relatively weak, these results provide preliminary evidence for a direct link between hnRNPM and signaling proteins downstream of cGAS and RIG-I.

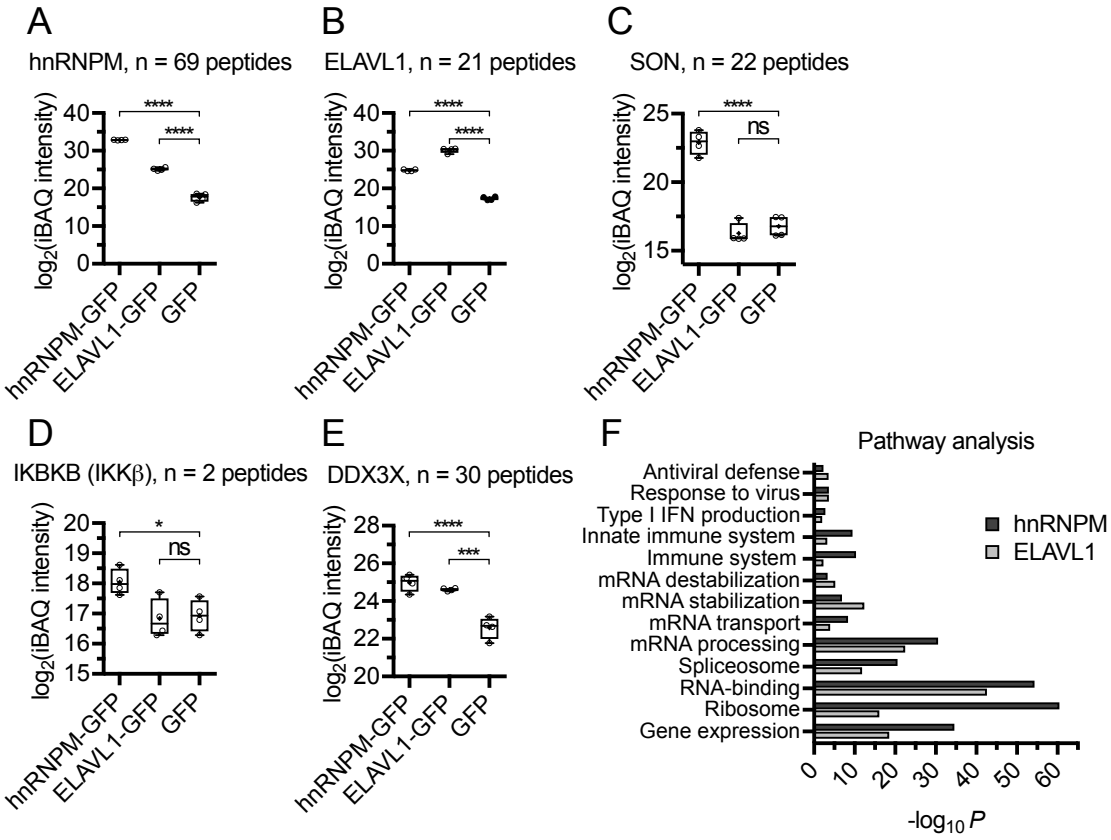

Fig. 3.33: hnRNPM interacts with IKKβ.
(**A**-**E**) Box plots show the abundance of hnRNPM, ELAVL1, SON, IKBKB (IKKβ), and DDX3X (log_2(iBAQ intensities, imputed) in the IPs of the interacting baits (hnRNPM-GFP, ELAVL1-GFP, or GFP) (Box-Whisker plot: boxes indicate the interquartile range and the median, + is the mean value, whiskers show minimum to maximum values) (n = 4, one-way ANOVA, Dunnett's multiple comparisons test). (**F**) Pathway analysis of differentially enriched protein groups that were detected in the hnRNPM or ELAVL1 condition when compared to the IP of GFP. All pathways/processes are significantly enriched, with a high $-log_{10}$ *P* indicating specific interactions of hnRNPM or ELAVL1 with several components of the respective pathways/processes. Significances are indicated as follows: * ($P < 0.05$), ** ($P < 0.01$), *** ($P < 0.001$), **** ($P \leq 0.0001$), ns: not significant.

3.4 hnRNPM and ELAVL1 form a multiprotein complex with TBK1

3.4.1 Activated TBK1 shows cytoplasmic and nuclear localization

TBK1 is a Ser/Thr protein kinase and plays a key role in cGAS and RIG-I signaling. It consists of 729 amino acids and folds into a three-domain structure, with an N-terminal kinase domain, an intermediate ubiquitin-like domain (ULD), and a C-terminal scaffold and dimerization domain (SDD) (Larabi et al., 2013; Shu et al., 2013; Tu et al., 2013). TBK1 and IKKε, the two non-canonical IKKs, are closely related and share 61 % sequence homology (Hiscott, 2007). Although both enzymes belong to the IKK kinase family, sequence homology to the canonical IKKs, IKKα and IKKβ, is limited with only 27 % (Hiscott, 2007). Considering that hnRNPM is a predominantly nuclear protein, it was asked whether hnRNPM and TBK1 are present in the same cellular compartments and thus putative interactions are not excluded by spatial separation. Therefore, the subcellular localization of TBK1 was analyzed in cytoplasmic and nuclear extracts of cGAS- (Fig. 3.34A) and RIG-I-activated THP-1 dual cells (Fig. 3.34B).

TBK1 was mainly present in cytoplasmic extracts, with weaker signals detectable in the nuclear fractions. Interestingly, considerable quantities of pTBK1-Ser172 were observed in both cytosolic and nuclear extracts 3 h after stimulation of cGAS or RIG-I. The localization of NF-κB p65 was very similar to that of TBK1 and NF-κB p65 phosphorylated at Ser536 (NF-κB pp65-Ser536) partially translocated to the nucleus in activated cells. Similar to hnRNPM, ELAVL1 was predominantly detected in the nuclear extracts. In contrast to hnRNPM and ELAVL1, SON was only found in the nuclear compartment. It should be noted that the protein content of the cytoplasmic extracts was approximately five times higher compared to the nuclear extracts (Fig. 3.34).

The nuclear localization of activated TBK1 was further evaluated by confocal immunofluorescence microscopy. After stimulation of cGAS with G_3-YSD-AF647, pTBK1-Ser172 formed distinct puncta concentrated around the cytoplasmic portion of the nuclear membrane and partially in the nucleus (Fig. 3.35). In summary, these data indicate that hnRNPM, ELAVL1, and activated TBK1 are not spatially separated, a prerequisite for interaction, and further imply that complex mechanisms might exist that regulate the TBK1-IRF3 signaling axis in different cellular compartments.

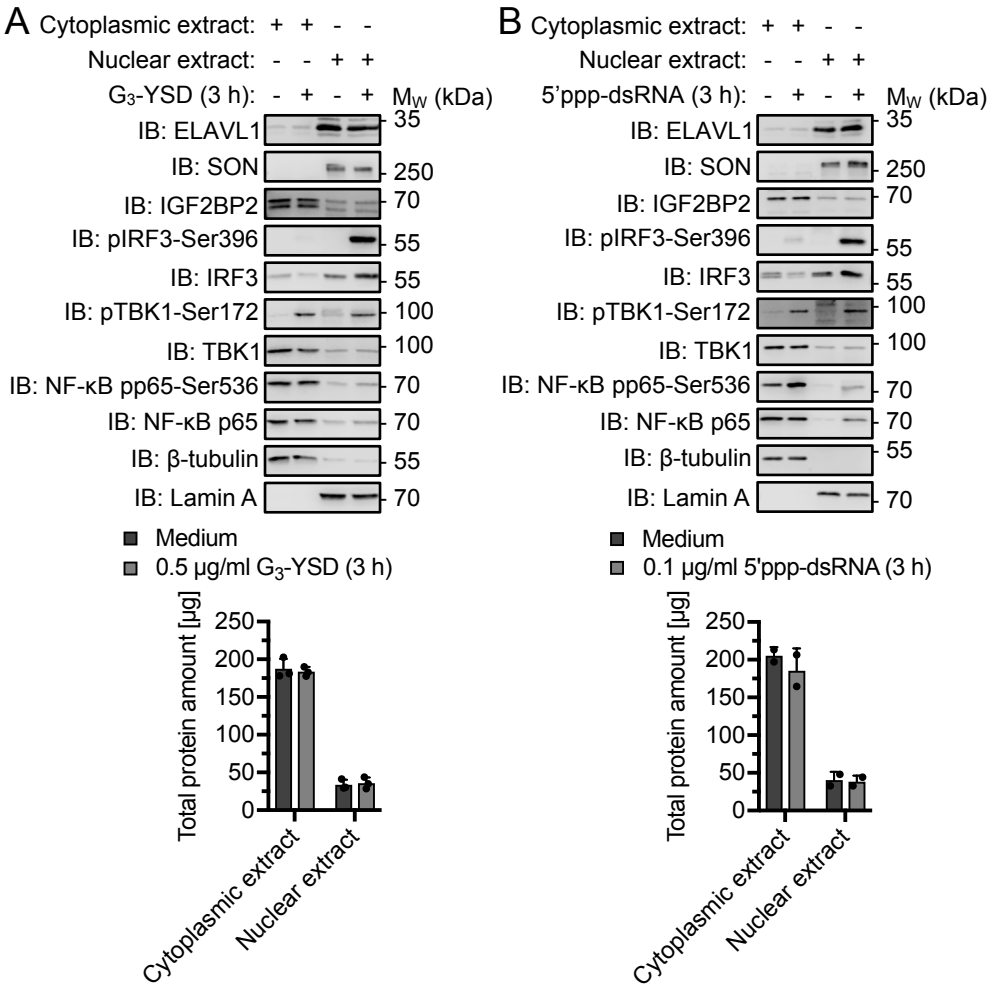

Fig. 3.34: pTBK1-Ser172 is present in nuclear extracts of THP-1 dual cells after activation of cGAS or RIG-I.

(**A**) Nuclear and cytoplasmic extracts were prepared from resting THP-1 dual cells (Medium) and THP-1 dual cells stimulated with 0.5 µg/ml G_3-YSD for 3 h. Equal protein amounts were analyzed by immunoblotting with the indicated antibodies. The total protein amount in the cytoplasmic/nuclear extracts of 1.86×10^6 THP-1 cells was determined by BCA. One representative experiment of two independent experiments is shown. (**B**) Nuclear and cytoplasmic extracts were prepared from resting THP-1 dual cells (Medium) and THP-1 dual cells stimulated with 0.1 µg/ml 5'ppp-dsRNA for 3 h. Equal protein amounts were analyzed by immunoblotting with the indicated antibodies. The total protein amount in the cytoplasmic/nuclear extracts of 1.86×10^6 THP-1 cells was determined by BCA. One representative experiment of two independent experiments is shown.

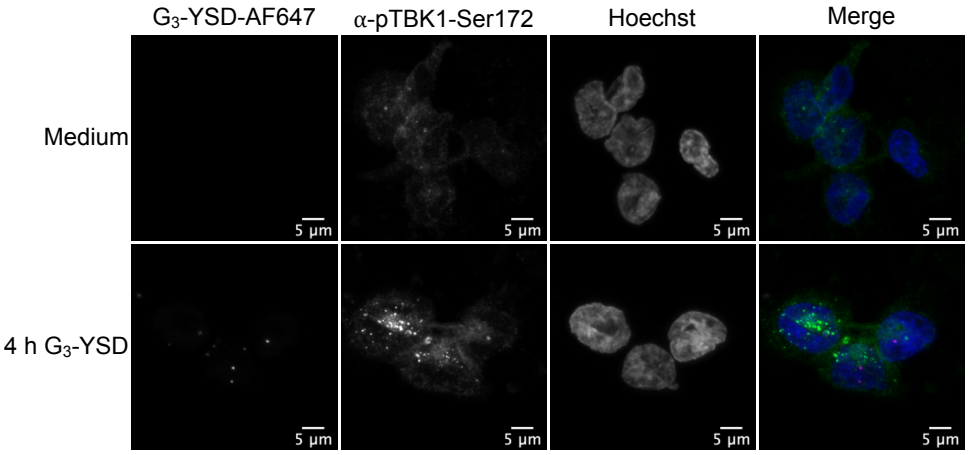

Fig. 3.35: pTBK1-Ser172 forms distinct cytoplasmic puncta and is also present in the nucleus of THP-1 dual cells.
PMA-differentiated THP-1 dual cells were lipofected with 0.5 µg/ml G_3-YSD-AF647 or left non-stimulated (Medium). After 4 h, the cells were fixed, permeabilized, blocked, and incubated with a pTBK1-Ser172-specific antibody for 2 h. Following, the cells were incubated with an AF488-conjugated secondary antibody for 1 h and then the nuclei were counterstained with Hoechst 33342. Z stack images were recorded in line sequential scan mode on a confocal microscope and visualized as maximum intensity projections (magenta: G_3-YSD, green: pTBK1-Ser172, blue: Hoechst 33342). One representative experiment of two independent experiments is shown.

3.4.2 TBK1, IKKβ, IKKε, and NF-κB p65 co-immunoprecipitate with hnRNPM

The results of this thesis suggest that hnRNPM and ELAVL1 regulate the cGAS- and RIG-I-dependent phosphorylation of TBK1 and IRF3. Since interactions between hnRNPM and IKKβ were detected by MS, it was analyzed whether hnRNPM also binds to other signaling proteins downstream of cGAS and RIG-I. Similar to before, hnRNPM-GFP and GFP were immunoprecipitated from lysates of resting and cGAS-activated THP-1 dual cells and co-immunoprecipitation was analyzed by immunoblotting. As previously observed, hnRNPM-GFP was significantly less expressed than GFP and, accordingly, the yield after IP of hnRNPM-GFP was also lower (Fig. 3.36). Nonetheless, TBK1 and pTBK1-Ser172 selectively co-immunoprecipitated with hnRNPM in an RNA-independent manner. The interactions between pTBK1-Ser172 and hnRNPM further increased after cGAS activation. It should be noted that for TBK1 and some other proteins, minor signals were also detectable after IP of GFP. However, the IPs of hnRNPM-GFP and GFP were analyzed on the same membrane, and in all experiments, the respective signal intensities were lower in the GFP condition. As previously shown by AP-MS, IKKβ and also IKKε selec-

tively co-immunoprecipitated with hnRNPM in a stimulation- and RNA-independent manner (Fig. 3.36).

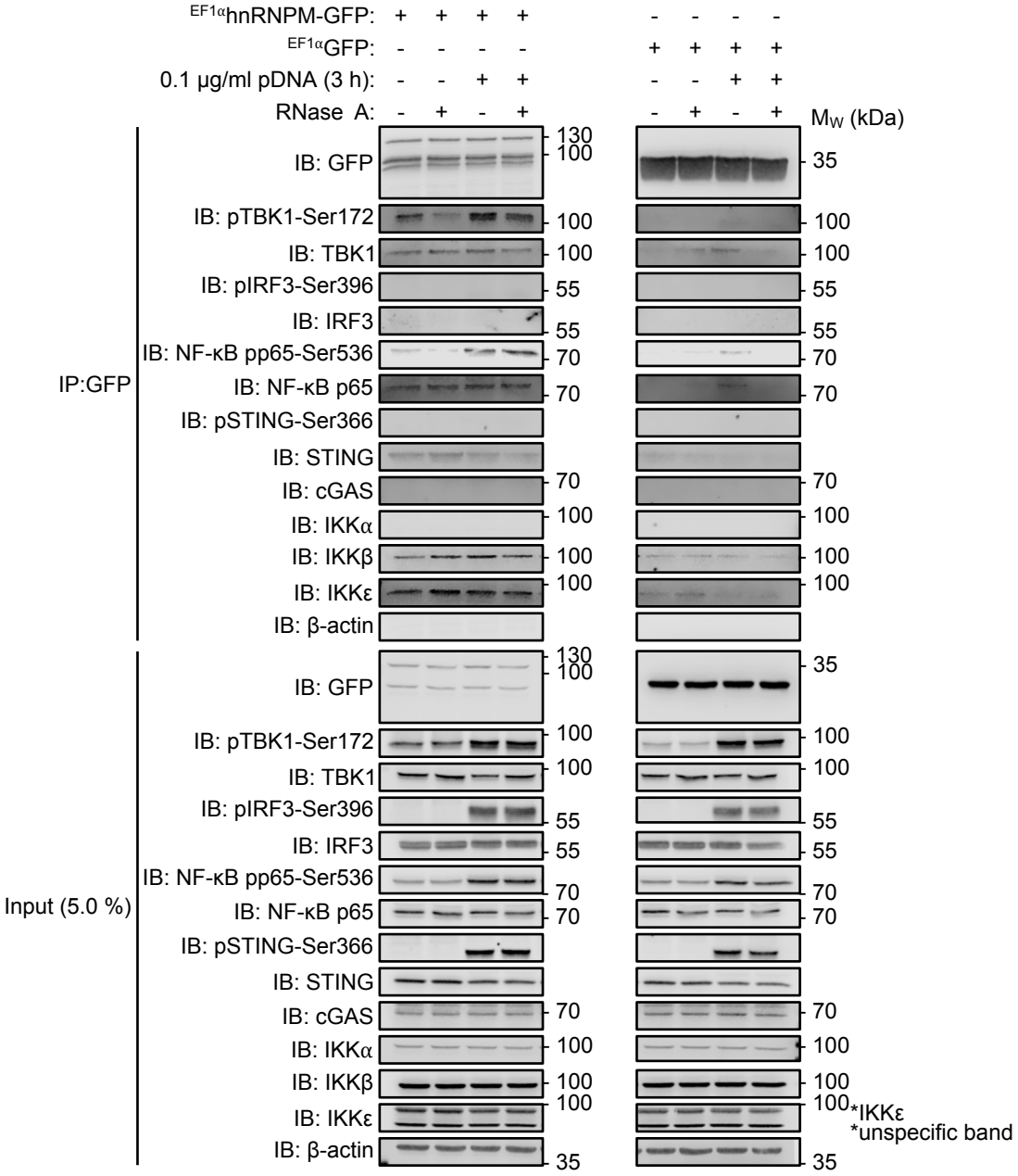

Fig. 3.36: TBK1, IKKβ, IKKε, and NF-κB p65 co-immunoprecipitate with hnRNPM. THP-1 dual cells stably expressing hnRNPM-GFP or GFP (EF1α promoter) were stimulated with 0.1 µg/ml pDNA or left non-stimulated. After 3 h, CCLs were generated and the GFP fusion proteins were immunoprecipitated at 4 °C overnight. If indicated, RNase A treatment was performed after IP. Bound proteins were analyzed by immunoblotting with the indicated antibodies and 5.0 % of the CCLs were used as input controls. Corresponding signals are from the same blot, with empty lanes removed. One representative experiment of at least two independent experiments is shown.

Of note, NF-κB p65 and NF-κB pp65-Ser536 also formed RNase-resistant complexes with hnRNPM. Similar to TBK1, cGAS activation further enhanced the interactions between hnRNPM and NF-κB pp65-Ser536 (Fig. 3.36). By contrast, hnRNPM did not interact with IRF3, pIRF3-Ser396, pSTNG-Ser366, cGAS, and IKKα. Interestingly, in contrast to pSTING-Ser366, low amounts of total STING protein co-immunoprecipitated with hnRNPM (Fig. 3.36).

To provide a second layer of specificity, putative interactions between ELAVL1 and pTBK1-Ser172 were also analyzed by co-IP. Notably, pTBK1-Ser172 selectively co-immunoprecipitated with ELAVL1 after activation of cGAS (Fig. 3.37). In summary, these data indicate that hnRNPM and ELAVL1 form a yet undescribed multiprotein complex *in vitro* that contains kinases and transcription of the cGAS and RIG-I signaling pathways.

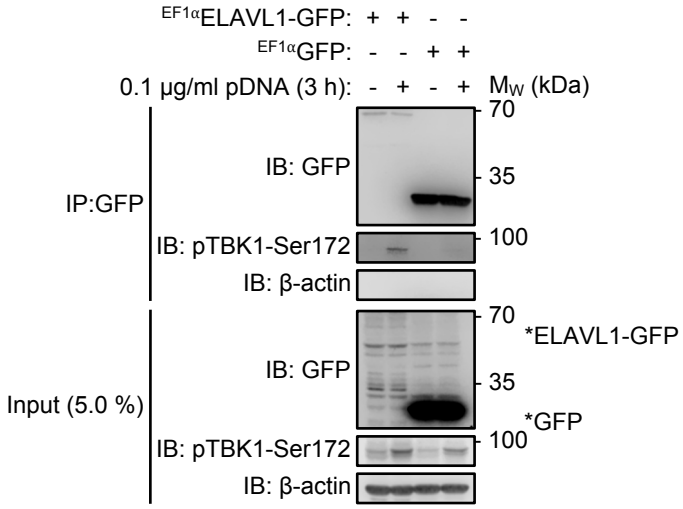

Fig. 3.37: Activated TBK1 co-immunoprecipitates with ELAVL1.
THP-1 dual cells stably expressing ELAVL1-GFP or GFP (EF1α promoter) were stimulated with 0.1 µg/ml pDNA or left non-stimulated. After 3 h, CCLs were generated and the GFP fusion proteins were immunoprecipitated at 4 °C overnight. Bound proteins were analyzed by immunoblotting with the indicated antibodies. 5.0 % of the CCLs were used as input controls. One representative experiment of two independent experiments is shown.

3.4.3 hnRNPM, ELAVL1, and TBK1 form a multiprotein complex *in cellulo*

To exclude the possibility that co-IP of pTBK1-Ser172 with hnRNPM/ELAVL1 resulted from non-specific interactions and to test whether these interactions also occur *in cellulo*, PLAs were performed. PLA makes use of an antibody-directed rolling circle amplification

and can resolve protein:protein interactions within a distance of 40 nm in cells. According to the manufacturer, the amplification step enhances the signal intensities up to 1,000-fold, thus allowing detection of weak/transient interactions.

For this assay, THP-1 dual cells expressing hnRNPM-GFP or GFP (biological control) were seeded in 96-well imaging chambers and incubated overnight with 100 ng/ml PMA to allow differentiation into an adherent, macrophage-like state. After stimulation of cGAS with G_3-YSD, the cells were fixed, permeabilized, and blocked. To analyze interactions between hnRNPM and TBK1 phosphorylated at Ser172 (hnRNPM:pTBK1-Ser172), the cells were incubated with a combination of GFP- and pTBK1-Ser172-specific antibodies. After adding species-specific oligonucleotide-coupled secondary antibodies, the PLA reaction was performed. Hybridization of fluorophore-coupled oligonucleotides with the amplification product was analyzed by confocal microscopy. Images of whole cells at different focal distances along the z axis were captured and Fiji was used for image processing. Before the signals were counted, a threshold was applied to the PLA channel to enhance the signal-to-noise ratio. The PLA score was defined as the total number of PLA signals per cell, providing a proportional measure to the degree of protein:protein interactions.

Experiences from different experiments showed that also incubation with only one primary antibody leads to a detectable number of PLA signals, averaging between 20 to 30 puncta per cell (Fig. 3.38B-3.40B). Therefore, GFP-expressing cells and specimens incubated with only one of the indicated antibodies were included as controls. It should be noted that due to the selected z step size of 0.5 µm, signals may be counted multiple times. Therefore, the actual number of PLA puncta per cell is lower than the calculated PLA score. However, since the z step size was fixed throughout all experiments and whole cells were imaged, this was considered a systematic error that would not distort the final results. Furthermore, it was observed that the PLA signals (Texas Red channel) were partially also detectable in the G_3-YSD-AF647 channel, explaining the low signal intensities in the G_3-YSD-AF647 channel in the non-stimulated condition. Because signal intensities varied between independent experiments, laser intensities and image processing parameters in Fiji (default threshold: 6 to 255 or 10 to 255; size of counted puncta: 5 to ∞ or 10 to ∞ pixel units) were adjusted to increase the signal-to-noise ratio. Within one experimental group, however, these settings remained unchanged.

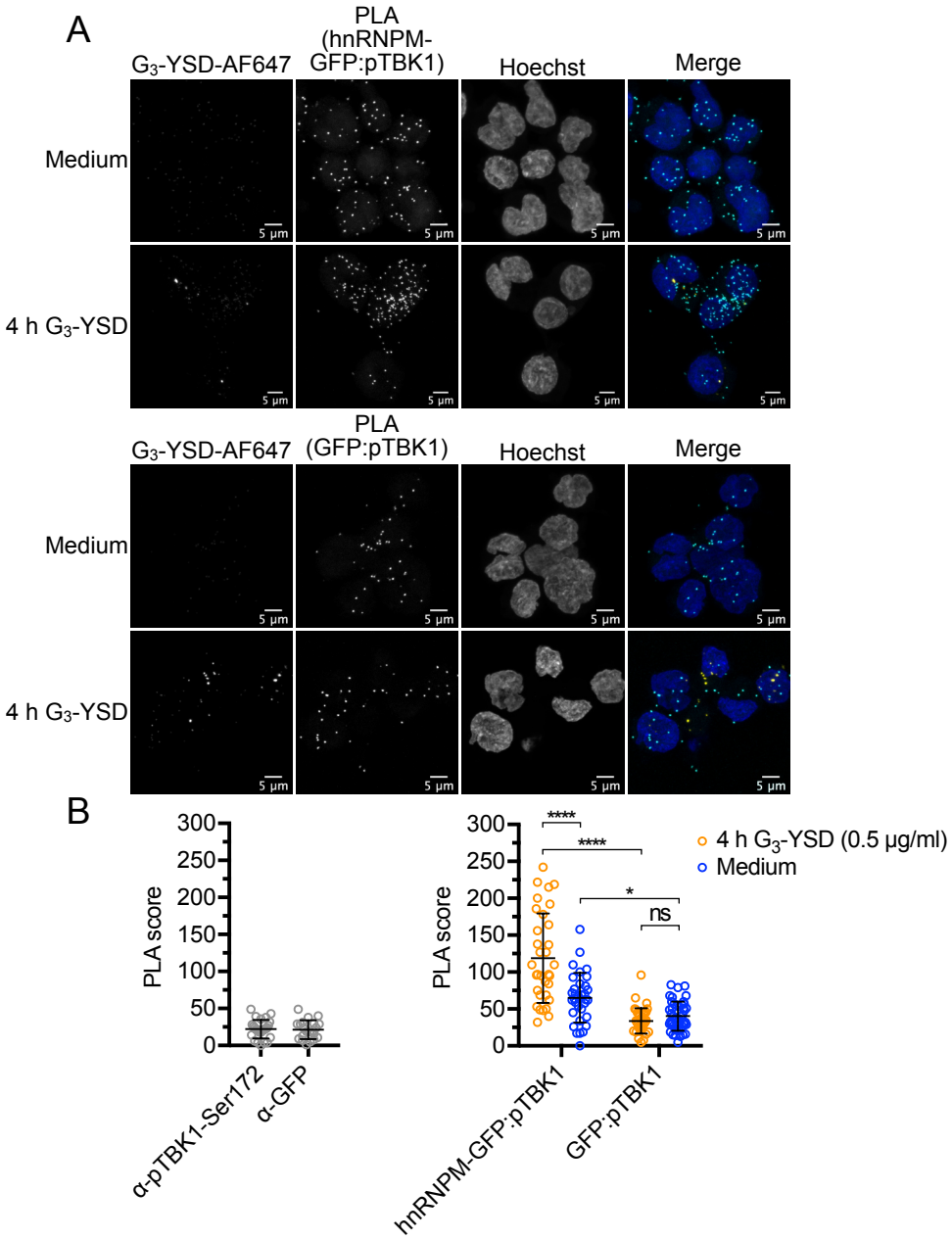

Fig. 3.38: hnRNPM and activated TBK1 are in close proximity *in cellulo*.
(**A**) PMA-differentiated THP-1 dual cells expressing hnRNPM-GFP (top) or GFP (bottom) were stimulated with 0.5 µg/ml G_3-YSD-AF647 or left non-stimulated (Medium). After 4 h, the PLA reaction was performed (primary antibody combination: rabbit α-pTBK1-Ser172 + mouse α-GFP). Hoechst 33342 was used to counterstain the nuclei. Z stack images were recorded on a confocal microscope. The image sequences are shown as maximum intensity projections (yellow: G_3-YSD, cyan: PLA, blue: Hoechst 33342). PLA signals indicate close proximity of proteins recognized by two different primary antibodies. (**B**) Fiji was used to determine the PLA scores (left: PLA scores after incubation with α-pTBK1-Ser172 mAb or α-GFP mAb; right: PLA scores of the hnRNPM-GFP:pTBK1-Ser172 and GFP:pTBK1-Ser172 interactions detected in (A) (n ≥ 29 cells, mean + SD, two-way ANOVA, Tukey's multiple comparisons test). Significances are indicated as follows: * ($P < 0.05$), ** ($P < 0.01$), *** ($P < 0.001$), **** ($P \leq 0.0001$), ns: not significant.

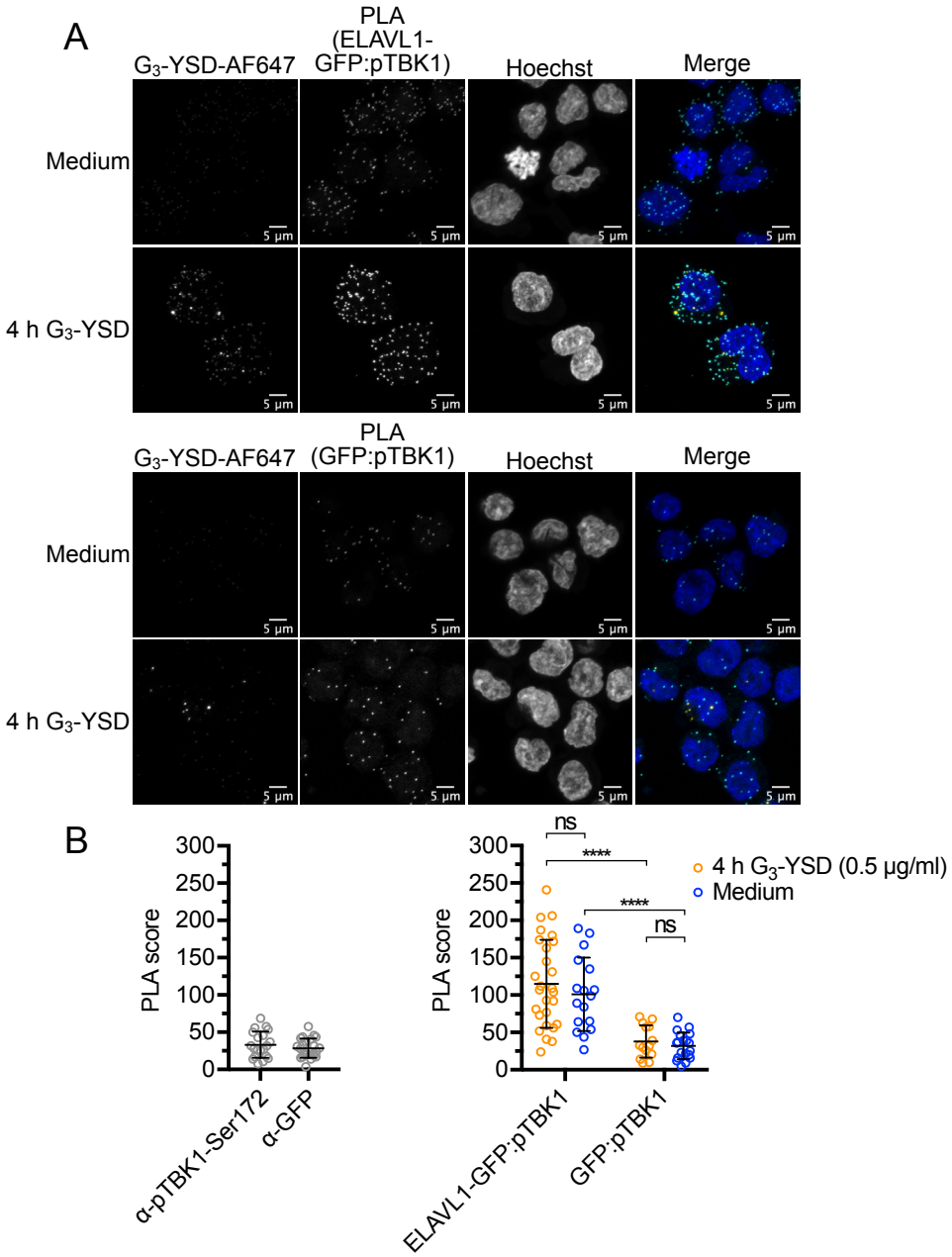

Fig. 3.39: ELAVL1 and activated TBK1 are in close proximity *in cellulo*.
(**A**) PMA-differentiated THP-1 dual cells expressing ELAVL1-GFP (top) or GFP (bottom) were stimulated with 0.5 µg/ml G_3-YSD-AF647 or left non-stimulated (Medium). After 4 h, the PLA reaction was performed (primary antibody combination: rabbit α-pTBK1-Ser172 + mouse α-GFP). Hoechst 33342 was used to counterstain the nuclei. Z stack images were recorded on a confocal microscope. The image sequences are shown as maximum intensity projections (yellow: G_3-YSD, cyan: PLA, blue: Hoechst 33342). PLA signals indicate close proximity of proteins recognized by two different primary antibodies. (**B**) Fiji was used to determine the PLA scores (left: PLA scores after incubation with α-pTBK1-Ser172 mAb or α-GFP mAb; right: PLA scores of the ELAVL1-GFP:pTBK1-Ser172 and GFP:pTBK1-Ser172 interactions detected in (A) (n ≥ 14 cells, mean + SD, two-way ANOVA, Tukey's multiple comparisons test). Significances are indicated as follows: * ($P < 0.05$), ** ($P < 0.01$), *** ($P < 0.001$), **** ($P \leq 0.0001$), ns: not significant.

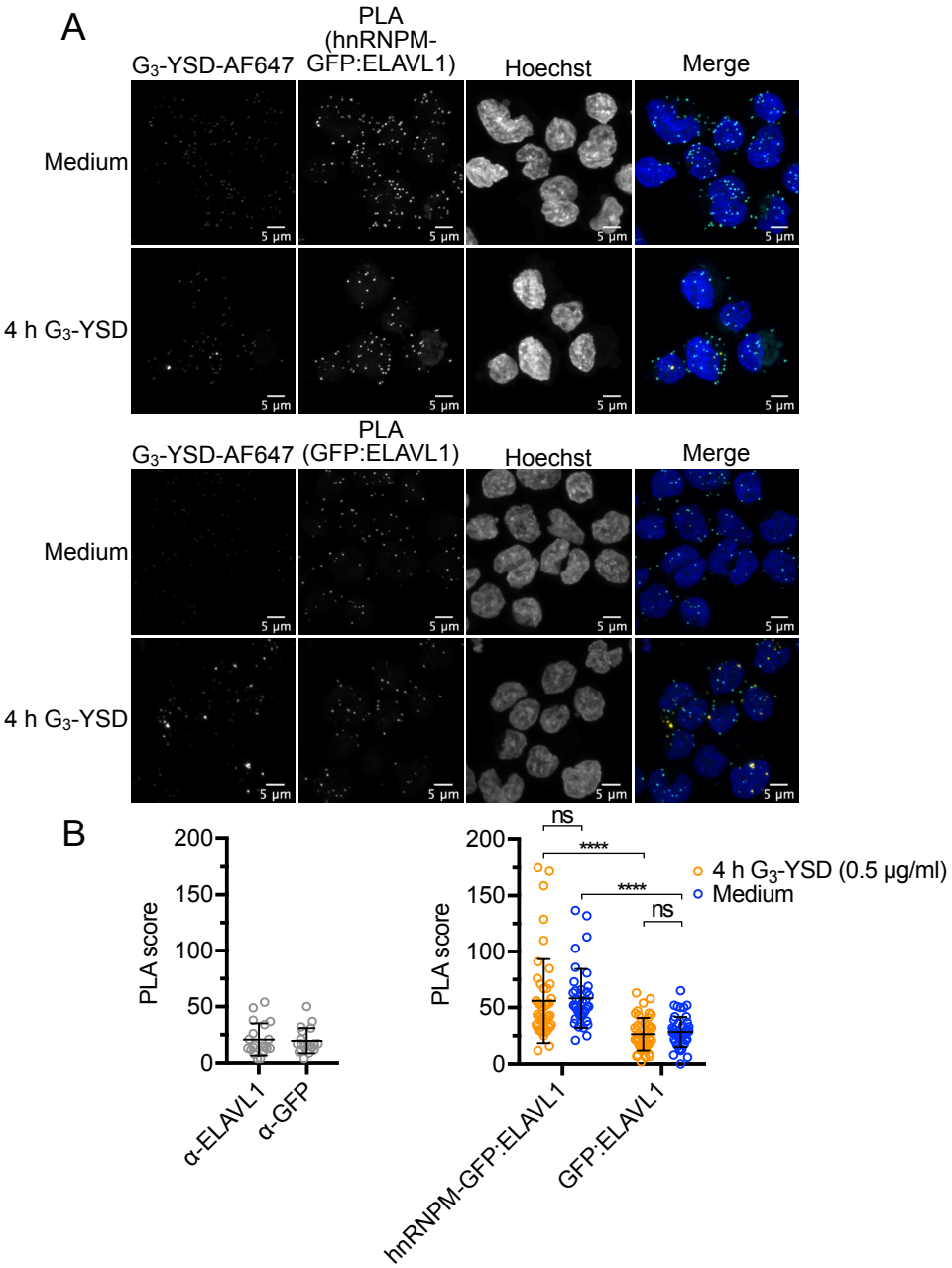

Fig. 3.40: hnRNPM and ELAVL1 are in close proximity *in cellulo*.
(**A**) PMA-differentiated THP-1 dual cells expressing hnRNPM-GFP (top) or GFP (bottom) were stimulated with 0.5 µg/ml G_3-YSD-AF647 or left non-stimulated (Medium). After 4 h, the PLA reaction was performed (primary antibody combination: rabbit α-ELAVL1 + mouse α-GFP). Hoechst 33342 was used to counterstain the nuclei. Z stack images were recorded on a confocal microscope. The image sequences are shown as maximum intensity projections (yellow: G_3-YSD, cyan: PLA, blue: Hoechst 33342). PLA signals indicate close proximity of proteins recognized by two different primary antibodies. (**B**) Fiji was used to determine the PLA scores (left: PLA scores after incubation with α-ELAVL1 mAb or α-GFP mAb; right: PLA scores of the hnRNPM-GFP:ELAVL1 and GFP:ELAVL1 interactions detected in (A) (n ≥ 38 cells, mean + SD, two-way ANOVA, Tukey's multiple comparisons test). Significances are indicated as follows: * (P < 0.05), ** (P < 0.01), *** (P < 0.001), **** (P ≤ 0.0001), ns: not significant.

Using the quantification strategy described above, close proximity of hnRNPM and pTBK1-Ser172 was detected in non-stimulated THP-1 dual monocytes (Fig. 3.38A-3.38B). Of note, the PLA score further increased upon cGAS stimulation. Assembly of the recorded images into 3D projections revealed that the majority of PLA puncta were present in the cytoplasm and close to the nuclear envelope, suggesting that hnRNPM regulates TBK1 phosphorylation in the cytoplasm (3D projections not shown).

Similarly, the interactions of ELAVL1:pTBK1-Ser172 and hnRNPM:ELAVL1 were analyzed. To analyze the interactions between ELAVL1 and activated TBK1, PLA was performed in THP-1 dual cells expressing ELAVL1-GFP or GFP using GFP- and pTBK1-Ser172-specific primary antibodies. As shown in Fig. 3.39A-3.39B, the PLA score of the ELAVL1-GFP:pTBK1-Ser172 interactions was significantly higher compared to the GFP:pTBK1-Ser172 condition, indicating close proximity of ELAVL1 and activated TBK1 *in cellulo*. The PLA signals were mainly detected in the cytoplasm, with no evident increase after cGAS stimulation (3D projections not shown). To analyze the interactions between hnRNPM and ELAVL1, PLA was performed in THP-1 dual cells expressing hnRNPM-GFP or GFP using GFP- and ELAVL1-specific primary antibodies. The calculated PLA score of the hnRNPM-GFP:ELAVL1 interactions was also significantly higher compared to GFP:ELAVL1, suggesting that hnRNPM and ELAVL1 also interact *in cellulo* (Fig. 3.40A-3.40B). 3D projections of the acquired images showed that most PLA signals are detectable in the cytoplasm and partially in the nucleus (3D projections not shown). Altogether, these findings complement the results of the *in vitro* co-IP experiments and indicate that hnRNPM, ELAVL1, and TBK1 form a so far undescribed multiprotein complex *in cellulo*. But how do hnRNPM and ELAVL1 regulate the phosphorylation of TBK1 mechanistically?

3.5 hnRNPM forms a multiprotein complex that augments the phosphorylation of TBK1 in the activation loop

ELAVL1 and hnRNPM control the type I IFN induction triggered by cGAS and RIG-I and interact with signaling proteins shared by both pathways. However, these findings do not explain how hnRNPM and ELAVL1 regulate signaling at a mechanistic level. In principle, hnRNPM and ELAVL1 could promote TBK1 activation (1) by inhibiting TBK1-specific phosphatases, (2) by regulating the nuclear translocation of IRF3, (3) by regulating the

phosphorylation-dependent activation of TBK1, or (4) by regulating unknown TBK1-specific kinases. In this thesis, the first three hypotheses were tested.

3.5.1 No evidence for a direct connection between hnRNPM, ELAVL1, and several phosphatases

It was hypothesized that the newly identified hnRNPM/ELAVL1 multiprotein complex sequesters TBK1 from inhibitory phosphatases to maintain signaling. Several phosphatases have been reported to dephosphorylate TBK1, including protein phosphatase 1 B (PPM1B), protein phosphatase 4 (PP4, encoded by *PPP4C*), and phosphatidylinositol 3,4,5-trisphosphate 5-phosphatase 1 (SHIP1, encoded by *INPP5D*) (Gabhann et al., 2010; Zhan et al., 2015; Zhao et al., 2012). To analyze whether these phosphatases inhibit the cGAS- and RIG-I-mediated type I IFN response in THP-1 dual cells, target-specific KD cell lines were generated (Fig. 3.41A-3.41B).

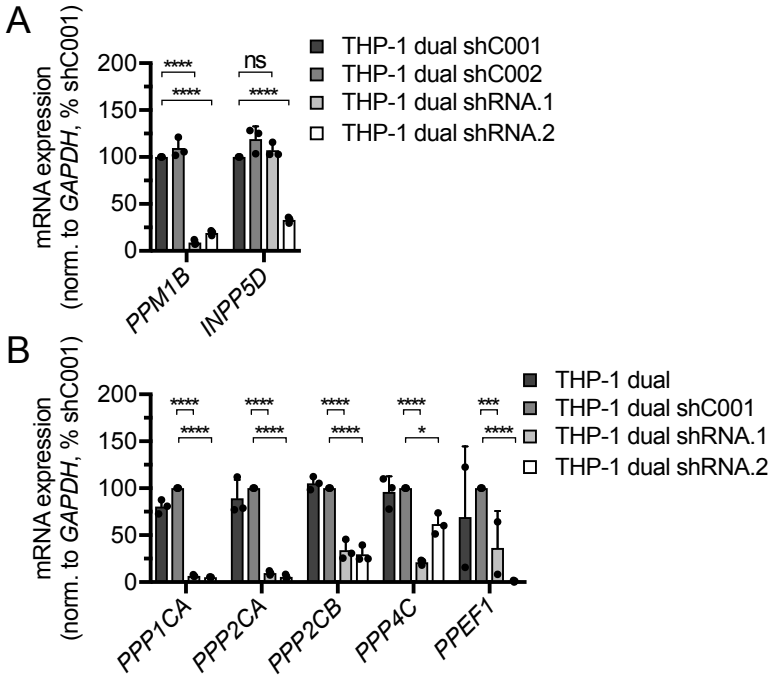

Fig. 3.41: KD of several phosphatases in THP-1 dual cells.
(**A**) Control cells (THP-1 dual shC001, THP-1 dual shC002) and cells expressing PPM1B- or SHIP1-specific shRNAs were analyzed by qPCR to determine relative target KD efficiency. The target mRNA expression was normalized to *GAPDH* mRNA (n = 3, mean + SD, two-way ANOVA, Dunnett's multiple comparisons test). (**B**) Control cells (THP-1 dual, THP-1 dual shC001) and cells expressing PP1-, PP2A-, PP2B-, PP4-, or PP7-specific shRNAs were analyzed by qPCR to determine relative target KD efficiency. The target mRNA expression was normalized to *GAPDH* mRNA (n ≥ 2, mean + SD, two-way ANOVA, Dunnett's multiple comparisons test). Significances are indicated as follows: * ($P < 0.05$), ** ($P < 0.01$), *** ($P < 0.001$), **** ($P \leq 0.0001$), ns: not significant.

Since phosphatases have a broad substrate specificity, additional phosphatases were included in the KD screen (i.e., PP1 (encoded by *PPP1CA*), PP2A (encoded by *PPP2CA*), PP2B (encoded by *PPP2CB*), and PP7 (encoded by *PPEF1*)) (Sparks and Brautigan, 1986). qPCR analysis showed that all shRNAs, except shRNA.2 against SHIP1, induce a target-specific KD (Fig. 3.41A-3.41B). However, the cGAS- or RIG-I-mediated ISRE reporter activities were not consistently increased in the phosphatase KD cell lines, indicating that PP1, PP2A, PP2B, PP4, PP7, PPM1B, and SHIP1 do not negatively regulate cGAS and RIG-I signaling in THP-1 dual cells (Fig. 3.42A-3.42B).

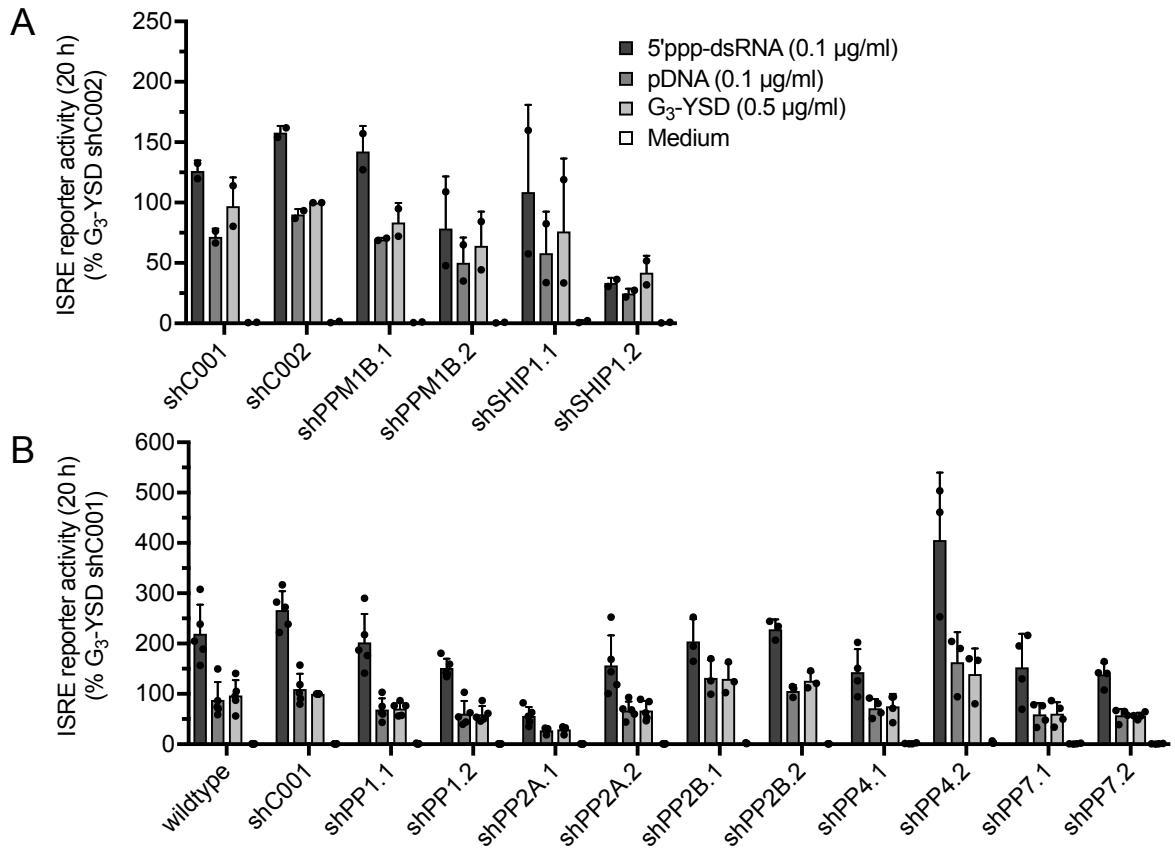

Fig. 3.42: The cGAS- and RIG-I-dependent type I IFN induction in THP-1 dual cells is not negatively regulated by PPM1B, SHIP1, PP1, PP2A, PP2B, PP4, and PP7.
(**A**) Control cells (THP-1 dual shC001, THP-1 dual shC002) and cells expressing PPM1B- or SHIP1-specific shRNAs (target-specific shRNAs are indicated on the X axis) were stimulated with ligands activating RIG-I (5'ppp-dsRNA), cGAS (pDNA, G_3-YSD), or left non-stimulated (Medium). After 20 h, ISRE reporter activation was analyzed (n = 2, mean + SD). (**B**) Control cells (THP-1 dual (wildtype), THP-1 dual shC001) and cells expressing PP1-, PP2A-, PP2B-, PP4-, or PP7-specific shRNAs (target-specific shRNAs are indicated on the X axis) were stimulated and analyzed as described in (A) (n ≥ 3, mean + SD).

It is conceivable that these phosphatases redundantly dephosphorylate TBK1. Therefore, wildtype and ELAVL1-deficient THP-1 dual cells were treated with OA, a potent inhibitor of PP1 and PP2A (Bialojan and Takai, 1988) as well as PP4 and PP5 (Swingle et al., 2007). Treating THP-1 dual wildtype cells with 10 nM and 20 nM OA slightly increased the cGAS- and RIG-I-dependent ISRE reporter activation (Fig. 3.43). At higher OA concentrations, ISRE reporter activities were reduced in THP-1 dual wildtype cells, presumably due to toxicity of OA. However, OA treatment did not rescue the cGAS- or RIG-I-induced type I IFN production in ELAVL1-deficient THP-1 dual cells, indicating that ELAVL1 does not positively regulate cGAS and RIG-I signaling by suppressing the activity of PP1, PP2A, PP4, and PP5. Interestingly, increasing concentrations of OA triggered a significant type I IFN response in non-stimulated wildtype cells but not in ELAVL1-deficient THP-1 dual cells. In summary, these results demonstrate that the phosphatases described above do not non-redundantly inhibit cGAS and RIG-I signaling in THP-1 dual cells. Therefore, it remains challenging to establish a direct link to hnRNPM/ELAVL1.

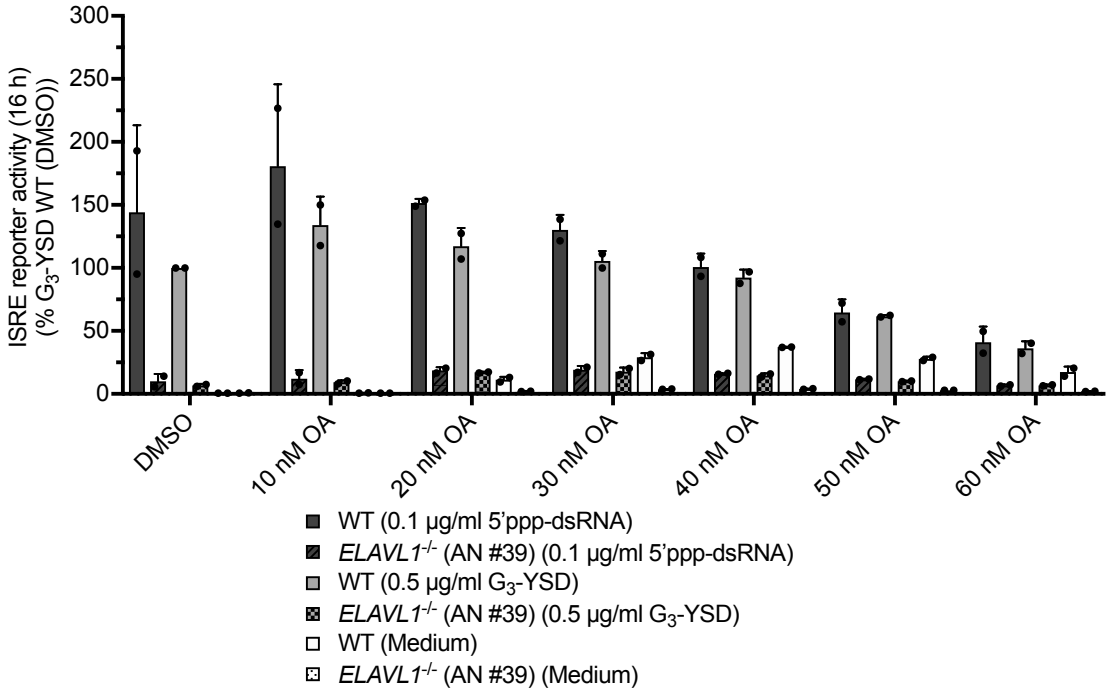

Fig. 3.43: OA treatment does not rescue the cGAS- and RIG-I-dependent production of type I IFNs in THP-1 dual *ELAVL1*$^{-/-}$ cells.
THP-1 dual (WT) and THP-1 dual *ELAVL1*$^{-/-}$ (AN #39) cells were incubated with the indicated concentrations of OA or DMSO for 6 h. The cells were kept in OA- or DMSO-containing medium and stimulated with 5'ppp-dsRNA, G_3-YSD, or left non-stimulated (Medium). After 16 h, ISRE reporter activation was analyzed (n = 2, mean + SD).

3.5.2 ELAVL1 does not mediate the nuclear transport of TBK1 and IRF3

Phosphorylation-induced IRF3 dimerization and translocation of dimeric IRF3 to the nucleus is a hallmark of cGAS and RIG-I signaling. It was previously reported that ELAVL1 stabilizes the mRNA of *PLK2*, a gene involved in the nuclear translocation of IRF3 (Sueyoshi et al., 2018). However, the 3'-mRNA expression analysis in this thesis showed that the mRNA expression of *PLK2* is unchanged between wildtype and ELAVL1-deficient THP-1 dual cells. Nonetheless, nuclear and cytoplasmic extracts were prepared to analyze the localization of IRF3 in THP-1 dual ELAVL1 KO cells (Fig. 3.44).

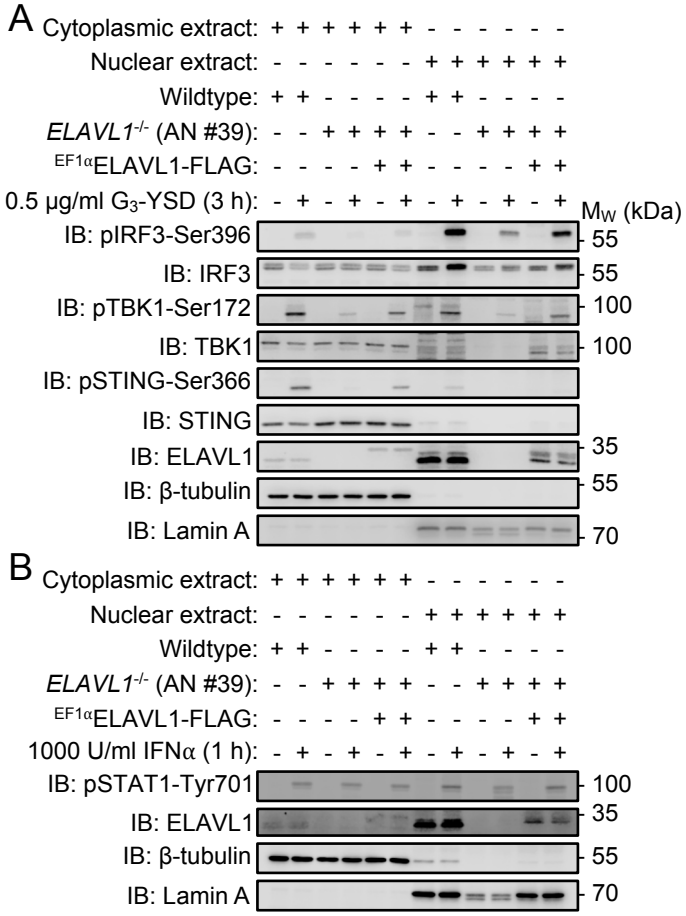

Fig. 3.44: ELAVL1 does not regulate the nuclear transport of IRF3 and TBK1 in THP-1 dual cells.
(**A**) THP-1 dual cells (wildtype), THP-1 dual *ELAVL1*$^{-/-}$ cells (AN #39), and THP-1 dual *ELAVL1*$^{-/-}$ (AN #39) ELAVL1-FLAG-expressing cells (EF1α promoter) were stimulated with 0.5 µg/ml G_3-YSD or left non-stimulated. After 3 h, nuclear and cytoplasmic extracts were prepared and analyzed by immunoblotting with the indicated antibodies. One representative experiment of two independent experiments is shown. (**B**) The cell lines depicted in (A), were stimulated with 1000 U/ml IFNα or left non-stimulated. After 1 h, nuclear and cytoplasmic extracts were prepared and analyzed by immunoblotting with the indicated antibodies. One representative experiment is shown.

Relative to wildtype and ELAVL1-FLAG-expressing THP-1 dual *ELAVL1*$^{-/-}$ cells, pIRF3-Ser396 and total IRF3 levels were significantly reduced in the nuclear extracts of ELAVL1-deficient cells 3 h after cGAS activation with 0.5 µg/ml G_3-YSD and did not accumulate in the cytoplasm, further arguing against the nuclear transport theory postulated by Sueyoshi *et al.* (Fig. 3.44A). Similar to pIRF3, the cytoplasmic and nuclear pTBK1-Ser172 levels were reduced to similar extents in THP-1 dual ELAVL1 KO cells. Total TBK1 protein was predominantly localized in the cytoplasm and not detectable in the nuclear extracts of ELAVL1-deficient cells (Fig. 3.44A). In contrast to wildtype and reconstituted ELAVL1 KO cells, no phosphorylated STING was found in the cytoplasmic extracts of cGAS-activated ELAVL1-deficient cells. Interestingly, lamin A was significantly less expressed in ELAVL1-deficient THP-1 dual cells, indicating that ELAVL1 regulates lamin A expression.

As a control, the localization of pSTAT1-Tyr701 was analyzed 1 h after stimulation of IFNAR with 1000 U/ml IFNα (Fig. 3.44B). Notably, the cytoplasmic pSTAT1-Tyr701 levels were unaltered in ELAVL1-deficient THP-1 dual cells and only modestly decreased in the nuclear fraction after IFNAR stimulation, further indicating that ELAVL1 is not connected to the JAK-STAT signaling pathway. Altogether, these results suggest that ELAVL1 does not mediate the nuclear transport of pIRF3-Ser396/IRF3 in THP-1 dual cells and indicate that ELAVL1 promotes cGAS and RIG-I signaling upstream of the nuclear transport machinery.

3.5.3 hnRNPM forms a multiprotein complex that enhances the phosphorylation of TBK1 in the activation loop

Because the nuclear transport of pIRF3-Ser396/IRF3 in THP-1 dual cells is not regulated by ELAVL1, it was hypothesized that ELAVL1 and hnRNPM directly modulate the activity of TBK1. Therefore, an *in vitro* kinase assay was established to analyze the influence of the hnRNPM/ELAVL1 multiprotein complex on the phosphorylation of TBK1 in the activation loop (Fig. 3.45). The first step of the assay was the IP of hnRNPM-GFP and GFP from lysates of resting or cGAS-activated THP-1 dual cells. Consistent with previous observations, pTBK1-Ser172, IKKβ, and IKKε selectively co-immunoprecipitated with hnRNPM (Fig. 3.45A). After IP, the beads were washed extensively to reduce non-specific protein binding and incubated with catalytically active TBK1-GST (produced in Sf9 cells) in the presence of 20 µM ATP at 30 °C for 30 min.

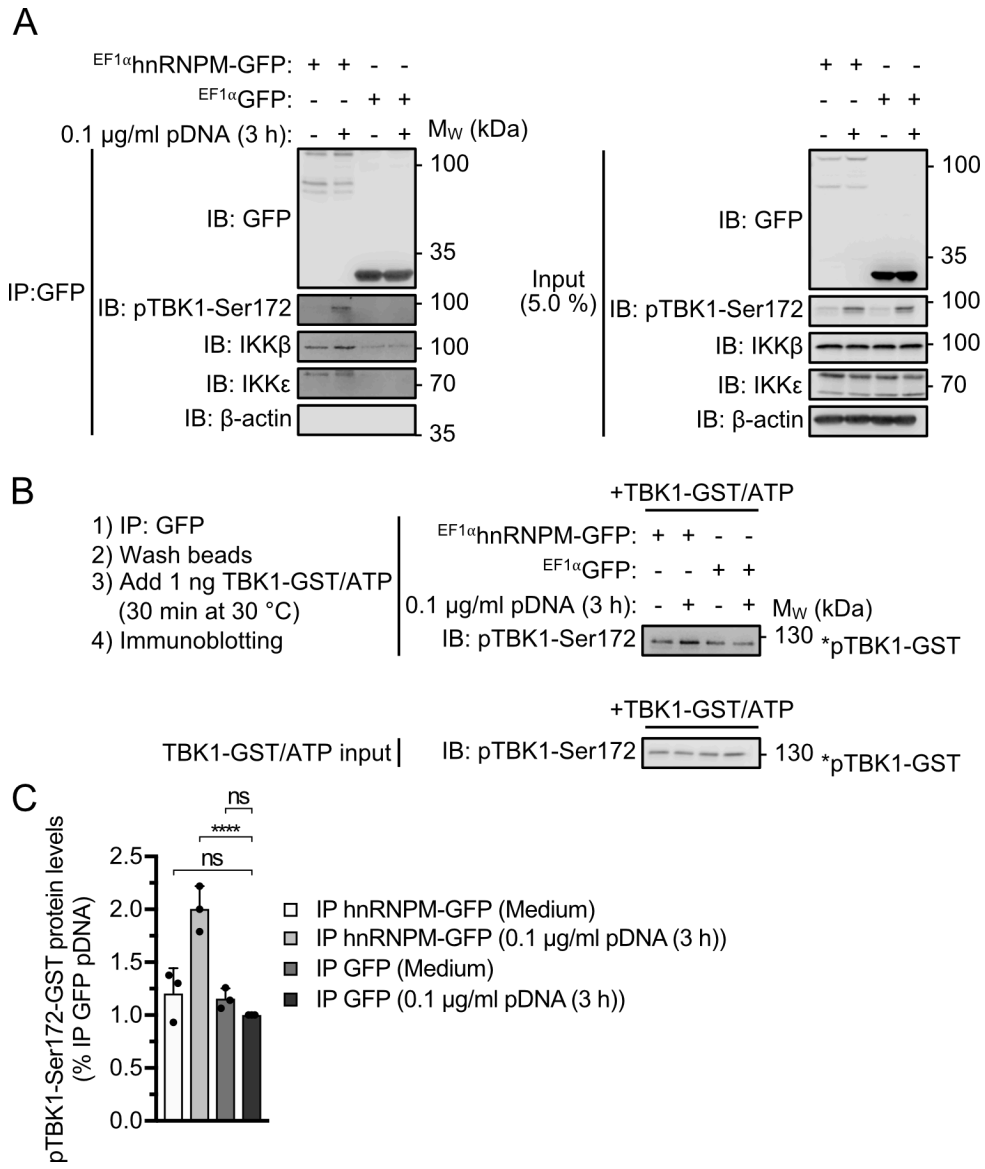

Fig. 3.45: hnRNPM forms a novel multiprotein complex that enhances the phosphorylation of TBK1 in the activation loop.

(**A**) THP-1 dual cells stably expressing hnRNPM-GFP or GFP (EF1α promoter) were stimulated with 0.1 µg/ml pDNA or left non-stimulated (Medium). After 3 h, CCLs were generated and the GFP fusion proteins were immunoprecipitated at 4 °C overnight. Bound proteins were analyzed by immunoblotting with the indicated antibodies. 5.0 % of the CCLs were used as input controls. (**B**) The IPs depicted in (A) were incubated with recombinant, catalytically active TBK1-GST in ATP-containing buffer at 30 °C for 30 min and then the phosphorylation of TBK1-GST was analyzed by immunoblotting with a pTBK1-Ser172-specific antibody (upper blot). As an input control, 1 ng TBK1-GST was incubated in ATP-containing buffer at 30 °C for 30 min (lower blot). One representative experiment of three independent experiments is shown. (**C**) Quantification of the pTBK1-Ser172-GST signals detected in (B) (n = 3, mean + SD, one-way ANOVA, Dunnett's multiple comparisons test). Significances are indicated as follows: * ($P < 0.05$), ** ($P < 0.01$), *** ($P < 0.001$), **** ($P \leq 0.0001$), ns: not significant.

Following, the phosphorylation of TBK1-GST was analyzed by immunoblotting. As expected, incubation of TBK1-GST in ATP-containing buffer induced a strong autophosphorylation pattern (Fig. 3.45B, lower blot), whereas almost no phosphorylated TBK1-GST was detected in the absence of ATP (data not shown). Of note, incubation of recombinant TBK1 with hnRNPM-GFP immunoprecipitated from CCLs of cGAS-activated cells increased the phosphorylation of TBK1-GST at Ser172 (pTBK1-Ser172-GST) by approximately 2-fold as compared to the GFP condition, indicating that the multiprotein complex formed by hnRNPM can enhance the phosphorylation of TBK1 in the activation loop *in vitro* (Fig. 3.45B-3.45C). In conjunction with the PLA results, these data suggest that the hnRNPM/ELAVL1 multiprotein complex exhibits scaffolding functions for active kinases of the cGAS and RIG-I signaling pathways and regulates the expression of type I IFNs by enhancing TBK1 activity.

4 Discussion

Detection of non-self nucleic acids by cGAS and RIG-I is crucial for the host to fight viral infections. Although several key adaptor proteins, kinases, and transcription factors have been described, important questions remain to be answered regarding the regulation and interplay of the underlying signal transmission cascades. This thesis has shown that hnRNPM functions as a non-redundant positive regulator of both cGAS and RIG-I signaling. Biochemical and genetic analyses have demonstrated that hnRNPM operates downstream of RIG-I, cGAS, and STING and upstream of TBK1 and IRF3 phosphorylation. Through a combined AP-MS/RNAi screening approach, ELAVL1 and SON were identified as novel interaction partners of hnRNPM. Genetic deletion of *ELAVL1* in THP-1 dual cells and reconstitution approaches revealed that ELAVL1 is a potent inducer of the cGAS- and RIG-I-dependent type I IFN response and promotes TBK1 and IRF3 phosphorylation. IPs showed that hnRNPM interacts with important signaling proteins downstream of both cGAS and RIG-I, including TBK1, IKKβ, IKKε, and NF-κB p65. Direct interactions between phosphorylated TBK1, hnRNPM, and ELAVL1 were also detected *in cellulo*. Mechanistically, hnRNPM and ELAVL1 form a multiprotein complex that promotes type I IFN induction by amplifying the phosphorylation of TBK1 in the activation loop.

4.1 hnRNPM is a non-redundant positive regulator of RIG-I and cGAS signaling

4.1.1 hnRNPM is a positive regulator of the RIG-I- and cGAS-dependent type I IFN response

hnRNPM, the central protein of this thesis, was originally identified by Dr. A.-M. Herzner as a G_3-YSD-binding protein. Initial RNAi experiments pointed towards an involvement of hnRNPM in the cGAS-mediated type I IFN production. However, the elementary function of hnRNPM remained elusive.

hnRNPM is a multifunctional protein and belongs to the hnRNP family. Rather than being classified by structural similarity, hnRNPs were originally identified by sucrose gradient centrifugation as RNA-binding proteins of the eukaryotic small ribosomal subunit (40S) (Beyer et al., 1977; Eekelen et al., 1981). hnRNPs participate in a wide range of RNA processing steps and have been shown to mediate splicing, translation, stabilization, and transport of RNAs (Han et al., 2010). hnRNPM consists of three RRMs and exhibits bind-

ing preferences towards G/U-rich sequences in distal intronic RNA (Huelga et al., 2012). In addition to its role in pre-mRNA splicing, accumulating evidence suggests that hnRNPM also regulates viral replication and type I IFN expression. Preliminary experiments prior to this thesis indicated that hnRNPM constitutes a novel candidate type I IFN-inducing DNA sensor because (1) it interacted with G_3-YSD and (2) KD of hnRNPM diminished the cGAS-dependent type I IFN response. Indeed, in this study, the N-terminus of hnRNPM was shown to mediate the interactions with G_3-YSD. However, *in vitro* pull-down experiments cannot clarify whether the interactions occur directly or depend on scaffold molecules (e.g., proteins, RNAs). It should be noted that in both the current G_3-YSD/C_3-YSD pull-down and the initial MS-based identification of hnRNPM, biotinylated G_3-YSD was not transfected into cells but was incubated with CCLs. The question therefore arises whether cytoplasmic G_3-YSD and hnRNPM, a predominantly nuclear protein, would also interact to such extent under more physiological conditions. To overcome this technical problem, G_3-YSD-binding proteins could be analyzed in future experiments by *in vivo* cross-linking MS, a technology that could lead to a more stringent identification of novel DNA sensors or cofactors of the cGAS-STING pathway (Kaake et al., 2014).

This thesis demonstrated that KD of hnRNPM in THP-1 dual cells attenuates both the cGAS- and RIG-I-dependent induction of type I IFNs, indicating that hnRNPM positively regulates a common signaling step downstream of these PRRs. These findings were surprising because cGAS and RIG-I sense fundamentally different PAMPs and both signaling pathways are considered independent of each other. However, both PRRs signal via shared kinases (i.e., TBK1, IKKε) and transcription factors (i.e., IRF3, NF-κB p65) and induce a comparable antiviral immune response that is dominated by type I IFNs and pro-inflammatory cytokines. Therefore, it is conceivable that cells have evolved a protein network that integrates signals from both pathways downstream of PRR activation. In addition, the 2'3'-cGAMP-induced type I IFN response was also reduced in THP-1 dual hnRNPM KD cells, indicating that hnRNPM functions downstream of STING and further arguing against the theory that hnRNPM represents a novel DNA sensor.

Although hnRNPM has been described in various cellular contexts, depletion of hnRNPM did not critically impair the metabolic activity of THP-1 dual cells, largely excluding the possibility that reduced cellular fitness inhibits the expression of type I IFNs. Additional evidence against a nonspecific phenotype is that the IFNα-induced JAK-STAT signaling

pathway is intact in THP-1 dual hnRNPM KD cells. Similarly, activation of TLR1/TLR2 and TLR8 induced low, unaltered levels of type I IFNs in THP-1 dual hnRNPM KD cells compared to wildtype and shC001-expressing cells. Only cells expressing shhnRNPM.2 exhibited a certain ISRE reporter hyperactivation after TL8-506 challenge, which was not observed in shhnRNPM.1-expressing cells. Because this effect was also detectable for the TLR8-dependent NF-κB response, it is conceivable that the expression of shhnRNPM.2 may have unintentionally downregulated a regulatory component of the TLR8 signaling pathway. However, since both hnRNPM-specific shRNAs reliably attenuated the type I IFN response induced by cGAS, STING, or RIG-I, this inconsistency was considered a non-specific effect.

In contrast to the markedly inhibited ISRE reporter activity, both THP-1 dual hnRNPM KD cell lines showed a differential NF-κB activation after cytosolic DNA or RNA challenge, arguing against the involvement of hnRNPM in the cGAS- and RIG-I-dependent NF-κB response. However, the observed signals were close to the detection limit. Thus, permanent genetic deletion of *HNRNPM* has clear advantages over shRNA-mediated KD. For THP-1 dual cells, several attempts to delete the *HNRNPM* gene failed, suggesting that hnRNPM deficiency is not tolerated by the cell. As will be discussed later, KO clones could be isolated for a newly characterized hnRNPM interactor, ELAVL1. Since the cGAS- and RIG-I-mediated activation of NF-κB was ELAVL1-dependent, it appears plausible that the hnRNPM/ELAVL1 multiprotein complex indeed mediates NF-κB activation and that the KD of hnRNPM was insufficient to observe this phenotype.

Overall, this study demonstrates for the first time that the cGAS- and RIG-I-dependent type I IFN response is non-redundantly regulated by a single protein, hnRNPM. Therefore, hnRNPM represents a convergence point of the cGAS and RIG-I signaling pathways. Other immune signaling cascades such as the TLR8-mediated type I IFN induction, IFNAR signaling, and the TLR1/TLR2-dependent activation of NF-κB are hnRNPM-independent.

4.1.2 hnRNPM promotes the phosphorylation-dependent activation of TBK1 and IRF3

To further investigate the function of hnRNPM, it was asked whether hnRNPM regulates the cGAS- and RIG-I-dependent type I IFN response (1) at the level of translation, (2) at the level of transcription, or (3) by directly enhancing the activity of signaling proteins. qPCR analysis showed that the cGAS-induced mRNA expression of *IFNB1*, *IFIT1*, *OAS1*, and *DDX60* is downregulated in THP-1 dual hnRNPM KD cells, suggesting that the translation of *IFNB1* mRNA is hnRNPM-independent and rather indicating that hnRNPM regulates transcriptional processes (i.e., regulation of RNA processing, RNA transport, or RNA stability) or signaling.

Ligand recognition by cGAS and RIG-I initiates complex signaling cascades that lead to the phosphorylation of key signaling proteins, including TBK1 and IRF3. In THP-1 dual wildtype cells, stimulation of cGAS induced high levels of pTBK1-Ser172 and pIRF3-Ser396, whereas RIG-I activation only led to a strong phosphorylation of IRF3. Surprisingly, hnRNPM was required for the cGAS- and RIG-I-mediated phosphorylation of IRF3. Similarly, reduced pTBK1-Ser172 levels were detectable in THP-1 dual hnRNPM KD cells after cGAS stimulation. These results indicate that hnRNPM promotes the cGAS- and RIG-I-dependent production of type I IFNs at stage (3). In contrast to IRF3, RIG-I activation only induced low levels of phosphorylated TBK1, which were not further diminished in THP-1 dual hnRNPM KD cells. It is conceivable that the hnRNPM KD efficiency was insufficient to also inhibit the RIG-I-dependent phosphorylation of TBK1. As described in the following chapters, this conclusion is supported by the observation that both pIRF3-Ser396 and pTBK1-Ser172 levels were significantly decreased in ELAVL1-deficient THP-1 dual cells after stimulation of cGAS or RIG-I.

Current data imply that cGAS and RIG-I trigger the oligomerization of STING and MAVS, respectively, thereby providing a suitable interaction surface for the recruitment and activation of TBK1 and IKKs. In turn, TBK1/IKKε/IKKβ phosphorylate MAVS at *p*L*x*IS^{442}, whereas STING is phosphorylated by TBK1 at *p*L*x*IS^{366}. These phosphorylated motifs serve as binding sites for IRF3 and are essential for the TBK1-dependent phosphorylation of IRF3. Considering the sequential nature of this multistep process, the results of this study imply that hnRNPM mediates a process upstream of TBK1 phosphorylation that is required for both cGAS and RIG-I signaling.

4.1.3 hnRNPM promotes the secretion of antiviral cytokines in myeloid and somatic cell lines

In addition to the THP-1-derived reporter cell line, HeLa cells were used as a somatic cell line to study the role of hnRNPM. It was shown that the RIG-I-dependent secretion of IP10, a surrogate parameter for type I IFNs, was significantly reduced in HeLa hnRNPM KD cells, indicating that the function of hnRNPM in nucleic acid immunity is not restricted to immune cells. By contrast, HeLa cells did not secrete IP10 after transfection of cGAS agonists. In line with these results, other groups have already reported that HeLa cells do not respond to lipofected DNA stimuli (Lahaye et al., 2018). Recently, however, it has been reported that cGAS activation actually induces the secretion of antiviral cytokines in HeLa cells (Morchikh et al., 2017). These discrepancies warrant further investigation and indicate that some HeLa populations may have lost cGAS expression. In future experiments, the type I IFN-inducing function of hnRNPM should also be investigated in primary human cells. KD of hnRNPM in primary human macrophages or fibroblasts could provide valuable insights into the role of hnRNPM in cGAS and RIG-I signaling under more physiological conditions.

4.1.4 hnRNPM promotes innate antiviral immunity to infections with HSV-1 and *L. monocytogenes* and is a restriction factor for HSV-1

Mimicking viral infections by lipofection of 5'ppp-dsRNA or dsDNA facilitates the analysis of cell signaling but does not provide information about viral replication. Therefore, THP-1 dual hnRNPM KD cells were infected with HSV-1. Interestingly, HSV-1 RNA levels inversely correlated with the expression of hnRNPM, indicating that hnRNPM is an anti-viral restriction factor for HSV-1. It should be noted that elevated viral RNA levels do not necessarily mean that more infectious viral particles have been produced. Here, viral plaque assays could be used to analyze the release of infectious HSV-1 particles in THP-1 dual hnRNPM KD cells.

It was speculated that hnRNPM restricts HSV-1 replication by promoting cGAS signaling. Indeed, the HSV-1-induced type I IFN response was hnRNPM-dependent. Previously, hnRNPM has been described to enhance the production of type I IFNs after *L. monocytogenes* infection (Luo et al., 2012). This effect could be reproduced in THP-1 dual cells in this thesis. Together, these results demonstrate that hnRNPM promotes the induction of

type I IFNs not only after transfection of RIG-I or cGAS ligands but also after infection with certain pathogens.

Replication of different alphaviruses, including Semliki Forest virus, Sindbis virus, and Chikungunya virus, has been described to be increased after RNAi-mediated KD of hnRNPM (Varjak et al., 2013). In this regard, it would be interesting to investigate whether hnRNPM also controls the expression of type I IFNs after infection with these viruses. Furthermore, coxsackievirus B3 and poliovirus were shown to target hnRNPM by 3C protease-dependent cleavage and to incorporate the hnRNPM degradation product into their life cycle to increase viral replication (Jagdeo et al., 2015). These seemingly contradictory functions of hnRNPM could be explained by reinterpreting the observations in light of the continuous evolutionary arms race between host and pathogen. On the one hand, hnRNPM might be able to restrict the replication of certain viruses. On the other hand, it is possible that some viruses have evolved to hijack hnRNPM and exploit it for their own replication, thereby simultaneously blocking the type I IFN response. Therefore, it is tempting to speculate whether these or other viral proteases cleave hnRNPM to evade the innate antiviral immune response. This strategy could represent an evolutionary advantage for viruses that are recognized by both cGAS and RIG-I (e.g., Dengue virus) (Aguirre et al., 2017).

4.1.5 hnRNPM is predominantly localized in the nucleus

Different groups have reported that hnRNPM is a nuclear protein and undergoes nucleocytoplasmic shuttling after infection with alphaviruses or picornaviruses (Jagdeo et al., 2015; Varjak et al., 2013). Considering the results of this thesis, it is conceivable that hnRNPM actively shuttles to the cytoplasm to promote the phosphorylation of TBK1 and IRF3. However, in THP-1 dual cells, hnRNPM was predominantly localized in the nuclear compartment, and activation of cGAS or RIG-I did not induce cytosolic translocation of hnRNPM. In contrast to cGAS, hnRNPM did not form distinct cytoplasmic puncta that colocalized with G_3-YSD, further arguing against the initial DNA sensor theory. These observations indicate that the immunologically active fraction of hnRNPM is present at local signaling sites at sufficient concentrations and is not actively recruited there. Nonetheless, it remains to be shown whether lipofection of cGAS or RIG-I stimuli can induce cytoplasmic translocation of hnRNPM as efficiently as actual viral infections. Future experiments

could address this question by analyzing the localization of hnRNPM after HSV-1 infection.

4.1.6 hnRNPM does not regulate the expression of core signaling proteins of the cGAS and RIG-I pathways

Considering the variety of functions reported for hnRNPM, it was asked whether hnRNPM promotes type I IFN induction by controlling the expression of genes involved in cGAS and RIG-I signaling. At the protein level, the expression of cGAS, RIG-I, key adaptor proteins (i.e., STING, MAVS), kinases (i.e., TBK1, IKKs), and transcription factors (i.e., IRF3, NF-κB p65) was unchanged between wildtype and hnRNPM-depleted THP-1 dual cells. Because this analysis only covered a limited number of proteins, global mRNA expression profiling was performed. Here, the mRNA levels of essential signaling components of the cGAS and RIG-I signaling pathways were also unaltered in hnRNPM-depleted THP-1 dual cells compared to the control cells. However, since the KD efficiency of hnRNPM was relatively low in this experiment, the results are preliminary and were not included in this thesis. Therefore, it would be worthwhile to repeat the global 3'-mRNA-sequencing analysis with maximal hnRNPM KD efficiency to obtain solid data.

Recently, hnRNPM has been described to regulate constitutive and alternative splice choices of more than 100 transcripts, including *IL6* and *MX1*, in the mouse macrophage cell line RAW 264.7 after infection with the gram-negative bacterium *Salmonella enterica* serovar Typhimurium, indicating that hnRNPM co-transcriptionally suppresses macrophage activation (West et al., 2019). In this regard, whole transcriptome sequencing could be performed to elucidate whether hnRNPM also regulates splicing of mRNAs associated with cytosolic nucleic acid sensing in human cells.

4.2 Mass spectrometric identification of ELAVL1 and SON as novel interactors of hnRNPM

4.2.1 Interactome of hnRNPM

Most proteins depend on direct protein:protein interactions to regulate cellular processes or to become activated (e.g., through post-translational modifications (PTMs), interaction-induced conformational changes, or oligomerization). Because hnRNPM lacks enzymatic activity, the interactome of hnRNPM was determined to uncover molecular details of how

hnRNPM supports the cGAS- and RIG-I-dependent type I IFN response. The majority of proteins, including RPLs, hnRNPs, and several RNA-binding proteins (i.e., IGF2BP2, RALY, or EBNA1BP2), interacted with hnRNPM in the resting and cGAS-activated state. For several proteins, interactions with hnRNPM were detected either preferentially under steady state conditions (e.g., LSM14A) or after cGAS activation (e.g., SUB1, DCD, SCL16A10). Interestingly, hnRNPM also interacted with proteins previously linked to innate antiviral immune responses, including LSM14A, ZC3HAV1, PRKDC, DHX9, DHX15, and ELAVL1. Therefore, it was hypothesized that hnRNPM regulates cGAS and RIG-I signaling by acting as a cofactor for one of these proteins. The following section briefly introduces the roles of these candidates in innate immunity.

LSM14A has been reported to promote the phosphorylation of IRF3 and the induction of type I IFNs by directly sensing immune-stimulatory DNA and RNA ligands (Li et al., 2012; Liu et al., 2016). ZC3HAV1 (also known as zinc finger antiviral protein (ZAP) and poly [ADP-ribose] polymerase 13 (PARP13)) represented another interesting target, as its shorter isoform, ZAPS, has been described to induce the oligomerization and activation of RIG-I (Hayakawa et al., 2011). PRKDC, like several other proteins, has been described to function as a cytoplasmic DNA sensor that induces the expression of type I IFNs via IRF3 (Ferguson et al., 2012). However, detailed genetic and biochemical analyses have established cGAS as *the* sensor of pathogenic DNA, raising the question of how different signaling pathways may all be essential for the DNA-mediated expression of type I IFNs (Vance, 2016). Interestingly, a recent study has described a STING-independent DNA sensing pathway (SIDSP) in human cells that is orchestrated by PRKDC and Heat shock cognate 71 kDa protein (HSPA8) (Burleigh et al., 2020). DHX9, a DExDc helicase family member, was described to sense CpG-DNA in pDCs and to induce NF-κB activation by interacting with MyD88 (Kim et al., 2010). The same group reported shortly afterwards that DHX9 also interacts with MAVS to induce the expression of type I IFNs and pro-inflammatory cytokines in myeloid DCs (Zhang et al., 2011). DHX15, a DExD/H box helicase, has been described to bind to both pathogenic RNA and the CARD of RIG-I, thereby increasing the ATPase activity of RIG-I (Pattabhi et al., 2019). Earlier studies identified DHX15 as an interactor of MAVS and specific inducer of the mitogen-activated protein kinase (MAPK) and NF-κB signaling pathways (Lu et al., 2014; Mosallanejad et al., 2014).

4.2.2 SON and ELAVL1 promote the RIG-I- and cGAS-dependent production of type I IFNs

To identify proteins that regulate the cGAS- and RIG-I-dependent production of type I IFNs in a manner similar to hnRNPM, 39 candidate hnRNPM interactors were targeted by shRNAs. As expected, KD of most targets (36/39) did not impair the cGAS- and RIG-I-mediated type I IFN response. These included different hnRNPs (hnRNPA1, hnRNPAB, hnRNPD, hnRNPH2, and SYNCRIP (also known as hnRNPQ)), indicating that the role of hnRNPM in cGAS and RIG-I signaling is unique within the hnRNP family. Although only one shRNA efficiently decreased the mRNA expression of hnRNPU and LSM14A, KD of these candidates did not compromise the cGAS- and RIG-I-dependent type I IFN induction. Similar to LSM14A, also PRKDC, DHX9, DHX15, and ZC3HAV1 were dispensable for the cGAS- and RIG-I-mediated type I IFN response in THP-1 dual monocytes. Discrepancies with other studies could be explained by the use of different model systems (LSM14A: HEK293, murine DCs; ZC3HAV1: HEK293T; PRKDC: mouse embryonic fibroblasts; DHX9: myeloid DCs, Gen2.2; DHX15: Huh7).

Intriguingly, KD of SON, ELAVL1, and IGF2BP2 significantly impaired the cGAS- and RIG-I-dependent type I IFN production. Importantly, SON and ELAVL1 were also required for the phosphorylation of IRF3 and/or TBK1 induced by cGAS or RIG-I. These results suggest that SON and ELAVL1, similar to hnRNPM, regulate the type I IFN response by promoting crucial phosphorylations downstream of cGAS and RIG-I. By contrast, TBK1 and IRF3 phosphorylation was independent of IGF2BP2, pointing to an involvement of IGF2BP2 in transcription or translation of *IFNB1* mRNA.

SON interacted with hnRNPM in resting and cGAS-stimulated cells in an RNA-independent manner, while interactions with IGF2BP2 were lost after RNase A treatment. Due to the lower sensitivity of the ELAVL1-specific antibody, no co-IP of endogenous ELAVL1 with hnRNPM could be detected. However, endogenous hnRNPM selectively co-immunoprecipitated with lentivirally expressed ELAVL1. Collectively, these data suggest that hnRNPM, ELAVL1, and SON form a multiprotein complex that promotes the cGAS- and RIG-I dependent induction of type I IFNs by regulating TBK1 and IRF3 phosphorylation. Currently, hnRNPM, ELAVL1, and SON represent the first non-redundant signaling components that merge the RIG-I-MAVS and cGAS-STING signaling pathways. In the following, some of the known functions of IGF2BP2, SON, and ELAVL1 are introduced.

IGF2BP2, together with IGF2BP1 and IGF2BP3, belong to a conserved family of RNA-binding proteins (Cao et al., 2018). IGF2BPs share a similar domain structure and bind RNAs via both their N-terminal RRMs and C-terminal hnRNP K homology (KH) domains (Nielsen et al., 1999). RNA-binding by IGF2BPs induces the formation of cytoplasmic ribonucleoprotein particles (RNPs) (Nielsen et al., 2003). In the nucleus, IGF2BPs stabilize nascent transcripts through direct interactions (Weidensdorfer et al., 2009). Via the nuclear export signal of the KH domains, IGF2BPs have been described to regulate the export of target transcripts to the cytoplasm (Nielsen et al., 2003). Furthermore, IGF2BPs have been reported to promote translation of bound transcripts and to be associated with the embryonic development of the central nervous system (Adolph et al., 2009; Nielsen et al., 2004; Schaeffer et al., 2012). The diversity of reported functions makes IGF2BP2 an interesting target for future studies, which should focus primarily on the transcriptional and translational regulation of the type I IFN response.

SON is a large, ubiquitously expressed DNA- and RNA-binding protein and comprises a glycine-rich motif (G-patch) and a double-stranded RNA-binding motif (DSRM), both located at the C-terminus, as well as an arginine/serine (RS)-rich domain (Ahn et al., 2011; Hickey et al., 2014). So far, these domains have been mainly associated with RNA processing (Aravind and Koonin, 1999; Saunders and Barber, 2003). SON colocalizes with nuclear speckles and has been described to regulate splicing of mRNAs associated with cell cycle progression and genome stability (Ahn et al., 2011; Huen et al., 2010; Sharma et al., 2010). Other groups have reported that SON can also bind to gene promoters, thereby repressing transcription (Ahn et al., 2013; Sun et al., 2001). Patients with mutations in *SON* suffer from Zhu-Tokita-Takenouchi-Kim (ZTTK) syndrome, a rare developmental disorder characterized by malformations of the cerebral cortex, intellectual disability, facial dysmorphism, epilepsy, vision problems, and musculoskeletal abnormalities (Kim et al., 2016). All of the reported ZTTK cases are caused by heterozygous *de novo* loss-of-function mutations in *SON* (Slezak et al., 2020). To date, SON has not been associated with the expression of type I IFNs. Recently, however, two new patients with ZTTK syndrome were reported who suffer from recurrent respiratory and inner ear infections (Slezak et al., 2020). Further research should clarify whether SON dysfunction inhibits cGAS and RIG-I signaling in these patients and is thus the cause of the reoccurring infections.

ELAVL1 (also known as human antigen R (HuR)) is an ubiquitously expressed, predominantly nuclear protein and has been described primarily in the context of post-transcriptional gene regulation. Similar to hnRNPM, ELAVL1 consists of three RRMs and displays binding preferences towards destabilizing adenylate-uridylate (A/U)-rich elements (AREs) of mRNAs, but has also been reported to bind AREs in the 5'-UTR (Abdelmohsen et al., 2008; Brennan and Steitz, 2001; Hinman and Lou, 2008; López De Silanes et al., 2004; Ma et al., 1996). ELAVL1 has been described to stabilize a variety of transcripts, including the mRNAs encoding for inducible nitric oxide synthase (iNOS), granulocyte macrophage-colony stimulating factor (GM-CSF), vascular endothelial growth factor (VEGF), TNF-α, cyclooxygenase (COX)-2, acetylcholinesterase (AChE), Fas ligand (FasL), TLR4, IL-3, IL-4, IL-6, and IL-8 (Srikantan and Gorospe, 2012). Although transcript stabilization by ELAVL1 is not fully understood, it is hypothesized that ELAVL1 sequesters bound mRNAs from turnover and translation regulatory RNA-binding proteins (TTR-RBPs) and RNA-induced silencing complex (RISC), thereby preventing their transport to sites of mRNA decay (Srikantan and Gorospe, 2012). In addition, ELAVL1 has also been described to promote the translation of certain mRNAs (Durie et al., 2011; Kim et al., 2009). Since ELAVL1 has been shown to stabilize various mRNAs, it is not surprising that ELAVL1 contributes to several cellular processes such as angiogenesis and development and has been associated with the onset of different pathologies, particularly inflammation and cancer (Dixon et al., 2001; Nabors et al., 2001). Previously, two groups have described ELAVL1 in the context of type I IFN production (Herdy et al., 2015; Sueyoshi et al., 2018). Herdy *et al.* identified ELAVL1 as an *in vitro* binder of AREs in the 3'-UTR of *IFNB1* mRNA and reported that KD of ELAVL1 decreases the poly(I:C)-induced production of type I IFNs in HeLa cells. Although the authors postulated that ELAVL1 stabilizes *IFNB1* mRNA, stabilization of *IFNB1* mRNA by ELAVL1 was not experimentally confirmed. By contrast, Sueyoshi *et al.* have proposed that ELAVL1 and PLK2 regulate the nuclear transport of IRF3 after RLR activation (Sueyoshi et al., 2018). In an earlier study, PLK2 and PLK4 were shown to mediate the nuclear translocation of IRF3 after poly(I:C) stimulation (Chevrier et al., 2011). This conclusion was based on the observation that treatment of primary bone marrow-derived DCs (BMDCs) with BI 2536, a pan-specific PLK inhibitor, blocks the nuclear transport but not the poly(I:C)-induced phosphorylation of IRF3. Later, Sueyoshi *et al.* found downregulated mRNA levels of *PLK2* in ELAVL1-deficient

RAW 264.7 cells and reported that KO of ELAVL1 decreases the nuclear translocation of IRF3 (Sueyoshi et al., 2018). In addition, Sueyoshi *et al.* observed reduced nuclear levels of pIRF3-Ser396 in RAW 264.7 ELAVL1 KO cells after poly(I:C) stimulation. On the one hand, these data suggest that ELAVL1 controls the nuclear transport of IRF3 in RAW 264.7 cells. On the other hand, these observations indicate that ELAVL1 may also promote the phosphorylation of IRF3, since PLK inhibition by BI 2536 has not been described to decrease pIRF3-Ser396 levels. However, in this thesis, ELAVL1 was identified as an interactor of hnRNPM that non-redundantly promotes the cGAS- and RIG-I-dependent induction of type I IFNs in human THP-1 dual monocytes and presumably enhances signaling by regulating TBK1 and/or IRF3 phosphorylation. These discrepancies warrant further investigation and may be caused by species- or cell-type-specific roles of ELAVL1 in innate immunity.

4.3 ELAVL1 constitutes a non-redundant signaling component that merges the RIG-I-MAVS and cGAS-STING signaling pathways

4.3.1 ELAVL1 induces the expression of type I IFNs and activation of NF-κB downstream of both cGAS and RIG-I

To further elucidate the role of ELAVL1, CRISPR/Cas9 was used to delete the *ELAVL1* genomic locus. Three different ELAVL1-deficient THP-1 dual clones were isolated (gRNA AN: clone #39, clone #44; gRNA AI: clone #7). For clone AN #39, a homozygous T insertion in exon 5 at position 499 of 978 was confirmed by Sanger sequencing. The sequencing chromatograms of the clones AN #44 and AI #7 showed multiple overlapping peaks. Therefore, KO of ELAVL1 could only be confirmed at the protein level. Nonetheless, the cGAS- and RIG-I-dependent type I IFN induction was severely compromised in all three clones, indicating that the observed phenotype is not caused by clonal defects or non-specific cleavage of Cas9. The type I IFN response was inhibited by approximately 6-fold to 8-fold in ELAVL1-deficient THP-1 dual monocytes, suggesting that ELAVL1 is not essential for cGAS and RIG-I signaling but represents a potent inducer. Importantly, stable expression of ELAVL1-FLAG reestablished the secretion of type I IFNs induced by cGAS or RIG-I, demonstrating that ELAVL1 is a specific and non-redundant enhancer of both pathways. Stimulation with 2'3'-cGAMP further showed that ELAVL1, similar to hnRNPM, also operates downstream of STING. Interestingly, ELAVL1 also amplified the

cGAS- and RIG-I-dependent NF-κB response, whereas the TLR1/TLR2-mediated activation of NF-κB was ELAVL1-independent. These data indicate that ELAVL1 regulates NF-κB signaling in a PRR-dependent manner. It should be noted that the TLR8-dependent activation of NF-κB was diminished in cells with *ELAVL1*$^{-/-}$ genetic background compared to THP-1 dual wildtype cells. This observation may be caused by non-specific cleavage of Cas9 and warrants further investigation.

Considering the heterogeneity of described functions of ELAVL1, MTT assay was used to exclude that ELAVL1 deficiency negatively affects the fitness of THP-1 dual monocytes, thereby inhibiting cGAS and RIG-I signaling. In fact, KO of ELAVL1 ameliorated the metabolic activity after cytosolic challenge with 5'ppp-dsRNA, pDNA, or G_3-YSD, presumably due to the reduced ability of ELAVL1-deficient cells to induce pro-apoptotic pathways via NF-κB and IRF3.

Because ELAVL1 has been shown to bind to numerous transcripts via its RRMs, it was hypothesized that these protein domains are also necessary to promote cGAS and RIG-I signaling. Deletion analyses showed that both the N-terminal RRM1 and C-terminal RRM3 of ELAVL1 are required for the cGAS- and RIG-I-dependent type I IFN response. It is conceivable that these domains bind to RNA species that have scaffold functions for important signaling proteins. Interactions with scaffold molecules may contribute to the spatial and temporal assembly of large signaling complexes. Recently, hexamethylene bis-acetamide-inducible protein 1 (HEXIM1) and the long non-coding RNA (lncRNA) nuclear paraspeckle assembly transcript 1 (NEAT1) were shown to serve as scaffolds for the multimeric assembly of cGAS signaling components (Morchikh et al., 2017). In light of these observations, it is possible that ELAVL1 also directly interacts with signaling proteins via its RRMs. However, it cannot be excluded that these relatively large N- and C-terminal deletions have led to the formation of misfolded ELAVL1 fusion proteins that are unable to promote signaling.

4.3.2 ELAVL1 promotes the phosphorylation of TBK1, STING, and IRF3

In the present study, ELAVL1 was shown to control the cGAS- and RIG-I-dependent mRNA expression of *IFNB1*, *CXCL10*, and *IFIT1*, eliminating the possibility that ELAVL1 is involved in the translation of these mRNAs. Curiously, the transcript levels were

downmodulated to different extents. While *IFNB1* and *CXCL10* mRNA expression was blunted in ELAVL1-deficient cells, the cGAS- or RIG-I-mediated induction of *IFIT1* was only decreased by approximately 4-fold to 5-fold. These data indicate that ELAVL1 might stabilize *IFNB1* and *CXCL10* mRNA in THP-1 dual cells. Interestingly, *IFIT1* mRNA expression induced by direct activation of IFNAR was independent of ELAVL1, further illustrating that the IFNAR signaling pathway is intact in THP-1 dual ELAVL1 KO cells.

In this study, KD of hnRNPM, ELAVL1, and SON was shown to impair the cGAS- and RIG-I-dependent phosphorylation of TBK1 and/or IRF3. It was hypothesized that this phenotype is even more pronounced in THP-1 dual ELAVL1 KO cells and can be rescued by overexpression of ELAVL1-FLAG. Indeed, overexpression of ELAVL1-FLAG in THP-1 dual *ELAVL1*$^{-/-}$ cells reestablished the phosphorylation of TBK1 at Ser172, IRF3 at Ser396, and STING at Ser366 after stimulation of cGAS or RIG-I, suggesting that ELAVL1, similar to hnRNPM, functions as a non-redundant, positive regulator downstream of cGAS/RIG-I and upstream of TBK1. Curiously, the Pam3CSK4-induced phosphorylation of TBK1 at Ser172 was ELAVL1-independent. These data are in line with the observation that the TLR1/TLR2-mediated activation of NF-κB was unchanged between wildtype and THP-1 dual ELAVL1 KO cells. Therefore, ELAVL1 promotes the phosphorylation of TBK1 in a PRR-dependent manner and may be able to discriminate TBK1 molecules of different signaling complexes. It can only be speculated how ELAVL1 amplifies TBK1 phosphorylation in a context-dependent manner. Adaptor proteins could recruit ELAVL1 to local signaling sites, where it may serve as a scaffold for signaling proteins known to activate TBK1. In addition, activation of cGAS or RIG-I could induce PTMs (e.g., phosphorylation, ubiquitination) of ELAVL1 that enable interactions with signaling proteins.

The current mechanistic model suggests that the phosphorylation of STING, MAVS, and IRF3 is a consequence of TBK1 activity. Because the cGAS- or RIG-I-mediated phosphorylation of TBK1 was shown to be dependent on ELAVL1, the results of this study suggest a direct or indirect connection between the kinase activity of TBK1 and the ELAVL1/hnRNPM complex. A direct link to TBK1 would explain why hnRNPM and ELAVL1 promote signaling downstream of both cGAS and RIG-I.

Considering that ELAVL1 may promote the expression of type I IFNs at two stages, both by promoting TBK1/IRF3 phosphorylation and *IFNB1* mRNA stability, it was asked which

of these functions predominates in THP-1 dual monocytes. In theory, stabilization of the *IFNB1* mRNA by ELAVL1 could indirectly decrease the PRR activation threshold through IFN-mediated upregulation of cGAS and RIG-I. This positive feed-forward loop should not enhance the induction of type I IFNs in cells with *IFNAR2*$^{-/-}$ genetic background. Indeed, RNAi against ELAVL1 in THP-1 dual IFNAR2 KO cells still significantly inhibited the production of type I IFNs induced by cGAS or RIG-I, demonstrating that ELAVL1 predominantly regulates signaling. Nevertheless, stabilization of *IFNB1* mRNA by ELAVL1 will contribute to its type I IFN-inducing capacities.

4.3.3 Analyzing the global gene expression pattern of ELAVL1-deficient THP-1 dual cells by 3'-mRNA sequencing

ELAVL1 is a multifunctional protein and involved in different steps of RNA processing, including mRNA stabilization. Previously, this work demonstrated that ELAVL1 promotes the cGAS- and RIG-I-dependent induction of type I IFNs by activating TBK1 and IRF3. However, it cannot be excluded that ELAVL1 also augments the type I IFN response by controlling the expression of essential signaling proteins of the cGAS-STING and RIG-I-MAVS pathways. Therefore, 3'-mRNA sequencing of THP-1 dual ELAVL1 KO cells was performed.

In general, more genes were downregulated than upregulated in ELAVL1-deficient THP-1 dual monocytes compared to wildtype cells, suggesting that ELAVL1 indeed controls gene expression. However, the expression of the principal components of the cGAS and RIG-I signaling pathways, including PRRs (i.e., cGAS, RIG-I), adaptor proteins (i.e., STING, MAVS), kinases (i.e., TBK1, IKKs), and transcription factors (i.e., IRFs, NF-κB), was independent of ELAVL1. Interestingly, the mRNA expression of *PLK2* was also ELAVL1-independent, contradicting the theory that ELAVL1 regulates the nuclear translocation of IRF3 by stabilizing *PLK2* transcripts. Further experiments, discussed in the following chapters, provide additional evidence that the nuclear translocation of IRF3 is not mediated by ELAVL1 and instead suggest a direct connection between ELAVL1/hnRNPM and TBK1/IRF3 in THP-1 dual cells.

After stimulation of IFNAR, 167 genes were upregulated and 251 genes were downregulated in ELAVL1-deficient cells as compared to THP-1 dual wildtype cells. Most ISGs, including the genes encoding for IFI16, IFITs, OAS proteins, RIG-I, and MDA5, were not

significantly regulated. Consistent with previous findings, these data demonstrate that the JAK-STAT signaling pathway is intact in THP-1 dual ELAVL1 KO cells and suggest that ELAVL1 is not involved in the expression of ISGs.

ELAVL1 regulated more genes significantly after stimulation of cGAS or RIG-I compared to IFNAR, presumably because direct PRR stimulation induced high levels of type I IFNs (> 1000 U/ml) and thus had a stronger effect on ISG expression. For 5'ppp-dsRNA stimulation, 207 genes were significantly upregulated and 584 genes were significantly downregulated in ELAVL1-deficient THP-1 dual cells. Relative to wildtype cells, cytosolic G_3-YSD challenge led to an upregulation of 186 genes and downregulation of 557 genes in THP-1 dual ELAVL1 KO cells. In both conditions, *IFNB1* mRNA levels were strongly downregulated. Consequently, the ISG response was also markedly diminished in ELAVL1-deficient THP-1 dual cells, providing further evidence that ELAVL1 is a potent inducer of the cGAS and RIG-I signaling pathways.

4.3.4 Overlapping protein:protein interactions of hnRNPM and ELAVL1

In this thesis, hnRNPM and ELAVL1 were shown to form a complex that promotes the cGAS- and RIG-I-dependent expression of type I IFNs and phosphorylation of TBK1/IRF3. Because hnRNPM and ELAVL1 exhibit similar functions in nucleic acid immunity, it is conceivable that both proteins share common binding partners. DDX3X (also known as DDX3), a DEAD box RNA helicase, was identified as the only common interactor of hnRNPM and ELAVL1 that is associated with the expression of type I IFNs. Several studies have reported a decisive role of DDX3X in combating viral infections. In this regard, DDX3X has been described to interact with TBK1 and to be phosphorylated by TBK1 (Soulat et al., 2008). In addition, DDX3X has been reported to link IKKε to IRF3, thereby promoting the production of type I IFNs (Gu et al., 2017; Schröder et al., 2008). Analyzing the function of DDX3X and its interaction with hnRNPM/ELAVL1 may therefore provide valuable insights into the regulation of cGAS and RIG-I signaling. TRIM25, PCBP2, SYK, HSPD1, and XRCC5 were additional candidate interactors of hnRNPM that have been linked to the type I IFN response and thus represent promising targets for further investigation.

IKKβ is one of the most interesting hnRNPM interactors, as IKKβ has been shown to phosphorylate MAVS at the conserved *p*L*x*IS motif at Ser442. The detection of only two

unique IKKβ-derived peptides indicates weak interactions with hnRNPM, but could also be explained by low ionization efficiencies. Compared to the first interactome analysis of hnRNPM (IP at 4 °C for 2 h), the IP of the analysis described here was performed at 4 °C overnight. In theory, prolonged incubation times should allow detection of weak interactions, but at the same time, the likelihood of non-specific interactions may increase. Indeed, IKKβ peptides were only detected after IP at 4 °C overnight. Nonetheless, these results were the first indications that hnRNPM directly interacts with signaling proteins involved in the type I IFN response and suggested to specifically analyze putative interactions between hnRNPM and other signaling proteins downstream of cGAS/RIG-I (i.e., TBK1, IKKε).

ELAVL1 and hnRNPM interacted with several common RNA-binding proteins, particularly RPLs and components of the splicing machinery. The interactions were consistently more enriched in the hnRNPM condition as compared to IP of ELAVL1, presumably due to the higher expression and pull-down efficiency of hnRNPM or because hnRNPM generally binds to proteins with greater affinity. This could also explain why interactions with SON and IKKβ could only be detected for hnRNPM. However, it is also conceivable that hnRNPM forms distinct, spatially separated complexes with ELAVL1 and SON, but further studies are needed to confirm this theory.

4.4 hnRNPM, ELAVL1, and TBK1 form a multiprotein complex *in cellulo*

4.4.1 Activated TBK1 is present in both cytoplasm and nucleus

hnRNPM and ELAVL1 are predominantly localized in the nucleus, whereas SON is exclusively found in the nuclear compartment. By contrast, TBK1 is thought to phosphorylate its context-dependent targets STING, MAVS, and IRF3 in the cytoplasm. Interestingly, pTBK1-Ser172 was detected in both cytoplasmic and nuclear extracts of THP-1 dual monocytes after activation of cGAS or RIG-I. In fact, considering that the majority of total TBK1 protein was present in the cytoplasm, these results indicate that nuclear TBK1 is phosphorylated to a greater extent than cytoplasmic TBK1. Similar findings were previously described by Du *et al.*, who detected phosphorylated TBK1 in nuclear extracts of L929 and RAW 264.7 cells stimulated with DMXAA, a murine STING ligand, indicating

that complex mechanisms may regulate IRF3 signaling in different cellular compartments (Conlon et al., 2013; Du et al., 2015).

It is also conceivable that the nuclear pTBK1-Ser172 signals result from inefficient separation of ER/Golgi and nuclei. However, since the signal intensities of pSTING-Ser366, an ER-/Golgi-resident protein, were significantly lower in the nuclear fraction compared to pTBK1-Ser172, it is indeed likely that activated TBK1 is present in the nucleus of THP-1 dual cells. It should be noted that the signal intensities in the nuclear fractions may be overrepresented because equal amounts of total protein were analyzed and the nuclear extracts were less concentrated than the cytoplasmic extracts. In support of this theory, confocal immunofluorescence microscopy showed that the majority of pTBK1-Ser172 is localized in the cytoplasm around the nuclear membrane, while weaker signals are also present in the nucleus of THP-1 dual monocytes challenged with G_3-YSD. Nonetheless, these data demonstrate that physical contacts between hnRNPM, ELAVL1, and TBK1 are not excluded by spatial separation. Considering that SON is a dominant nuclear protein, it would be interesting to explore a putative connection to nuclear TBK1.

4.4.2 hnRNPM forms a novel type I IFN-inducing multiprotein complex

Physical interactions between proteins drive signaling cascades and thus determine cellular activities. The AP-MS analysis in this study demonstrated that IKKβ constitutes a weak but significant interactor of hnRNPM. The complex formation between hnRNPM and IKKβ was subsequently confirmed by co-IP. These interactions were further shown to be RNase A-resistant and detectable under both steady state and cGAS-activated conditions. TBK1 was previously reported to phosphorylate IKKβ, thereby inducing IκBα degradation and activation of NF-κB (Tojima et al., 2000). Because TBK1 shares approximately 27 % sequence homology with the canonical IKKs (Hiscott, 2007), it was hypothesized that TBK1 represents a putative interactor of hnRNPM. Indeed, TBK1 and pTBK1-Ser172 co-immunoprecipitated with hnRNPM in an RNA-independent manner. Interactions between hnRNPM and pTBK1-Ser172 further increased upon cGAS activation. hnRNPM also interacted with IKKε, NF-κB p65, and NF-κB pp65-Ser536. These results indicate that hnRNPM forms a multiprotein complex *in vitro* that contains at least four active signaling proteins shared by the RIG-I-MAVS and cGAS-STING signaling pathways. Inter-

estingly, total STING protein also co-immunoprecipitated with hnRNPM. However, these interactions need to be further evaluated, as no interactions between phosphorylated STING and hnRNPM were detected. In addition, activated TBK1 also co-immunoprecipitated with ELAVL1, further indicating that the interactions of the hnRNPM/ELAVL1 complex are specific. These discoveries may explain how hnRNPM and ELAVL1 regulate cGAS- and RIG-I signaling. It is conceivable that hnRNPM is a scaffold for TBK1, IKKε, and IKKβ, thereby controlling the expression of type I IFNs. Close proximity of hnRNPM/ELAVL1 to IKKβ, TBK1, and NF-κB p65 would also explain why the cGAS- and RIG-I-mediated NF-κB response is ELAVL1-dependent.

According to current knowledge, hnRNPM, ELAVL1, and SON are the first proteins capable of merging the cGAS-STING and RIG-I-MAVS signaling pathways and thus represent potential therapeutic targets for the treatment of diseases characterized by excessive type I IFN secretion. In theory, this means that the development of only one specific inhibitor could treat diseases resulting from dysfunction of different PRRs (e.g., AGS (amongst others, caused by excessive cGAS activation), SMS (caused by gain-of-function mutations in the RIG-I- and MDA5-encoding genes), or SAVI (caused by gain-of-function mutations in the STING-encoding gene)). Since hnRNPM, ELAVL1, and SON are involved in a variety of cellular processes, pharmacological inhibitors need to be carefully designed to disrupt only the formation/function of the immunologically active multiprotein complex. A high-throughput screen has identified MS-444, a chrysanthone-like compound, as a homodimerization inhibitor of ELAVL1 (Meisner et al., 2007). Dimerization has been shown to be essential for RNA-binding by ELAVL1 and cytoplasmic translocation of ELAVL1 (Meisner et al., 2007). Intriguingly, ELAVL1 inhibition by MS-444 was reported to impair the poly(I:C)-induced type I IFN production in HeLaS3 cells (Herdy et al., 2015). Therefore, it would be interesting to investigate whether MS-444 represses signaling by interfering with the formation of the hnRNPM/ELAVL1 protein complex.

The interactome analysis of hnRNPM captured weak interactions with IKKβ. However, in contrast to the IPs, no interactions were observed with TBK1, IKKε, and NF-κB p65. It is conceivable that these interactions could not be detected due to low ionization efficiencies of TBK1, IKKε, and NF-κB p65. Another explanation could be the limited sensitivity of the mass spectrometer. In general, a well-functioning monoclonal antibody offers high sensi-

tivity and is able to resolve 10^2 to 10^3 protein copies, while identification of proteins with state-of-the-art mass spectrometers typically requires at least 10^6 copies (Timp and Timp, 2020).

4.4.3 Activated TBK1 interacts with hnRNPM and ELAVL1 *in cellulo*

In this thesis, hnRNPM and ELAVL1 were shown to form a multiprotein complex with several signaling proteins downstream of both cGAS and RIG-I. However, these *in vitro* experiments do not necessarily clarify whether the interactions of hnRNPM/ELAVL1 with TBK1, IKKβ, IKKε, and NF-κB p65 also occur *in cellulo*. To address this issue, PLAs were performed. PLA requires two different primary antibodies raised in different species and a pair of oligonucleotide-conjugated secondary antibodies. If the primary antibodies recognize epitopes in immediate vicinity (distance ≤ 40 nm), the complementary oligonucleotides can form a DNA loop that serves as a template for a rolling circle amplification. Hybridization of fluorescent probes can be followed by confocal microscopy and is proportional to the degree of protein:protein interactions.

This study demonstrated that hnRNPM and pTBK1-Ser172 are indeed in close proximity *in cellulo*. The calculated PLA score of hnRNPM-GFP:pTBK1-Ser172 interactions further increased upon cGAS activation and was significantly higher compared to GFP:pTBK1-Ser172 interactions. These data indicate that either activated TBK1 is recruited to hnRNPM or that hnRNPM serves as a docking platform for the phosphorylation of TBK1. Most interactions between hnRNPM and activated TBK1 occurred in the cytoplasm and at the nuclear membrane. However, due to the presence of background signals, the identification of true physical interactions is limited and therefore these results only suggest a clustering of hnRNPM-GFP:pTBK1-Ser172 interactions in these regions. Nonetheless, these data indicate that the cytoplasmic rather than the nuclear portion of hnRNPM mediates cGAS and RIG-I signaling.

In a similar manner, PLA confirmed *in cellulo* interactions between ELAVL1 and pTBK1-Ser172. 3D assembly of the individual z stack images showed that the majority of ELAVL1-GFP:pTBK1-Ser172 interactions occurred in the cytoplasm, suggesting that the cytoplasmic component of ELAVL1, similar to hnRNPM, promotes the type I IFN induction. In contrast to the IPs, which only resolved interactions between ELAVL1 and pTBK1-Ser172 in the cGAS-activated condition, ELAVL1-GFP:pTBK1-Ser172 interactions were

also detected in resting cells and did not further increase after cGAS activation. It is conceivable that the potential weak/transient interactions between ELAVL1 and pTBK1-Ser172 under steady state conditions could only be resolved by the more sensitive PLA. Since the interactions between hnRNPM and ELAVL1 were also confirmed by PLA, it appears plausible that both proteins form a cytoplasmic protein complex with activated TBK1 *in cellulo*. It should be noted that the number of PLA puncta per cell was decreased for hnRNPM-GFP-ELAVL1 interactions compared to hnRNPM-GFP:pTBK1-Ser172 or ELAVL1-GFP:pTBK1-Ser172. It is possible that the lower sensitivity of the ELAVL1-specifc antibody might have reduced the signal-to-noise ratio. However, because laser intensities and image processing parameters may have been adjusted between the experimental groups, the PLA scores cannot be easily compared.

4.5 hnRNPM organizes a multiprotein complex that enhances the phosphorylation of TBK1 in the activation loop

How do hnRNPM and ELAVL1 regulate cGAS and RIG-I signaling mechanistically? This work evaluated whether hnRNPM and ELAVL1 promote the production of type I IFNs (1) by inhibiting TBK1-specific phosphatases, (2) by regulating the nuclear transport of IRF3, or (3) by enhancing the phosphorylation of TBK1 in the activation loop.

To test the first theory, different TBK1-specific phosphatases were targeted by shRNAs. Unexpectedly, KD of PPM1B, SHIP1, and PP4 did not enhance the cGAS- or RIG-I-mediated type I IFN response, suggesting that dephosphorylation of TBK1 by these enzymes depends on the cellular context. It is also conceivable that these phosphatases are functionally redundant and that redundancy provides a safeguard mechanism for the cell to limit exuberant immune responses. Similarly, it was shown that PP1, PP2A, PP2B, and PP7 do not negatively regulate the cGAS- and RIG-I-dependent expression of type I IFNs. Simultaneous inhibition of PP1, PP2A, PP4, and PP5 by OA also did not ameliorate cGAS and RIG-I signaling in THP-1 dual ELAVL1 KO cells, suggesting that ELAVL1 does not prevent TBK1 dephosphorylation by these phosphatases. Interestingly, THP-1 dual wildtype cells induced significant levels of type I IFNs after prolonged exposure to more than 10 nM OA. Because this effect was ELAVL1-dependent, it appears plausible that PP1, PP2A, PP4, and PP5 inhibit a signaling protein upstream of ELAVL1. In conclusion,

linking hnRNPM/ELAVL1 to inhibitory phosphatases remains a major challenge, as no TBK1-specific phosphatase could be identified in THP-1 dual cells.

Previously, ELAVL1 was described to regulate the RLR-dependent production of type I IFNs by stabilizing the mRNA of *PLK2*, a gene implicated in the nuclear transport of IRF3 (Sueyoshi et al., 2018). This work provides several pieces of evidence that argue against the nuclear transport theory: (1) the *PLK2* mRNA expression was unchanged between wildtype and THP-1 dual ELAVL1 KO cells; (2) pIRF3-Ser396/IRF3 did not accumulate in the cytoplasm of ELAVL1-deficient THP-1 dual monocytes; (3) ELAVL1 regulated both cGAS and RIG-I signaling; (4) the phosphorylation of IRF3, TBK1, and STING was proportional to the expression of ELAVL1. Discrepancies may be explained by the use of different model systems, as Sueyoshi *et al.* studied the function of ELAVL1 in the mouse macrophage cell line RAW 264.7.

According to the third theory, hnRNPM and ELAVL1 assemble signaling proteins of the cGAS-STING and RIG-I-MAVS pathways into a multiprotein complex to enhance TBK1 phosphorylation. Indeed, incubation of recombinant TBK1-GST with immunoprecipitated hnRNPM-GFP significantly increased the phosphorylation of TBK1-GST in the activation loop in the cGAS-activated condition compared to IP of GFP. These data indicate that binding of hnRNPM to active signaling components (i.e., endogenous TBK1, IKKε, and IKKβ) increases the capacity of the cell to activate TBK1 and thus induce the production of type I IFNs. It is hypothesized that both hnRNPM and ELAVL1 have scaffold functions for TBK1, IKKε, IKKβ, and NF-κB p65 and form a multiprotein complex that positively regulates cGAS and RIG-I signaling in the cytoplasm (Fig. 4.1). Permanent assembly of TBK1, IKKε, IKKβ, and NF-κB p65 into a multiprotein complex may benefit the cell to integrate incoming messages from functionally distinct nucleic acid receptors. In general, formation of preformed multiprotein complexes might also accelerate signal transmission and help to gain spatiotemporal control over the immune response, limit hyperactivation, and restore homeostasis once the infection is controlled. Furthermore, it is speculated that hnRNPM forms a distinct nuclear complex with SON (Fig. 4.1). However, the role of SON in cGAS and RIG-I signaling is poorly understood and requires further investigation.

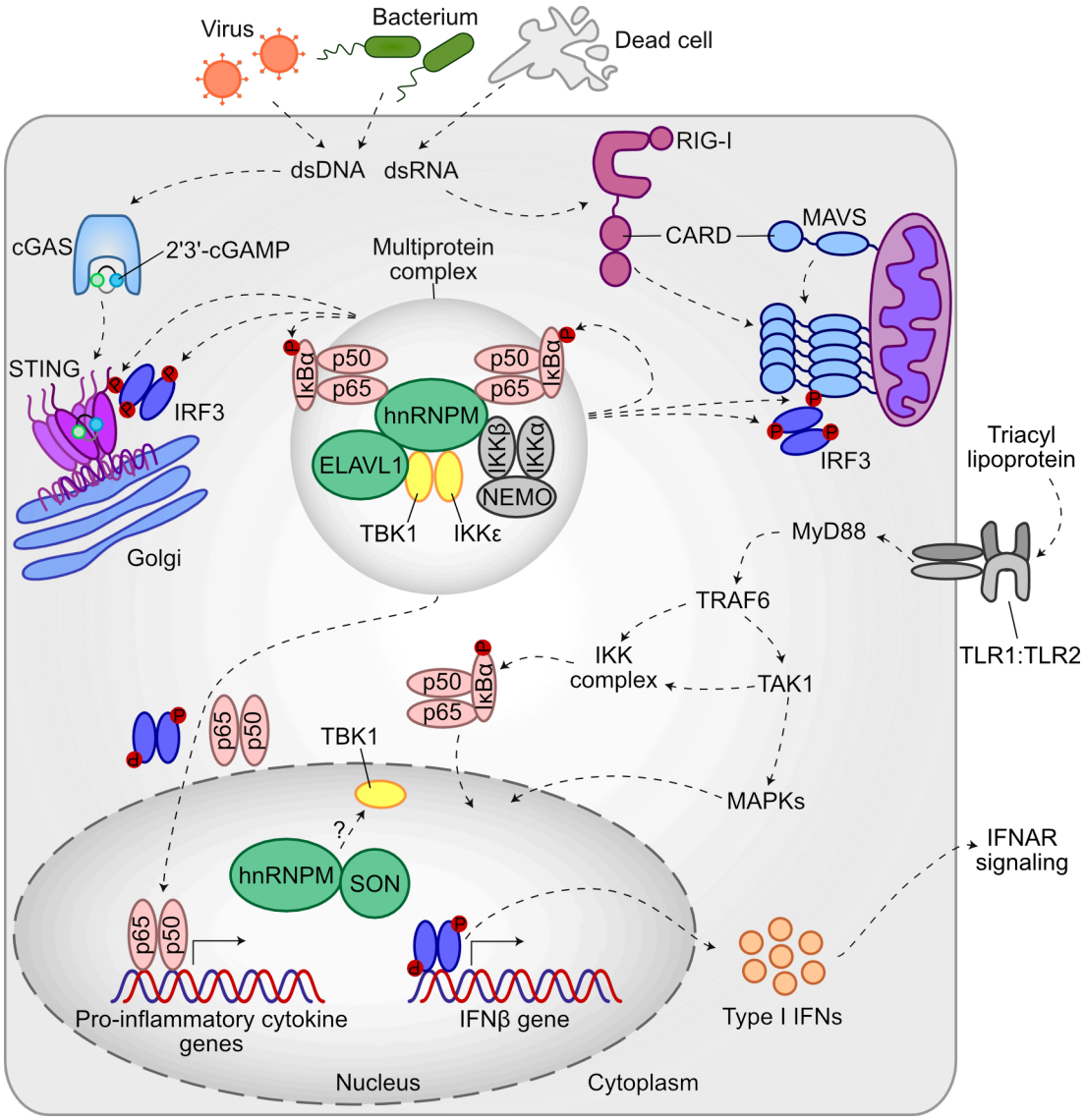

Fig. 4.1: Proposed model of how hnRNPM, ELAVL1, and SON promote signal transduction downstream of cGAS and RIG-I.
Nucleic acids of viruses, bacteria, and dead cells can be recognized by the cytoplasmic immune sensors cGAS and RIG-I. cGAS senses dsDNA and catalyzes the formation of 2'3'-cGAMP to activate STING. Binding of RNA with tri-/diphosphorylated 5'-ends by RIG-I induces the activation of MAVS at the mitochondrial membrane. Although both receptors recognize distinct ligands and activate unrelated adaptor proteins, cGAS and RIG-I use a common signaling machinery involving TBK1, IKKs, IRF3, and NF-κB p65. hnRNPM and ELAVL1 connect both pathways downstream of STING/MAVS. They form a multiprotein complex with TBK1, IKKε, IKKβ, and NF-κB p65 and promote TBK1/IRF3 phosphorylation, ultimately leading to the expression of type I IFNs and pro-inflammatory cytokines. Additionally, hnRNPM might form a distinct complex with the nuclear protein SON. The TLR1/TLR2-mediated phosphorylation of TBK1 and activation of NF-κB is independent of ELAVL1.

In addition to RIG-I-MAVS, MDA5-MAVS, and cGAS-STING signaling, the TLR3-TRIF and TLR4-TRIF-MyD88 signaling pathways also induce type I IFNs via TBK1 and IRF3 (Tanaka and Chen, 2012). Activation of TBK1, however, does not necessarily lead to IRF3 phosphorylation. As shown by Clark et al., activation of MyD88-dependent PRRs (i.e., TLR1/TLR2, TLR2/TLR6, TLR7, TLR9) induces TBK1 phosphorylation but does not trigger an IRF3-dependent type I IFN response (Clark et al., 2011a, 2011b). Further research will reveal how signal integration and decision-making work mechanistically for different signaling pathways, but engagement of specific adaptor proteins might play a crucial role. For example, it is known that STING and MAVS are required for the recruitment of TBK1 and subsequent activation of IRF3 (Tanaka and Chen, 2012). Thus, IRF3 is activated by TBK1 only if a specific adaptor protein is activated in advance, and it is conceivable that hnRNPM and ELAVL1 exhibit similar scaffolding functions for TBK1, IKKβ, and IKKε.

Considering that TBK1, IKKε, and IKKβ are structurally related, it appears plausible that these kinases have overlapping substrate specificities. In the following, a brief overview of the known substrates of TBK1, IKKβ, and IKKε is given. IKKβ has been shown to phosphorylate MAVS at the *p*L*x*IS motif at Ser442 and NF-κB p65 at Ser536 (Buss et al., 2004; Liu et al., 2015; Sakurai et al., 1999). In the context of TLR3 signaling, IKKβ has been described to phosphorylate TBK1 in the activation loop at Ser172, thereby allowing IRF3 recruitment to TRIF (Abe et al., 2020). In addition, the canonical IKKs were reported to phosphorylate TBK1 and IKKε after activation of TLR3 or TLR4 (Clark et al., 2011a). IKKβ has also been described to catalyze an activating phosphorylation of IRF3 after TLR3 activation, whereas IKKβ has not yet been linked to STING phosphorylation (Han et al., 2004). Similarly, IKKε has been shown to phosphorylate NF-κB p65 at Ser536 (Bao et al., 2010; Buss et al., 2004) and IRF3 at Ser396 (Fitzgerald et al., 2003). Recently, IKKε has also been described to phosphorylate STING at Ser366 in mouse myeloid cells (Balka et al., 2020). To date, IKKε has not been shown to phosphorylate MAVS or TBK1. TBK1 is well-known to phosphorylate STING at *p*L*x*IS^{366} and MAVS at *p*L*x*IS^{442} after cytosolic DNA or 5'ppp-dsRNA challenge, and TBK1 has also been reported to phosphorylate NF-κB p65 at Ser536 (Buss et al., 2004; Liu et al., 2015). Interestingly, TBK1 was also shown to phosphorylate IKKβ in the activation loop, thereby inducing IκBα degradation and subse-

quent activation of NF-κB (Tojima et al., 2000), whereas phosphorylation of IKKε by TBK1 has not yet been described.

Considering that TBK1, IKKβ, and IKKε have similar substrate specificities, it is possible that unexpected and unexplored functional relationships exist between these proteins that may have enhanced the phosphorylation of TBK1 in the *in vitro* kinase assay of this study. An intricate kinase network could facilitate signal integration and add an additional layer of regulation to balance the inflammatory response after viral clearance. Functional redundancy may also make the cell less susceptible to certain viral immune evasion mechanisms, in which viral proteases attempt to inhibit phosphorylations essential for the type I IFN response.

TBK1 and IKKε have been reported to bind to the scaffold proteins TRAF family member-associated NF-kappa-B activator (TANK), NF-kappa-B-activating kinase-associated protein 1 (NAP1), and TANK-binding kinase 1-binding protein 1 (TBKBP1, also known as similar to NAP1 TBK1 adaptor (SINTBAD)) (Chau et al., 2008; Goncalves et al., 2011). However, the functions of TANK, NAP1, and SINTBAD are still controversial since KO of the encoding genes did not affect the TLR- and RLR-mediated expression of type I IFNs and pro-inflammatory cytokines in primary mouse macrophages (Fukasaka et al., 2013; Kawagoe et al., 2009). No interactions with TANK, NAP1, and SINTBAD were detected in the interactome analyses of this work, suggesting that the multiprotein complex assembled by hnRNPM and ELAVL1 is functionally distinct.

It should be noted that hnRNPM has recently been assigned a negative regulatory role in RLR signaling and has been described to compete with RIG-I and MDA5 for binding to viral RNAs (Cao et al., 2019). However, these findings could not be reproduced in this thesis and it would therefore be of great importance to identify the origins of these controversies.

4.6 Outlook

This work has identified a novel multiprotein complex consisting of at least hnRNPM, ELAVL1, and TBK1 that functions downstream of cGAS and RIG. IKKβ, IKKε, and NF-κB p65 were identified as additional *in vitro* interactors of hnRNPM. In future experiments, these interactions should also be evaluated *in cellulo*. Moreover, deletion analyses could

identify the domains of hnRNPM that mediate the interactions with TBK1, IKKβ, IKKε, and NF-κB p65. Phos-tag-containing SDS-PAGE gels could be used to elucidate whether different TBK1 phosphoforms interact with hnRNPM and whether phosphorylation of TBK1 is a prerequisite for binding to hnRNPM. It should also be investigated whether nuclear TBK1 can activate IRF3 and thus induce a type I IFN response. Although numerous publications have already described important functions of the canonical and non-canonical IKKs in innate immunity, their interplay and overlapping substrate specificities in the cellular context have not yet been systematically characterized. This gap could be filled by generating TBK1/IKK-deficient cell lines. Screening of additional hnRNPM/ELAVL1 interactors could certainly provide valuable insights into the regulation of the newly identified multiprotein complex. However, future efforts should first focus on a more detailed genetic analysis of SON and the putative connection to nuclear TBK1. IGF2BP2 represents another interesting candidate that, although not directly controlling the phosphorylation of TBK1 and IRF3, could regulate the expression of type I IFNs at the level of transcription or translation. Considering that hnRNPM is frequently associated with splicing, total RNA sequencing could be performed to examine whether hnRNPM mediates splicing of genes involved in the type I IFN response. Future experiments should also evaluate whether hnRNPM and ELAVL1 control MDA5 signaling. This is likely to be expected since both MDA5 and RIG-I signal via MAVS. The newly discovered signaling complex would gain further relevance if the function of hnRNPM and ELAVL1 could be confirmed in primary human cells and mice.

5 Abstract

Detection of viral nucleic acids by specialized PRRs of the innate immune system triggers the expression of type I IFNs, a hallmark of antiviral defense. In vertebrates, the cGAS-STING pathway and the RLR-MAVS pathway have emerged as the major cytosolic type I IFN-inducing nucleic acid sensing systems. Although both systems sense the genetic material of different virus classes, signaling downstream of the initial receptor-ligand contact involves common kinases (i.e., TBK1, IKKε) and transcription factors (i.e., IRF3, NF-κB p65).

This thesis has characterized the role of hnRNPM, a predominantly nuclear protein, in cytosolic nucleic acid sensing in the monocytic cell line THP-1. hnRNPM positively regulated both the cGAS-STING- and RIG-I-dependent type I IFN induction by promoting the phosphorylation of TBK1 and/or IRF3. A combined AP-MS/RNAi screen identified ELAVL1 and SON as hnRNPM interactors that also promote cGAS and RIG-I signaling by enhancing TBK1 and/or IRF3 phosphorylation. IGF2BP2, an RNA-dependent hnRNPM interactor, amplified the cGAS- and RIG-I-induced type I IFN response in a TBK1 phosphorylation-independent manner.

To further evaluate the function of ELAVL1, the *ELAVL1* gene locus was deleted in THP-1 cells. A more detailed investigation revealed that ELAVL1 promoted both the expression of type I IFNs and activation of NF-κB after stimulation of cGAS or RIG-I. The type I IFN response was downregulated by approximately 6-fold to 8-fold in ELAVL1 KO cells and was dependent on the N- and C-terminal RRMs of ELAVL1. Overexpression of ELAVL1-FLAG in ELAVL1-deficient THP-1 dual cells rescued the cGAS- or RIG-I-induced phosphorylation of TBK1/IRF3 and the subsequent ISG response. By contrast, the TLR1/TLR2-mediated phosphorylation of TBK1 was ELAVL1-independent, indicating that ELAVL1 might regulate the activation of different TBK1 subpopulations in a PRR-dependent manner. Analyzing the global mRNA expression profile further demonstrated that ELAVL1 does not regulate the expression of genes associated with cGAS and RIG-I signaling.

A comparative interactome analysis identified common interactors of hnRNPM and ELAVL1, including RNA-binding proteins, ribosomal proteins, splicing factors, and also type I IFN-inducing proteins (i.e., DDX3X). The interactions with SON were restricted to

hnRNPM, suggesting that hnRNPM forms distinct complexes with ELAVL1 and SON. In addition, hnRNPM also interacted with TBK1, IKKε, IKKβ, and NF-κB p65. PLAs confirmed that the interactions between hnRNPM, ELAVL1, and TBK1 phosphorylated at Ser172 occur *in cellulo* and primarily in the cytoplasm, indicating that the minor cytoplasmic rather than the predominant nuclear portions of hnRNPM and ELAVL1 mediate TBK1 phosphorylation. Furthermore, the antibody-based purification of the multiprotein complex assembled by hnRNPM enhanced the phosphorylation of recombinant TBK1 in the activation loop.

In summary, this thesis provides new insights into the signaling cascades downstream of cGAS and RIG-I and has identified a novel multiprotein complex that positively regulates both pathways at a common point of convergence, TBK1 phosphorylation. A better understanding of the newly identified multiprotein complex might contribute to the development of new therapies for the treatment of inflammatory diseases resulting from dysregulation of cGAS-STING or RIG-I-MAVS signaling (i.e., AGS, SMS, or SAVI).

6 List of figures

7 List of tables

8 References

Abdelmohsen, K., Kuwano, Y., Kim, H.H., and Gorospe, M. (2008). Posttranscriptional gene regulation by RNA-binding proteins during oxidative stress: Implications for cellular senescence. Biol. Chem. *389*, 243–255.

Abe, H., Satoh, J., Shirasaka, Y., Kogure, A., Kato, H., Ito, S., and Fujita, T. (2020). Priming Phosphorylation of TANK-Binding Kinase 1 by IκB Kinase β Is Essential in Toll-Like Receptor 3/4 Signaling. Mol. Cell. Biol. *40*.

Ablasser, A., and Chen, Z.J. (2019). CGAS in action: Expanding roles in immunity and inflammation. Science *363*, eaat8657.

Ablasser, A., and Hur, S. (2020). Regulation of cGAS- and RLR-mediated immunity to nucleic acids. Nat. Immunol. *21*, 17–29.

Ablasser, A., Goldeck, M., Cavlar, T., Deimling, T., Witte, G., Röhl, I., Hopfner, K.P., Ludwig, J., and Hornung, V. (2013). CGAS produces a 2′-5′-linked cyclic dinucleotide second messenger that activates STING. Nature *498*, 380–384.

Adolph, S.K., DeLotto, R., Nielsen, F.C., and Christiansen, J. (2009). Embryonic expression of Drosophila IMP in the developing CNS and PNS. Gene Expr. Patterns *9*, 138–143.

Aguirre, S., Luthra, P., Sanchez-Aparicio, M.T., Maestre, A.M., Patel, J., Lamothe, F., Fredericks, A.C., Tripathi, S., Zhu, T., Pintado-Silva, J., et al. (2017). Dengue virus NS2B protein targets cGAS for degradation and prevents mitochondrial DNA sensing during infection. Nat. Microbiol. *2*, 17037.

Ahn, E.-Y., DeKelver, R.C., Lo, M.-C., Nguyen, T.A., Matsuura, S., Boyapati, A., Pandit, S., Fu, X.-D., and Zhang, D.-E. (2011). SON Controls Cell-Cycle Progression by Coordinated Regulation of RNA Splicing. Mol. Cell *42*, 185–198.

Ahn, E.E.-Y., Higashi, T., Yan, M., Matsuura, S., Hickey, C.J., Lo, M.-C., Shia, W.-J., DeKelver, R.C., and Zhang, D.-E. (2013). SON protein regulates GATA-2 through transcriptional control of the microRNA 23a~27a~24-2 cluster. J. Biol. Chem. *288*, 5381–5388.

Ahn, J., Gutman, D., Saijo, S., and Barber, G.N. (2012). STING manifests self DNA-dependent inflammatory disease. Proc. Natl. Acad. Sci. *109*, 19386–19391.

Alexopoulou, L., Holt, A.C., Medzhitov, R., and Flavell, R.A. (2001). Recognition of double-stranded RNA and activation of NF-kappaB by Toll-like receptor 3. Nature *413*, 732–738.

An, J., Durcan, L., Karr, R.M., Briggs, T.A., Rice, G.I., Teal, T.H., Woodward, J.J., and Elkon, K.B. (2017). Expression of Cyclic GMP-AMP Synthase in Patients With Systemic Lupus Erythematosus. Arthritis Rheumatol. (Hoboken, N.J.) *69*, 800–807.

Anders, S., Pyl, P.T., and Huber, W. (2015). HTSeq-A Python framework to work with high-throughput sequencing data. Bioinformatics *31*, 166–169.

Aravind, L., and Koonin, E. V. (1999). G-patch: A new conserved domain in eukaryotic RNA-processing proteins and type D retroviral polyproteins. Trends Biochem. Sci. *24*, 342–344.

Balka, K.R., Louis, C., Saunders, T.L., Smith, A.M., Calleja, D.J., D'Silva, D.B., Moghaddas, F., Tailler, M., Lawlor, K.E., Zhan, Y., et al. (2020). TBK1 and IKKε Act Redundantly to Mediate STING-Induced NF-κB Responses in Myeloid Cells. Cell Rep. *31*, 107492.

Bao, X., Indukuri, H., Liu, T., Liao, S.-L., Tian, B., Brasier, A.R., Garofalo, R.P., and Casola, A. (2010). IKKε modulates RSV-induced NF-κB-dependent gene transcription. Virology *408*, 224–231.

Barbuddhe, S.B., and Chakraborty, T. (2009). Listeria as an enteroinvasive gastrointestinal pathogen. Curr. Top. Microbiol. Immunol. *337*, 173–195.

Barchet, W., Wimmenauer, V., Schlee, M., and Hartmann, G. (2008). Accessing the therapeutic potential of immunostimulatory nucleic acids. Curr. Opin. Immunol. *20*, 389–395.

Bartok, E., and Hartmann, G. (2020). Immune Sensing Mechanisms that Discriminate Self from Altered Self and Foreign Nucleic Acids. Immunity *53*, 54–77.

Berke, I.C., Yu, X., Modis, Y., and Egelman, E.H. (2012). MDA5 assembles into a polar helical filament on dsRNA. Proc. Natl. Acad. Sci. *109*, 18437–18441.

Beyer, A.L., Christensen, M.E., Walker, B.W., and LeStourgeon, W.M. (1977). Identification and characterization of the packaging proteins of core 40S hnRNP particles. Cell *11*, 127–138.

Bialojan, C., and Takai, A. (1988). Inhibitory effect of a marine-sponge toxin, okadaic acid, on protein phosphatases. Specificity and kinetics. Biochem. J. *256*, 283–290.

Brennan, C.M., and Steitz, J.A. (2001). HuR and mRNA stability. Cell. Mol. Life Sci. *58*, 266–277.

Burleigh, K., Maltbaek, J.H., Cambier, S., Green, R., Gale, M., James, R.C., and Stetson, D.B. (2020). Human DNA-PK activates a STING-independent DNA sensing pathway. Sci. Immunol. *5*, 1–14.

Buss, H., Dörrie, A., Schmitz, M.L., Hoffmann, E., Resch, K., and Kracht, M. (2004). Constitutive and interleukin-1-inducible phosphorylation of p65 NF-{kappa}B at serine 536 is mediated by multiple protein kinases including I{kappa}B kinase (IKK)-{alpha}, IKK{beta}, IKK{epsilon}, TRAF family member-associated (TANK)-binding kinase 1 (TB. J. Biol. Chem. *279*, 55633–55643.

Cai, X., Chen, J., Xu, H., Liu, S., Jiang, Q.-X., Halfmann, R., and Chen, Z.J. (2014). Prion-like Polymerization Underlies Signal Transduction in Antiviral Immune Defense and Inflammasome Activation. Cell *156*, 1207–1222.

Cao, J., Mu, Q., and Huang, H. (2018). The roles of insulin-like growth factor 2 mRNA-binding protein 2 in cancer and cancer stem cells. Stem Cells Int. *2018*, 4217259.

Cao, P., Luo, W.W., Li, C., Tong, Z., Zheng, Z.Q., Zhou, L., Xiong, Y., and Li, S. (2019). The heterogeneous nuclear ribonucleoprotein hnRNPM inhibits RNA virus-triggered innate immunity by antagonizing RNA sensing of RIG-I-like receptors. PLoS Pathog. *15*, 1–20.

Chau, T.L., Gioia, R., Gatot, J.S., Patrascu, F., Carpentier, I., Chapelle, J.P., O'Neill, L., Beyaert, R., Piette, J., and Chariot, A. (2008). Are the IKKs and IKK-related kinases TBK1 and IKK-ε similarly activated? Trends Biochem. Sci. *33*, 171–180.

Chen, W.Y., Lin, C.L., Chuang, J.H., Chiu, F.Y., Sun, Y.Y., Liang, M.C., and Lin, Y. (2017). Heterogeneous nuclear ribonucleoprotein M associates with mTORC2 and regulates muscle differentiation. Sci. Rep. *7*, 1–13.

Chevrier, N., Mertins, P., Artyomov, M.N., Shalek, A.K., Iannacone, M., Ciaccio, M.F., Gat-Viks, I., Tonti, E., Degrace, M.M., Clauser, K.R., et al. (2011). Systematic discovery of TLR signaling components delineates viral-sensing circuits. Cell *147*, 853–867.

Choe, J., Kelker, M.S., and Wilson, I.A. (2005). Crystal structure of human toll-like receptor 3 (TLR3) ectodomain. Science *309*, 581–585.

Christensen, M.H., Jensen, S.B., Miettinen, J.J., Luecke, S., Prabakaran, T., Reinert, L.S., Mettenleiter, T., Chen, Z.J., Knipe, D.M., Sandri-Goldin, R.M., et al. (2016). HSV-1 ICP27 targets the TBK1-activated STING signalsome to inhibit virus-induced type I IFN expression. EMBO J. *35*, 1385–1399.

Clark, K., Peggie, M., Plater, L., Sorcek, R.J., Young, E.R.R., Madwed, J.B., Hough, J., McIver, E.G., and Cohen, P. (2011a). Novel cross-talk within the IKK family controls innate immunity. Biochem. J. *434*, 93–104.

Clark, K., Takeuchi, O., Akira, S., and Cohen, P. (2011b). The TRAF-associated protein TANK facilitates cross-talk within the IκB kinase family during Toll-like receptor signaling. Proc. Natl. Acad. Sci. *108*, 17093–17098.

Conlon, J., Burdette, D.L., Sharma, S., Bhat, N., Thompson, M., Jiang, Z., Rathinam, V.A.K., Monks, B., Jin, T., Xiao, T.S., et al. (2013). Mouse, but not Human STING, Binds and Signals in Response to the Vascular Disrupting Agent 5,6-Dimethylxanthenone-4-Acetic Acid. J. Immunol. *190*, 5216–5225.

Coppé, J.-P., Patil, C.K., Rodier, F., Sun, Y., Muñoz, D.P., Goldstein, J., Nelson, P.S., Desprez, P.-Y., and Campisi, J. (2008). Senescence-associated secretory phenotypes reveal cell-nonautonomous functions of oncogenic RAS and the p53 tumor suppressor. PLoS Biol. *6*, 2853–2868.

Crow, Y.J., and Manel, N. (2015). Aicardi-Goutières syndrome and the type I interferonopathies. Nat. Rev. Immunol. *15*, 429–440.

Crow, Y.J., Hayward, B.E., Parmar, R., Robins, P., Leitch, A., Ali, M., Black, D.N., van Bokhoven, H., Brunner, H.G., Hamel, B.C., et al. (2006). Mutations in the gene encoding the 3'-5' DNA exonuclease TREX1 cause Aicardi-Goutières syndrome at the AGS1 locus. Nat. Genet. *38*, 917–920.

Datar, K. V., Dreyfuss, G., and Swanson, M.S. (1993). The human hnRNP M proteins: Identification of a methionine/arginine-rich repeat motif in ribonucleoproteins. Nucleic Acids Res. *21*, 439–446.

Deane, J.A., Pisitkun, P., Barrett, R.S., Feigenbaum, L., Town, T., Ward, J.M., Flavell, R.A., and Bolland, S. (2007). Control of toll-like receptor 7 expression is essential to restrict autoimmunity and dendritic cell proliferation. Immunity *27*, 801–810.

Dixon, D.A., Tolley, N.D., King, P.H., Nabors, L.B., McIntyre, T.M., Zimmerman, G.A., and Prescott, S.M. (2001). Altered expression of the mRNA stability factor HuR promotes cyclooxygenase-2 expression in colon cancer cells. J. Clin. Invest. *108*, 1657–1665.

Dobin, A., Davis, C.A., Schlesinger, F., Drenkow, J., Zaleski, C., Jha, S., Batut, P., Chaisson, M., and Gingeras, T.R. (2013). STAR: Ultrafast universal RNA-seq aligner. Bioinformatics *29*, 15–21.

Dou, Z., Ghosh, K., Vizioli, M.G., Zhu, J., Sen, P., Wangensteen, K.J., Simithy, J., Lan, Y., Lin, Y., Zhou, Z., et al. (2017). Cytoplasmic chromatin triggers inflammation in senescence and cancer. Nature *550*, 402–406.

Du, M., and Chen, Z.J. (2018). DNA-induced liquid phase condensation of cGAS activates innate immune signaling. Science *361*, 704–709.

Du, M., Liu, J., Chen, X., Xie, Y., Yuan, C., Xiang, Y., Sun, B., Lan, K., Chen, M., James, S.J., et al. (2015). Casein Kinase II Controls TBK1/IRF3 Activation in IFN Response against Viral Infection. J. Immunol. *194*, 4477–4488.

Durie, D., Lewis, S.M., Liwak, U., Kisilewicz, M., Gorospe, M., and Holcik, M. (2011). RNA-binding protein HuR mediates cytoprotection through stimulation of XIAP translation. Oncogene *30*, 1460–1469.

Ea, C.-K., Deng, L., Xia, Z.-P., Pineda, G., and Chen, Z.J. (2006). Activation of IKK by TNFalpha requires site-specific ubiquitination of RIP1 and polyubiquitin binding by NEMO. Mol. Cell *22*, 245–257.

Eekelen, C.A. va., Riemen, T., and Venrooij, W.J. va. (1981). Specificity in the interaction of hnRNA and mRNA with proteins as revealed by in vivo cross linking. FEBS Lett. *130*, 223–226.

Ferguson, B.J., Mansur, D.S., Peters, N.E., Ren, H., and Smith, G.L. (2012). DNA-PK is a DNA sensor for IRF-3-dependent innate immunity. Elife *2012*, 1–17.

Fitzgerald, K.A., McWhirter, S.M., Faia, K.L., Rowe, D.C., Latz, E., Golenbock, D.T., Coyle, A.J., Liao, S.M., and Maniatis, T. (2003). IKKE and TBKI are essential components of the IRF3 signalling pathway. Nat. Immunol. *4*, 491–496.

Fukasaka, M., Ori, D., Kawagoe, T., Uematsu, S., Maruyama, K., Okazaki, T., Kozaki, T., Imamura, T., Tartey, S., Mino, T., et al. (2013). Critical role of AZI2 in GM-CSF-induced dendritic cell differentiation. J. Immunol. *190*, 5702–5711.

Gabhann, J.N., Higgs, R., Brennan, K., Thomas, W., Damen, J.E., Ben Larbi, N., Krystal, G., and Jefferies, C.A. (2010). Absence of SHIP-1 Results in Constitutive Phosphorylation of Tank-Binding Kinase 1 and Enhanced TLR3-Dependent IFN-β Production. J. Immunol. *184*, 2314–2320.

Gack, M.U., Shin, Y.C., Joo, C.-H., Urano, T., Liang, C., Sun, L., Takeuchi, O., Akira, S., Chen, Z., Inoue, S., et al. (2007). TRIM25 RING-finger E3 ubiquitin ligase is essential for RIG-I-mediated antiviral activity. Nature *446*, 916–920.

Gall, A., Treuting, P., Elkon, K.B., Loo, Y.-M., Gale, M.J., Barber, G.N., and Stetson, D.B. (2012). Autoimmunity initiates in nonhematopoietic cells and progresses via lymphocytes in an interferon-dependent autoimmune disease. Immunity *36*, 120–131.

Gao, D., Li, T., Li, X.-D., Chen, X., Li, Q.-Z., Wight-Carter, M., and Chen, Z.J. (2015). Activation of cyclic GMP-AMP synthase by self-DNA causes autoimmune diseases. Proc. Natl. Acad. Sci. *112*, E5699-705.

Gattoni, R., Mahé, D., Mähl, P., Fischer, N., Mattei, M.G., Stévenin, J., and Fuchs, J.P. (1996). The human hnRNP-M proteins: Structure and relation with early heat shock-induced splicing arrest and chromosome mapping. Nucleic Acids Res. *24*, 2535–2542.

Gauzzi, M.C., Barbieri, G., Richter, M.F., Uzé, G., Ling, L., Fellous, M., and Pellegrini, S. (1997). The amino-terminal region of Tyk2 sustains the level of interferon alpha receptor 1, a component of the interferon alpha/beta receptor. Proc. Natl. Acad. Sci. *94*, 11839–11844.

Glück, S., Guey, B., Gulen, M.F., Wolter, K., Kang, T.W., Schmacke, N.A., Bridgeman, A., Rehwinkel, J., Zender, L., and Ablasser, A. (2017). Innate immune sensing of cytosolic chromatin fragments through cGAS promotes senescence. Nat. Cell Biol. *19*, 1061–1070.

Goncalves, A., Bürckstümmer, T., Dixit, E., Scheicher, R., Górna, M.W., Karayel, E., Sugar, C., Stukalov, A., Berg, T., Kralovics, R., et al. (2011). Functional dissection of the TBK1 molecular network. PLoS One *6*, e23971.

Greenlund, A.C., Morales, M.O., Viviano, B.L., Yan, H., Krolewski, J., and Schreiber, R.D. (1995). Stat recruitment by tyrosine-phosphorylated cytokine receptors: an ordered reversible affinity-driven process. Immunity *2*, 677–687.

Gu, L., Fullam, A., McCormack, N., Höhn, Y., and Schröder, M. (2017). DDX3 directly regulates TRAF3 ubiquitination and acts as a scaffold to co-ordinate assembly of signalling complexes downstream from MAVS. Biochem. J. *474*, 571–587.

Häcker, H., Redecke, V., Blagoev, B., Kratchmarova, I., Hsu, L.-C., Wang, G.G., Kamps, M.P., Raz, E., Wagner, H., Häcker, G., et al. (2006). Specificity in Toll-like receptor signalling through distinct effector functions of TRAF3 and TRAF6. Nature *439*, 204–207.

Han, K.J., Su, X., Xu, L.G., Bin, L.H., Zhang, J., and Shu, H.B. (2004). Mechanisms of the TRIF-induced Interferon-stimulated Response Element and NF-κB Activation and Apoptosis Pathways. J. Biol. Chem. *279*, 15652–15661.

Han, S.P., Tang, Y.H., and Smith, R. (2010). Functional diversity of the hnRNPs: Past, present and perspectives. Biochem. J. *430*, 379–392.

Hansen, K., Prabakaran, T., Laustsen, A., Jørgensen, S.E., Rahbæk, S.H., Jensen, S.B., Nielsen, R., Leber, J.H., Decker, T., Horan, K.A., et al. (2014a). Listeria monocytogenes induces IFNβ expression through an IFI16-, cGAS- and STING-dependent pathway . EMBO J. *33*, 1654–1666.

Harding, S.M., Benci, J.L., Irianto, J., Discher, D.E., Minn, A.J., and Greenberg, R.A. (2017). Mitotic progression following DNA damage enables pattern recognition within micronuclei. Nature *548*, 466–470.

Hayakawa, S., Shiratori, S., Yamato, H., Kameyama, T., Kitatsuji, C., Kashigi, F., Goto, S., Kameoka, S., Fujikura, D., Yamada, T., et al. (2011). ZAPS is a potent stimulator of signaling mediated by the RNA helicase RIG-I during antiviral responses. Nat. Immunol. *12*, 37–44.

Heim, M.H., Kerr, I.M., Stark, G.R., and Darnell, J.E.J. (1995). Contribution of STAT SH2 groups to specific interferon signaling by the Jak-STAT pathway. Science *267*, 1347–1349.

Hein, M.Y., Hubner, N.C., Poser, I., Cox, J., Nagaraj, N., Toyoda, Y., Gak, I.A., Weisswange, I., Mansfeld, J., Buchholz, F., et al. (2015). A Human Interactome in Three Quantitative Dimensions Organized by Stoichiometries and Abundances. Cell *163*, 712–723.

Heinz, L.X., Lee, J.E., Kapoor, U., Kartnig, F., Sedlyarov, V., Papakostas, K., César-Razquin, A., Essletzbichler, P., Goldmann, U., Stefanovic, A., et al. (2020). TASL is the SLC15A4-associated adaptor for IRF5 activation by TLR7–9. Nature *581*, 316–322.

Hemmi, H., Kaisho, T., Takeuchi, O., Sato, S., Sanjo, H., Hoshino, K., Horiuchi, T., Tomizawa, H., Takeda, K., and Akira, S. (2002). Small anti-viral compounds activate immune cells via the TLR7 MyD88-dependent signaling pathway. Nat. Immunol. *3*, 196–200.

Herdy, B., Karonitsch, T., Vladimer, G.I., Tan, C.S.H., Stukalov, A., Trefzer, C., Bigenzahn, J.W., Theil, T., Holinka, J., Kiener, H.P., et al. (2015). The RNA-binding protein HuR/ELAVL1 regulates IFN-β mRNA abundance and the type I IFN response. Eur. J. Immunol. *45*, 1500–1511.

Herzner, A.-M. (2013). Mechanismen der Immunmodulation durch Erkennung zytosolischer DNA. Dissertation, Rheinische Friedrich-Wilhelms-Universität Bonn.

Herzner, A.M., Hagmann, C.A., Goldeck, M., Wolter, S., Kübler, K., Wittmann, S., Gramberg, T., Andreeva, L., Hopfner, K.P., Mertens, C., et al. (2015). Sequence-specific activation of the DNA sensor cGAS by Y-form DNA structures as found in primary HIV-1 cDNA. Nat. Immunol. *16*, 1025–1033.

Hickey, C.J., Kim, J.H., and Ahn, E.Y.E. (2014). New discoveries of old SON: A link between RNA splicing and cancer. J. Cell. Biochem. *115*, 224–231.

Hinman, M.N., and Lou, H. (2008). Diverse molecular functions of Hu proteins. Cell. Mol. Life Sci. *65*, 3168–3181.

Hiscott, J. (2007). Convergence of the NF-κB and IRF pathways in the regulation of the innate antiviral response. Cytokine Growth Factor Rev. *18*, 483–490.

Honda, K., Yanai, H., Negishi, H., Asagiri, M., Sato, M., Mizutani, T., Shimada, N., Ohba, Y., Takaoka, A., Yoshida, N., et al. (2005). IRF-7 is the master regulator of type-I interferon-dependent immune responses. Nature *434*, 772–777.

Hooks, J.J., Moutsopoulos, H.M., Geis, S.A., Stahl, N.I., Decker, J.L., and Notkins, A.L. (1979). Immune interferon in the circulation of patients with autoimmune disease. N. Engl. J. Med. *301*, 5–8.

Hopfner, K.P., and Hornung, V. (2020). Molecular mechanisms and cellular functions of cGAS–STING signalling. Nat. Rev. Mol. Cell Biol. *21*, 501–521.

Hornung, V., Ellegast, J., Kim, S., Brzózka, K., Jung, A., Kato, H., Poeck, H., Akira, S., Conzelmann, K.K., Schlee, M., et al. (2006). 5′-Triphosphate RNA is the ligand for RIG-I. Science *314*, 994–997.

Hou, F., Sun, L., Zheng, H., Skaug, B., Jiang, Q.-X., and Chen, Z.J. (2011). MAVS forms functional prion-like aggregates to activate and propagate antiviral innate immune response. Cell *146*, 448–461.

Huang, Y.-H., Liu, X.-Y., Du, X.-X., Jiang, Z.-F., and Su, X.-D. (2012). The structural basis for the sensing and binding of cyclic di-GMP by STING. Nat. Struct. Mol. Biol. *19*, 728–730.

Huelga, S.C., Huelga, S.C., Vu, A.Q., Vu, A.Q., Arnold, J.D., Arnold, J.D., Liang, T.Y., Liang, T.Y., Liu, P.P., Liu, P.P., et al. (2012). Integrative genome-wide analysis reveals cooperative regulation of alternative splicing by hnRNP proteins. Cell Rep. *1*, 167–178.

Huen, M.S.Y., Sy, S.M.H., Leung, K.M., Ching, Y.-P., Tipoe, G.L., Man, C., Dong, S., and Chen, J. (2010). SON is a spliceosome-associated factor required for mitotic progression. Cell Cycle *9*, 2679–2685.

Ishikawa, H., and Barber, G.N. (2008). STING is an endoplasmic reticulum adaptor that facilitates innate immune signalling. Nature *455*, 674–678.

Jagdeo, J.M., Dufour, A., Fung, G., Luo, H., Kleifeld, O., Overall, C.M., and Jan, E. (2015). Heterogeneous Nuclear Ribonucleoprotein M Facilitates Enterovirus Infection. J. Virol. *89*, 7064–7078.

Janeway, C.A.J. (1989). Approaching the asymptote? Evolution and revolution in immunology. Cold Spring Harb. Symp. Quant. Biol. *54 Pt 1*, 1–13.

Jang, M.-A., Kim, E.K., Now, H., Nguyen, N.T.H., Kim, W.-J., Yoo, J.-Y., Lee, J., Jeong, Y.-M., Kim, C.-H., Kim, O.-H., et al. (2015). Mutations in DDX58, which encodes RIG-I, cause atypical Singleton-Merten syndrome. Am. J. Hum. Genet. *96*, 266–274.

Jiang, F., Ramanathan, A., Miller, M.T., Tang, G.-Q., Gale, M.J., Patel, S.S., and Marcotrigiano, J. (2011). Structural basis of RNA recognition and activation by innate immune receptor RIG-I. Nature *479*, 423–427.

Jiang, X., Kinch, L.N., Brautigam, C.A., Chen, X., Du, F., Grishin, N. V, and Chen, Z.J. (2012). Ubiquitin-induced oligomerization of the RNA sensors RIG-I and MDA5 activates antiviral innate immune response. Immunity *36*, 959–973.

Jin, L., Waterman, P.M., Jonscher, K.R., Short, C.M., Reisdorph, N.A., and Cambier, J.C. (2008). MPYS, a novel membrane tetraspanner, is associated with major histocompatibility complex class II and mediates transduction of apoptotic signals. Mol. Cell. Biol. *28*, 5014–5026.

Judge, A.D., Sood, V., Shaw, J.R., Fang, D., McClintock, K., and MacLachlan, I. (2005). Sequence-dependent stimulation of the mammalian innate immune response by synthetic siRNA. Nat. Biotechnol. *23*, 457–462.

Jurk, M., Heil, F., Vollmer, J., Schetter, C., Krieg, A.M., Wagner, H., Lipford, G., and Bauer, S. (2002). Human TLR7 or TLR8 independently confer responsiveness to the antiviral compound R-848. Nat. Immunol. *3*, 499.

Kaake, R.M., Wang, X., Burke, A., Yu, C., Kandur, W., Yang, Y., Novtisky, E.J., Second, T., Duan, J., Kao, A., et al. (2014). A new in vivo cross-linking mass spectrometry platform to define protein-protein interactions in living cells. Mol. Cell. Proteomics *13*, 3533–3543.

Kang, D., Gopalkrishnan, R. V, Wu, Q., Jankowsky, E., Pyle, A.M., and Fisher, P.B. (2002). mda-5: An interferon-inducible putative RNA helicase with double-stranded RNA-dependent ATPase activity and melanoma growth-suppressive properties. Proc. Natl. Acad. Sci. *99*, 637–642.

Kato, H., Takeuchi, O., Mikamo-Satoh, E., Hirai, R., Kawai, T., Matsushita, K., Hiiragi, A., Dermody, T.S., Fujita, T., and Akira, S. (2008). Length-dependent recognition of double-stranded ribonucleic acids by retinoic acid-inducible gene-I and melanoma differentiation-associated gene 5. J. Exp. Med. *205*, 1601–1610.

Kawagoe, T., Takeuchi, O., Takabatake, Y., Kato, H., Isaka, Y., Tsujimura, T., and Akira, S. (2009). TANK is a negative regulator of Toll-like receptor signaling and is critical for the prevention of autoimmune nephritis. Nat. Immunol. *10*, 965–972.

Kawai, T., Sato, S., Ishii, K.J., Coban, C., Hemmi, H., Yamamoto, M., Terai, K., Matsuda, M., Inoue, J., Uematsu, S., et al. (2004). Interferon-alpha induction through Toll-like receptors involves a direct interaction of IRF7 with MyD88 and TRAF6. Nat. Immunol. *5*, 1061–1068.

Kawai, T., Takahashi, K., Sato, S., Coban, C., Kumar, H., Kato, H., Ishii, K.J., Takeuchi, O., and Akira, S. (2005). IPS-1, an adaptor triggering RIG-I- and Mda5-mediated type I interferon induction. Nat. Immunol. *6*, 981–988.

Kawamura, M., McVicar, D.W., Johnston, J.A., Blake, T.B., Chen, Y.Q., Lal, B.K., Lloyd, A.R., Kelvin, D.J., Staples, J.E., and Ortaldo, J.R. (1994). Molecular cloning of L-JAK, a Janus family protein-tyrosine kinase expressed in natural killer cells and activated leukocytes. Proc. Natl. Acad. Sci. *91*, 6374–6378.

Kim, H.H., Kuwano, Y., Srikantan, S., Lee, E.K., Martindale, J.L., and Gorospe, M. (2009). HuR recruits let-7/RISC to repress c-Myc expression. Genes Dev. *23*, 1743–1748.

Kim, J.-H., Shinde, D.N., Reijnders, M.R.F., Hauser, N.S., Belmonte, R.L., Wilson, G.R., Bosch, D.G.M., Bubulya, P.A., Shashi, V., Petrovski, S., et al. (2016). De Novo Mutations in SON Disrupt RNA Splicing of Genes Essential for Brain Development and Metabolism, Causing an Intellectual-Disability Syndrome. Am. J. Hum. Genet. *99*, 711–719.

Kim, T., Pazhoor, S., Bao, M., Zhang, Z., Hanabuchi, S., Facchinetti, V., Bover, L., Plumas, J., Chaperot, L., Qin, J., et al. (2010). Aspartate-glutamate-alanine-histidine box motif (DEAH)/RNA helicase a helicases sense microbial DNA in human plasmacytoid dendritic cells. Proc. Natl. Acad. Sci. *107*, 15181–15186.

Kowalinski, E., Lunardi, T., McCarthy, A.A., Louber, J., Brunel, J., Grigorov, B., Gerlier, D., and Cusack, S. (2011). Structural basis for the activation of innate immune pattern-recognition receptor RIG-I by viral RNA. Cell *147*, 423–435.

Kumar, H., Kawai, T., Kato, H., Sato, S., Takahashi, K., Coban, C., Yamamoto, M., Uematsu, S., Ishii, K.J., Takeuchi, O., et al. (2006). Essential role of IPS-1 in innate immune responses against RNA viruses. J. Exp. Med. *203*, 1795–1803.

Lahaye, X., Gentili, M., Silvin, A., Conrad, C., Picard, L., Jouve, M., Zueva, E., Maurin, M., Nadalin, F., Knott, G.J., et al. (2018). NONO Detects the Nuclear HIV Capsid to Promote cGAS-Mediated Innate Immune Activation. Cell *175*, 488-501.e22.

Larabi, A., Devos, J.M., Ng, S.L., Nanao, M.H., Round, A., Maniatis, T., and Panne, D. (2013). Crystal Structure and Mechanism of Activation of TANK-Binding Kinase 1. Cell Rep. *3*, 734–746.

Leonard, J.N., Ghirlando, R., Askins, J., Bell, J.K., Margulies, D.H., Davies, D.R., and Segal, D.M. (2008). The TLR3 signaling complex forms by cooperative receptor dimerization. Proc. Natl. Acad. Sci. *105*, 258–263.

Li, S., Strelow, A., Fontana, E.J., and Wesche, H. (2002). IRAK-4: a novel member of the IRAK family with the properties of an IRAK-kinase. Proc. Natl. Acad. Sci. *99*, 5567–5572.

Li, X., Shu, C., Yi, G., Chaton, C.T., Shelton, C.L., Diao, J., Zuo, X., Kao, C.C., Herr, A.B., and Li, P. (2013). Cyclic GMP-AMP Synthase Is Activated by Double-Stranded DNA-Induced Oligomerization. Immunity *39*, 1019–1031.

Li, Y., Chen, R., Zhou, Q., Xu, Z., Li, C., Wang, S., Mao, A., Zhang, X., He, W., and Shu, H.B. (2012). LSm14A is a processing body-associated sensor of viral nucleic acids that initiates cellular antiviral response in the early phase of viral infection. Proc. Natl. Acad. Sci. *109*, 11770–11775.

Lin, S.-C., Lo, Y.-C., and Wu, H. (2010). Helical assembly in the MyD88-IRAK4-IRAK2 complex in TLR/IL-1R signalling. Nature *465*, 885–890.

Liu, L., Botos, I., Wang, Y., Leonard, J.N., Shiloach, J., Segal, D.M., and Davies, D.R. (2008). Structural basis of toll-like receptor 3 signaling with double-stranded RNA. Science *320*, 379–381.

Liu, S., Chen, J., Cai, X., Wu, J., Chen, X., Wu, Y.-T., Sun, L., and Chen, Z.J. (2013). MAVS recruits multiple ubiquitin E3 ligases to activate antiviral signaling cascades. Elife *2*, e00785.

Liu, S., Cai, X., Wu, J., Cong, Q., Chen, X., Li, T., Du, F., Ren, J., Wu, Y.T., Grishin, N. V., et al. (2015). Phosphorylation of innate immune adaptor proteins MAVS, STING, and TRIF induces IRF3 activation. Science *347*, aaa2630.

Liu, T.-T., Yang, Q., Li, M., Zhong, B., Ran, Y., Liu, L.-L., Yang, Y., Wang, Y.-Y., and Shu, H.-B. (2016). LSm14A Plays a Critical Role in Antiviral Immune Responses by Regulating MITA Level in a Cell-Specific Manner. J. Immunol. *196*, 5101–5111.

Liu, Y., Jesus, A.A., Marrero, B., Yang, D., Ramsey, S.E., Sanchez, G.A.M., Tenbrock, K., Wittkowski, H., Jones, O.Y., Kuehn, H.S., et al. (2014). Activated STING in a vascular and pulmonary syndrome. N. Engl. J. Med. *371*, 507–518.

Llères, D., Denegri, M., Biggiogera, M., Ajuh, P., and Lamond, A.I. (2010). Direct interaction between hnRNP-M and CDC5L/PLRG1 proteins affects alternative splice site choice. EMBO Rep. *11*, 445–451.

Lopez-Pelaez, M., Lamont, D.J., Peggie, M., Shpiro, N., Gray, N.S., and Cohen, P. (2014). Protein kinase IKKβ-catalyzed phosphorylation of IRF5 at Ser462 induces its dimerization and nuclear translocation in myeloid cells. Proc. Natl. Acad. Sci. *111*, 17432–17437.

López De Silanes, I., Zhan, M., Lal, A., Yang, X., and Gorospe, M. (2004). Identification of a target RNA motif for RNA-binding protein HuR. Proc. Natl. Acad. Sci. *101*, 2987–2992.

Love, M.I., Huber, W., and Anders, S. (2014). Moderated estimation of fold change and dispersion for RNA-seq data with DESeq2. Genome Biol. *15*.

Lu, H., Lu, N., Weng, L., Yuan, B., Liu, Y., and Zhang, Z. (2014). DHX15 Senses Double-Stranded RNA in Myeloid Dendritic Cells. J. Immunol. *193*, 1364–1372.

Luo, D., Ding, S.C., Vela, A., Kohlway, A., Lindenbach, B.D., and Pyle, A.M. (2011). Structural insights into RNA recognition by RIG-I. Cell *147*, 409–422.

Luo, Z., Li, Z., Chen, K., Liu, R., Li, X., Cao, H., and Zheng, S.J. (2012). Engagement of heterogeneous nuclear ribonucleoprotein M with listeriolysin O induces type I interferon expression and restricts Listeria monocytogenes growth in host cells. Immunobiology *217*, 972–981.

Ma, W.J., Cheng, S., Campbell, C., Wright, A., and Furneaux, H. (1996). Cloning and characterization of HuR, a ubiquitously expressed Elav-like protein. J. Biol. Chem. *271*, 8144–8151.

Mackenzie, K.J., Carroll, P., Martin, C.-A., Murina, O., Fluteau, A., Simpson, D.J., Olova, N., Sutcliffe, H., Rainger, J.K., Leitch, A., et al. (2017). cGAS surveillance of micronuclei links genome instability to innate immunity. Nature *548*, 461–465.

Marko, M., Leichter, M., Patrinou-Georgoula, M., and Guialis, A. (2010). hnRNP M interacts with PSF and p54nrb and co-localizes within defined nuclear structures. Exp. Cell Res. *316*, 390–400.

Meisner, N.C., Hintersteiner, M., Mueller, K., Bauer, R., Seifert, J.M., Naegeli, H.U., Ottl, J., Oberer, L., Guenat, C., Moss, S., et al. (2007). Identification and mechanistic characterization of low-molecular-weight inhibitors for HuR. Nat. Chem. Biol. *3*, 508–515.

Meylan, E., Curran, J., Hofmann, K., Moradpour, D., Binder, M., Bartenschlager, R., and Tschopp, J. (2005). Cardif is an adaptor protein in the RIG-I antiviral pathway and is targeted by hepatitis C virus. Nature *437*, 1167–1172.

Morchikh, M., Cribier, A., Raffel, R., Amraoui, S., Cau, J., Severac, D., Dubois, E., Schwartz, O., Bennasser, Y., and Benkirane, M. (2017). HEXIM1 and NEAT1 Long Non-coding RNA Form a Multi-subunit Complex that Regulates DNA-Mediated Innate Immune Response. Mol. Cell *67*, 387-399.e5.

Mosallanejad, K., Sekine, Y., Ishikura-Kinoshita, S., Kumagai, K., Nagano, T., Matsuzawa, A., Takeda, K., Naguro, I., and Ichijo, H. (2014). The DEAH-Box RNA helicase DHX15 activates NF-κB and MAPK signaling downstream of MAVS during antiviral responses. Sci. Signal. *7*, ra40.

Motshwene, P.G., Moncrieffe, M.C., Grossmann, J.G., Kao, C., Ayaluru, M., Sandercock, A.M., Robinson, C. V, Latz, E., and Gay, N.J. (2009). An oligomeric signaling platform formed by the Toll-like receptor signal transducers MyD88 and IRAK-4. J. Biol. Chem. *284*, 25404–25411.

Mukherjee, A., Morosky, S.A., Delorme-Axford, E., Dybdahl-Sissoko, N., Oberste, M.S., Wang, T., and Coyne, C.B. (2011a). The coxsackievirus B 3C protease cleaves MAVS and TRIF to attenuate host type I interferon and apoptotic signaling. PLoS Pathog. *7*, e1001311.

Mukherjee, N., Corcoran, D.L., Nusbaum, J.D., Reid, D.W., Georgiev, S., Hafner, M., Ascano, M., Tuschl, T., Ohler, U., and Keene, J.D. (2011b). Integrative Regulatory Mapping Indicates that the RNA-Binding Protein HuR Couples Pre-mRNA Processing and mRNA Stability. Mol. Cell *43*, 327–339.

Nabors, L.B., Gillespie, G.Y., Harkins, L., and King, P.H. (2001). HuR, a RNA stability factor, is expressed in malignant brain tumors and binds to adenine- and uridine-rich elements within the 3′ untranslated regions of cytokine and angiogenic factor mRNAs. Cancer Res. *61*, 2154–2161.

Namjou, B., Kothari, P.H., Kelly, J.A., Glenn, S.B., Ojwang, J.O., Adler, A., Alarcón-Riquelme, M.E., Gallant, C.J., Boackle, S.A., Criswell, L.A., et al. (2011). Evaluation of the TREX1 gene in a large multi-ancestral lupus cohort. Genes Immun. *12*, 270–279.

Napirei, M., Karsunky, H., Zevnik, B., Stephan, H., Mannherz, H.G., and Möröy, T. (2000). Features of systemic lupus erythematosus in Dnase1-deficient mice. Nat. Genet. *25*, 177–181.

Nielsen, J., Christiansen, J., Lykke-Andersen, J., Johnsen, A.H., Wewer, U.M., and Nielsen, F.C. (1999). A Family of Insulin-Like Growth Factor II mRNA-Binding Proteins Represses Translation in Late Development. Mol. Cell. Biol. *19*, 1262–1270.

Nielsen, J., Adolph, S.K., Rajpert-De Meyts, E., Lykke-Andersen, J., Koch, G., Christiansen, J., and Nielsen, F.C. (2003). Nuclear transit of human zipcode-binding protein IMP1. Biochem. J. *376*, 383–391.

Nielsen, J., Kristensen, M.A., Willemoës, M., Nielsen, F.C., and Christiansen, J. (2004). Sequential dimerization of human zipcode-binding protein IMP1 on RNA: A cooperative mechanism providing RNP stability. Nucleic Acids Res. *32*, 4368–4376.

Oganesyan, G., Saha, S.K., Guo, B., He, J.Q., Shahangian, A., Zarnegar, B., Perry, A., and Cheng, G. (2006). Critical role of TRAF3 in the Toll-like receptor-dependent and -independent antiviral response. Nature *439*, 208–211.

Ohto, U., Shibata, T., Tanji, H., Ishida, H., Krayukhina, E., Uchiyama, S., Miyake, K., and Shimizu, T. (2015). Structural basis of CpG and inhibitory DNA recognition by Toll-like receptor 9. Nature *520*, 702–705.

Oshiumi, H., Matsumoto, M., Funami, K., Akazawa, T., and Seya, T. (2003). TICAM-1, an adaptor molecule that participates in Toll-like receptor 3-mediated interferon-beta induction. Nat. Immunol. *4*, 161–167.

Oshiumi, H., Matsumoto, M., Hatakeyama, S., and Seya, T. (2009). Riplet/RNF135, a RING finger protein, ubiquitinates RIG-I to promote interferon-beta induction during the early phase of viral infection. J. Biol. Chem. *284*, 807–817.

Oshiumi, H., Miyashita, M., Inoue, N., Okabe, M., Matsumoto, M., and Seya, T. (2010). The ubiquitin ligase Riplet is essential for RIG-I-dependent innate immune responses to RNA virus infection. Cell Host Microbe *8*, 496–509.

Ostendorf, T., Zillinger, T., Andryka, K., Schlee-Guimaraes, T.M., Schmitz, S., Marx, S., Bayrak, K., Linke, R., Salgert, S., Wegner, J., et al. (2020). Immune Sensing of Synthetic, Bacterial, and Protozoan RNA by Toll-like Receptor 8 Requires Coordinated Processing by RNase T2 and RNase 2. Immunity *52*, 591-605.e6.

Ouyang, S., Song, X., Wang, Y., Ru, H., Shaw, N., Jiang, Y., Niu, F., Zhu, Y., Qiu, W., Parvatiyar, K., et al. (2012). Structural analysis of the STING adaptor protein reveals a hydrophobic dimer interface and mode of cyclic di-GMP binding. Immunity *36*, 1073–1086.

Panne, D., McWhirter, S.M., Maniatis, T., and Harrison, S.C. (2007). Interferon regulatory factor 3 is regulated by a dual phosphorylation- dependent switch. J. Biol. Chem. *282*, 22816–22822.

Passacantilli, I., Frisone, P., De Paola, E., Fidaleo, M., and Paronetto, M.P. (2017). HNRNPM guides an alternative splicing program in response to inhibition of the PI3K/AKT/mTOR pathway in Ewing sarcoma cells. Nucleic Acids Res. *45*, 12270–12284.

Pattabhi, S., Knoll, M.L., Gale, M., and Loo, Y.M. (2019). DHX15 Is a Coreceptor for RLR Signaling That Promotes Antiviral Defense Against RNA Virus Infection. J. Interf. Cytokine Res. *39*, 331–346.

Peisley, A., Lin, C., Wu, B., Orme-Johnson, M., Liu, M., Walz, T., and Hur, S. (2011). Cooperative assembly and dynamic disassembly of MDA5 filaments for viral dsRNA recognition. Proc. Natl. Acad. Sci. *108*, 21010–21015.

Peisley, A., Jo, M.H., Lin, C., Wu, B., Orme-Johnson, M., Walz, T., Hohng, S., and Hur, S. (2012). Kinetic mechanism for viral dsRNA length discrimination by MDA5 filaments. Proc. Natl. Acad. Sci. *109*, E3340–E3349.

Pichlmair, A., Schulz, O., Tan, C.P., Näslund, T.I., Liljeström, P., Weber, F., and Reis e Sousa, C. (2006). RIG-I-mediated antiviral responses to single-stranded RNA bearing 5'-phosphates. Science *314*, 997–1001.

Pisitkun, P., Deane, J.A., Difilippantonio, M.J., Tarasenko, T., Satterthwaite, A.B., and Bolland, S. (2006). Autoreactive B cell responses to RNA-related antigens due to TLR7 gene duplication. Science *312*, 1669–1672.

Polymenidou, M., Lagier-Tourenne, C., Hutt, K.R., Huelga, S.C., Moran, J., Liang, T.Y., Ling, S.C., Sun, E., Wancewicz, E., Mazur, C., et al. (2011). Long pre-mRNA depletion and RNA missplicing contribute to neuronal vulnerability from loss of TDP-43. Nat. Neurosci. *14*, 459–468.

Ren, J., Chen, X., and Chen, Z.J. (2014). IKKβ is an IRF5 kinase that instigates inflammation. Proc. Natl. Acad. Sci. *111*, 17438–17443.

Robinson, T., Kariuki, S.N., Franek, B.S., Kumabe, M., Kumar, A.A., Badaracco, M., Mikolaitis, R.A., Guerrero, G., Utset, T.O., Drevlow, B.E., et al. (2011). Autoimmune disease risk variant of IFIH1 is associated with increased sensitivity to IFN-α and serologic autoimmunity in lupus patients. J. Immunol. *187*, 1298–1303.

Rowland, M.A., Harrison, B., and Deeds, E.J. (2015). Phosphatase specificity and pathway insulation in signaling networks. Biophys. J. *108*, 986–996.

Sakurai, H., Chiba, H., Miyoshi, H., Sugita, T., and Toriumi, W. (1999). IkappaB kinases phosphorylate NF-kappaB p65 subunit on serine 536 in the transactivation domain. J. Biol. Chem. *274*, 30353–30356.

Saunders, L.R., and Barber, G.N. (2003). The dsRNA binding protein family: critical roles, diverse cellular functions. FASEB J. *17*, 961–983.

Schaeffer, V., Hansen, K.M., Morris, D.R., LeBoeuf, R.C., and Abrass, C.K. (2012). RNA-binding protein IGF2BP2/IMP2 is required for laminin-β2 mRNA translation and is modulated by glucose concentration. Am. J. Physiol. Renal Physiol. *303*, F75-82.

Schindler, C., Shuai, K., Prezioso, V.R., and Darnell, J.E.J. (1992). Interferon-dependent tyrosine phosphorylation of a latent cytoplasmic transcription factor. Science *257*, 809–813.

Schlee, M., and Hartmann, G. (2016). Discriminating self from non-self in nucleic acid sensing. Nat. Rev. Immunol. *16*, 566–580.

Schlee, M., Roth, A., Hornung, V., Hagmann, C.A., Wimmenauer, V., Barchet, W., Coch, C., Janke, M., Mihailovic, A., Wardle, G., et al. (2009). Recognition of 5′ Triphosphate by RIG-I Helicase Requires Short Blunt Double-Stranded RNA as Contained in Panhandle of Negative-Strand Virus. Immunity *31*, 25–34.

Schnare, M., Holt, A.C., Takeda, K., Akira, S., and Medzhitov, R. (2000). Recognition of CpG DNA is mediated by signaling pathways dependent on the adaptor protein MyD88. Curr. Biol. *10*, 1139–1142.

Schneider, W.M., Chevillotte, M.D., and Rice, C.M. (2014). Interferon-stimulated genes: A complex web of host defenses. Annu. Rev. Immunol. *32*, 513–545.

Schröder, M., Baran, M., and Bowie, A.G. (2008). Viral targeting of DEAD box protein 3 reveals its role in TBK1/IKKε-mediated IRF activation. EMBO J. *27*, 2147–2157.

Schuberth-Wagner, C., Ludwig, J., Bruder, A.K., Herzner, A.M., Zillinger, T., Goldeck, M., Schmidt, T., Schmid-Burgk, J.L., Kerber, R., Wolter, S., et al. (2015). A Conserved Histidine in the RNA Sensor RIG-I Controls Immune Tolerance to N1-2'O-Methylated Self RNA. Immunity *43*, 41–51.

Seth, R.B., Sun, L., Ea, C.-K., and Chen, Z.J. (2005). Identification and characterization of MAVS, a mitochondrial antiviral signaling protein that activates NF-kappaB and IRF 3. Cell *122*, 669–682.

Shang, G., Zhu, D., Li, N., Zhang, J., Zhu, C., Lu, D., Liu, C., Yu, Q., Zhao, Y., Xu, S., et al. (2012). Crystal structures of STING protein reveal basis for recognition of cyclic di-GMP. Nat. Struct. Mol. Biol. *19*, 725–727.

Shang, G., Zhang, C., Chen, Z.J., Bai, X., and Zhang, X. (2019). Cryo-EM structures of STING reveal its mechanism of activation by cyclic GMP–AMP. Nature *567*, 389–393.

Sharma, A., Takata, H., Shibahara, K.I., Bubulya, A., and Bubulya, P.A. (2010). Son is essential for nuclear speckle organization and cell cycle progression. Mol. Biol. Cell *21*, 650-663.

Shaw, A.E., Hughes, J., Gu, Q., Behdenna, A., Singer, J.B., Dennis, T., Orton, R.J., Varela, M., Gifford, R.J., Wilson, S.J., et al. (2017). Fundamental properties of the mammalian innate immune system revealed by multispecies comparison of type I interferon responses. PLoS Biol. *15*, e2004086.

Shi, Y., Yuan, B., Qi, N., Zhu, W., Su, J., Li, X., Qi, P., Zhang, D., and Hou, F. (2015). An autoinhibitory mechanism modulates MAVS activity in antiviral innate immune response. Nat. Commun. *6*, 7811.

Shu, C., Sankaran, B., Chaton, C.T., Herr, A.B., Mishra, A., Peng, J., and Li, P. (2013). Structural insights into the functions of TBK1 in innate antimicrobial immunity. Structure *21*, 1137–1148.

Slezak, R., Smigiel, R., Rydzanicz, M., Pollak, A., Kosinska, J., Stawinski, P., Malgorzata Sasiadek, M., and Ploski, R. (2020). Phenotypic expansion in Zhu-Tokita-Takenouchi-Kim syndrome caused by de novo variants in the SON gene. Mol. Genet. Genomic Med. *8*, 1–7.

Soulat, D., Bürckstümmer, T., Westermayer, S., Goncalves, A., Bauch, A., Stefanovic, A., Hantschel, O., Bennett, K.L., Decker, T., and Superti-Furga, G. (2008). The DEAD-box helicase DDX3X is a critical component of the TANK-binding kinase 1-dependent innate immune response. EMBO J. *27*, 2135–2146.

Sparks, J.W., and Brautigan, D.L. (1986). Molecular basis for substrate specificity of protein kinases and phosphatases. Int. J. Biochem. *18*, 497–504.

Srikantan, S., and Gorospe, M. (2012). HuR function in disease. Front. Biosci. *17*, 189–205.

Srikanth, S., Woo, J.S., Wu, B., El-Sherbiny, Y.M., Leung, J., Chupradit, K., Rice, L., Seo, G.J., Calmettes, G., Ramakrishna, C., et al. (2019). The Ca 2+ sensor STIM1 regulates the type I interferon response by retaining the signaling adaptor STING at the endoplasmic reticulum. Nat. Immunol. *20*, 152–162.

Stetson, D.B., Ko, J.S., Heidmann, T., and Medzhitov, R. (2008). Trex1 prevents cell-intrinsic initiation of autoimmunity. Cell *134*, 587–598.

Sueyoshi, T., Kawasaki, T., Kitai, Y., Ori, D., Akira, S., and Kawai, T. (2018). Hu Antigen R Regulates Antiviral Innate Immune Responses through the Stabilization of mRNA for Polo-like Kinase 2. J. Immunol. *200*, 3814–3824.

Sun, C.T., Lo, W.Y., Wang, I.H., Lo, Y.H., Shiou, S.R., Lai, C.K., and Ting, L.P. (2001). Transcription repression of human hepatitis B virus genes by negative regulatory element-binding protein/SON. J. Biol. Chem. *276*, 24059–24067.

Sun, L., Wu, J., Du, F., Chen, X., and Chen, Z.J. (2013). Cyclic GMP-AMP synthase is a cytosolic DNA sensor that activates the type I interferon pathway. Science *339*, 786–791.

Sun, Q., Sun, L., Liu, H.-H., Chen, X., Seth, R.B., Forman, J., and Chen, Z.J. (2006). The specific and essential role of MAVS in antiviral innate immune responses. Immunity *24*, 633–642.

Sun, W., Li, Y., Chen, L., Chen, H., You, F., Zhou, X., Zhou, Y., Zhai, Z., Chen, D., and Jiang, Z. (2009). ERIS, an endoplasmic reticulum IFN stimulator, activates innate immune signaling through dimerization. Proc. Natl. Acad. Sci. *106*, 8653–8658.

Swingle, M., Ni, L., and Honkanen, R.E. (2007). Small-molecule inhibitors of ser/thr protein phosphatases: specificity, use and common forms of abuse. Methods Mol. Biol. *365*, 23–38.

Takaoka, A., Yanai, H., Kondo, S., Duncan, G., Negishi, H., Mizutani, T., Kano, S.-I., Honda, K., Ohba, Y., Mak, T.W., et al. (2005). Integral role of IRF-5 in the gene induction programme activated by Toll-like receptors. Nature *434*, 243–249.

Tan, X., Sun, L., Chen, J., and Chen, Z.J. (2018). Detection of Microbial Infections Through Innate Immune Sensing of Nucleic Acids. Annu. Rev. Microbiol. *72*, 447–478.

Tanaka, Y., and Chen, Z.J. (2012). STING specifies IRF3 phosphorylation by TBK1 in the cytosolic DNA signaling pathway. Sci. Signal. *5*, 1–12.

Tanji, H., Ohto, U., Shibata, T., Taoka, M., Yamauchi, Y., Isobe, T., Miyake, K., and Shimizu, T. (2015). Toll-like receptor 8 senses degradation products of single-stranded RNA. Nat. Struct. Mol. Biol. *22*, 109–115.

Tatematsu, M., Ishii, A., Oshiumi, H., Horiuchi, M., Inagaki, F., Seya, T., and Matsumoto, M. (2010). A molecular mechanism for Toll-IL-1 receptor domain-containing adaptor molecule-1-mediated IRF-3 activation. J. Biol. Chem. *285*, 20128–20136.

Timp, W., and Timp, G. (2020). Beyond mass spectrometry, the next step in proteomics. Sci. Adv. *6*, 1–17.

Tojima, Y., Fujimoto, A., Delhase, M., Chen, Y., Hatekeyama, S., Nakayama, K.I., Kaneko, Y., Nimura, Y., Motoyama, N., Ikeda, K., et al. (2000). NAK is an IκB kinase-activating kinase. Nature *404*, 778–782.

Tu, D., Zhu, Z., Zhou, A.Y., Yun, C. hong, Lee, K.E., Toms, A. V., Li, Y., Dunn, G.P., Chan, E., Thai, T., et al. (2013). Structure and Ubiquitination-Dependent Activation of TANK-Binding Kinase 1. Cell Rep. *3*, 747–758.

Tyanova, S., Temu, T., Sinitcyn, P., Carlson, A., Hein, M.Y., Geiger, T., Mann, M., and Cox, J. (2016). The Perseus computational platform for comprehensive analysis of (prote)omics data. Nat. Methods *13*, 731–740.

Uematsu, S., Sato, S., Yamamoto, M., Hirotani, T., Kato, H., Takeshita, F., Matsuda, M., Coban, C., Ishii, K.J., Kawai, T., et al. (2005). Interleukin-1 receptor-associated kinase-1 plays an essential role for Toll-like receptor (TLR)7- and TLR9-mediated interferon-{alpha} induction. J. Exp. Med. *201*, 915–923.

Vance, R.E. (2016). Cytosolic DNA Sensing: The Field Narrows. Immunity *45*, 227–228.

Varjak, M., Saul, S., Arike, L., Lulla, A., Peil, L., and Merits, A. (2013). Magnetic Fractionation and Proteomic Dissection of Cellular Organelles Occupied by the Late Replication Complexes of Semliki Forest Virus. J. Virol. *87*, 10295–10312.

Warner, J.D., Irizarry-Caro, R.A., Bennion, B.G., Ai, T.L., Smith, A.M., Miner, C.A., Sakai, T., Gonugunta, V.K., Wu, J., Platt, D.J., et al. (2017). STING-associated vasculopathy develops independently of IRF3 in mice. J. Exp. Med. *214*, 3279–3292.

Weidensdorfer, D., Stöhr, N., Baude, A., Lederer, M., Köhn, M., Schierhorn, A., Buchmeier, S., Wahle, E., and Hüttelmaier, S. (2009). Control of c-myc mRNA stability by IGF2BP1-associated cytoplasmic RNPs. RNA *15*, 104–115.

West, K.O., Scott, H.M., Torres-Odio, S., West, A.P., Patrick, K.L., and Watson, R.O. (2019). The Splicing Factor hnRNP M Is a Critical Regulator of Innate Immune Gene Expression in Macrophages. Cell Rep. *29*, 1594-1609.e5.

Woo, S.R., Fuertes, M.B., Corrales, L., Spranger, S., Furdyna, M.J., Leung, M.Y.K., Duggan, R., Wang, Y., Barber, G.N., Fitzgerald, K.A., et al. (2014). STING-dependent cytosolic DNA sensing mediates innate immune recognition of immunogenic tumors. Immunity *41*, 830–842.

Wu, B., Peisley, A., Richards, C., Yao, H., Zeng, X., Lin, C., Chu, F., Walz, T., and Hur, S. (2013). Structural Basis for dsRNA Recognition, Filament Formation, and Antiviral Signal Activation by MDA5. Cell *152*, 276–289.

Wu, B., Peisley, A., Tetrault, D., Li, Z., Egelman, E.H., Magor, K.E., Walz, T., Penczek, P.A., and Hur, S. (2014). Molecular imprinting as a signal-activation mechanism of the viral RNA sensor RIG-I. Mol. Cell *55*, 511–523.

Wu, C.-J., Conze, D.B., Li, T., Srinivasula, S.M., and Ashwell, J.D. (2006). Sensing of Lys 63-linked polyubiquitination by NEMO is a key event in NF-κB activation. Nat. Cell Biol. *8*, 398–406.

Xu, H., He, X., Zheng, H., Huang, L.J., Hou, F., Yu, Z., de la Cruz, M.J., Borkowski, B., Zhang, X., Chen, Z.J., et al. (2015). Correction: Structural basis for the prion-like MAVS filaments in antiviral innate immunity. Elife *4*.

Xu, L.-G., Wang, Y.-Y., Han, K.-J., Li, L.-Y., Zhai, Z., and Shu, H.-B. (2005). VISA is an adapter protein required for virus-triggered IFN-beta signaling. Mol. Cell *19*, 727–740.

Xu, Y., Gao, X.D., Lee, J.H., Huang, H., Tan, H., Ahn, J., Reinke, L.M., Peter, M.E., Feng, Y., Gius, D., et al. (2014). Cell type-restricted activity of hnRNPM promotes breast cancer metastasis via regulating alternative splicing. Genes Dev. *28*, 1191–1203.

Yamamoto, M., Sato, S., Hemmi, H., Hoshino, K., Kaisho, T., Sanjo, H., Takeuchi, O., Sugiyama, M., Okabe, M., Takeda, K., et al. (2003). Role of adaptor TRIF in the MyD88-independent toll-like receptor signaling pathway. Science *301*, 640–643.

Yang, Y.-G., Lindahl, T., and Barnes, D.E. (2007). Trex1 exonuclease degrades ssDNA to prevent chronic checkpoint activation and autoimmune disease. Cell *131*, 873–886.

Yin, Q., Tian, Y., Kabaleeswaran, V., Jiang, X., Tu, D., Eck, M.J., Chen, Z.J., and Wu, H. (2012). Cyclic di-GMP sensing via the innate immune signaling protein STING. Mol. Cell *46*, 735–745.

Yoneyama, M., Kikuchi, M., Natsukawa, T., Shinobu, N., Imaizumi, T., Miyagishi, M., Taira, K., Akira, S., and Fujita, T. (2004). The RNA helicase RIG-I has an essential function in double-stranded RNA-induced innate antiviral responses. Nat. Immunol. *5*, 730–737.

Zeng, W., Sun, L., Jiang, X., Chen, X., Hou, F., Adhikari, A., Xu, M., and Chen, Z.J. (2010). Reconstitution of the RIG-I pathway reveals a signaling role of unanchored polyubiquitin chains in innate immunity. Cell *141*, 315–330.

Zhan, Z., Cao, H., Xie, X., Yang, L., Zhang, P., Chen, Y., Fan, H., Liu, Z., and Liu, X. (2015). Phosphatase PP4 Negatively Regulates Type I IFN Production and Antiviral Innate Immunity by Dephosphorylating and Deactivating TBK1. J. Immunol. *195*, 3849–3857.

Zhang, C., Shang, G., Gui, X., Zhang, X., Bai, X.-C., and Chen, Z.J. (2019). Structural basis of STING binding with and phosphorylation by TBK1. Nature *567*, 394–398.

Zhang, G., Chan, B., Samarina, N., Abere, B., Weidner-Glunde, M., Buch, A., Pich, A., Brinkmann, M.M., and Schulz, T.F. (2016a). Cytoplasmic isoforms of Kaposi sarcoma herpesvirus LANA recruit and antagonize the innate immune DNA sensor cGAS. Proc. Natl. Acad. Sci. *113*, E1034-43.

Zhang, X., Wu, J., Du, F., Xu, H., Sun, L., Chen, Z., Brautigam, C.A., Zhang, X., and Chen, Z.J. (2014). The cytosolic DNA sensor cGAS forms an oligomeric complex with DNA and undergoes switch-like conformational changes in the activation loop. Cell Rep. *6*, 421–430.

Zhang, X., Bai, X. chen, and Chen, Z.J. (2020). Structures and Mechanisms in the cGAS-STING Innate Immunity Pathway. Immunity *53*, 43–53.

Zhang, Z., Yuan, B., Lu, N., Facchinetti, V., and Liu, Y.-J. (2011). DHX9 Pairs with IPS-1 To Sense Double-Stranded RNA in Myeloid Dendritic Cells. J. Immunol. *187*, 4501–4508.

Zhang, Z., Ohto, U., Shibata, T., Krayukhina, E., Taoka, M., Yamauchi, Y., Tanji, H., Isobe, T., Uchiyama, S., Miyake, K., et al. (2016b). Structural Analysis Reveals that Toll-like Receptor 7 Is a Dual Receptor for Guanosine and Single-Stranded RNA. Immunity *45*, 737–748.

Zhao, B., Shu, C., Gao, X., Sankaran, B., Du, F., Shelton, C.L., Herr, A.B., Ji, J.-Y., and Li, P. (2016). Structural basis for concerted recruitment and activation of IRF-3 by innate immune adaptor proteins. Proc. Natl. Acad. Sci. *113*, E3403-12.

Zhao, B., Du, F., Xu, P., Shu, C., Sankaran, B., Bell, S.L., Liu, M., Lei, Y., Gao, X., Fu, X., et al. (2019). A conserved PLPLRT/SD motif of STING mediates the recruitment and activation of TBK1. Nature *569*, 718–722.

Zhao, Y., Liang, L., Fan, Y., Sun, S., An, L., Shi, Z., Cheng, J., Jia, W., Sun, W., Mori-Akiyama, Y., et al. (2012). PPM1B negatively regulates antiviral response via dephosphorylating TBK1. Cell. Signal. *24*, 2197–2204.

Zhong, B., Yang, Y., Li, S., Wang, Y.-Y., Li, Y., Diao, F., Lei, C., He, X., Zhang, L., Tien, P., et al. (2008a). The adaptor protein MITA links virus-sensing receptors to IRF3 transcription factor activation. Immunity *29*, 538–550.

9 Appendix

For space reasons, a tabular listing of all generated interaction and expression data sets is not included in the printed version of this thesis. Instead, these data sets can be found in the digital appendix of this work (DOI: https://doi.org/10.22000/473).

9.1 Interactome data of hnRNPM in resting and cGAS-activated THP-1 dual cells

The interactomes of hnRNPM in resting and cGAS-activated THP-1 dual cells (related to Fig. 3.13) can be found in folder `9.1_Interactome-hnRNPM` of the digital appendix.

9.2 3'-mRNA expression data of ELAVL1-deficient THP-1 dual cells

The 3'-mRNA expression data of ELAVL1-deficient THP-1 dual cells vs. THP-1 dual wildtype cells in the non-stimulated state (related to Fig. 3.28) can be found in folder `9.2_Medium.ko_vs_wt.deseq2` of the digital appendix.

The 3'-mRNA expression data of ELAVL1-deficient THP-1 dual cells vs. THP-1 dual wildtype cells after IFNAR activation (related to Fig. 3.29) can be found in folder `9.2_IFNa.ko_vs_wt.deseq2` of the digital appendix.

The 3'-mRNA expression data of ELAVL1-deficient THP-1 dual cells vs. THP-1 dual wildtype cells after RIG-I activation (related to Fig. 3.30) can be found in folder `9.2_IVT4.ko_vs_wt.deseq2` of the digital appendix.

The 3'-mRNA expression data of ELAVL1-deficient THP-1 dual cells vs. THP-1 dual wildtype cells after cGAS activation (related to Fig. 3.31) can be found in folder `9.2_G3_YSD.ko_vs_wt.deseq2` of the digital appendix.

9.3 Interactome data of hnRNPM and ELAVL1

The interactomes of hnRNPM and ELAVL1 in THP-1 dual cells (related to Fig. 3.32) can be found in folder `9.3_Interactome-hnRNPM-ELAVL1` of the digital appendix.

10 Acknowledgements

This doctoral thesis would not have been possible without the contribution and help of many people. I would like to thank all colleagues, friends, and my family for their constant support during the last years:

First of all, I would like to thank Prof. Dr. Martin Schlee for giving me the opportunity to pursue my PhD project in his group, for introducing me to the exciting field of nucleic acid immunity, his guidance, his seemingly unlimited ideas for new experiments, and many fruitful discussions.

I would also like to express my sincere gratitude to the other members of the dissertation committee, Prof. Dr. Matthias Geyer, Prof. Dr. Eicke Latz, and Prof. Dr. Andreas Schlitzer, for devoting their valuable time to the review of this thesis.

I am thankful to Prof. Dr. Gunther Hartmann for building an excellent institute in an inspiring research environment.

I am very grateful to Prof. Dr. Andreas Pichlmair, Dr. Antonio Piras, and Christian Urban for a truly excellent collaboration.

I would like to thank Dr. Gabor Horvath of the Microscopy Core Facility for practical tips on confocal imaging, Dr. André Heimbach of the Next Generation Sequencing Core Facility for 3'-mRNA seq library preparation and sequencing, Peter Wurst and Maximilian Germer of the Flow Cytometry Core Facility for cell sorting, and Dr. Maria Hønholt Christensen for providing HSV-1.

I thank all current and former members of the Institute of Clinical Chemistry and Clinical Pharmacology for their support, advice, and assistance. Particularly, I am grateful to Thais for the 3'-mRNA sequencing data analysis and for introducing me to R. I thank Anna for initiating this interesting project. I thank Kasia for her help with all confocal microscopy-related issues and my former student Petro for his interest in my research and his help with the RNAi screen.

In particular, I thank the whole AG Schlee for the great working atmosphere, continuous support, and help throughout the years. A big thanks to Agathe and Christina, whose

technical support at the end of this project helped me a lot, and Heike for keeping things running smoothly in the lab. A special thanks to Anne, Steven, Marvin, Julia, Katrin, and Adham for being great colleagues, sharing ideas, coffee breaks, and fun times outside of the lab.

I am deeply grateful to my family for their continuous and unparalleled love and support. I owe you everything and I wouldn't be here without you. Katrin, your love, patience, and encouragement during the last years only made all this possible. Thank you for always being by my side no matter what.